



Norwegian University of  
Science and Technology

# Numerical Simulation of Viscous Shear Flow Around Tandem Cylinders

**Dhanushi Nayanatara Attanapola**

Marine Technology

Submission date: June 2018

Supervisor: Bjørnar Pettersen, IMT

Co-supervisor: Tale Egeberg Aasland, IMT

Norwegian University of Science and Technology  
Department of Marine Technology





## MASTER THESIS IN MARINE HYDRODYNAMICS

SPRING 2018

FOR

**Stud.techn. Dhanushi N. Attanapola**

### **NUMERICAL SIMULATION OF VISCOUS SHEAR FLOW AROUND TANDEM CYLINDERS.**

The candidate shall investigate the viscous flow around two circular cylinders in a tandem configuration exposed to shear current. The numerical simulation tool to be used is OpenFOAM, at low Reynolds numbers.

Focus of the study shall be on the physical flow field details, especially in the flow zone between the two cylinders. All the results obtained should be discussed and compared to relevant data available from the literature. Proper visualization of results are important.

The candidate's choice of flow parameters should be argued for. Computational parameters shall be investigated and documented. The proper parameters and detailed settings of the numerical simulations (including pre- and post-processing) should be documented for later use.

In the thesis the candidate shall present his personal contribution to the resolution of the problem within the scope of the thesis work. Theories and conclusions should be based on mathematical derivation and logic reasoning identifying the various steps in the deduction. The original contribution of the candidate and material taken from other sources shall be clearly defined. Work from other sources shall be properly referenced. The candidate should utilize the existing possibilities for obtaining relevant literature.

The thesis should be organized in a rational manner to give a clear exposition of results, assessments and conclusions. The text should be brief and to the point, with a clear language.

The thesis shall contain the following elements: A text defining the scope, preface, list of contents, summary, main body of thesis, conclusions with recommendations for further work, list of symbols and acronyms, references and appendices. All figures, tables and equations shall be numerated.

It is supposed that Department of Marine Technology, NTNU, can use the results freely in its research work by referring to the student's thesis.

The thesis shall be submitted June 11<sup>th</sup>, 2018, in two copies.



Bjørnar Pettersen  
Professor/supervisor

Co-supervisor: PhD-student Tale E. Aasland



# Abstract

The project, Coastal Highway E39, introduces the concept of *Submerged Floating Tube Bridge (SFTB)*. The bridge is simplified as tandem cylinders with longitudinal length-diameter ratio  $L/D = 3.2$ , diameter  $D = 1.0$  and span-wise length  $l = 6D$ . The tandem cylinders are subjected by a linearly varying profile called *Shear Flow*, with a shear rate  $K = 0.2$ , gradient  $G = 0.1$  1/s and center-line velocity  $U_c = 0.5$ . The flow problems are analyzed numerical with OpenFOAM, for two-dimensional (2D) domains with Reynolds number ( $R_e$ ) 100, 300 and 500, and three-dimensional (3D) domains with Reynolds number ( $R_e$ ) 100 and 500.

The numerical analysis is performed with a laminar solver, where mean values for drag - and lift coefficients are found with root mean square values. The oscillation periods  $T_v$  [s], frequencies  $f_v$  [1/s] and Strouhals numbers ( $S_t$ ) are found behind each cylinder, with use of Power Spectral Density (PSD) curves. ParaView is used to visualize the distribution of velocity U, pressure P and vorticity in z-direction  $\omega_z$ .

Results obtained for flow problem with Reynolds number 100 are approximately identical for both 2D and 3D domains, since there are no 3D effects occurring for this Reynolds number. When increasing the Reynolds number  $R_e$ , one must take in account the 3D effects occurring span-wise. The thesis discusses the effects of a shear flow versus a uniform flow, and the effect of having tandem configurations versus a single cylinder.

Tandem cylinders will experience drag forces on each cylinder, with oscillating lift forces close to zero. A uniform - or shear flow will move around the tandem cylinders, with some vorticity and approximately no velocities in-between the cylinders. Turbulent behaviour is observed downstream, when a shear flow is subjected on the tandem configuration. When subjecting a flow towards a single cylinder, the alternating vortex sheddings will occur for an earlier time instant, compared to tandem flow problems. Pressure distribution around tandem cylinders follows the same pressure curve, when subjected either to a shear - or a uniform flow. The pressure magnitude and fluctuation values are larger around the cylinders, when subjected to shear flow.

Designing Submerged Floating Tube Bridges (SFTB), one must understand the flow behaviour in-between the tandem configuration and flow phenomena downstream when subjected to a shear flow versus a uniform flow.



# Sammendrag

*Ferjefri E39* introduserer rørbrokonseptet som skal erstatte ferjeovergangene langs Vestlandet. Rørbroen er forenklet som tandem sylindere med lengde-diameter ratio  $L/D = 3,2$ , diameter  $D = 1,0$  og sylindrelengde på  $l = 6D$ . Sylinderne blir påført en linear varierende skjærstrøm, med skjærrate  $K = 0.2$ , gradient  $G = 0.1$  1/s og normalhastighet på  $U_c = 0.5$ .

Dette strømningsproblemet er analysert numerisk ved bruk av OpenFOAM. Analysen blir utført på todimensjonale (2D) domener ved Reynolds tall 100, 300 og 500, mens ved tredimensjonale (3D) domene utføres analysen ved Reynoldstall 100 og 500. Det blir brukt en laminær kode for å løse problemet, hvor middelverdier for drag- og løftekoeffisienter med oscillerende amplitude via minste kvadraters metode er funnet. Oscillasjonsperioder  $T_v$  [s], frekvenser  $f_v$  [1 / s] og Strouhals-tall ( $S_t$ ) er funnet bak hver sylinder, ved bruk av spektralanalyse. ParaView brukes til å visualisere fordeling av hastighet U, trykk P og virvling i z-retning  $\omega_z$ .

Resultatene ved Reynolds nummer 100 er omtrent identiske for både 2D og 3D-domener, siden det ikke forekommer 3D-effekter ved Reynoldstall 100. Økes Reynoldstallet  $R_e$ , må man ta hensyn til 3D-effektene som forekommer langs sylinderaksen. Masteravhandlingen diskuterer effektene av en skjærstrøm og uniform strømning, og effekten av å ha tandemkonfigurasjon og en enkel sylinder.

Tandem sylindere vil oppleve dragkrefter på hver av sylinderne, med oscillerende løftekrefter lik null. En uniform- eller skjærstrøm vil bevege seg rundt sylinderne, slik at man får noe virvling og omtrent ingen hastigheter imellom sylinderne. Virvelavløsningen ved skjærstrøm på tandemkonfigurasjon vil oppføre seg turbulent ettersom 3D effektene påvirker strømningen. Virvelavløsningsfenomenet vil oppstå for et tidligere tidssteg for en enkel sylinder, sammenliknet med tandem sylindere.

Trykkfordelingen rundt tandem sylindere vil følge lik trykkurve, ved påført skjær- og uniformstrømning. Ved skjærstrømning, vil trykkfordelingen vil være større for den første sylinderen, mens den andre sylinderen vil oppleve større trykkendringer.

Når man skal utforme og prosjektere rørbroene, må man ta hensyn til strømningsprofilen, f.eks en skjærstrøm kontra en uniform strømning. I tillegg må man forstå konsekvensene av å ta i bruk tandem sylindere i stedet for en enkel sylinder.





# Preface

The thesis is a results of my final semester at the five year integrated master program in Marine Technology at Norwegian University of Science and Technology (NTNU). The thesis is inspired by the fjord crossing concept of Submerged Floating Tube Bridges (SFTB), proposed by the Norwegian Public Road Administration (NPRA) in their project of Coastal Highway E39.

The thesis simplifies the SFTB as 3D tandem cylinders, and investigates the effect of shear flow around the cylinders. The investigation is performed numerically with use of OpenFOAM as a Computational Fluid Dynamic' tool in laminar regime. Taking use of OpenFOAM has given me valuable experience in the use of Computational Fluid Dynamics. The use of post-processing tools MATLAB and ParaView became important when evaluating, visualizing and discussing the obtained results. Using NTNU's computer Vilje gave insight in the performance and limitations within numerical simulations, and understanding of computer power versus computational time.

My supervisor Bjørnar Pettersen, Professor at the Department for Marine Technology, has inspired and motivated me to understand the importance of hydrodynamics in the scope of my thesis. Professor Bjørnar Pettersen is a supervisor that is available for questions, help and discussions throughout my final year.

Bjørnar Pettersen has also arranged a cooperation with Tale Egeberg Aasland, PhD-student and employee at Norwegian Public Road Administration (NPRA). Tale E. Aasland has been a huge resource when discussing the potential of the Submerged Floating Tube Bridge (SFTB), and she has engaged me to understand how hydrodynamics can be applied in infrastructural problems. I would also like to thank PhD-student Håkon Strandenes, which has been available for help regarding use of OpenFOAM and ParaView.

Writing my own thesis has given me the possibility to experience how marine technology and hydrodynamics can be applied in various of problems in different industries.

Trondheim, Norway  
June 8th, 2018  
Dhanushi Nayanatara Attanapola



# Nomenclature

$\alpha$	Angle between the cylinders with a staggered configuration
$\delta$	Boundary Layer Thickness
$\delta(x)$	Boundary layer
$\Delta t$	Time step
$\Delta x$	Cell size in x-direction
$\Delta y$	Cell size in y-direction
$\Delta z$	Cell size in z-direction
$\theta$	The angle around the circular cross-section presented in Chapter 6
$\lambda$	Blockage ratio, ratio between cylinder diameter and tunnel diameter in experimental set-up
$\mu$	Dynamic viscosity
$\nu$	Kinematic viscosity
$\rho$	Fluid density
$\tau_w$	Shear wall stress
$\phi$	Angle around the circular cross-section [Igarashi, 1981]
$\omega_z$	Vorticity in z-direction
$R_e$	Reynolds number
$T_v$	Vortex shedding period or oscillation period
$f_v$	Vortex shedding frequency or oscillation frequency
$S_t$	Strouhals number
$L_c$	Characteristic length, defined in Reynolds number & Strouhals number
$P$	Pressure
$U$	Incoming freestream velocity

$U_0$	Stream-wise velocity component
$U(y)$	Planar shear flow
$U(z)$	Axial shear flow
$U_x$	Velocity in x-direction
$U_y$	Velocity in y-direction
$U_z$	Velocity in z-direction
$U_{mag}$	Velocity magnitude
$U_{y=-5.0}$	Inlet velocity at bottom boundary of computational domain
$U_{y=5.0}$	Inlet velocity at top boundary of computational domain
$F_x$	Drag force
$F_y$	Lift force
$C_D$	Drag force coefficient
$C_L$	Lift force coefficient
$\bar{C}_D$	Mean drag force coefficient
$\bar{C}_L$	Mean lift force coefficient
$\bar{C}_{dp}$	Drag force with pressure contribution
$\bar{C}_{df}$	Drag force with frictional contribution
$C_p$	Pressure coefficient
$A_{ref}$	Projected area of cylinder, defined as cylinder length $l$ times diameter $D$
$D$	Diameter
$L$	Longitudinal length, the length between cylinders in tandem configuration
$l$	Span-wise length of cylinder in z-direction
$T$	Transverse length, the length between cylinders in side-by-side configuration
$P$	Length between two cylinders in staggered configuration
$L/D$	Longitudinal length - diameter ratio between tandem cylinders
$l/D$	Ratio between span-wise length and diameter of a cylinder
$T/D$	Transverse length - diameter ratio between side-by-side cylinders
$K$	Shear rate
$G$	Shear flow gradient
$U_c$	Center-line velocity, velocity normal on cylinder
$t$	Time or time instant

*2D* Two-dimensions or two-dimensional  
*3D* Three-dimensions or three-dimensional  
*NTNU* Norwegian University of Science and Technology  
*NPRA* Norwegian Public Road Administration  
*SFTB* Submerged Floating Tube Bridge  
*CFD* Computational Fluid Dynamics  
*RMS* Root mean square  
*PDE* Partial Differential Equations  
*FVM* Finite Volume Method  
*OpenFOAM* Open Field Operation And Manipulation  
*PISO* Pressure Implicit with Splitting of Operators  
*MEGA* Mesh generating program  
*CFL* Courant-Friedrichs-Levy condition  
*PSD* Power Spectral Density  
*m* meter, SI unit for length  
*s* seconds, SI unit for time  
*1/s* frequency [Hz], SI unit for number of periods pr. time  
*m/s* meters pr. second, SI unit for velocity



# Contents

<b>Assignment</b>	<b>I</b>
<b>Abstract</b>	<b>III</b>
<b>Sammendrag</b>	<b>V</b>
<b>Preface</b>	<b>VII</b>
<b>Nomenclature</b>	<b>IX</b>
<b>1 Introduction</b>	<b>1</b>
<b>2 Background Motivation</b>	<b>3</b>
2.1 Coastal Highway: Ferry Free E39 . . . . .	3
2.1.1 Submerged floating tunnel bridge (SFTB) . . . . .	5
2.1.2 pontoons and Tethers as Vertical Stiffness . . . . .	6
2.2 Simplification of Submerged Floating Tube Bridge Concept . . . . .	7
<b>3 Background Theory</b>	<b>9</b>
3.1 Properties of Fluid Dynamics . . . . .	9
3.1.1 Assumptions and Limitations of the Fluid . . . . .	9
3.1.2 Fluid Properties and Flow Regimes . . . . .	10
3.2 Classification of Fundamental Equations . . . . .	11
3.2.1 Conservation of Mass . . . . .	11
3.2.2 Conservation of Momentum . . . . .	11
3.3 Flow Phenomena . . . . .	12
3.3.1 Stagnation Point . . . . .	12
3.3.2 Flow Separation . . . . .	13
3.3.3 Vortex Shedding . . . . .	16
3.3.4 Relationship between Strouhals number $S_t$ and Reynolds number $R_e$ . . . . .	18
3.3.5 Vorticity . . . . .	22
3.3.6 Boundary Layer . . . . .	22
3.4 Drag - and Lift Forces . . . . .	23

3.4.1	Force Coefficients . . . . .	23
3.4.2	Root Mean Square of fluctuations . . . . .	23
3.4.3	Relationship between mean drag $\bar{C}_D$ and Reynolds number $Re$ . . . . .	24
3.5	Uniform Flow around a Circular Cylinder . . . . .	25
3.6	Shear Flow around a Circular Cylinder . . . . .	27
3.7	Configuration of Circular Cylinders . . . . .	30
3.7.1	Tandem Cylinders . . . . .	31
<b>4</b>	<b>Numerical Methods in Fluid Dynamics and Computational Domain</b>	<b>40</b>
4.1	Computational Fluid Dynamics (CFD) . . . . .	40
4.2	OpenFOAM . . . . .	41
4.2.1	Finite Volume Method (FVM) . . . . .	42
4.2.2	PISO Algorithm as Solver . . . . .	42
4.2.3	Time Step Analysis . . . . .	43
4.3	Set-up of Computational Domain & Fluid Flow Problem . . . . .	44
4.3.1	Computational Domain Size . . . . .	44
4.3.2	Mesh and Grid refinement . . . . .	46
4.3.3	Boundary Conditions . . . . .	49
4.3.4	Grid Verification . . . . .	50
<b>5</b>	<b>Results</b>	<b>54</b>
5.1	Shear Flow and Tandem Cylinder Characteristics . . . . .	54
5.2	Results obtained for 2D Shear Flow Around Tandem Cylinders . . . . .	56
5.3	Results obtained for 3D Shear Flow Around Tandem Cylinders . . . . .	56
<b>6</b>	<b>Discussion</b>	<b>57</b>
6.1	Comparison between the 2D and 3D simulation of Shear Flow Around Tandem Cylinders . . . . .	58
6.2	Comparison of the Shear Flow Around Tandem Cylinders with Other Flow Problems . . . . .	59
6.2.1	Comparison of Velocity Magnitude $U_{mag}$ and Velocity in x-direction $U_x$ . . . . .	62
6.2.2	Comparison of Pressure Distribution P . . . . .	69
6.2.3	Comparison of Vorticity in z-direction $\omega_z$ . . . . .	74
<b>7</b>	<b>Conclusion</b>	<b>79</b>
7.1	Future Work . . . . .	82
	<b>References</b>	<b>83</b>
	<b>Appendix</b>	<b>88</b>
.1	2D Shear Flow Around Tandem Cylinders at $Re = 100$ and $K = 0.2$ . . . . .	88



.2	2D Shear Flow Around Tandem Cylinders at $R_e = 300$ and $K = 0.2$ . . . . .	93
.3	2D Shear Flow Around Tandem Cylinders at $R_e = 500$ and $K = 0.2$ . . . . .	97
.4	3D Shear Flow Around Tandem Cylinders at $R_e = 100$ and $K = 0.2$ . . . . .	101
.5	3D Shear Flow Around Tandem Cylinders at $R_e = 500$ and $K = 0.2$ . . . . .	110
.6	Uniform Flow around a 3D Circular Cylinder . . . . .	123
.7	Uniform Flow around a 3D Circular cylinder with Boundary conditions for Slip and Symmetry . . . . .	136
.8	Shear Flow around a 2D Circular Cylinder . . . . .	140
.9	Shear Flow with Shear Rate $K = 0.2$ around a 2D & 3D Circular Cylinders . . . . .	151
.10	Uniform Flow around 2D Tandem Cylinder . . . . .	180
.11	Uniform Flow around a 3D Tandem Cylinder . . . . .	196
.12	MATLAB SCRIPTS: . . . . .	218
.13	BASH SCRIPTS: . . . . .	226
.14	OpenFOAM SCRIPTS . . . . .	227
.14.1	OpenFOAM: boundary . . . . .	227
.14.2	OpenFOAM: velocity U . . . . .	229
.14.3	OpenFOAM: pressure P . . . . .	231
.14.4	OpenFOAM: vorticity . . . . .	233
.14.5	OpenFOAM: controlDict . . . . .	234
.14.6	OpenFOAM: decomposeParDict . . . . .	237



# Chapter 1

## Introduction

Marine engineering and offshore technology have found it's potential in the infrastructural project of Coastal Highway E39, or better known as Ferry Free E39. The goal of this project is to replace every ferry connections along Kristiansand to Trondheim, with fixed links. The proposed fixed links are existing and new bridge structures, which are to be built in fjord conditions with vast distances and environmental conditions. The final thesis *TMR 4930 Master Thesis in Marine Technology*, studies the concept of the *Submerged Floating Tube Bride (SFTB)*, where the thesis approaches the problem numerically with Computational Fluid Dynamics' (CFD) tool, OpenFOAM.

The Master Thesis has title *Numerical Simulation of Viscous Shear Flow Around Tandem Cylinders*. The concept of *Submerged Floating tube Bridge (SFTB)* is simplified as tandem cylinders with a chosen longitudinal length ( $L$ ) between the cylinders, a diameter and a span-wise length. The inlet velocity is a linearly varying current profile, which is subjected on the tandem cylinders. This current profile is called Shear Flow.

Introduction to the Coastal Highway E39 and the proposed concept *Submerged Floating Tube Bridge (SFTB)* is described in Chapter 2. Chapter 3 explains the fluid properties, assumptions and hydrodynamic phenomena. The chapter also contains literature review about uniform - and shear flow around single and tandem cylinders.

Chapter 4: *Numerical Methods in Fluid Dynamics and Computational Domain* describes the numerical methods used to solve the fluid flow problems, description of the computational domain used for the numerical simulation and the implemented boundary conditions. Chapter 5 presents the results obtained for both two-dimensional (2D) and three-dimensional (3D) shear flow problem around tandem cylinders with shear rate  $K = 0.2$  for various Reynolds number. The solutions are obtained with laminar solvers.

Chapter 6 discusses the main difference between the results obtain for the 2D and 3D shear flow problems. The chapter also analyzes the main differences and effects of a shear flow versus a uniform flow subjected on a single cylinder versus tandem cylinders.

Chapter 7 presents the final conclusion and present the crucial factors of having a shear flow subjected on tandem cylinders. The chapter also presents the possibility of future work in terms of extending the numerical simulation by taking use of turbulence models, larger computational domain and longer time simulation.

There are several flow problems analyzed for different Reynolds number with both shear flow and uniform flow around single and tandem cylinders. These results are presented in Appendix.

## Chapter 2

# Background Motivation

### 2.1 Coastal Highway: Ferry Free E39

The Coastal Highway Route E39 is a national infrastructural project, where the goal is to replace ferry connections with fixed links across the fjords of coastal areas in Western Norway.

Western Norway is known for its scenic terrain of vast fjords, mountains and hills, therefore the use of ferries are required. The ferry itself represent the transportation culture in several areas in Western Norway. Unfortunately, the travelling time is time-costly, as the ferries are restricted to a schedule and capacity.

The project of a fixed Coastal Highway E39 is planned and executed by the Norwegian Public Road Administration (NPRA). The challenge lies in creating a *Ferry Free E39* of 1100 km from Kristiansand to Trondheim.

The coastal highway will reduce travel time from 21 hours to 11 hours by replacing 6 ferry connections with fixed roads, through tunnels and bridges presented in figure 2.1 [Reinertsen et al., 2016].



Figure 2.1: Planned route for the Coastal Highway E39 [Dunham, 2016].

Challenges regarding planning and executing the project, is to implement new concepts and new technology. One must understand the environmental loads from wind, waves and current, but also solving challenges that comes with extreme fjord crossing as distance and depth. The challenges regarding risks, safety and how the road will impact society must be evaluated and taken into account [Larsen and Jakobsen, 2010] & [Tveit, 2010].

This project is executed with the goal of creating both local and regional interaction from south of Norway towards mid region, through the western coast. The Coastal Highway Route E39 will connect industries that are found along the route, predicting an increase in both labour, living and service within the industries of oil, gas, fisheries and shipping [Dimmen et al., 2016], [NPRA and NVF, 2017] & [Dunham, 2016].

## 2.1.1 Submerged floating tunnel bridge (SFTB)

The Norwegian Public Road Administration (NPRA) have proposed the following concepts for the extreme fjord crossings of Coastal Highway E39:

- Suspension bridge
- Floating bridge
- Tension Leg Platforms (TLP) with suspension bridge
- Gravity Based Structures (GBS)
- Submerged floating tunnel/tube bridge (SFTB)

The bridge concept evaluated in the present study is the Submerged Floating Tube Bridges (SFTB). The concept takes the land based concrete tunnels, and submerges the tunnels under water, thereby the name *Submerged Floating Tube Bridge* with either two - or three lane crossings for each direction, presented in figure 2.2 and 2.3.

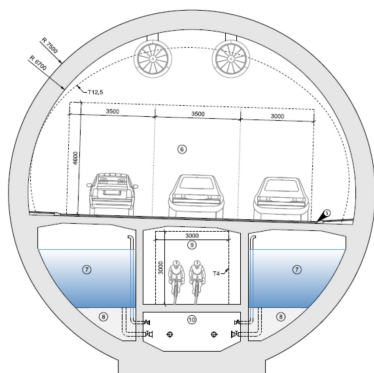


Figure 2.2: Cross-section of floating tube bridge with three driving lanes, with outer-diameter  $OD = 15.0$  m [Minoretta et al., 2016].

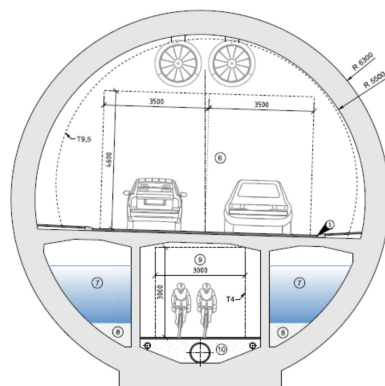


Figure 2.3: Cross-section of floating tube bridge with two driving lanes, with outer-diameter  $OD = 12.6$  m [Minoretta et al., 2016].

The advantages regarding the Submerged Floating Tube Bridge (SFTB) are low environmental impact, such as visibility, noise and almost no wind loading on the structure. Challenges regarding Submerged Floating Tube Bridges (SFTB) are the hydrodynamic loads as waves and current in a fjord [Myhr et al., 2016].

The Coastal Highway E39 project faces challenges when combining existing structural bridge technology with offshore technology in a fjord crossing environment. The proposed bridge structure is a new system, which will experience different global response and behavior. The structure itself will impact the environment and society in Western Norway.

The fjord bottom introduces challenges regarding ground conditions as unstable sediment areas. The existing ship traffic will experience larger risk in collision and interaction between a vessel and a proposed bridge structure [Johansen, 2016].

### 2.1.2 Pontoons and Tethers as Vertical Stiffness

The Submerged Floating Tube Bridges (SFTB) are designed to float under the free surface. Vertical stiffness' elements as pontoons or mooring systems are used to prevent the Submerged Floating Tube Bridge (SFTB) from drifting. The principles of Submerged Floating Tube Bridge (SFTB) is to immerse concrete tubes, which are to be connected to pontoons floating at surface, illustrated in figure 2.4. Tethers are used as mooring systems between the bridge structure and the fjord bottom, illustrated in figure 2.5. The two concrete tunnels are connected in-between for every 200 meter, which is designed as emergency exits [Reinertsen et al., 2016].

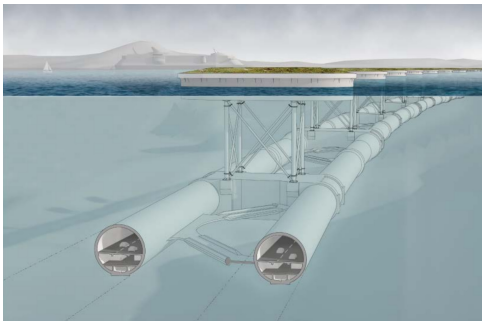


Figure 2.4: Submerged Floating Tube Bridge (SFTB) with pontoons [Minoretta et al., 2016].

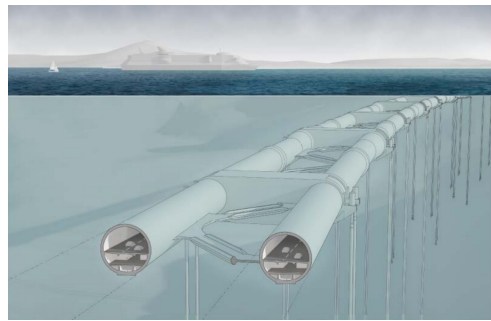


Figure 2.5: Submerged Floating Tube Bridge (SFTB) with tethers [Minoretta et al., 2016].

The advantages by using pontoons as vertical stiffness are the low visual impact in the environment. Challenges with pontoons are the risk of collision between ship traffic and the floating pontoons. The pontoons are also subjected to larger wave loads, compared to tethers.

The tethers have no visual impact, but the disadvantages are the risk of collision between the tethers and submarines. Tethers are connected to sea bed, where in a fjord have more varying underwater terrain than ocean floor. A fjord will also contain current velocities, which will effect the layout and strength of the tethers [Johansen, 2016], [Minoretta et al., 2016] & [Reiso et al., 2015].



## 2.2 Simplification of Submerged Floating Tube Bridge Concept

Analyzing hydrodynamic loads from currents on a proposed fjord crossing concept, there is a need for assumptions and simplifications. In this study the Submerged Floating Tube Bridge (SFTB) are simplified in terms of geometry as two parallel or tandem circular cylinders.

The dimensions are chosen to obtain desired longitudinal length-diameter ratio of  $L/D = 3.2$ . The outer diameter for the simplified geometry is  $OD = 12.6m$ , as shown in figure 2.3 for the proposed 'two driving lane' tunnels. The horizontal or longitudinal length between the tandem cylinders are:  $L = 40m$ . The  $L/D$ -ratios becomes important when analyzing tandem cylinders in current flow. Flow phenomena and wake interference will vary for different  $L/D$ -ratios and different Reynolds number.

The underwater view of the Submerged Floating Tube Bridge (SFTB) is shown in figure 2.6, while an inside layout is presented in figure 2.7.



Figure 2.6: General underwater view of the Submerged Floating Tube Bridge with pontoons [NPRA and NVF, 2017].



Figure 2.7: Inside view of the Submerged Floating Tube Bridge [NPRA and NVF, 2017].

Table 2.1: Current velocities in Bjørnafjord for various depth and return period [Reinertsen et al., 2016].

Depth	10 year	100 year	10000*
Surface	1.13 [m/s]	1.33 [m/s]	1.69 [m/s]
30 [m]	0.46 [m/s]	0.54 [m/s]	0.69 [m/s]

The hydrodynamic loads are simplified to a shear current profile. The wave and wind loads are neglected in this study, and the current velocity profile is analyzed as a linear varying shear current along the circular cross-section. Assumption and limitations for the current flow are presented in section 3 which describes the properties of the fluid, assumptions and limitations of the model, and shear flow properties and behaviour.

Project report *Bjørnafjord Submerged Floating Tube Bridge* [Reinertsen et al., 2016] gives the extreme current velocity for a given return period at Bjørnafjord. The current velocities are presented in table 2.1 and are the extreme current velocities given for return period of 10, 100 and 10000\* years, where the 10000\*year value is extrapolated from the 10 year and 100 year values.

Many studies have been performed on tandem cylinders with uniform current flow, while studies with shear current flow are mostly performed on single circular cylinders. A study of tandem cylinders in shear current flow will be performed in this thesis, simplifying the Submerged Floating Tube Bridge (SFTB) as tandem cylinders subjected by a linearly varying current flow.

The extreme current value  $U_c$  will be the magnitude which hits the cylinder surface as the centre-line. The Submerged Tube Bride is to be placed 30 m under free surface and the computation domain will initially be chosen as infinite fluid.

The analysis is performed to understand how shear flow will effect tandem cylinders, especially in-between the tandem cylinders and downstream flow behaviour. The analysis is motivated by the concept of Submerged Floating Tube Bridges (SFTB) as a fjord-crossing, and the effect of the local current loads on the bridge-formation.

# Chapter 3

## Background Theory

Theory regarding fluid properties and fluid flows are described in this chapter. Description of a uniform flow versus a shear flow and different cylinder configurations are presented.

### 3.1 Properties of Fluid Dynamics

#### 3.1.1 Assumptions and Limitations of the Fluid

A fluid flow is described as a moving fluid. Analyzing fluid problems, assumptions and limitations are used to simplify the flow problem. The assumptions and limitations are:

- Single-component fluid
- Newtonian fluid: fluid can obtain friction and shear stresses, when the fluid acts against a solid surface or on another fluid. The shear stress leads to deformation, and the deformation rate is linearly proportional to the shear stress.
- Incompressible: assuming constant fluid density  $\rho$  (mass per unit volume).
- Constant viscosity  $\nu$

### 3.1.2 Fluid Properties and Flow Regimes

A moving fluid or a fluid flow can either be described as: laminar, transient or turbulent. The laminar flow regime is described as a stable and well-ordered state of fluid flow. The fluid particles appear to move along each other, in contrast to a turbulent flow where there is no form of stability in the movement of fluid particles.

Turbulence flow regime is characterized as unstable, unsteady with vorticities, large mixing rate and shear stress. Transient flow regime is defined as the flow regime between laminar and turbulent regimes.

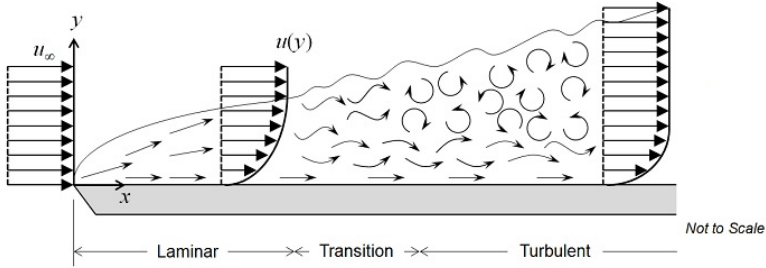


Figure 3.1: Laminar, transient and turbulent flow [Bejan and Kraus, 2003].

Figure 3.1 illustrates how the flow acts in laminar, transient and turbulent regimes for a flat-plate problem. The difference between a laminar and a turbulent flow regimes is characterized by the Reynolds numbers, which includes the fluid flow velocity, density and dynamic viscosity. In theory, low Reynolds numbers describe laminar flow regime, and high Reynolds numbers describe turbulent flow regime.

The definition of the Reynolds number is given by equation (3.1), where  $U$  is the fluid velocity and  $L_c$  is the characteristic length in the fluid domain. In this study, the characteristic length will be considered as the diameter  $D$ . The kinematic viscosity  $\nu$  is defined with both the dynamic viscosity  $\mu$  and density of a fluid  $\rho$ .

$$Re = \frac{\rho U L_c}{\mu} = \frac{UD}{\nu} \qquad \nu = \frac{\mu}{\rho} \left[ \frac{m^2}{s} \right] \qquad (3.1)$$

Figure 3.7 presents the flow-body interacting between an incoming flow and a circular cylinder. A laminar flow is observed for Reynolds number  $40 < Re < 200$ , and turbulent flow is observed in the wake region behind the circular cylinder for  $300 < Re < 10^5$ . Above  $Re > 10^5$  the boundary layer on the cylinder is also turbulent.

## 3.2 Classification of Fundamental Equations

The fundamental equations describing fluid dynamic problems are the conservation of mass, better known as the (1) continuity equations and (2) the momentum equation, which is further derived as the Navier-Stokes equation.

### 3.2.1 Conservation of Mass

A fundamental principle in nature is conservation of mass. In fluid flow problems, conservation of mass describes how the mass flows enters and leaves a control volume. The conservation law requires a net mass flow in and out of a control volume, for a given time interval.

The conservation of mass can be expressed by the continuity equation. This expression can be modified to fit a fluid flow with different properties. The equation (3.2) describes the mass conservation for a three-dimensional steady and in-compressible flow problem of a Newtonian fluid.

$$\left[ \frac{\partial u}{\partial x} + \frac{\partial v}{\partial y} + \frac{\partial w}{\partial z} \right] = 0 \quad (3.2)$$

### 3.2.2 Conservation of Momentum

The second fundamental conservation law is conservation of momentum, and is derived from Newton's 2nd law. The general equation for conservation of momentum is given by equation (3.3), where  $i = 1, 2, 3$  and  $j = 1, 2, 3$  for each direction of  $x, y, z$ .

$$\frac{\partial u_i}{\partial t} + u_j \left[ \frac{\partial u_i}{\partial x_j} \right] = -\frac{1}{\rho} \frac{\partial p}{\partial x_i} + \nu \left[ \frac{\partial^2 u_i}{\partial x_j \partial x_j} \right] \quad (3.3)$$

The conservation of the fluid momentum equation consists of components, where they describe the flow properties. The left-hand side consists of the time-dependent component, which describes the change in velocity. The second component on the left-hand side describes the fluid velocity in each direction.

At the right-hand side of the momentum equation, the pressure gradient and the kinematic viscosity term with the second derivative are presented. The momentum equation can be written with the general formula (3.4). Further, the general momentum equation (3.4) is expressed as the well-known Navier-Stokes equation (3.5):

$$\rho \frac{DU}{Dt} = -\nabla P + \mu \nabla^2 U + \rho f \quad (3.4)$$

$$\frac{DU_i}{Dt} = -\frac{1}{\rho} \frac{\partial P}{\partial x_i} + \nu \left[ \frac{\partial^2 U_i}{\partial x_j \partial x_j} \right] + f_i \quad (3.5)$$

### 3.3 Flow Phenomena

A fluid flow will experience different flow phenomena. The fluid flow is described with fluid velocity, viscosity, Reynolds number, and be characterized as laminar, transient or turbulent based on the flow behaviour and Reynolds number. Observing a fluid flow interacting with a fixed body, different flow phenomena will occur, as stagnation point, flow separation, vortex shedding and boundary layer.

Figure 3.2 illustrates how an incoming flow hits a fixed body, as a two-dimensional circular cross-section. The figure shows a boundary layer close to the fixed body, a stagnation point in-front of the body and the wake region behind the separation point.

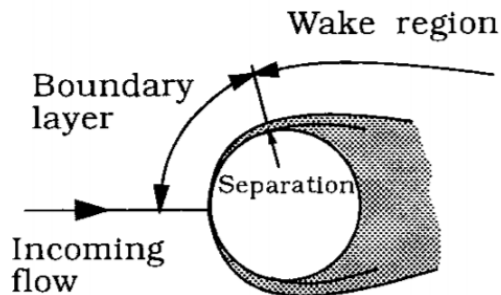


Figure 3.2: Definitions of flow phenomena [Sumer, 1997].

#### 3.3.1 Stagnation Point

A stagnation point is defined as the point where the flow obtains zero velocity, as the incoming flow hits normal on a fixed body. Stagnation points have also high pressure zones located in-front of the stagnation point, as the velocity becomes zero, the pressure increases at stagnation point [Cengel and Cimbala, 2014].

### 3.3.2 Flow Separation

Flow separation is a phenomenon which occurs between a fluid flow and a fixed body. When a fluid is forced to flow over a curved body, the flow will no longer be attached to the fixed surface and will separate. The flow separation comes from the no-slip condition between the fluid flow and the fixed surface, where the fluid is assumed to have direct contact with the solid surface [Cengel and Cimbala, 2014].

For the two-dimensional flow problem, the momentum equation will be simplified at the wall  $y = 0$  to expression (3.6), with only the pressure gradient and the viscous term left.

$$\nu \frac{\partial^2 u}{\partial y^2} \Big|_{y=0} = -U \frac{dU}{dx} = \frac{1}{\rho} \frac{dP}{dx} \quad (3.6)$$

Figure 3.3 presents the different stages from (a) to (e) of interaction between fluid flow and solid surface. The stages illustrated how the flow and solid surface are dependant on a balance between the pressure gradient and the viscous term from expression 3.6. Illustrated in figure 3.3 presents the velocity profile  $U(x)$  and the boundary layer  $\delta(x)$  in the axis-system of  $x$  and  $y$ .

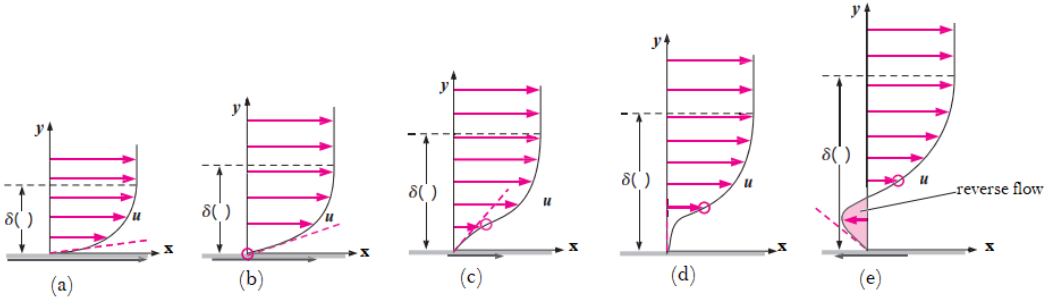


Figure 3.3: Illustration of flow separation [Cengel and Cimbala, 2014]

- (a): Fluid flow interaction where  $\frac{dU}{dx} > 0$ , such that  $\frac{\partial^2 u}{\partial y^2} < 0$  &  $\frac{1}{\rho} \frac{dP}{dx} < 0$ .
- (b): Linear growth of  $u(y)$ , such that  $\frac{\partial^2 u}{\partial y^2} = 0$  &  $\frac{1}{\rho} \frac{dP}{dx} = 0$ .
- (c): Obtaining mild adverse boundary layer profile:  $\frac{dU}{dx} < 0$ , such that  $\frac{\partial^2 u}{\partial y^2} > 0$  &  $\frac{1}{\rho} \frac{dP}{dx} > 0$ . Shear wall stress is still present at this point.
- (d): Critical adverse boundary layer, such that separation occurs as wall stress  $\tau_w = \mu \frac{\partial u}{\partial y} \Big|_{y=0} = 0$  or  $\frac{\partial u}{\partial y} \Big|_{y=0} = 0$ . The pressure gradient is  $\frac{1}{\rho} \frac{dP}{dx} > 0$  and the second derivative of the velocity  $\frac{\partial^2 u}{\partial y^2} > 0$ .
- (e): Obtaining reverse flow. Shear wall stress will be negative, as  $\mu \frac{\partial u}{\partial y} \Big|_{y=0} < 0$ .

Separation as a flow phenomenon between a current and a circular cylinder have been analyzed with both numerical tools and by experiments. Figure 3.4 presents how the separation angles on a circular cylinder will vary with Reynolds number.

The figure presents separation angles for different experimental measurements and numerical computations. For the experimental measurements, the experiments are performed in a tunnel with a given diameter. Therefore the figure presents the results with a given blockage ratio  $\lambda$ , which is the ratio between the cylinder diameter  $D$  and the tunnel diameter in the experiment.

The differences in blockage ratio  $\lambda$ , and how the experiments and numerical computations are performed will give errors in the results presented in figure 3.4.

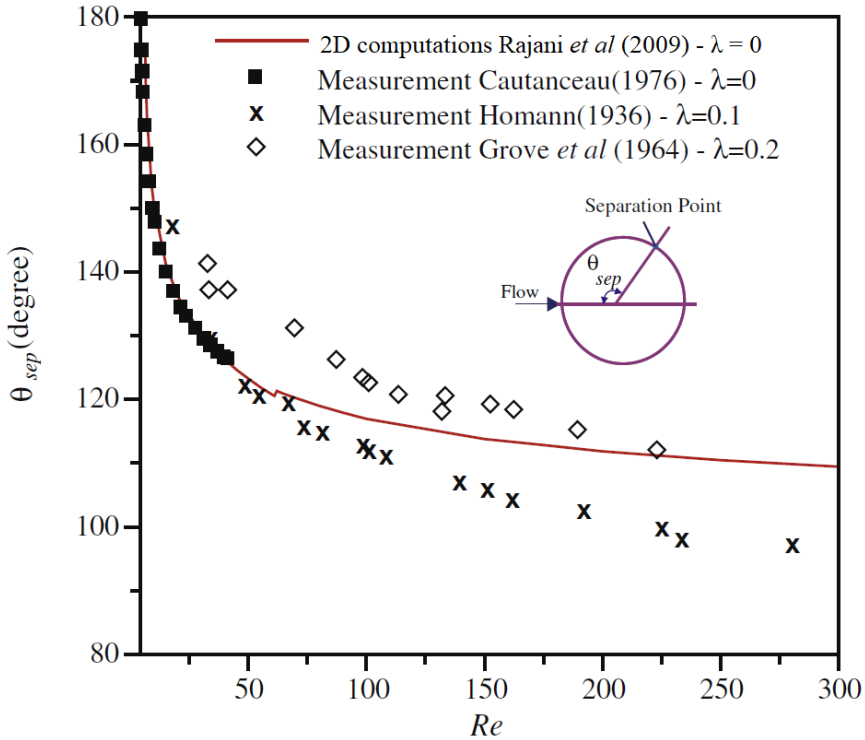


Figure 3.4: Separation angle with respect to Reynolds number for 2D computation for Rajanu *er al.* (2009), measurements from Cautanceau (1976), Hormann (1936) and Grove *et al.* (1964) [Rajani *et al.*, 2009].



A comparison between experimental and numerical studies of separation angle for flow around circular cylinder are performed. In experiments, the results obtained are averaged values of measurements. Averaged separation angles are obtained directly from finite-time-exposed photographs or time-averaged images for the separation, where as the actual separation occurs when the wall-shear stress becomes zero.

A numerical analysis is performed by Wu et al. (2004) where a comparison is performed. The experimental results are gathered from literature about time-averaged separation angle with results obtained by Wu et al. (2004). These results are presented in figure 3.5 [Wu et al., 2004].

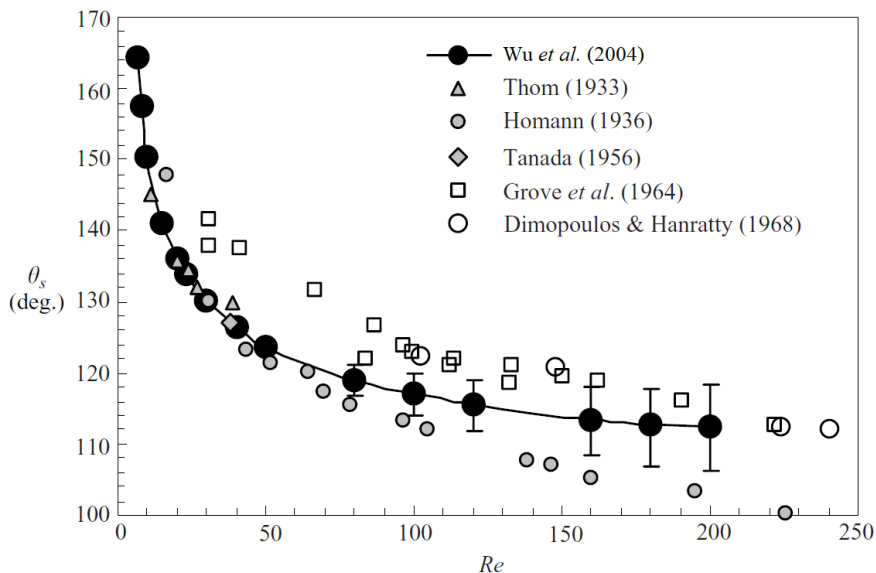


Figure 3.5: Separation angle with respect to Reynolds number for numerical results from Wu et al. (2004), measurements from Thom (1933), Hormann (1936), Tanda (1956), Grove et al. (1964) and Dimopoulos & Hanratty (1968) [Wu et al., 2004].

### 3.3.3 Vortex Shedding

Vortex shedding is a phenomena that occurs when the Reynolds number reaches value of 48 or higher, and is a common feature for all flow regimes. At  $5 < Re < 40$ , a pair of vortices or twin vortices are formed in the near wake of the cylinder and stays there for a steady flow. When the Reynolds number increase, the vortices begin to shed alternately from each side of the cylinder, as the wake becomes more and more unstable with a varying pressure field [Braza et al., 1986], [Rajani et al., 2009] & [Pettersen, 2007].

The vortex shedding will at a time instant 0 have a vortex that is being cut off by a second vortex, shown in figure 3.7. The first vortex will then be free to travel downstream, where a clockwise circulation (A) around the cylinder is created. A third vortex will form where the first vortex took place, and it will cut off the second one at a time instant 1. The second vortex will then travel downstream and cause an anti-clockwise circulation (B). This process will continue in an alternating manner. An illustration of clockwise (A) and anti-clockwise (B) circulation is shown in figure 3.6, and it is often referred to *Von Kármán* vortices [Sumer, 1997].

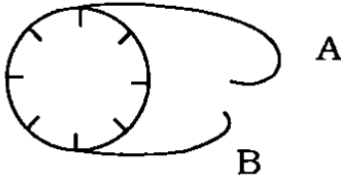


Figure 3.6: Vortex shedding: clock wise (A) and anti-clock wise (B), [Sumer, 1997]

Vortex shedding can be measured as vortex shedding frequency  $f_v$ , which is expressed dimensionless by the Strouhals number, given in equation (3.7).  $L_c$  is the characteristic length, diameter  $D$ , and  $U$  is the incoming current velocity.

$$S_t = \frac{L_c f_v}{U} = \frac{D f_v}{U} \quad (3.7)$$

Figure 3.7 illustrated the wake pattern behind a circular cross-section for different Reynolds numbers.


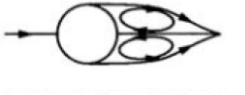







	No separation. Creeping flow	$Re < 5$
	A fixed pair of symmetric vortices	$5 < Re < 40$
	Laminar vortex street	$40 < Re < 200$
	Transition to turbulence in the wake	$200 < Re < 300$
	Wake completely turbulent. A: Laminar boundary layer separation	$300 < Re < 3 \times 10^5$  Subcritical
	A: Laminar boundary layer separation B: Turbulent boundary layer separation; but boundary layer laminar	$3 \times 10^5 < Re < 3.5 \times 10^5$  Critical (Lower transition)
	B: Turbulent boundary layer separation; the boundary layer partly laminar partly turbulent	$3.5 \times 10^5 < Re < 1.5 \times 10^6$  Supercritical
	C: Boundary layer comple- tely turbulent at one side	$1.5 \times 10^6 < Re < 4 \times 10^6$  Upper transition
	C: Boundary layer comple- tely turbulent at two sides	$4 \times 10^6 < Re$  Transcritical

Figure 3.7: Vortex Shedding phenomena [Sumer, 1997]

### 3.3.4 Relationship between Strouhals number $S_t$ and Reynolds number $R_e$

Both Reynolds number  $R_e$  and Strouhals numbers  $S_t$  are dimensionless, and the relation between Strouhals- and Reynolds number is shown in figure 3.8.

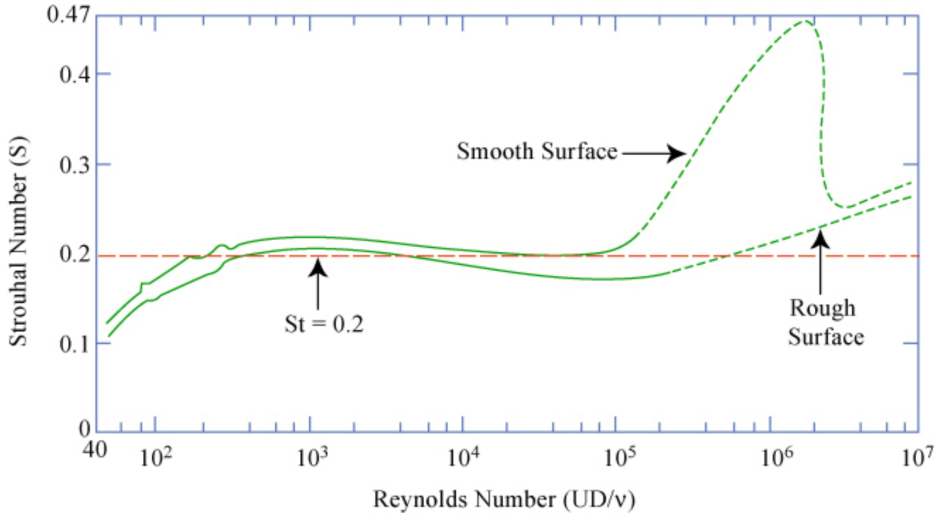
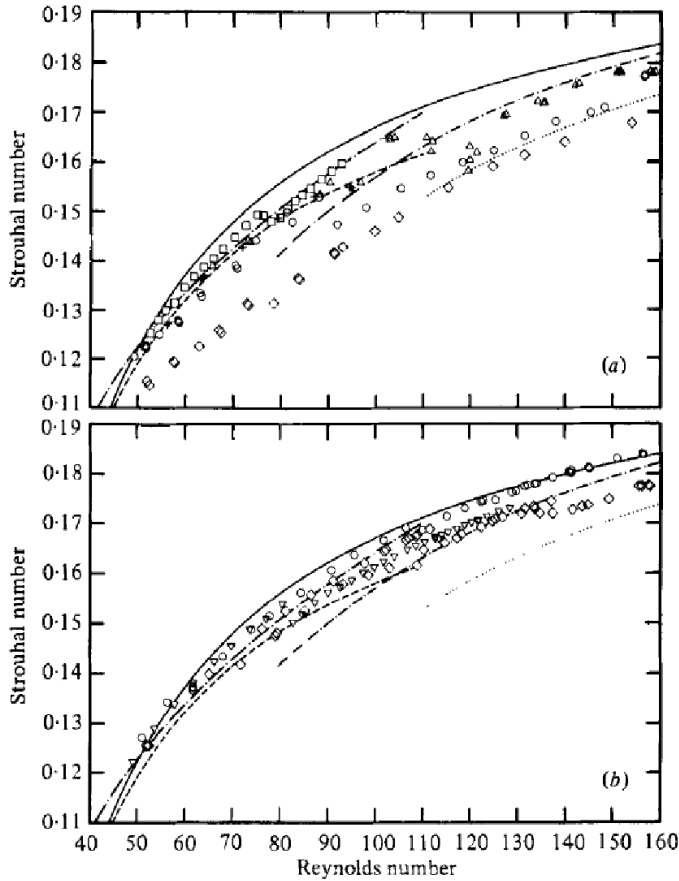


Figure 3.8: Relation between Strouhals number and Reynolds number [Pettersen, 2007]

For Reynolds number 40 – 48, two fixed pair of vortices behind the circular cross-section will occur. The Strouhal number will therefore be around 0.1. For increasing in Reynolds number, the Strouhals number will increase and stabilize around 0.2. For very large Reynolds numbers ( $\leq 1000000$ ),  $S_t$  is dependent on a smooth or rough body.

Friehe (1980) obtained experimental data from a laminar flow on cylinders with various diameters and cylinder lengths. The quantitative relationship between the Strouhals number and the Reynolds number is presented, where the Strouhals number is changing for different Reynolds numbers.

In experiments, the vortex shedding frequency will be affected by the interference of freestream velocity  $U$ . Therefore Friehe (1980) measures Strouhals number and Reynolds number for experiments by jet flows and wind tunnels. The results are presented in figure 3.9 where the results follows a certain curve. The results are presented for different cylinder with diameter  $D$  (notation for diameter:  $d$  in figure 3.9) and cylinder length  $l$  [Friehe, 1980].



Experimental  $St-Re$  data. (a) Data in 1.5 cm and 5 cm jet flows:  $\square$ ,  $d = 0.0107$  cm,  $l/d = 150$ ;  $+$ ,  $\triangle$ ,  $d = 0.0107$  cm,  $l/d = 467$ ;  $\circ$ ,  $d = 0.0208$  cm,  $l/d = 77$ ;  $\diamond$ ,  $d = 0.0348$  cm,  $l/d = 46$ . (b) Data in wind tunnel:  $\circ$ ,  $d = 0.0208$  cm,  $l/d = 3605$ ;  $\nabla$ ,  $d = 0.0160$  cm,  $l/d = 4688$ ;  $\diamond$ ,  $d = 0.0246$  cm,  $l/d = 3049$ . Reference data from Tritton (1959): —, Roshko (1954); - - -, Tritton (1959), low-speed mode; - - - - -, Berger (1964), low-speed mode; - · - ·, Tritton and Berger high-speed mode; ·····, Berger basic mode.

Figure 3.9: Relationship between Strouhals number and Reynolds number for different cylinders with diameter  $d$  and length  $l$ . (a) Experiment in jet flow, and (b) experiment in wind turbine [Friehe, 1980].

From experiments performed by the American Institute of Physics presents a graphical display of various Reynolds numbers in figure 3.10. The figure shows how the Strouhals number will vary for a cylinder with different diameters  $D$  and lengths  $l$ , where the results are approximately equal for the performed experiments [Fey et al., 1998].

Figure 3.10 presents the experimental data with the Strouhals number along the vertical axis (with notation  $S_r$ ) and Reynolds number  $R_e$  on the horizontal axis. The upper axis represent the true Reynolds number  $R_e$ , while the lower horizontal axis represents the value:  $\frac{1}{\sqrt{(R_e)}}$ . The slopes of Strouhals - Reynolds number will vary as instabilities in the flow will occur near the wake region for the cylinder.

The laminar regime will dominate for lower Reynolds numbers. For increasing Reynolds number at laminar regime will give increasing Strouhals number towards  $R_e = 180$ . Further the Strouhals number will reach a peak around  $S_t = 0.22$  as vortex shedding continuous in shear layer regime. The Strouhals number will slowly decrease as  $R_e \geq 2 * 10^4$  for turbulence flow regime.

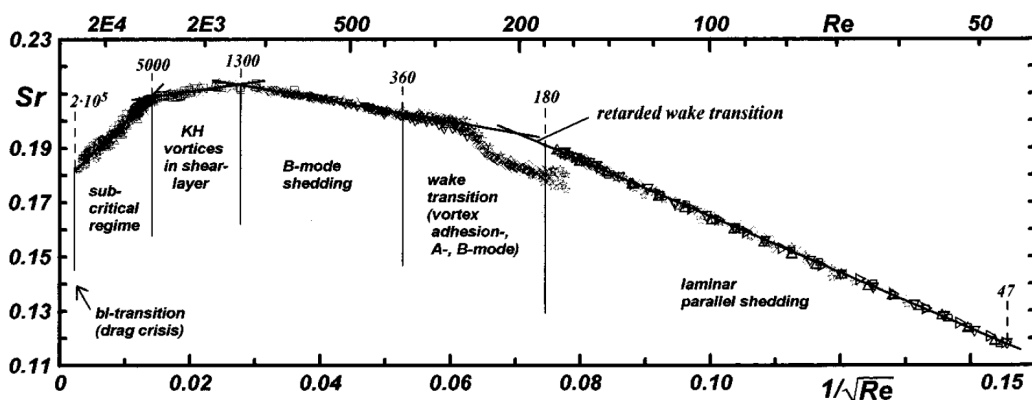


Figure 3.10: Relation between Strouhals number and Reynolds number. The various changes in slope are due to the different instabilities occurring in the near wake region. The different cylinder dimensions are not presented in the figure, but cylinder length  $l$  and diameter  $D$  ratio  $l/D$  varies from 50 to 400 [Fey et al., 1998].

Figure 3.11 presents how the Strouhals number will vary for different Reynolds number with comparison of a two-dimensional (2D) numerical computation from Rajani et al. (2009) and measurements from Norberg (1993) and Williamson (1992) [Rajani et al., 2009].

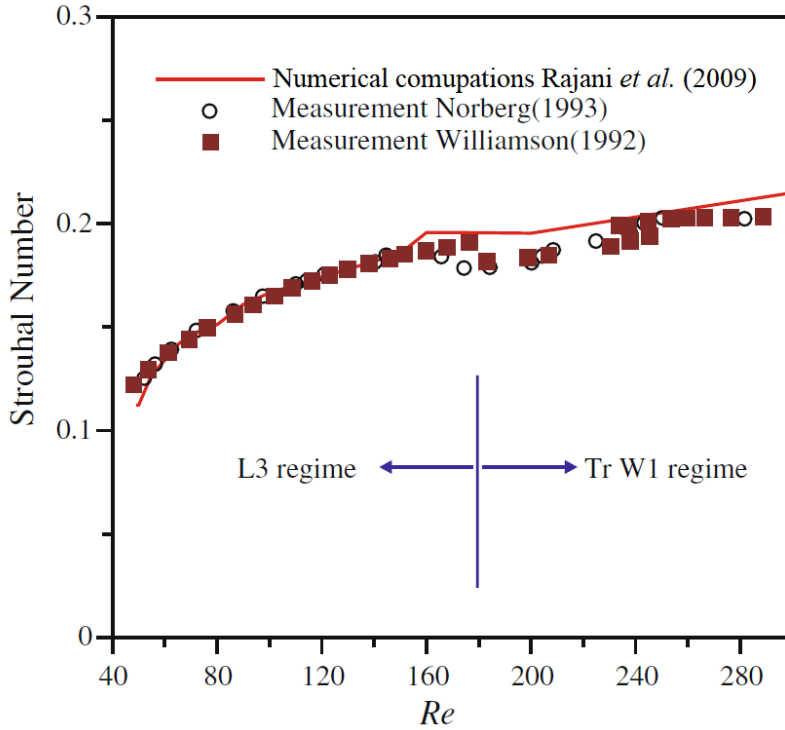


Figure 3.11: Relation between Strouhals number and Reynolds number [Rajani et al., 2009].

The figures 3.9, 3.10 and 3.11 presents results from numerical computations and experimental measurements, and shows a correlation between the Strouhals number  $S_t$  and the Reynolds number  $Re$ .

### 3.3.5 Vorticity

The vorticity is a measure of the rotational effect in a fluid, and can be defined in equation (3.8) [White, 2006].

$$\vec{\omega} = \nabla \times \vec{u} = \left(\frac{\partial w}{\partial y} - \frac{\partial v}{\partial z}\right)\vec{i} + \left(\frac{\partial u}{\partial z} - \frac{\partial w}{\partial x}\right)\vec{j} + \left(\frac{\partial v}{\partial x} - \frac{\partial u}{\partial y}\right)\vec{k} \quad (3.8)$$

The vorticity is not a primary variable in flow analysis, but it is an important aspect when examining the impact of Navier-Stokes equation. In general, vorticity is generated by the relative motion near solid walls, i.e. solid cylinder surface. Vorticity and turbulence are often referred about to one and another. Many vortices or vortex' are often included in the definition of a turbulent flow, such that the existence of vortices will determine a turbulent flow [White, 2006], [Tennekes and Lumley, 1972] & [Hussain, 1995].

### 3.3.6 Boundary Layer

The boundary layer  $\delta(x)$  is defined with a boundary layer thickness  $\delta$ , which is defined as the point where streamwise velocity component is 99 percent of the freestream velocity. The boundary layer thickness is then referred to as  $\delta_{99}$ , where  $u(y) = 0.99U(x)$ , and is estimated roughly with the expression (3.9) [White, 2006].

$$\delta = \frac{D}{\sqrt{Re}} \quad (3.9)$$

A thin boundary layer should exist for large Reynolds numbers. How large the Reynolds number should be, is dependent on the geometry of the fixed body. Boundary layers are characterized by high shear with large velocities away from the surface. Frictional force, viscous stress, and vorticity do occur in the boundary layers.

The figure 3.12 presents the stream-wise velocity component  $U_0$ , where the boundary layer thickness is illustrated in the gray region with thickness  $\delta$ . The illustration shows vorticity, where vortex shedding is occurring.

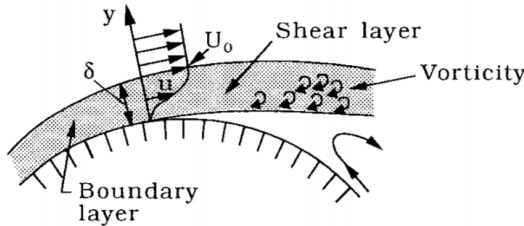


Figure 3.12: Boundary layer, separation and occurrence of vorticity [Sumer, 1997].



## 3.4 Drag - and Lift Forces

Vortex shedding phenomena creates instabilities in the flow. The alternating vortex shedding will give oscillating forces in cross-flow direction and in-flow direction. A lift force,  $F_y$ , will act normal to the incoming flow (cross-flow direction) and oscillates harmonically around zero. A drag force,  $F_x$ , will act in the flow direction and oscillates at twice the frequency of the lift force.

### 3.4.1 Force Coefficients

Drag force is the force which is excited in the inflow direction, while the lift force is normal to the incident flow direction. Both drag- and lift force can be expressed with the force coefficients,  $C_D$  and  $C_L$ , presented in equation (3.10). The uniform current velocity is given by  $U$ , while the projected area is given as  $A_{ref}$ , which is simplified as the cylinder length times the cylinder diameter [Faltinsen, 1990].

$$C_D = \frac{F_x}{\frac{1}{2}\rho U^2 A_{ref}} \qquad C_L = \frac{F_y}{\frac{1}{2}\rho U^2 A_{ref}} \qquad (3.10)$$

### 3.4.2 Root Mean Square of fluctuations

The Root Mean Square (RMS) or typically called quadratic mean, is based on having a set of data values, where the RMS is the square root of the mean value of  $x_i^2$ .

The RMS is given by:

$$x_{rms} = \sqrt{\frac{\sum_{i=1}^n x_i^2}{n}}. \qquad (3.11)$$

Finding the Root Mean Square for the drag coefficient and lift coefficient is a method to find the level of fluctuation around the mean value, or the mean amplitude for drag and lift forces. The value of fluctuation presents how much the mean is oscillating between a maximum and minimum [Cengel and Cimbala, 2014].

### 3.4.3 Relationship between mean drag $\bar{C}_D$ and Reynolds number $Re$

Analyzing flow around circular cylinders, the relation between the mean drag force coefficient  $\bar{C}_D$  with respect to Reynolds number  $Re$  is compared. Figure 3.13 present data of mean drag coefficient  $\bar{C}_D$  including pressure drag part and viscous drag part in a function of Reynolds number  $Re$ . The figure presents how the drag force coefficients stabilizes at a constant value for higher Reynolds number.

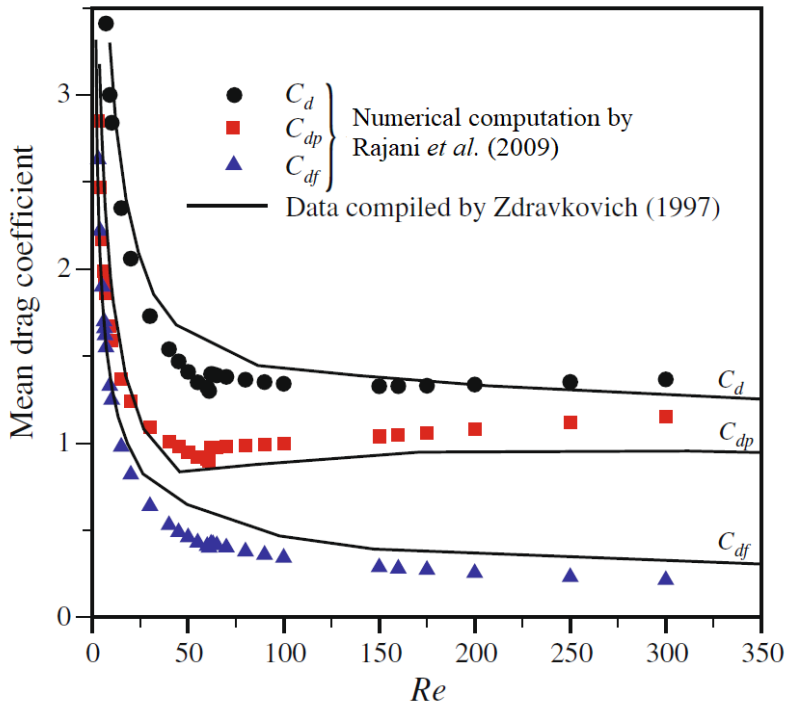


Figure 3.13: Graphical presentation of the relation between the mean drag coefficient  $\bar{C}_D$  and the Reynolds number  $Re$  for 2D numerical analysis. The comparison presents different data: Black dot  $\bar{C}_d$ : presents the total drag force from the 2D computation. Red square  $\bar{C}_{dp}$ : drag force with pressure contribution. Blue triangle  $\bar{C}_{df}$ : drag force with frictional contribution. The straight line are the data compiled from Zdravkovich (1997), [Rajani et al., 2009].

### 3.5 Uniform Flow around a Circular Cylinder

Section 3.3 introduces to flow phenomena for two-dimensional (2D) flow problems. Analyzing a three-dimensional (3D) circular cylinder, the cross-sectional diameter  $D$  and cylinder length  $l$  are important parameters. The ratio between the cylinder length  $l$  and cylinder diameter  $D$  are important when discuss the effects of cylinder-ends, cylinder roughness and flow behaviour for a three-dimensional (3D) flow problem.

Vortex shedding phenomena for a 3D problem will occur for the same Reynolds numbers as presented in figure 3.7. Flow problems with Reynolds number  $40 < Re < 200$ , *Von Kármán* vortices will occur with alternating clockwise and anti-clockwise vortices. The figure 3.14 presents a three-dimensional illustration of alternating vortex shedding for steady flow case with  $40 < Re < 200$ .

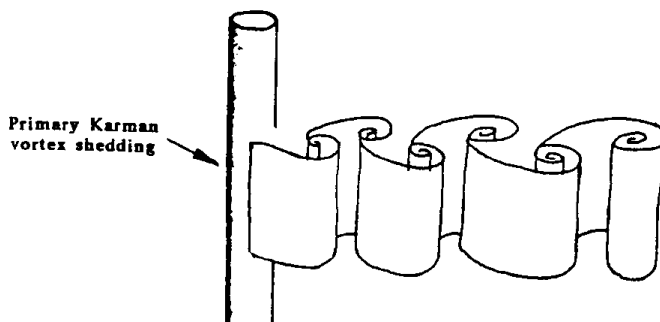


Figure 3.14: Three-dimensional illustration of alternating vortex shedding with  $40 < Re < 200$  [Williamson, 1996].

For increased Reynolds number, instability modes will arrive in the fluid. Around  $Re = 180 - 190$  or extended to  $Re = 194 - 200$  the three-dimensional instabilities in the wake will appear. Figures 3.15 and 3.16 present how instabilities occur as shear layers. The transition to turbulence exists in the separating shear layers, just before the vortices are formed and shedded.

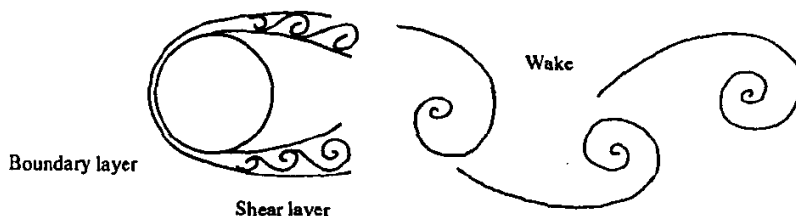


Figure 3.15: Illustration of unsteady flow and vortex shedding in 2D [Williamson, 1996].

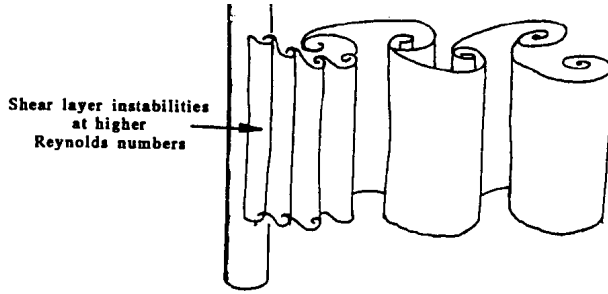


Figure 3.16: Illustration of unsteady flow and vortex shedding in 3D [Williamson, 1996].

In three-dimensional (3D) flow problems, vortex shedding phenomena can be described with two different modes of shedding. A three-dimensional (3D) wake will comprise into two distinct instabilities of Mode A and B. These modes describes the *secondary instabilities* behaviour. While the *primary instabilities* are described as the occurrence of the twin vortices between  $5 < R_e < 40$ .

The appearance of mode A is due to elliptical instability, which is characterized by a vortex core during shedding process. Mode A comprises streamwise vortices, where instabilities will occur as  $R_e > 180$ . There will be irregular drag - and lift force on the cylinder, with changing vortex shedding frequency  $f_v$ . Mode B will occur due to instability in scale of thickness of vorticity on each alternating braid. Mode B will have an in-line arrangement, and will occur for fluid cases with  $R_e > 270$  [Williamson, 1996] & [Cao and Wan, 2010].

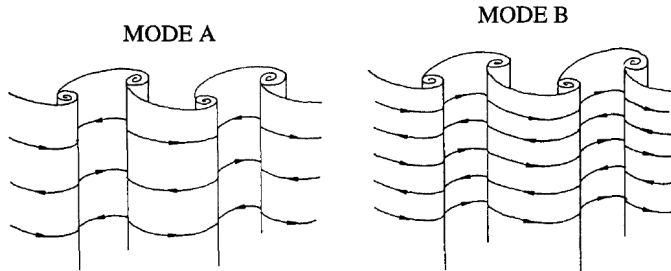


Figure 3.17: Illustration of modes A and B [Williamson, 1996].

For Reynolds number close to 300, observations of a period-doubling bifurcation occurs, as it may lead to turbulence. A bifurcation in fluid problems are described as a change in flow behavior due to a change of a fluid parameter, as the Reynolds number. One has not discovered the true origin of Mode A and B. The flow phenomena are observed for both numerical and experimental flow problems, but still there are unsolved mysteries which are not explained of flow behaviour and change of Reynolds number [Williamson, 1996], [Behara and Mittal, 2010], [Aarnes and Haugen, 2018] & [Barkley and Henderson, 1996].

### 3.6 Shear Flow around a Circular Cylinder

Several numerical and experimental fluid problems are analyzed for uniform flow around circular bodies. These analysis are performed to understand the flow phenomena in engineering challenges at sea. Unfortunately, many fluid problems are not uniform. Therefore shear flow would be more representative for currents flows at sea and in fjords.

Analyzing cylindrical structures, the analysis can be performed with an axial shear flow or a planar shear flow. The illustration in figure 3.18 and 3.19 presents an axial shear flow with a velocity  $U(z)$  which varies along the cylinder length with the z-axis, while the planar shear has velocity varying along the defined diameter with y-axis,  $U(y)$ .

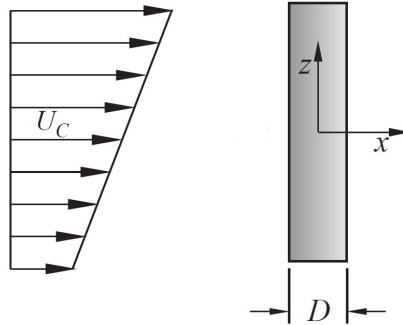


Figure 3.18: Circular cylinder in axial shear flow  $U(z)$  [Akosile and Sumner, 2003].

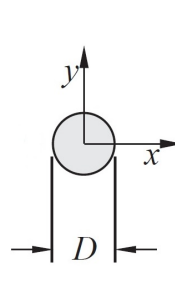


Figure 3.19: Circular cylinder in planar shear flow  $U(y)$  [Akosile and Sumner, 2003].

To be able to observe flow phenomena described in section 3.3, the planar shear flow analysis of an immersed cylindrical structure is preferable. The planar shear flow is defined as a varying shear current with respect to  $y$ , expressed for  $U(y)$  in equation (3.12). The expression consist of the current velocity at center-line  $U_c$ , where the velocity  $U_c$  acts normal on the cylinder. The linearly varying component  $Gy$  consists of  $y$  and  $G$ , where  $y$  is the cross-flow coordinate and  $G$  is the velocity gradient.

$$U(y) = U_c|_{y=0} + Gy \qquad G = \frac{dU}{dy} = \frac{U_A - U_B}{D} \left[ \frac{1}{s} \right] \quad (3.12)$$

The schematic illustration given in figure 3.20, presents a varying shear flow in planar direction on a two-dimensional (2D) circular cross-section. The cross-section is defined with the axis system of  $x$  and  $y$ .

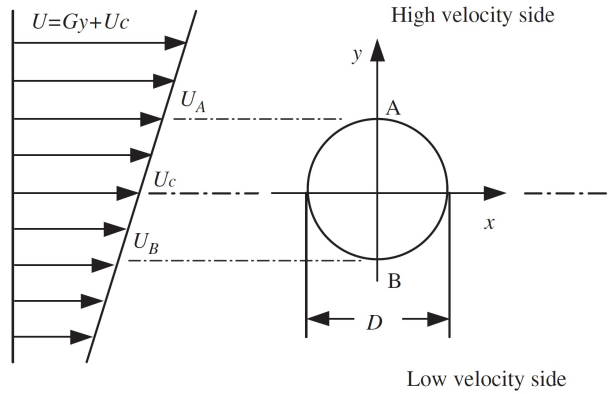


Figure 3.20: Schematic illustration of planar shear flow over a two-dimensional circular cross-section [Cao et al., 2010]

Figure 3.20 illustrated point  $A$  on the high-velocity side of the cross-section, while point  $B$  is on the low-velocity side. The difference in high - and low - velocity is due to the planar shear. This property of the shear flow will give new flow phenomena due to varying velocity over the cylinder, and varying Reynolds number.

Shear flow problems, introduces new dimensionless parameters which are used to compare measured results and describe the properties of the shear flow. The dimensionless shear parameter, or shear rate  $K$  is presented in equation (3.13). The shear rate is defined with cross-section diameter  $D$ , velocity gradient  $G$ , and the centre-line velocity  $U_c$ . The shear rate is a measure for the shear magnitude of a flow.

$$K = \frac{GD}{U_c} = \frac{U_A - U_B}{U_c} \quad (3.13)$$

A flow will experience low shear, when the shear parameter is identified between  $0.02 \leq K \leq 0.07$ . A flow experience large shear, when the shear rate is around  $K = 0.2$  [Akosile and Sumner, 2003].

Twin vortices and alternating vortex shedding are analyzed for the Reynolds numbers  $40 \leq Re \leq 80$  and shear rates  $0 \leq K \leq 0.20$  in the numerical analysis by [Tamura et al., 1980].

The shear parameter  $K$ , Reynolds number  $Re$  can be used to describe vortex shedding with frequency  $f_v$  and Strouhals number  $S_t$  [Kang, 2006].

Comparing the shear rate  $K$  with Reynolds number  $Re$  and Strouhals number  $S_t$ , one can observe a strong correlation between the dimensionless parameters. The Strouhals number will experience to decrease for  $K = 0.2$ , compared to uniform flow and smaller shear rate values of  $0.02 \leq K \leq 0.07$  [Lei et al., 2000], [Kiya et al., 1980] & [Kwon et al., 1992].

Lei et al. (2000) concludes that the stagnation point in a shear flow problem occurs on the high velocity side of the circular cross-section. Wu & Chen (1999) analyzes separation point at the laminar boundary-layer separation, where separation occurs at windward side of cylinder. Shear flow will also give periodic velocity, drag - and lift fluctuations which occur for larger Reynolds number in shear flow, compared to uniform flow [Kiya et al., 1980], [Lei et al., 2000] & [Wu and Chen, 1999].

The observations, comparison of dimensionless parameters and discussions regarding vortex shedding for shear flow problem, are all to be considered when further performing analysis of 3D tandem cylinders in a shear current flow.

### 3.7 Configuration of Circular Cylinders

”When more than one bluff body is placed in a fluid flow, the resulting forces and vortex shedding pattern may be completely different from those found on a single bluff body at the same Reynolds number” - [Zdravkovich, 1987].

Explaining the difference in a flow problem with a single cylinder to configurations of two cylinders, will give new flow phenomena. Phenomena as stagnation point, separation and vortex shedding will now be observed with respect to the interaction of the fluid flow and two cylinders with a given configuration.

From Zdravkovich (1987) and Sumner (2010), the arrangements of two cylinders are illustrated in figure 3.21 [Zdravkovich, 1987] & [Sumner, 2010]:

- (a) *Tandem arrangement*: are two cylinders with a longitudinal length  $L$  between the two cylinder centre, and gap  $G$  is the closest distance between the cylinder surface.
- (b) *Side-by-Side arrangement*: are two cylinder with a transverse distance  $T$  between the two cylinder centre.
- (c) *Staggered arrangement*: are two cylinders placed with an angle  $\alpha$  and distance  $P$ .

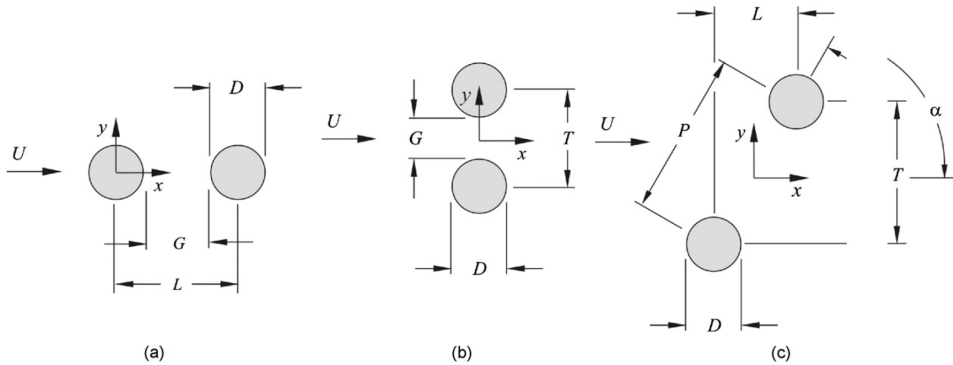


Figure 3.21: Configuration of circular cylinders [Sumner, 2010].



### 3.7.1 Tandem Cylinders

Tandem configuration arranges two cylinders in-line and parallel to the mean flow. This configurations places one cylinder in immediate upstream, while the second cylinder is placed downstream. This arrangement is further to be studied regarding the Submerged Floating Tube Bridge (SFTB) analysis subjected to a planar shear flow.

The important factors regarding the interaction between two circular cylinders, are Reynolds number, longitudinal length ( $L$ ) between the circular cylinders  $L$  and the cylinder diameter  $D$ . The flow phenomena discussed in section 3.3 can be analyzed and observed with respect to cylinder configuration and length-diameter-ratio  $L/D$ .

Figure 3.22 presents the regions of *wake interference* and *proximity interference* for a circular cross section in uniform flow. The horizontal axis presents the cylinder ratio of length  $L$  and diameter  $D$ . Along the vertical axis the ratio of vertical spacing  $T$  and diameter  $D$ . It is assumed that both cylinders have the same diameter size.

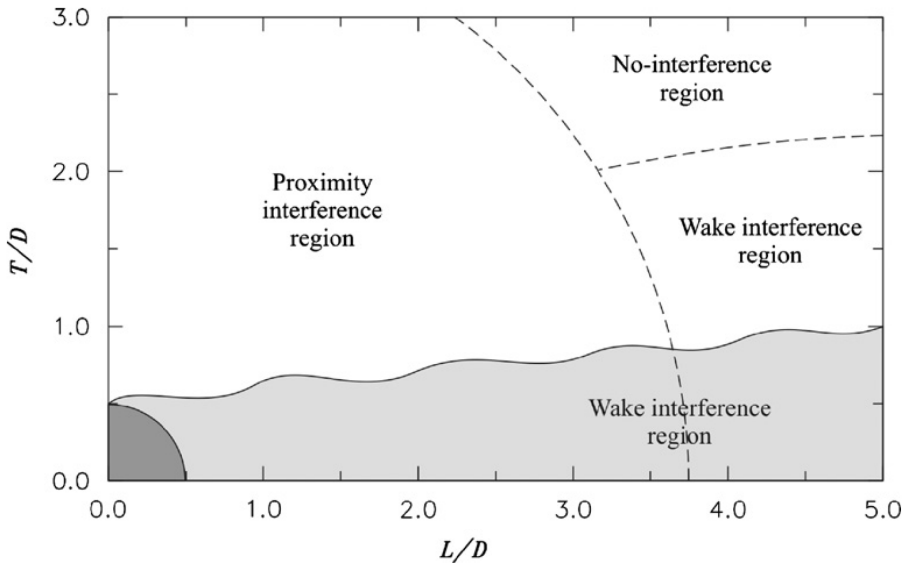


Figure 3.22: Illustration of the regions of wake interference and proximity interference for a circular cross-section subjected to a uniform flow [Zdravkovich, 1987].

*Wake interference* is when one cylinder is partially or completely submerged in the wake of the other cylinder for tandem configurations. Wake interference is observed as the wakes from one cylinder is transported immediately upstream of the second cylinder. The vortex shedding from the first cylinder will be suppressed when meeting the second cylinder. *Proximity interference* is when the two cylinders are located close to one another in side-by-side configurations, but will not be affected by each others wake [Sumner, 2010].

## Wake Interference

Flow patterns occurring when a uniform flow is subjected on cylinders in tandem configuration are sensitive to changes in Reynolds number and ratio of  $L/D$ . Flow patterns are described in three different types of wake interference [Xu and Zhou, 2004] & [Zhou and Yiu, 2006]:

- (i) Single bluff-body behaviour is also called "extended-body regimes as  $1.0 < L/D < 1.2 - 1.8$  [Zdravkovich, 1987] or  $1.0 < L/D < 2.0$  [Zhou and Yiu, 2006]. The cylinders are sufficiently close, and will behave as a single structure immersed in the fluid problem.
- (ii) Shear layer re-attachment behaviour or the re-attachment regime: Occurs at intermediate ratio of around  $1.2 - 1.8 < L/D < 3.4 - 3.8$  [Zdravkovich, 1987] or  $2.0 < L/D < 5.0$  [Zhou and Yiu, 2006], where the shear layers from the upstream cylinder will reattach on the downstream cylinder. There may be vortices occurring in-between the cylinders.
- (iii) Von Kármán vortex shedding from each cylinder or the co-shedding regime: Occurring for ratios of  $L/D > 3.4 - 3.8$  [Zdravkovich, 1987] or  $L/D > 5.0$  [Zhou and Yiu, 2006].

Flow separation occurs as the fluid detaches from the solid surface as no shear stress is present  $\tau_w = \mu \frac{\partial u}{\partial y}_{y=0} = 0$  or  $\frac{\partial u}{\partial y}_{y=0} = 0$ .

Reattachment will describe the phenomenon when the fluid attaches to a solid surface, during adverse pressure gradient only. *Reattachment* occurs when the flow separate from the upstream cylinder, and further be reattached to the downstream cylinder as the static pressure increases in the direction of the flow:  $\frac{\partial P}{\partial x}_{y=0} > 0$  [Xu and Zhou, 2004] & [Zhou and Yiu, 2006].

Figure 3.23 presents the different wake interference levels with respect to  $L/D$  ratio and Reynolds number [ $*10^4$ ] from (A) - (G). The map presents the regions of when vortex shedding, stable flow, unstable flow or reattachment will occur [Sumner, 2010], [Xu and Zhou, 2004] & [Zhou and Yiu, 2006].

- (A) *Over shot*: presents the wake interference case as (i) with *Single bluff-body behaviour*.
- (B) *Alternate reattachment*: increase in longitudinal length, such that alternate reattachment from upstream cylinder roll up behind the downstream cylinder. Similar to case (ii) *Reattachment regime*.
- (C) *Quasi-Steady reattachment with symmetric vortices between tandem cylinders*. Similar to case (ii) *Reattachment regime*.
- (D) *Quasi-Steady reattachment with asymmetric vortices between tandem cylinders*.
- (E) *intermittent reattachment*, where  $2.0 < L/D < 5.0$  [Zhou and Yiu, 2006].

- (F) *Co-shedding*: clearly presents the Von Kármán vortex shedding for case (iii) with vortex shedding for cylinder upstream and downstream.
- (G) Describes an unstable wake between region A, B and C.

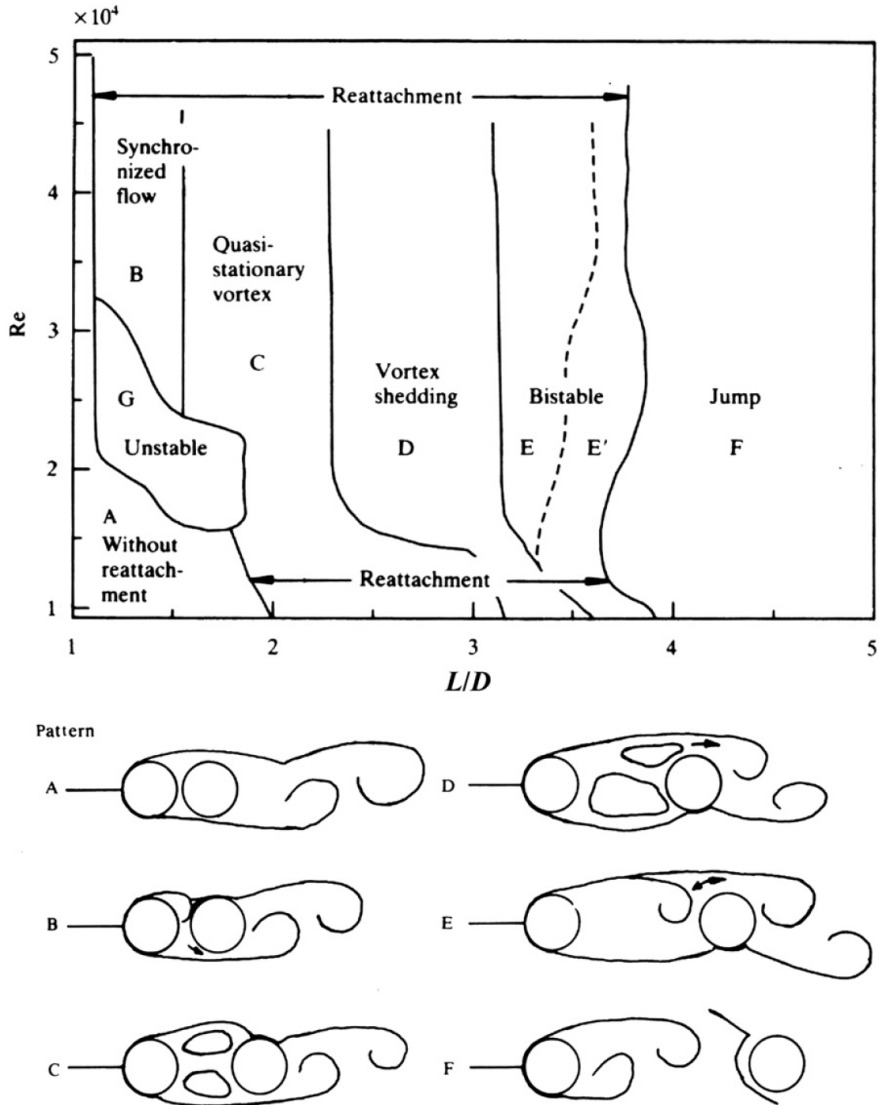


Figure 3.23: Wake interference map: Comparing ratio  $L/D$  and Reynolds number with wake pattern [Sumner, 2010].

Tandem configuration will consist of an upstream and a downstream cylinder with a distance  $L$  between the cylinder centres. The upstream cylinder will experience the incoming current velocity. The downstream cylinder will experience different flow phenomena, as the incoming flow on the downstream cylinder is affected by the wake of the upstream cylinder. The observed flow phenomena on the downstream cylinder are dependant on the Reynolds number and the ratio between the longitudinal length of diameter  $L/D$  of the tandem cylinders.

Kalvig et al. (2016) performs a numerical analysis with the computational fluid dynamics tool, OpenFOAM with Large Eddy Simulations of tandem cylinders with  $L/D = 5$  and turbulent flow with  $Re = 13100$ . The lift forces for the upstream and downstream cylinder have phase shift, as a result of the vortices shedding from upstream cylinder and travels towards downstream cylinder. The total lift force is also larger on the downstream cylinder, compared to the upstream cylinder. The downstream cylinder will be effected by the vortices travelling from the upstream cylinder and the formation of vortices around the downstream cylinder, which will induce lift force. Measurements of drag force, presents irregular root mean square (RMS) amplitudes for both upstream and downstream cylinder. This is due to various strength in vortices which are shedded from upstream cylinder, and how vortices interact with the downstream cylinder as a part of the co-shedding regime [Kalvig et al., 2016].

Meneghini et al. (2001) and Ding et al. (2007) presents how the mean value of drag for the downstream cylinder changes from negative magnitude value,  $\bar{C}_D < 0$ , to positive magnitude value,  $\bar{C}_D > 0$ , as the longitudinal length is three times larger than the cylinder diameter,  $L > 3D$ . The downstream cylinder will only shed vortices for  $L < 3D$  where negative mean drag force is measured. When  $L > 3D$ , the upstream cylinder will shed vortices too, with a positive mean drag force. This is described as the co-shedding regime.

A longitudinal length of  $L = 3D$  gives an equal lift amplitude for the downstream cylinder and a single cylinder subjected to the same flow. The upstream cylinder, will obtain a lower lift amplitude. This observation occurs for the drag force in both upstream and downstream cylinder. This phenomena can be described as the reattachment regime, where shear layers from the cylinder upstream will reattach on the downstream cylinder [Meneghini et al., 2001] & [Ding et al., 2007]

The figures 3.24 and 3.25 presents the drag and lift force coefficient with given time history for simulation with Reynolds number 200. The results are presented for both upstream and downstream cylinder for (a)  $L = 1.5D$ , (b)  $L = 2D$ , (c)  $L = 3D$  and (d)  $L = 4D$  [Meneghini et al., 2001].

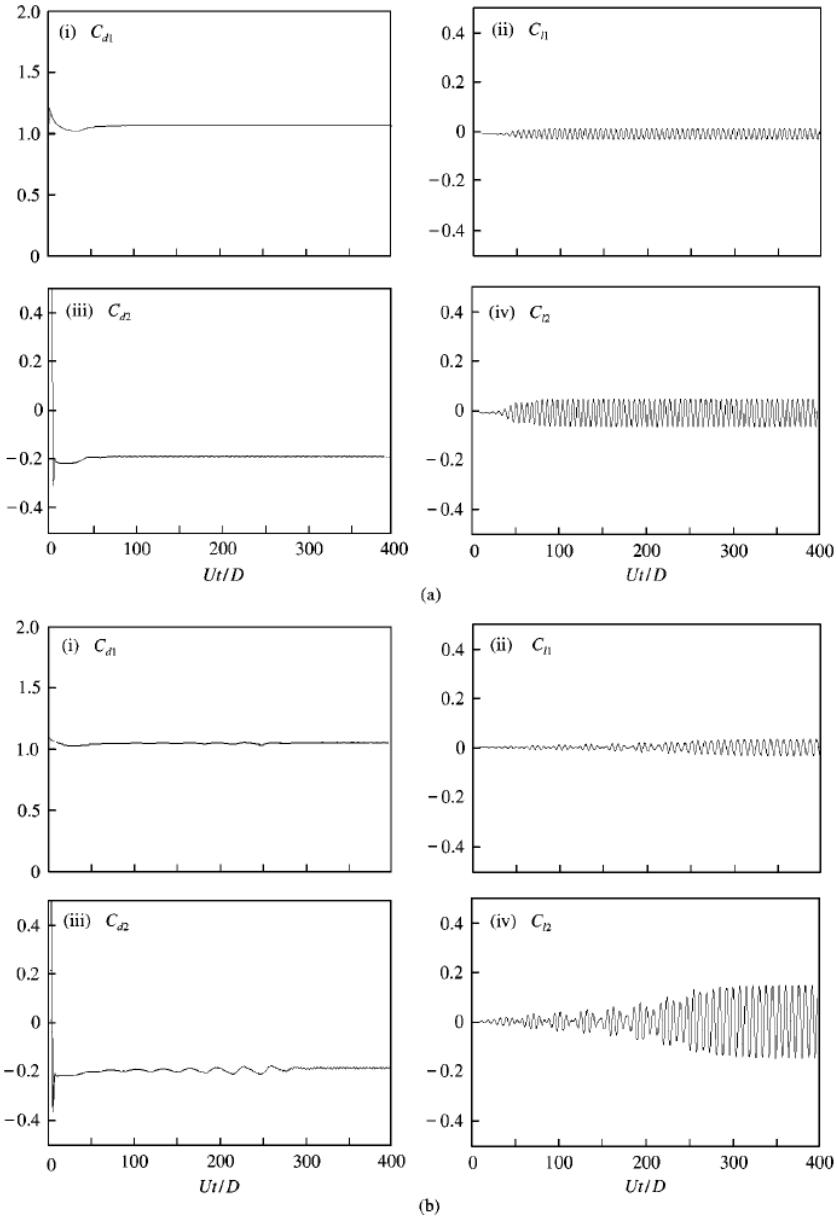


Figure 3.24: Force coefficient for drag and lift for  $Re = 200$  with time history. (a)  $L = 1.5D$ , (b)  $L = 2D$ . Index 1: Upstream circular cylinder, index 2: downstream circular cylinder [Meneghini et al., 2001].

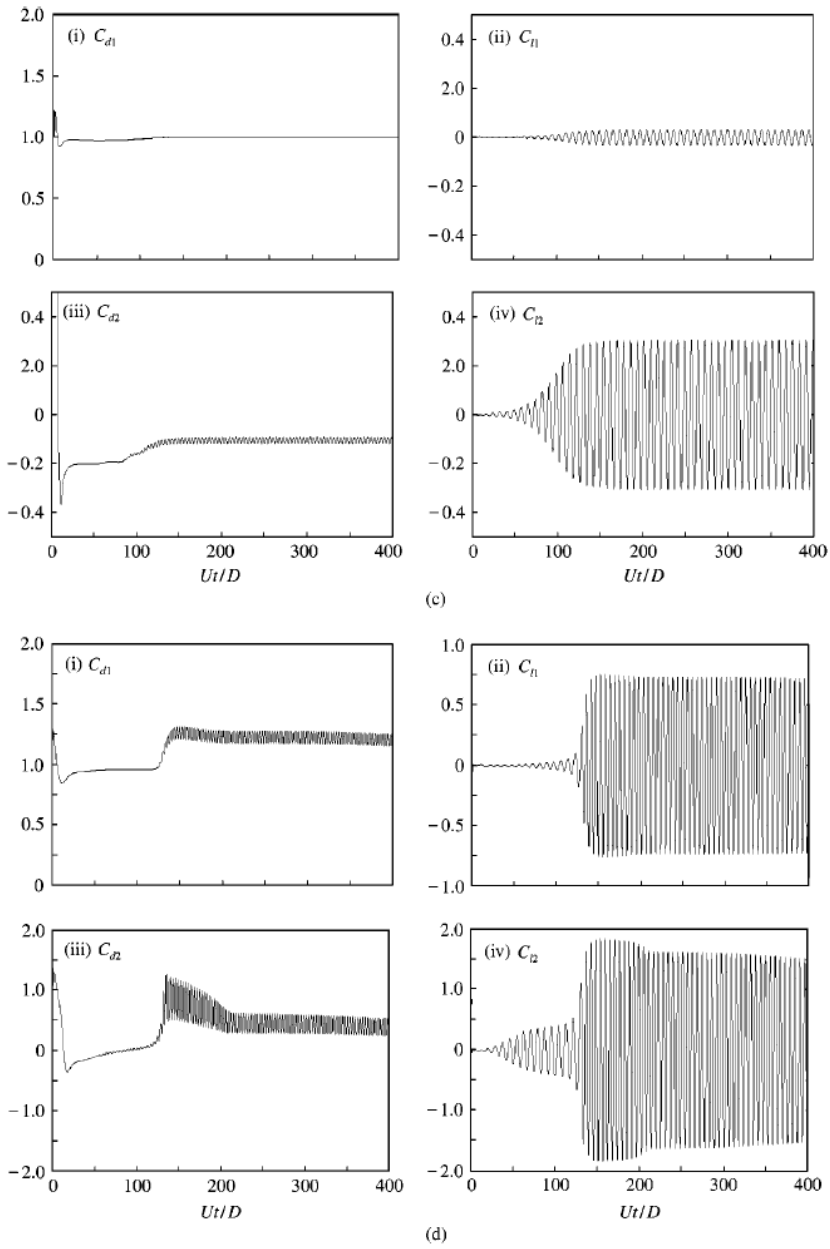


Figure 3.25: Force coefficient for drag and lift for  $Re = 200$  with time history. (c)  $L = 3D$ , (d)  $L = 4D$ . Index 1: Upstream circular cylinder, index 2: downstream circular cylinder [Meneghini et al., 2001].

## Pressure Distribution

Pressure distribution is an important scalar in studying flow phenomena. Pressure distribution and the velocity profiles reveals how the fluid behaves and how velocity and pressure interacts. The pressure coefficient is given by equation (3.14), where  $p$  is static pressure at chosen point and  $p_0$  is static pressure at freestream.  $u_0$  is the freestream velocity with the fluid density  $\rho$ .

$$C_p = \frac{p - p_0}{\frac{1}{2}\rho u_0^2} \quad (3.14)$$

Pressure distribution around upstream and downstream cylinders are measured for different longitudinal length-diameter ratio  $L/D$ . Figure 3.26 shows the tandem configuration with corresponding freestream velocity  $u_0$ , angle  $\phi$ , longitudinal length  $L$  and cylinder diameter  $D$  (diameter will be referred as:  $d$ ) [Igarashi, 1981].

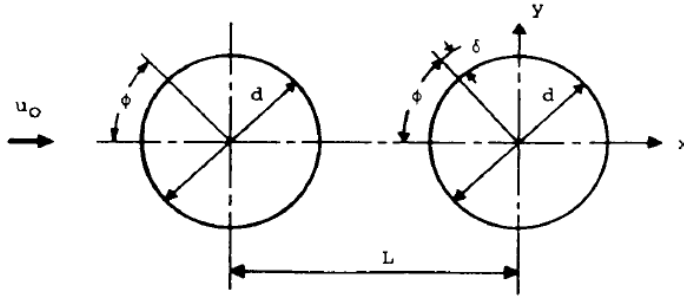


Figure 3.26: Tandem configuration with longitudinal length ( $L$ )  $L$  and circumference angle  $\phi$  and diameter  $d$  [Igarashi, 1981].

The pressure distribution for five different ratios  $L/D = 1.03, 1.18, 1.91, 3.09, 3.97$  are presented in figure 3.27 and 3.28 for upstream and downstream cylinder respectively. The pressure distribution is presented by the coefficient  $C_p$  around the cylinder surface for  $\phi$  degrees.

Upstream cylinder experience a drop in pressure along the cylinder surface. For all ratios, there is a low peak at  $\phi = 70$ . Comparing the results to a single cylinder, the single cylinder experience lower pressure distribution than the upstream cylinders in tandem configuration.

There is one remark to point out considering ratio  $L/D = 3.97$ . At this ratio shear layers are separated from the upstream cylinder and travels in-front of the downstream cylinder. The pressure distribution at  $L/D = 3.97$  for upstream cylinder in figure 3.27 will therefore be similar to the single cylinder, while the downstream cylinder will experience a negative pressure drop from stagnation point towards  $\phi = 90$ . Figure 3.28 presents the pressure distribution for the downstream cylinders with different  $L/D$ -ratios.

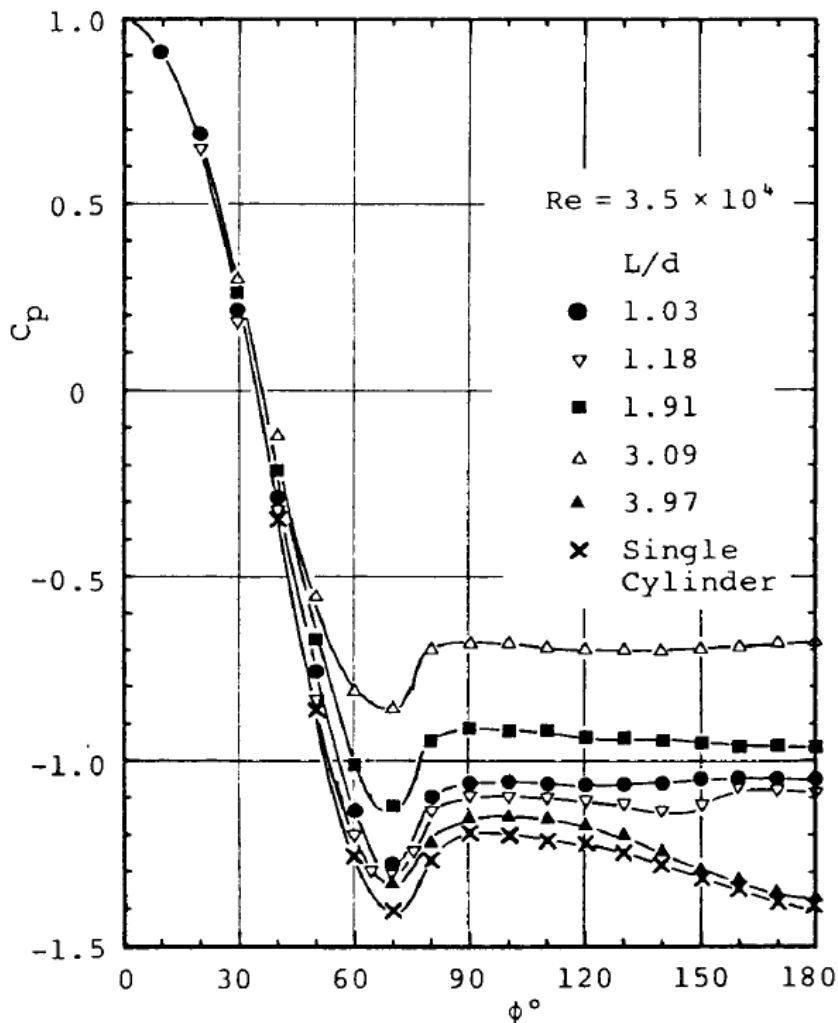


Figure 3.27: Pressure distribution  $C_p$  around upstream cylinder for different  $L/D$ -ratios [Igarashi, 1981].



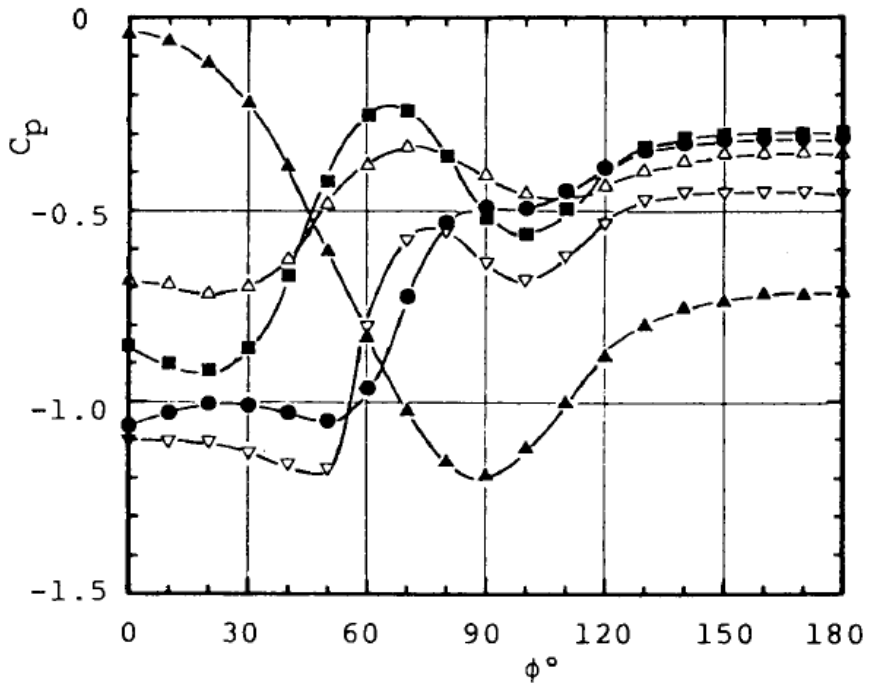


Figure 3.28: Pressure distribution  $C_p$  around downstream cylinder for different  $L/D$ -ratios [Igarashi, 1981].

## Chapter 4

# Numerical Methods in Fluid Dynamics and Computational Domain

### 4.1 Computational Fluid Dynamics (CFD)

Fluid dynamic problems can be analyzed by experimental testing or numerical simulations. Using numerical methods to solve fluid flow problems, one must introduce mathematical models to solve partial differential equations (PDE). The fundamental equations as the Continuity equation (3.2) and the generalized Momentum equation (3.4) will describe the fluid dynamics in a flow problem.

The generalized Momentum equation, can further be written as the well known PDE, Navier-Stokes equation (3.5). This equation is implemented in Computational Fluid Dynamics solvers. Computational Fluid Dynamics (CFD) is a method to solve viscous fluid problems in marine industry. Experimental solutions regarding model testing have dominated the industry in testing and validating structures at sea. The development in computer power gives CFD the advantage of analyzing fluid and hydrodynamic problems with respect to computational domain and for desired time intervals, which would not be visible with use of experimental methods.

The ideal solution from computational fluid dynamics is to solve the Navier-Stokes equation (3.5) for unsteady and three-dimensional (3D) flow with direct simulation of turbulence. Several assumptions are used to simplify the fluid problem, and boundary conditions are introduced to simulated the fluid problem in a computational domain. Taking use of computer methods to solve real life phenomena, computer power and computational time are limiting factors. Limitation regarding costs occurs when taking use of super computers and the cost of running time.

Numerical models are simplified by discretizing fundamental equations and choosing numerical methods to obtain converged solution. When discretizing equations, approximated results are obtained with respect to tolerance level, residual and error.

There are limitations with use of numerical methods as discretization - and iteration errors. Creating a fine enough mesh and large enough domain are crucial factors when analyzing fluid flow problems numerically. Today many numerical solutions are used to compare and validate experimental analysis and model testing, since experimental results are still preferable in industrial fluid flow problems.

## 4.2 OpenFOAM

OpenFOAM stands for Open Field Operator And Manipulation, and is an open source code for different engineering and science problems, i.e. CFD-problems. OpenFOAM is based on the programming language C++, such that the user can modify files with respect to the desired fluid flow problem.

The OpenFOAM package contains run folders with following items:

- *0*: Contains information of zero time instant. The folder contains definitions of boundary conditions for the quantities of velocity  $U$  and pressure  $P$ .
- *system*: Contains files that defined solver techniques, numerical schemes and controlDict. The controlDict contains information for solver, time step, start time, end time and write interval.
- *constant*: Contains files that described the mesh and defines the physical fluid properties, i.e. water density, viscosity, turbulence model etc.

The OpenFOAM analysis is performed with fluid assumption of in-compressible, where the partial differential equations (PDEs) are discretized with the Finite Volume Method (FVM). The solution is found by using the solver Pressure Implicit with Splitting of Operators (PISO) algorithm, where the pressure and velocity components are found for the fluid problem [Kalvig, 2015] & [Greenshields, 2015].

The results are visualized by using the tool ParaView. The program is used to obtain velocity-, pressure - and vorticity distribution.

### 4.2.1 Finite Volume Method (FVM)

OpenFOAM uses the *fvSchemes*, where *Finite Volume Method* is used to solve partial differential equations (PDEs). The numerical scheme, Finite Volume Method is an iterative method which discretizes the PDE with respect to desired variables. For the fluid flow problem, the Navier-Stokes equation is discretized with respect to the variables, velocity  $U$  and pressure  $P$ .

The Navier-Stokes equation is transformed into discrete equations over a finite volume. The volume is considered as hexahedral elements or cells that build up the computational domain. These variables are solved for each cell centre for the grid system [Moukalled and Darwish, 2015].

Conservation principles are applied for each cell or element, which represents a fixed region or space in our control volume. OpenFOAM uses Finite Volume Method to calculate desired values for each cell. The total result for the computational domain is obtained by integrating over the chosen control volume or computational domain [Müller, 2017] & [Pletcher et al., 2013].

### 4.2.2 PISO Algorithm as Solver

The PISO algorithm is chosen to perform the numerical analysis with respect to Finite Volume Method. PISO stands for Pressure Implicit with Splitting of Operators, which calculated the pressure-velocity coupling.

PISO algorithm contains one (1) predictor and two (2) corrector steps, where the predictor step guesses a value for the pressure field. The momentum equations are used, since the pressure term is expressed. The pressure distribution is found by with use of the continuity equation.

The first corrector step introduces the velocity fields to the discretized continuity equation, while the other corrector step introduces the velocity field into the discretized momentum equations. Both corrector steps finds pressure correction, where this process is performed in iterations until desired convergence is obtained [Kalvig, 2015] & [Greenshields, 2015].

### 4.2.3 Time Step Analysis

In a numerical analysis, the time step  $\Delta t$  represents what time interval the analysis is performed for each cell. It is required that time step  $\Delta t$  is large enough to give sufficient results without instabilities, but small enough to avoid heavy computational time.

OpenFOAM has a built-in break function, where the numerical analysis stops, if the computational stability criterion of Courant-Friedrichs-Levy (CFL) condition is not satisfied for time step  $\Delta t$ . The Courant-Friedrichs-Levy (CFL) condition is a stability condition used for advection problems, which describes transportation of a physical quantity as fluid with properties as temperature, velocity and pressure [Pletcher et al., 2013].

The criterion can be defined with the condition below, where  $U_x$  is velocity in x-direction,  $U_y$  is velocity in y-direction and  $U_z$  is the velocity in z.-direction.  $\Delta x$ ,  $\Delta y$  and  $\Delta z$  are the size of an element in the mesh in each direction x, y and z:

$$CFL = \frac{U_x \Delta t}{\Delta x} + \frac{U_y \Delta t}{\Delta y} + \frac{U_z \Delta t}{\Delta z} \leq 1.0 \quad (4.1)$$

OpenFOAM calculates the Courant-Friedrichs-Levy (CFL) number for each time step analysis. The solution will break if the CFL number exceeds its limitation. The Courant-Fredrichs-Levy condition is not measured for the performed analysis, but it discussed for simulations which breaks.

## 4.3 Set-up of Computational Domain & Fluid Flow Problem

### 4.3.1 Computational Domain Size

The computational domain determines how the fluid will act in a chosen control volume. The domain size has to be large enough, to produce results which are not affected by the given boundary conditions, but small enough to get sufficient results with respect to computational time. Too small computational domain can give inaccurate results, since the boundary conditions will give undesired effects in fluid flow analysis.

Table 4.1 presents the size of the computation domain and cylinder dimensions. The axis system is located between the tandem cylinders, where the cylinders have a longitudinal length ( $L$ ) of 3.2 times the diameter length ( $D$ ). The cylinder will have a span-wise length ( $l$ ) of 6 times the diameter.

Table 4.1: Domain size and Cylinder dimensions.

Domain Range and Dimensions:	
$X_{range}$ :	$-6.0 < x < 15.0$
$Y_{range}$ :	$-5.0 < y < 5.0$
$Z_{range}$ , 3D:	$0.0 < z < 6.0$
Diameter $D$	1
Upstream cylinder origo:	$(x,y,z) = (-1.6, 0, 0)$
Downstream cylinder origo:	$(x,y,z) = (1.6, 0, 0)$
longitudinal length ( $L$ )	3.2D

The 2D set-up of the computational domain is presented in figure 4.1, with range in x-direction and y-direction, diameter  $D$  of cylinders and longitudinal length ( $L$ ).

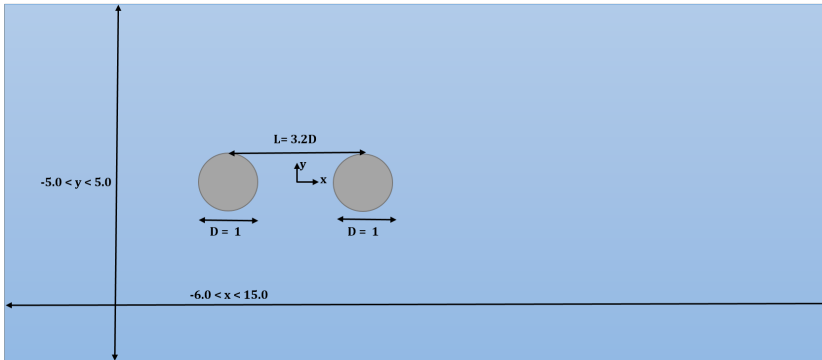


Figure 4.1: Set-up of computational domain with dimensions and sizes.

Figure 4.2 presents the shear flow problem which is analyzed. The shear flow will begin at bottom boundary, where  $U_c$  is the inlet velocity normal on the cylinders. The Reynolds number is defined with the inlet velocity normal on the cylinder  $U_c$ , such that a flow problem will have larger Reynolds number at the upper boundary, and Reynolds number approximately to zero at the bottom boundary. The dimensions given in the figure are the dimensions proposed for the Submerged Floating Tube Bridge (SFTB) concept in section 2.

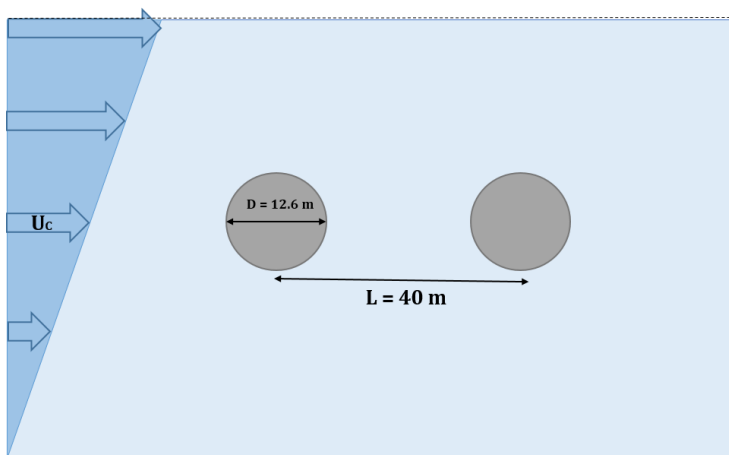


Figure 4.2: Set-up of shear flow problem around tandem cylinders. Dimensions are from section 2.

Figure 4.3 presents the location of the probes in the computational domain. Probe 1 is located at  $(x, y, z) = (-1.0, 0.354, 3.0)$ , probe 2 at  $(x, y, z) = (0.0, 0.354, 3.0)$ , probe 3 at  $(x, y, z) = (2.2, 0.354, 3.0)$  and probe 4 at  $(x, y, z) = (3.5, 0.354, 3.0)$ . The probes are only placed along the x-range and measures values for velocities  $U_x$ ,  $U_y$  and  $U_z$  and pressure at the probe location.

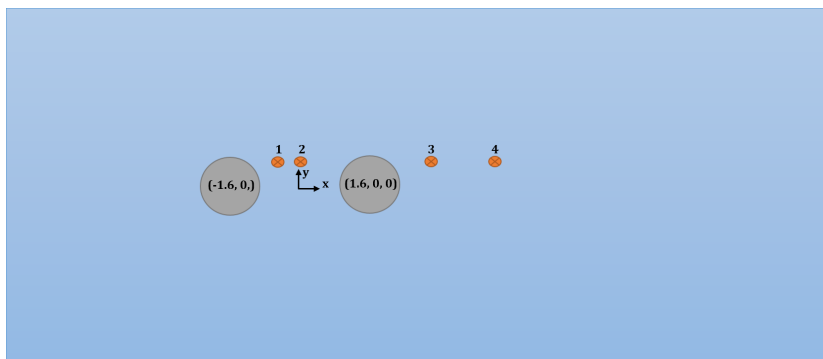


Figure 4.3: Illustration of probe location, which measures values for velocity and pressure.

### 4.3.2 Mesh and Grid refinement

Analyzing a flow problem where a current is subjected on a solid body, the flow phenomena occurring are of interest. Designing the computational domain, mesh and grid size, one has to determine the critical regions of a flow problem.

The mesh generator MEGA is used to generate a mesh with respect to number of elements, patches and domain size. The computational domain is constructed by defining all nodes, lines and patches, before the mesh is applied, such that the domain obtains a stable and consistent solution.

It is desired to have a finer mesh close to the fixed body, in terms of boundary layer resolution and to get sufficient simulation of flow phenomena close to the immersed body. A more coarse mesh is used to simulate the wake far downstream. The number of elements or cells will effect the computational time, as larger number of elements will give increased computational time.

Figure 4.4 presents the computational domain and how the domain is constructed with different patches around the tandem cylinders and in the wake region.

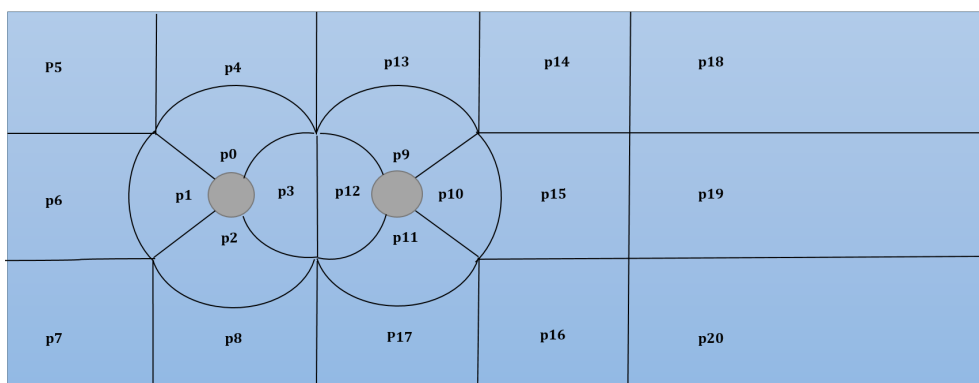


Figure 4.4: Illustration of patches in computational domain.



Table 4.2 presents the number of element in each patch, and around the important areas in the domain. The upstream cylinder has a total of 300 elements around the body, while the downstream cylinder has 310 elements. The span-wise length of the cylinder is 6 timer the diameter with 180 elements.

Table 4.2: Number of elements in each patch and total in the computational domain.

Number of Elements:					
Patch nr.	Elements	Patch nr.	Elements	Cylinders & Totals	Elements
$p_0$	5100	$p_{11}$	5100	Upstream Cylinder	300
$p_1$	3600	$p_{12}$	4200	Downstream Cylinder	310
$p_2$	5100	$p_{13}$	5950	Span-wise: z- direction	180
$p_3$	4900	$p_{14}$	4200	Total 2D	111900
$p_4$	5950	$p_{15}$	4200	Total 3D	20 142 000
$p_5$	4200	$p_{16}$	4200		
$p_6$	3600	$p_{17}$	5950		
$p_7$	4200	$p_{18}$	8400		
$p_8$	5950	$p_{19}$	8400		
$p_9$	5100	$p_{20}$	8400		
$p_{10}$	4200				

Figure 4.5 presents the 2D mesh used to simulate shear flow around tandem cylinders. The tandem cylinders are places close to the inlet, such that the domain is larger downstream to simulate the flow phenomena occurring behind flow-body interaction.

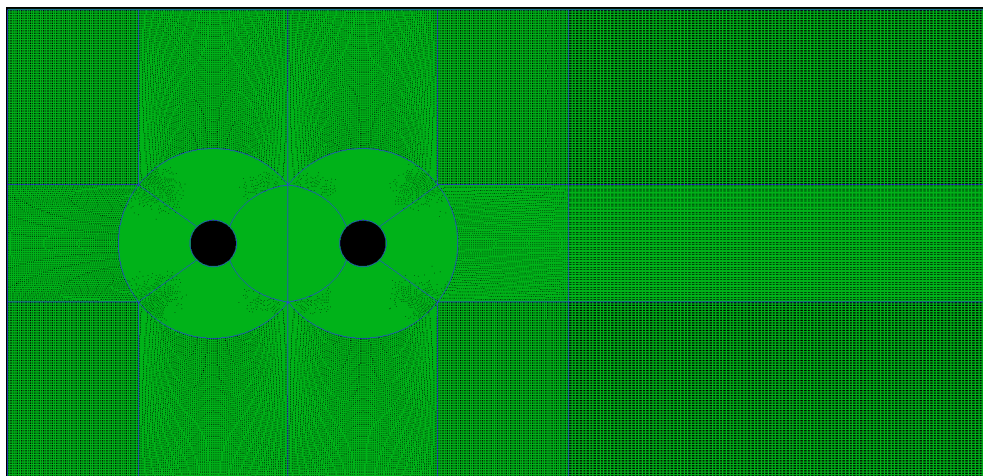


Figure 4.5: 2D Mesh generated in MEGA of Tandem Cylinders.

Figure 4.6 presents a close-up of grid around and in-between the cylinders. Figure 4.7 presents the grid system closed to the fixed upstream cylinders for the upper right quarter.

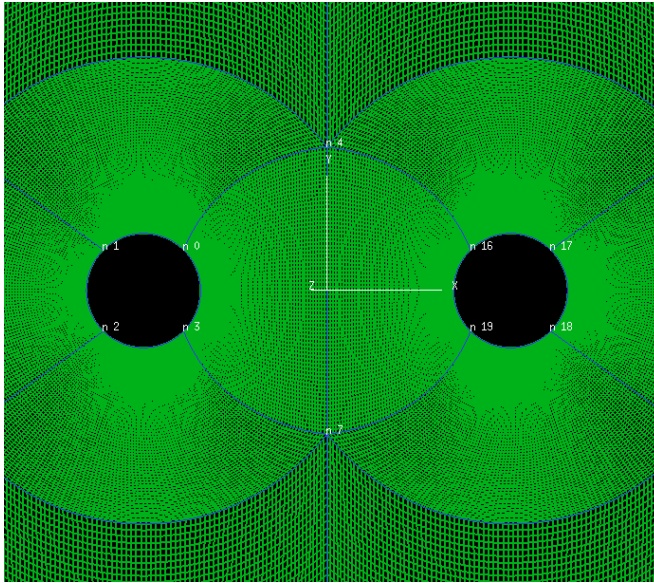


Figure 4.6: Close-up of mesh around the tandem cylinders.

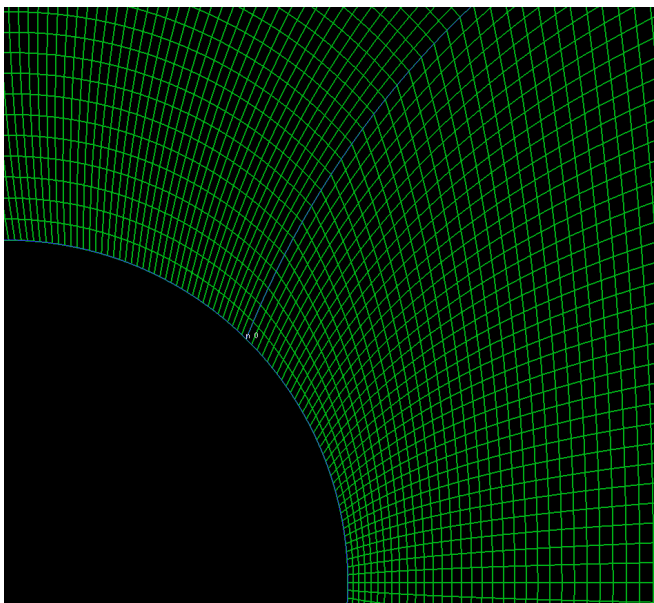


Figure 4.7: Close-up of mesh around upper right quarter of upstream cylinder.

### 4.3.3 Boundary Conditions

Defining a computational domain, the boundary conditions must be defined in order to create a fluid flow problem. The boundary conditions sets the restrictions for the flow, in terms of geometrical constraints, characteristics in velocity  $U$  and pressure  $P$  in the computational domain.

The boundaries are set to simulate the domain as infinite fluid with submerged cylinders. The analysis is performed for two-dimensional (2D) and three-dimensional (3D) circular cylinders, where the inflow boundary simulates a shear current moving towards the fixed body. The outflow will simulate how the current flow past the cylinder. The computational domain must therefore be large enough behind the body to visualize the interaction between flow and fixed body.

The computed boundaries for the domain are *inlet* - and *outlet* boundary, *topAndBottom* boundary and the circular cylinders as *upstreamCyl* and *downstreamCyl* within the domain. The *front* - and *back* boundary patches are marked as empty for a 2D analysis. For a 3D analysis, the cyclic boundary condition is used for both *front* and *back* boundaries to create the 3D effects along the tandem cylinders.

Table 4.3 presents the notation used in OpenFOAM to describe the boundary conditions and restrictions.

Table 4.3: Defining boundary conditions in OpenFOAM [Greenshields, 2015].

Defined boundaries:	Geometric constraint:	Velocity U:	Pressure P:
front	empty (2D) cyclic (3D)	empty (2D) cyclic (3D)	empty (2D) cyclic (3D)
back	empty (2D) cyclic (3D)	empty (2D) cyclic (3D)	empty (2D) cyclic (3D)
upstreamCyl	wall	fixedValue	zeroGradient
downstreamCyl	wall	fixedValue	zeroGradient
inlet	patch	fixedValue	zeroGradient
outlet	patch	zeroGradient	fixedValue
topAndBottom	slip	slip	slip

Description of OpenFOAM's boundary conditions used to analyze 2D and 3D flow problems around tandem cylinders:

- *Wall* boundary condition: Define the cylinder as a fixed rigid body.
- *Cyclic* boundary condition: is a geometric constraint for the domain and properties of pressure and velocity. A cyclic boundary condition is set in pairs, where the end effects for the cylinder is set to be periodic or cyclic, such that the boundaries *front* and *back* are treated as they were physically connected.
- *Empty* boundary condition: is applied on the *front* - and *back* boundaries, where the boundary conditions ensures 2D domain.
- *Patch* boundary condition: is set on boundaries with no geometric information about the grid and domain boundaries.
- *Slip* boundary condition: The *topAndBottom* boundary are the critical boundaries, which restrict the domain width and how the flow will move around the fixed circular cylinder. The *slip* condition is defined for the *topAndBottom* boundaries where it is desired a slip constraint on velocity and pressure, where the conditions allows change in both properties along the boundaries.
- *zeroGradient* boundary condition: sets the normal gradient of velocity  $U$  and pressure  $P$  equals to zero. Zero pressure gradients (*zeroGradient*) which is defined as:  $\frac{\partial P}{\partial n} = 0$ .

Further for inlet and outlet, the same notations are used to describe velocity and pressure at inlet and outlet. At outlet, the *zeroGradient* in velocity is defined as:

$$\frac{\partial \vec{U}}{\partial n} = \frac{\partial u}{\partial x} = \frac{\partial v}{\partial y} = \frac{\partial w}{\partial z} = 0,$$

such that change of each velocity component in  $\vec{U}$  is equal to zero:

$$\vec{U} = \vec{u}_i + \vec{v}_j + \vec{w}_k$$

- *FixedValue* boundary condition: is chosen for the properties to simulate inlet velocity or pressure at outlet.

#### 4.3.4 Grid Verification

The computed grid presented in figure 4.5 is verified for the Boundary layer resolution above the cylinder surfaces for upstream and downstream cylinder. The top and bottom boundaries are verified for the slip conditions. The validation is performed for the shear flow problem with Reynolds number 100 presented in section 5 and Appendix .4.

Grid verification is performed to check if the used grid gives results without significant deviation. The boundary layer resolution and *TopAndBottom* slip boundary condition are validated for the section at  $z = 3.0$ . This section is at the middle point of the 3D cylinder.

## Boundary Layer Resolution

Figure 4.8 presents the velocity in x-direction  $U_x$  and y-direction  $U_y$  along an arc with range  $0.5 < y < 5.0$ . The velocity above the upstream and downstream cylinder are measured at the cylinder surface towards the top boundary at time instant  $t = 500s$ .

The wall boundary condition is implemented at upstream and downstream cylinder at surface to simulate no velocities at the solid surface. The velocity in x-direction  $U_x$  at the surface is close to zero, but not zero. This could be due to few elements around the cylinder surfaces. The velocity in y - direction  $U_y$  is zero at cylinder surface, and is close to zero towards the top boundary. The velocity in z-direction  $U_z$  is zero along the arc and is not plotted in figure 4.8.

The velocity magnitude  $U_{mag}$  has it's contribution from the velocity in x-direction  $U_x$ :

$$U_{mag} = \sqrt{U_x^2 + U_z^2 + U_z^2}$$

Velocities  $U_x$  at top boundary  $y = 5.0$  are approaching absolute value of 1.0, which is the inlet velocity at at top boundary.

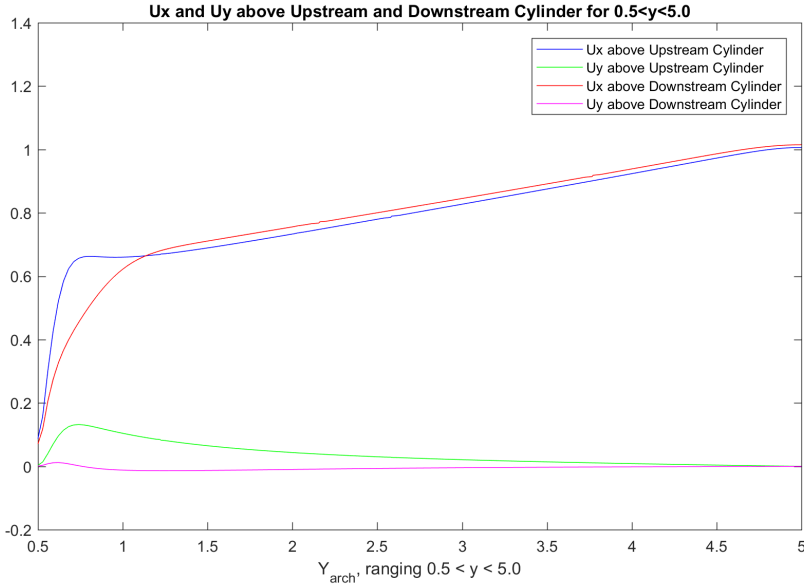


Figure 4.8: Validation of Boundary Layer Resolution on Upstream and Downstream Cylinder in Shear Flow  $K = 0.2$  and  $R_e = 100$ .

## Top and Bottom Slip Boundary Condition

Figure 4.9 and 4.10 presents the velocities  $U_x$ ,  $U_y$  and pressure P along the top boundary  $y = 5.0$  and bottom boundary  $y = -5.0$  for the x-range of  $-6.0 < x < 15$  at  $z = 3.0$ .

The top boundary experiences a velocity  $U_x$  approximately around 1.0, as expected due to the inlet velocity at top boundary. The velocity in y-direction  $U_y$  is approximately zero along the top boundary, the same applies for the velocity in z-direction  $U_z$ . Pressure along the top boundary is fluctuating close to zero.

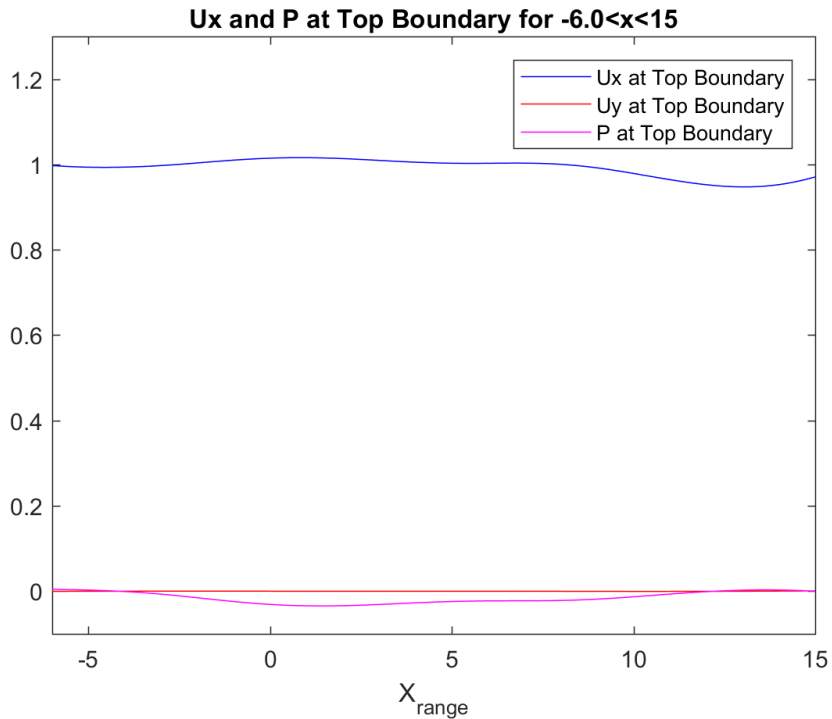


Figure 4.9: Validation of Top Boundary  $y = 5.0$  for Slip Condition in Shear Flow  $K = 0.2$  and  $R_e = 100$ .

The bottom boundary experiences jump in the velocity  $U_x$  and pressure P. The velocity in y-direction  $U_y$  and z-direction  $U_z$  are zero along the bottom boundary. The inlet velocity is close to zero at the bottom boundary, such that the peak value of  $U_x$  occur as the flow moves around the tandem cylinders.

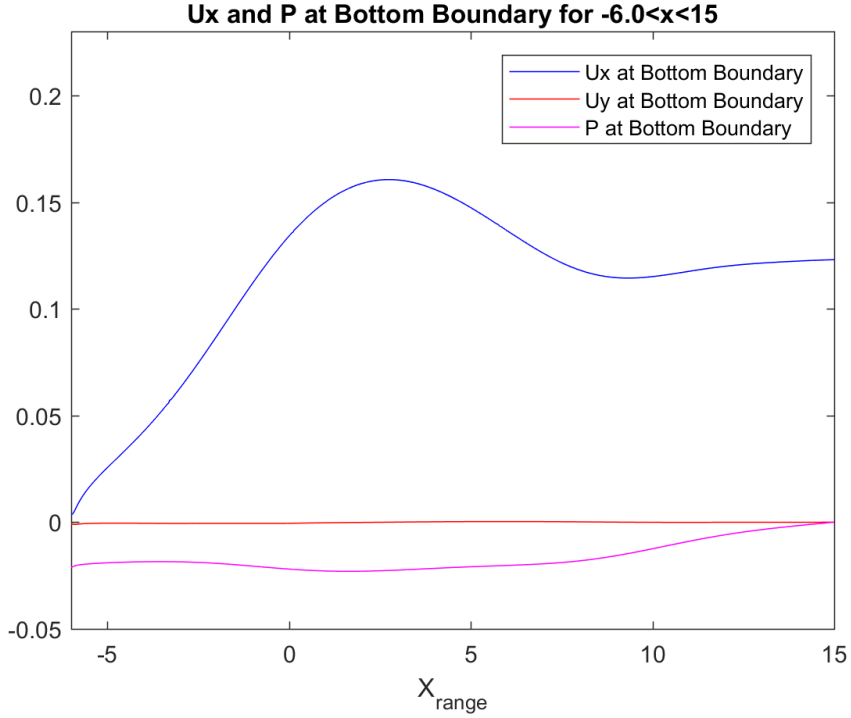


Figure 4.10: Validation of Top Boundary  $y = -5.0$  for Slip Condition in Shear Flow  $K = 0.2$  and  $R_e = 100$ .

# Chapter 5

## Results

### 5.1 Shear Flow and Tandem Cylinder Characteristics

The fjord crossing concept of Submerged Floating Tube Bridges (SFTB) described in section 2 is simplified to tandem cylinder with both cylinder diameter equals to 1, and a longitudinal length ( $L$ ) of 3.2 times the diameter. The tandem cylinders are modelled with a span-wise length ( $l$ ) of 6 times the diameter length, to simulate the three-dimensional (3D) effects along the cylinder.

The tandem cylinders are subjected to a planar shear flow  $U(y)$  described with a gradient  $G$  and the velocity normal to the tandem cylinders,  $U_c$ . The Reynolds number given in equation 3.1 uses the inlet velocity  $U_c$ , normal on the cylinders.

Numerical analysis with a shear inlet flow described with shear rate  $K = 0.2$  is performed for two-dimensional (2D) flow problem with Reynolds number 100, 300 and 500, and three-dimensional (3D) flow problem with Reynolds number 100 and 500.



Table 5.1 presents the properties of the planar shear flow and the dimensions of the tandem cylinders. The computational domain is described in table 4.1 in section 4.

Table 5.1: Flow and cylinder properties.

Properties of Shear Flow:	
Shear Flow	$K = 0.2$
Inlet origin	$y = -5.0$
$G$	1/10
$Uc$ (MagUInf)	0.5
$U_{y=-5.0}$ , bottom	0.0
$U_{y=5.0}$ , top	1.0
Cylinder dimensions:	
Diameter (D)	1
Span-wise cylinder length	6D
Longitudinal length (L)	3.2D
Kinematic viscosity $\nu$ :	
$R_e = 100$	$\nu = 1/200$
$R_e = 300$	$\nu = 1/600$
$R_e = 500$	$\nu = 1/1000$

The results include oscillation of force coefficients, velocity fluctuation behind upstream and downstream cylinders, Power Spectral Density curves and visualization of velocity -, pressure - and vorticity distribution. The results are presented in appendices .1, .2, .3 for the 2D shear flow problems and appendices .4 and .5 for the 3D shear flow problems.

## 5.2 Results obtained for 2D Shear Flow Around Tandem Cylinders

Table 5.2 presents the values for the 2D Shear Flow problem for given Reynolds numbers.

Table 5.2: Shear Flow Around 2D Tandem Cylinders for  $K = 0.2$ .

Desired values for 2D Shear Flow problem:						
$R_e$	$R_e = 100$		$R_e = 300$		$R_e = 500$	
Cylinder	Upstream	Downstream	Upstream	Downstream	Upstream	Downstream
mean $C_L$	-0.19738	-0.07390	-0.12246	0.00254	-0.08031	0.11545
mean $C_D$	1.23694	0.01960	1.44934	0.40348	1.54587	0.60668
RMS $C_L$	0.01247	0.10647	0.86768	1.49092	1.04621	1.60544
RMS $C_D$	0.00382	0.03073	0.10777	0.39394	0.16791	0.73532
$T_v[s]$	16.67	16.67	5.32 & 10.6	5.32 & 10.6	5.05 & 10	10 & 20
$f_v[Hz]$	0.06	0.06	0.19 & 0.09	0.19 & 0.09	0.2 & 0.1	0.1 & 0.05
$S_t$	0.12	0.12	0.37 & 0.19	0.37 & 0.12	0.4 & 0.2	0.2 & 0.1

## 5.3 Results obtained for 3D Shear Flow Around Tandem Cylinders

Table 5.3 presents the values obtained for the 3D shear flow problem with Reynolds number 100 and 500. The results for the 2D and 3D shear flow problem with  $R_e = 100$  are approximately identical. Comparing the results between 2D and 3D analysis for higher Reynolds number, the 3D simulations will allow the flow to obtain three-dimensional (3D) effects span-wise ( $l$ ) along the cylinder, while the 2D simulations will restrict this to occur.

Table 5.3: Shear Flow Around 3D Tandem Cylinders for  $K = 0.2$

Desired values for 3D Shear Flow problem:				
$R_e$	$R_e = 100$		$R_e = 500$	
Cylinder	Upstream	Downstream	Upstream	Downstream
mean $C_L$	-0.19737	-0.07394	-0.12319	-0.07862
mean $C_D$	1.23695	0.01960	1.02754	-0.15829
RMS $C_L$	0.01248	0.10656	0.01325	0.39875
RMS $C_D$	0.00383	0.03075	0.00838	0.14509
$T_v[s]$	16.67	16.67	(5 & 9.804)	13.89
$f_v[Hz]$	0.06	0.06	(0.2 & 0.102)	0.072
$S_t$	0.12	0.12	(0.4 & 0.204)	0.144

# Chapter 6

## Discussion

This chapter discusses and compares the results obtained for the two-dimensional (2D) and three-dimensional (3D) analysis with shear flow. The 2D flow problems are analyzed with Reynolds number 100, 300 and 500, and the 3D flow problems are analyzed with Reynolds number 100 and 500. The properties of the shear flow and the dimensions of tandem cylinders are given in table 5.1.

The difference and deviations between 2D and 3D shear flow problems are discussed with respect to restrictions in the 2D plane and the occurrence of 3D effects along the span-wise direction. Further, the 3D shear flow problem with Reynolds number 500 is compared to the flow problems: *a Shear Flow around a Single Cylinder* and *a Uniform Flow around Tandem Cylinders*. These flow problems are both analyzed with Reynolds number 500. The results obtained for the shear flow problem around a single cylinder is presented in Appendix .9, and results obtained for the uniform flow problem are presented in Appendix .11.

Plots of velocity distribution and pressure distributions are compared for each flow problem. The vorticity distributing in z-direction is compared with respect to vortex shedding behavior downstream and flow behavior in-between the tandem cylinders. The pressure distribution around upstream and downstream cylinders are measured for both shear - and uniform flow around the tandem configuration.

The tandem cylinders experience stable flow at the last time step  $t = 500s$ . For the shear flow problem around a single cylinder, the plots present the last time step, as the flow problem breaks it's simulation at time instant  $t = 142 - 143s$ . The velocity-, pressure- and vorticity distribution are plotted for the last time step of the simulation.

The values for mean drag -and lift coefficients, root mean square values, oscillation period, frequency and Strouhals number are presented in table 5.2 for the 2D shear flow problem and in table 5.3 for the 3D shear flow problem in section 5. The mean values are calculated for the 65 % last stable values for the simulation. For the shear flow problem around a single cylinder, the results are obtained for the stable values, right before the simulation breaks.

## 6.1 Comparison between the 2D and 3D simulation of Shear Flow Around Tandem Cylinders

The 2D shear flow problem with Reynolds number 100, 300 and 500 obtains a lift coefficient oscillating close to zero for both upstream and downstream cylinder. The drag coefficient for the upstream cylinder is increasing with Reynolds number from  $\bar{C}_D = 1.237$  to  $\bar{C}_D = 1.545$ . The downstream cylinder obtains a mean drag coefficient which is oscillating close to zero, but increasing from  $\bar{C}_D = 0.00196$  to  $\bar{C}_D = 0.6066$  with Reynolds number 100 to 500.

Oscillation periods and frequencies for the velocity behind upstream and downstream cylinders are stable with  $Re = 100$ , and obtains a value for Strouhals number  $S_t = 0.12$  for both tandem cylinders. For 2D shear flow with Reynolds number 300 and 500, there are obtained two oscillation periods and frequencies. This is due to the restriction of 3D effects in a 2D domain. The shear flow problem with Reynolds number 300 has the same oscillation period and frequency between upstream and downstream cylinder, with Strouhals numbers  $S_t = 0.376$  and  $S_t = 0.188$ . At Reynolds number 500, the Strouhals number for the downstream cylinder is almost half the value for the upstream cylinder. An increase in Reynolds number will give different oscillation periods and frequencies between the upstream and downstream cylinder.

Analyzing three-dimensional (3D) shear flow problems, one must take in account the 3D effects along the span-wise length of the cylinder. Comparing the 2D and 3D results for the shear flow problem at Reynolds number 100, one can observe that the results are approximately identical. The same applies for the oscillation of force coefficients, and distribution of velocity and pressure around the domain. This implies that there are no 3D effects occurring for flow problems with Reynolds number 100.

Comparing the 2D and 3D shear flow problem with Reynolds number 500, the 3D upstream cylinder has obtained a smaller mean drag coefficient at  $\bar{C}_D = 1.02754$ , compared to the mean drag coefficient obtained for the 2D upstream cylinder  $\bar{C}_D = 1.54587$ . The mean drag coefficient obtained for the 2D downstream cylinder is close to zero with  $\bar{C}_D = 0.606$ , while the 3D downstream cylinder obtains  $\bar{C}_D = -0.158$ . The inlet velocity will obtain it's stagnation point as the flow is subjected normal on the upstream cylinder. The flow will continue around the downstream cylinder with some wake interference shedded from the upstream cylinder. The upstream cylinder will obtain a larger mean drag force, than the cylinder downstream.

The Strouhals number is obtained for upstream and downstream cylinders with respect to velocity in x-direction  $U_x$ . By using Fourier Transform, one can obtain the oscillation periods and frequencies with Power Spectral Density curves. The velocity fluctuation behind the upstream cylinder is oscillating close to zero with irregular peaks and amplitudes, such that the obtained periods and frequencies are not an ideal representation of the flow behind the upstream cylinder. The velocity fluctuation behind the downstream cylinder will oscillate periodically for the shear flow problem. The velocity fluctuation will give oscillation period of  $T_v = 13.89$ , frequency of  $f_v = 0.072$  and a Strouhals number equals to  $S_t = 0.144$ .

## 6.2 Comparison of the Shear Flow Around Tandem Cylinders with Other Flow Problems

Further, the results obtained for the shear flow around tandem cylinders with Reynolds number 500 are compared to flow problems: *a Shear Flow around a Single Cylinder* and *a Uniform Flow around Tandem Cylinders*, where both flow problems are simulated with  $R_e = 500$ .

Table 6.1 presents the the domain size, cylinder dimensions and the properties of inlet velocity for the different flow problems. All cylinders will have a span-wise ( $l$ ) length of 6 times the diameter length. The inlet velocity is normal on the cylinder with  $U_c = 0.5$  for all three flow problems. Else, the overall domain size will deviate in x-and-y range.

Table 6.1: Domain size, cylinder dimensions and inlet velocity properties.

	a Cylinder:	Tandem Cylinder:	
	Shear $K = 0.2$ :	Uniform:	Shear $K = 0.2$ :
$X_{range}$ :	$-5 < x < 12.5$	$-6 < x < 12$	$-6 < x < 15$
$Y_{range}$ :	$-5 < y < 5$	$-6 < y < 6$	$-5 < y < 5$
$Z_{range}$ , 3D:	$0 < z < 6$	$0 < z < 6$	$0 < z < 6$
Diameter D	1	1	1
Origo (x,y,z):	(0, 0, 0)	-	-
Upstream cylinder origo:	-	(-1.6, 0, 0)	((-1.6, 0, 0)
Downstream cylinder origo:	-	(1.6, 0, 0)	(1.6, 0, 0)
longitudinal length (L)	-	3.2xD	3.2xD
Shear Rate	$K = 0.2$	$K = 0.0$	$K = 0.2$
$G$	1/10	$G = 0.0$	1/10
$U_c$ (MagUInf)	0.5	0.5	0.5
inlet origin	$y = -5.0$	$-5.0 < y < 5.0$	$y = -5.0$

Table 6.2 presents the obtained values for the different flow problems with Reynolds number 500. The oscillating drag - and lift force coefficients, velocity fluctuations behind cylinders, Power Spectral Density curves and visualization plots for velocity magnitude, pressure and vorticity are presented in Appendix .5, .9, and .11.

Table 6.2: Comparison of values for different 3D flow problems at  $R_e = 500$

	a Cylinder:	Tandem Cylinder:			
	Shear $K = 0.2$ :	Uniform:		Shear $K = 0.2$ :	
Cylinder	Single	Upstream	Downstream	Upstream	Downstream
mean $C_L$	-0.10392	0.00312	0.00505	-0.12319	-0.07862
mean $C_D$	1.29849	1.05257	-0.17424	1.02754	-0.15829
RMS $C_L$	0.43352	0.01562	0.35311	0.01325	0.39875
RMS $C_D$	0.08907	0.00241	0.04071	0.00838	0.14509
$T_v$ [s]	8.936	-	13.16	(5 & 9.804)	13.89
$f_v$ [Hz]	0.1119	-	0.076	(0.2 & 0.102)	0.072
$S_t$	0.2238	-	0.152	(0.4 & 0.204)	0.144

Subjecting an inlet velocity with shear rate  $K = 0.2$  and Reynolds number 500 towards a single circular cylinder, the mean force coefficients obtained are  $\bar{C}_D = 1.298$  and  $\bar{C}_L = -0.104$ . The oscillation period and frequency of the velocity behind the cylinder are  $T_v = 8.936$  and  $f_v = 0.1119$ , with a Strouhals number of  $S_t = 0.2238$ .

Subjecting the same shear flow around 3D tandem cylinder, one must analyze at the effects of having tandem cylinders instead of a single cylinder. The upstream cylinder obtains mean force coefficients of  $\bar{C}_D = 1.02754$  and  $\bar{C}_L = -0.123$ . The drag coefficient obtained for the upstream cylinder in a tandem formation is smaller, compared to the mean drag coefficient obtained for the single cylinder. The downstream cylinder will experience mean force coefficients of  $\bar{C}_D = -0.158$  and  $\bar{C}_L = -0.0786$ , where the drag force is oscillating close to zero. The lift coefficients around the tandem cylinders and for the single cylinder are all oscillating close to zero.

The upstream cylinder subjected to a shear flow will obtain two oscillation periods and frequencies, even though the velocities are fluctuating close to zero. These values are not ideal as the velocities are fluctuating unstable and close to zero.

Vortices will be shedded from the downstream cylinder in the shear flow problem, where the cylinder experiences periodical velocity fluctuation with oscillation period  $T_v = 13.89$ , frequency  $f_v = 0.072$  and Strouhals number  $S_t = 0.144$ . The frequency is 36 % smaller than for the single cylinder, such that vortices are shedded 36 % more frequently from the downstream cylinder than the single cylinder.

In tandem configuration, the upstream and downstream cylinder will experience the flow travelling around both cylinders, with almost no velocity in-between the tandem cylinder. The flow problem where a uniform flow is subjected on tandem cylinders, the velocity behind the upstream cylinder is also fluctuating close to zero. The downstream cylinder will obtain an oscillation period and frequency of  $T_v = 13.16$  and  $f_v = 0.076$ , which is approximately the same values obtained for the shear flow problem.

The Strouhals number for the uniform flow problem is  $S_t = 0.152$ , while the shear flow problem is  $S_t = 0.144$ . Values for the force coefficients are also approximately the same for the shear flow problem. The mean drag coefficient around the upstream cylinder is  $\bar{C}_D = 1.0526$ , and  $\bar{C}_D = -0.174$  for the downstream cylinder.

When tandem cylinders are subjected to shear - or uniform current flows, the downstream cylinder experience negative mean drag coefficient which is close to zero. Meneghini et al. (2001) and Ding et al. (2007) explains how the mean drag changes from negative mean value  $\bar{C}_D < 0$  to positive mean value  $\bar{C}_D > 0$  as the longitudinal length - diameter ratio  $L/D > 3$  in a uniform flow. For both shear and uniform flow problem around tandem cylinder at  $Re = 500$  and  $L/D = 3.2$ , the values for drag are close to zero and are negative.

In Appendices .4 and .11, the flow problems around 3D tandem cylinders with Reynolds number 100 and 300 presents a mean drag force coefficient oscillating close to zero. It is expected that the downstream cylinder shed vortices when  $L/D < 3$ . When  $L/D > 3$ , the upstream cylinder will shed vortices towards the downstream cylinder [Meneghini et al., 2001] & [Ding et al., 2007].

## 6.2.1 Comparison of Velocity Magnitude $U_{mag}$ and Velocity in x-direction $U_x$

This section discusses the similarities and differences between the velocity magnitude  $U_{mag}$  and velocity in x-direction  $U_x$  for the flow problems: *a Shear Flow subjected on Tandem Cylinders*, *a Shear Flow subjected on a Single Cylinder* and *a Uniform Flow subjected on Tandem Cylinders*. These flow problems are also discussed with respect to pressure distribution and vorticity distribution in z-direction.

The flow problems are analyzed for Reynolds number 500, where the shear flow is described with a shear rate of  $K = 0.2$  and velocity  $U_c = 0.5$  normal on cylinder. The shear inlet velocity ranges from  $U_{y=-5.0} = 0.0$  to value  $U_{t=5.0} = 1.0$  with gradient  $G = 0.1$  from equation 3.12. The Reynolds number is defined with use of velocity  $U_c$ , such that the Reynolds number will also vary linearly within the domain.

The velocity distributions are presented with legend values that ranges from  $0.0 < U < 1.0$  for  $U_{mag}$ ,  $U_x$ ,  $U_y$  and  $U_z$ . The velocity magnitude  $U_{mag}$  and velocity in x-direction  $U_x$  are presented for the shear flow problem at time instant  $t = 500s$  in figure 6.1 and 6.2. From the figures, one can observe the top boundary consisting of velocities near 1.0, and bottom boundary consisting of approximately zero velocity.

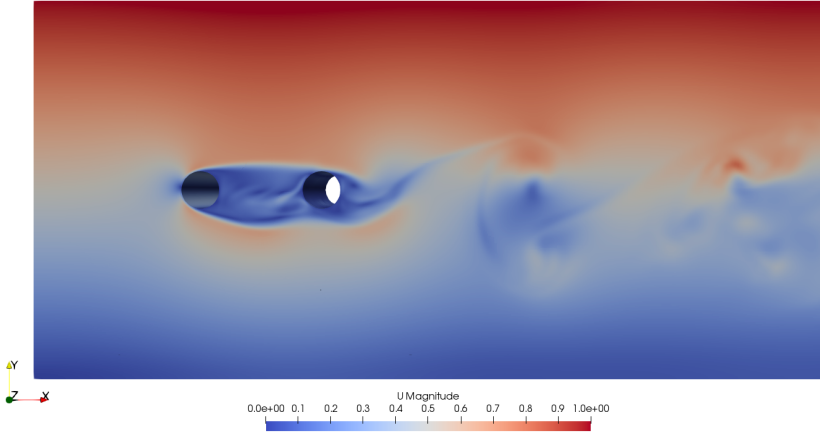


Figure 6.1: Velocity magnitude  $U_{mag}$  for shear flow around tandem cylinders for  $Re = 500$  &  $K = 0.2$  at time instant  $t = 500s$ .

The velocity in x-direction  $U_x$  is dominating its contribution in the absolute velocity magnitude  $U_{mag}$ , as the figures 6.1 and 6.2 are similar in terms of flow details and magnitude. Figure A.61 and A.62 in Appendix .5 presents the velocity distribution in y - and - z - direction, which is approximately zero. This is due to the inlet velocity is subjected along the x-direction, such that  $U_x$  becomes greater than  $U_y$  and  $U_z$ .



The velocity distribution in x-direction  $U_x$  in-between the tandem cylinders are approximately zero, as the velocity fluctuation is oscillating irregular and close to zero.

Vortices are shedded from the downstream cylinder. The flow behaviour in-between the tandem cylinders and downstream are visualized with the vorticity distributions in z-direction.

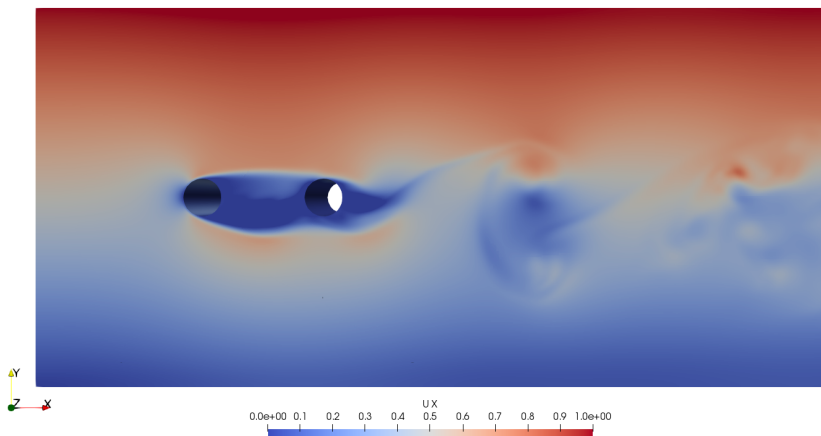


Figure 6.2: Velocity in x-direction  $U_x$  for shear flow around tandem cylinders for  $Re = 500$  &  $K = 0.2$  at time instant  $t = 500s$ .

The velocity magnitude  $U_{mag}$  and velocity in x-direction  $U_x$  for the uniform flow problem around tandem cylinders are presented in figure 6.3 and 6.4 with Reynolds number 500 at time instant  $t = 500s$ .

The velocity in x-direction will dominate the absolute velocity magnitude in the domain, as there are approximately no velocities in y - and - z - direction. The velocity distribution of  $U_y$  and  $U_z$  are presented in Appendix .11 in figure A.220 and A.221.

The velocity magnitude for the uniform flow around tandem cylinders, has a constant inlet velocity of  $U(y) = 0.5$  subjected in x-direction. The upper and lower domain have velocities close to the inlet velocity, while alternating vortex shedding are visualized as high and low velocity changes as vortices travel downstream.

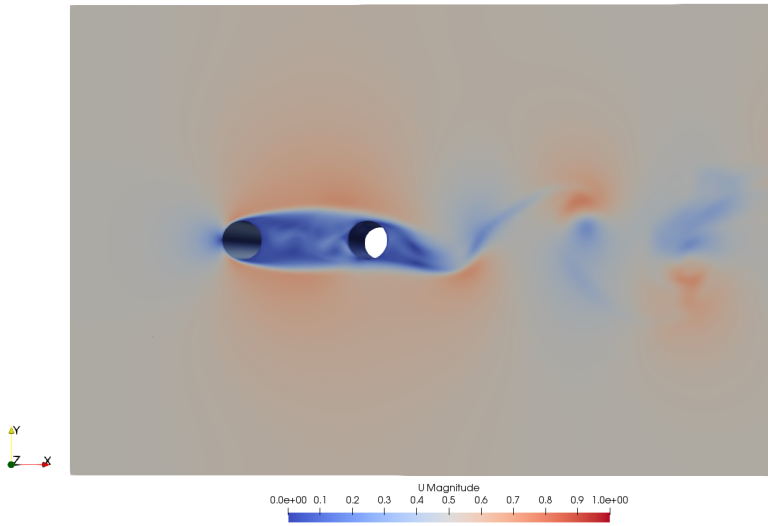


Figure 6.3: Velocity magnitude  $U_{mag}$  for uniform flow around tandem cylinders for  $Re = 500$  at time instant  $t = 500s$ .

There is almost no velocity in x-direction  $U_x$  in-between the tandem cylinders, as the flow moves around the tandem cylinders.

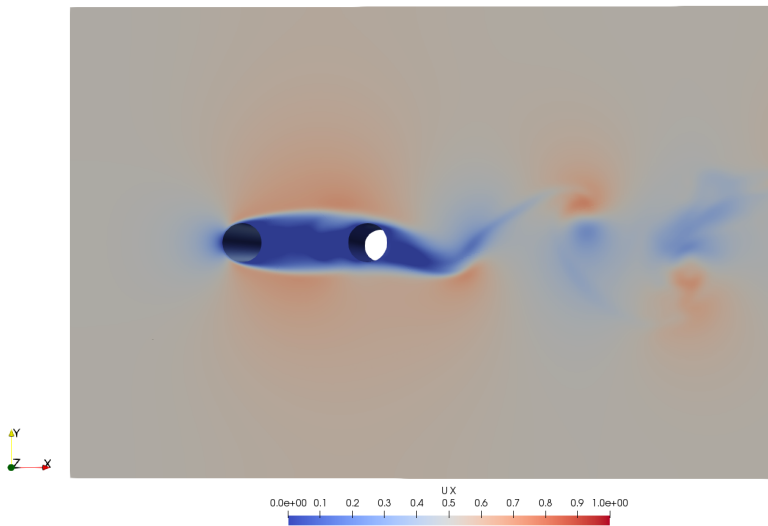


Figure 6.4: Velocity in x-direction  $U_x$  for uniform flow around tandem cylinders for  $Re = 500$  at time instant  $t = 500s$ .

The tandem cylinders subjected by uniform flow will experience the flow phenomena called *Wake Interference* for given longitudinal length - diameter ratio ( $L/D$ ). The illustration presented in figure 3.22 from section 3, describes the wake interference as a Shear Layer Re-Attachment behaviour for intermediate ratios of  $L/D = 3.2$ . The Re-attachment behaviour is characterized by one cylinder that is partially or completely submerged in the wake of the other cylinder [Sumner, 2010], [Zdravkovich, 1987] & [Zhou and Yiu, 2006].

The observations obtained for tandem cylinders subjected to a flow, illustrates how the wake region consist of alternating vortices, which are shedded from the downstream cylinder. The inlet velocity will first hit the upstream cylinder, where the stagnation point occurs. The velocity will move around the tandem cylinders, and the upstream cylinder will experience irregular and small velocities fluctuating close to zero. These small velocities are visualized as the dark blue area between the cylinders at time instant  $t = 500s$  in figure 6.1, 6.3 for the velocity magnitude  $U_{mag}$ , and in figure 6.2 and 6.4 for the velocity in x-direction  $U_x$ . The illustration in figure 3.22 describes the Wake Interference for uniform flow around tandem cylinders with Reynolds number 10000 to 50000, which is not suited in predicting wake interference and behaviour downstream for the analyzed shear and uniform flow problem around tandem cylinders with Reynolds number 500.

Figure 6.5 and 6.6 presents the velocity fluctuation in x-, y- and z - direction and the pressure fluctuation behind the upstream cylinder at location  $(-1.0, 0.354, 3.0)$  for the shear - and uniform flow around tandem cylinders. The figures present velocity  $U_x$ ,  $U_y$  and  $U_z$  which is oscillating irregular and close to zero for both shear - and uniform flow.

The pressure is negative at fluctuating at a mean value of  $\bar{p} = -0.1$  for both shear - and uniform flow. The magnitude of velocity in-between the tandem cylinder is approximately zero. One can conclude that there will be no clear oscillation periods or frequencies behind the upstream cylinder when subjected to shear - or uniform flow.

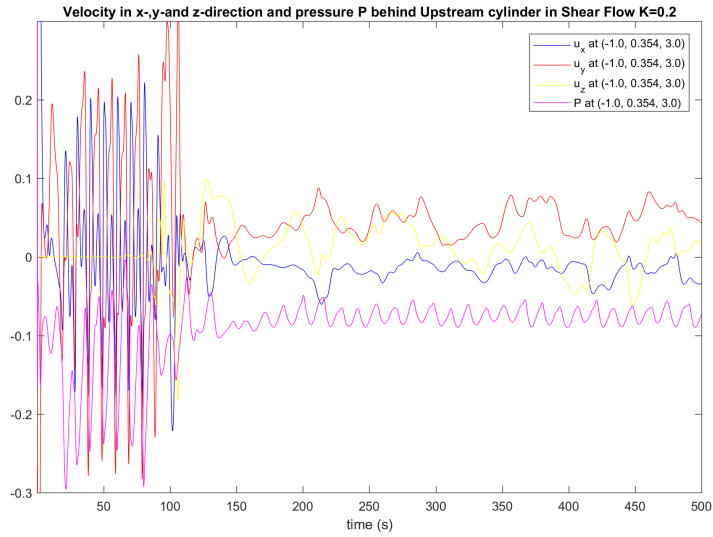


Figure 6.5: Velocity  $U_x$ ,  $U_y$ ,  $U_z$  and pressure  $P$  at Probe1  $(-1.0, 0.354, 3.0)$  behind upstream cylinder in tandem configuration subjected to shear flow with  $K = 0.2$  and  $Re = 500$ .

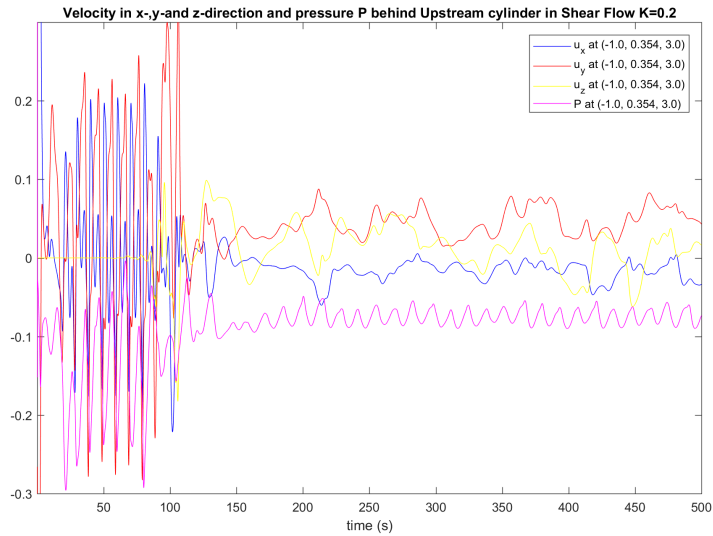


Figure 6.6: Velocity  $U_x$ ,  $U_y$ ,  $U_z$  and pressure  $P$  at Probe1  $(-1.0, 0.354, 3.0)$  behind upstream cylinder in tandem configuration subjected to uniform flow with  $Re = 500$ .

The shear flow problem around the single cylinder presents plots of velocity, pressure and vorticity at time instant  $t = 140s$ , as the simulation breaks at time instant  $t = 142 - 143s$ .

Figure 6.7 presents the velocity magnitude  $U_{mag}$  and figure 6.8 presents the velocity in x-direction  $U_x$ . The flow has an inlet velocity which is distributed from  $U_{y=-5.0} = 0.0$  to  $U_{y=5.0} = 1.0$ , with  $U_c = 0.5$  and gradient  $G = 0.1$ , which is the same inlet shear velocity subjected on tandem cylinders. This flow problem gives velocities close zero at the bottom boundary, and velocities around 1.0 for the upper half of the domain. The single cylinder will shed alternating vortices towards time instant  $t = 140s$ , before becoming unstable.

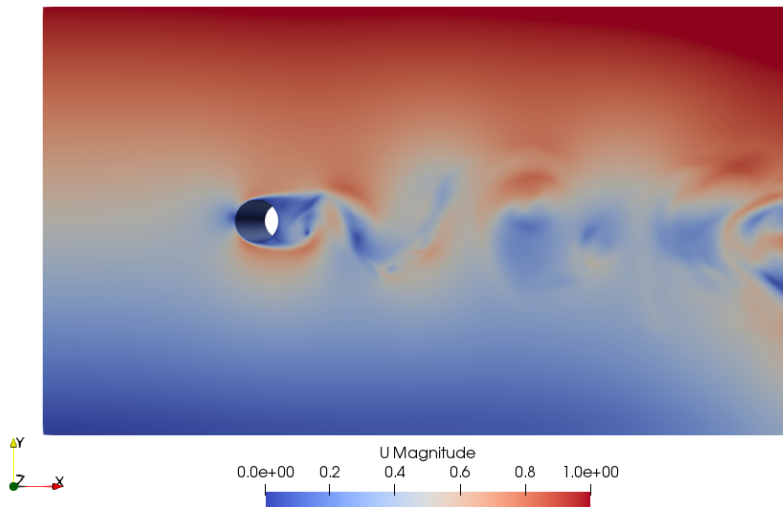


Figure 6.7: Velocity magnitude for Shear flow at  $R_e = 500$  for  $K = 0.2$  at time instant  $t = 140s$  before breaking the simulation with  $\Delta t = 0.002$ .

Figure 6.8 presents the velocity in x-direction. Comparing the velocity distribution  $U_x$  with the absolute velocity magnitude  $U_{mag}$ , the velocity and flow details around the domain are similar.

The velocity distribution in y-and-z-direction  $U_y$  and  $U_z$  are both close to zero, and are presented in figure A.152 and A.153 in Appendix .9.  $U_x$  gives the largest contribution of the velocity magnitude  $U_{mag}$ . This applies also for the flow problems with tandem cylinders, as the inlet velocity is subjected in x-direction.

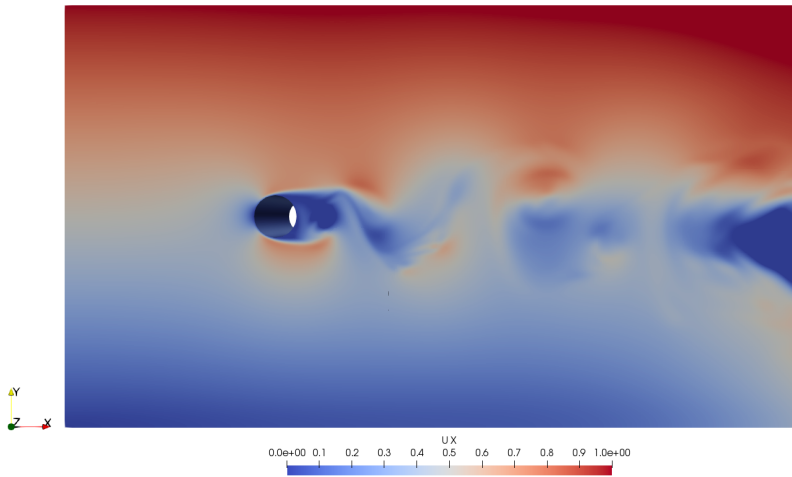


Figure 6.8: Velocity in x-direction  $U_x$  for shear flow around a single cylinder for  $Re = 500$  &  $K = 0.2$  at time instant  $t = 140s$  before breaking the time simulation.

## 6.2.2 Comparison of Pressure Distribution P

This section presents the pressure distribution with range of  $-0.15 < P < 0.15$ . The pressure distributions are presented in figure 6.9 and 6.10 for the shear flow - and uniform flow around tandem cylinders.

Comparing the pressure distributions presented in figure 6.9 and 6.10, the details show similar flow behaviour of the pressure. Both figures presents stagnation point as a high pressure zone in-front of the upstream cylinder. Vortex shedding phenomena occurs downstream, as alternating vortices are shedded from the downstream cylinder. Vortex sheddings are visualized by the high and low pressure zones downstream, which occurs for vortices travelling downstream.

From section 3.6, the stagnation point should occur at the high velocity area of the upstream cylinder when subjected by a shear flow. The stagnation point occurs for the upstream cylinder and single cylinders subjected to a shear low, and is visualized with a high pressure zone in-front of the upstream cylinder. The pressure distribution do not visualize in detail the actual location of the stagnation point, such that one can't conclude if the stagnation point is at the high velocity area [Lei et al., 2000].

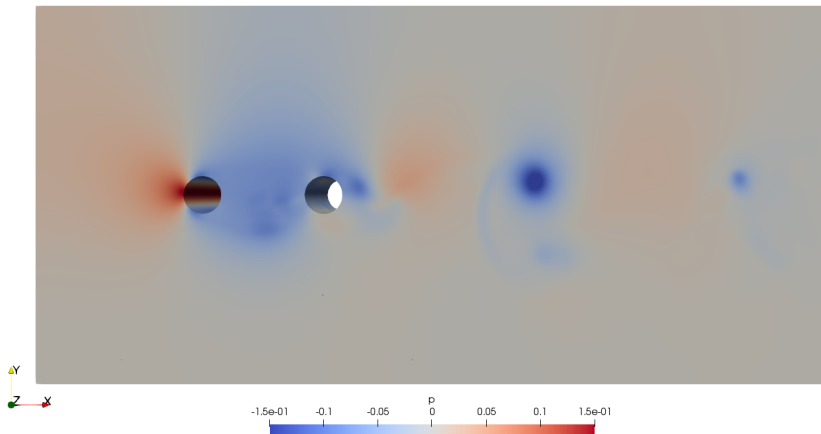


Figure 6.9: Pressure distribution for shear flow around tandem cylinders for  $R_e = 500$  &  $K = 0.2$  at time instant  $t = 500s$

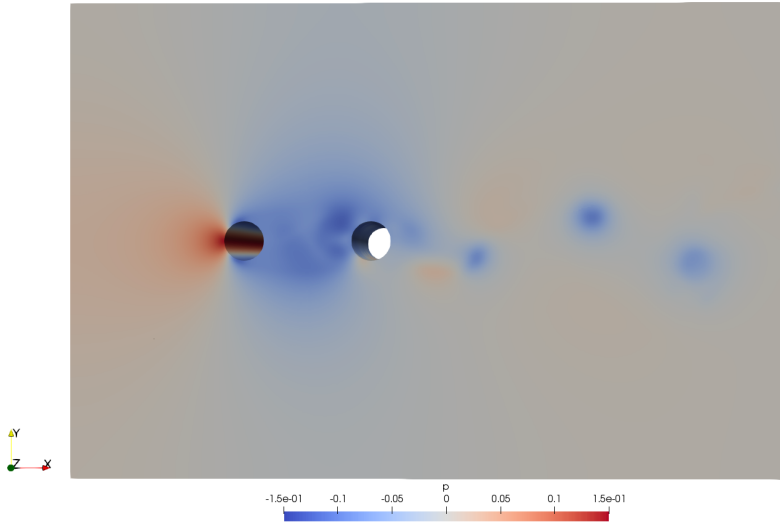


Figure 6.10: Pressure distribution for uniform flow around tandem cylinders for  $R_e = 500$  at time instant  $t = 500s$ .

Pressure Distribution around the cylinder surface is found by taking use of the pressure coefficient  $C_p$  from equation 3.14. The pressure distribution along the upper half of the upstream and downstream cylinders are presented in figure 6.11 and 6.12 at time instant  $t = 500s$ , when subjected to a shear flow and uniform flow.

Figure 6.11 presents the  $C_p$  around  $0 < \theta < 180$  degrees of the upstream cylinder for both uniform inlet flow and shear inlet flow. The pressure field for both upstream cylinders follow the same curve, where the bottom peak pressure is at  $\theta = 72$  degrees.

Figure 6.12 presents the  $C_p$  for the downstream cylinder subjected to shear - and uniform inlet flow. The downstream cylinder will experience larger pressure fluctuations when subjected to a shear flow, compared to a uniform inlet. The pressure around the downstream cylinder is negative for the upper half of the cylinder from  $0 < \theta < 180$  degrees.

The pressure distributions follows the same curve as in figure 3.27 and 3.28 for a turbulent flow problem with various longitudinal lengths (L) [Igarashi, 1981].



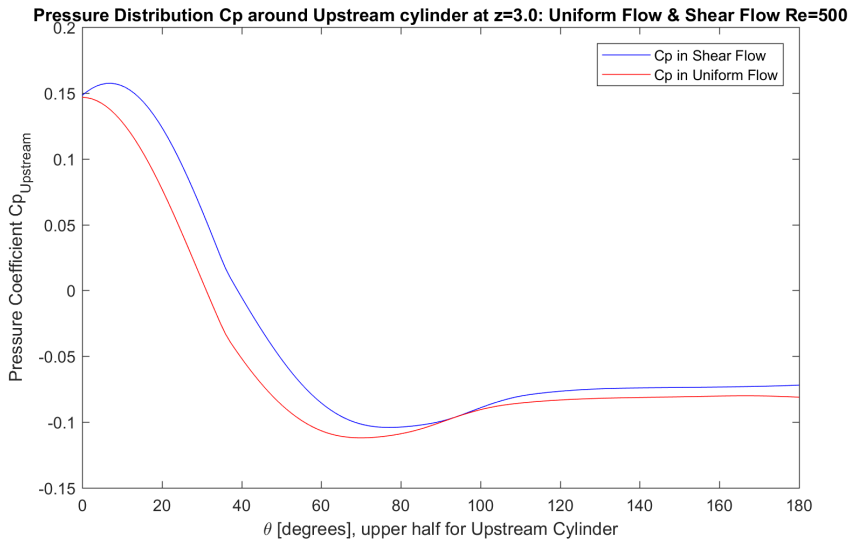


Figure 6.11: Pressure distribution around the upper half  $0 < \theta < 180$  degrees of the Upstream Cylinder for Shear Flow  $K = 0.2$  and Uniform Flow at Reynolds number 500 at  $t = 500s$ . The flow problems are presented in Appendices .5 and .11.

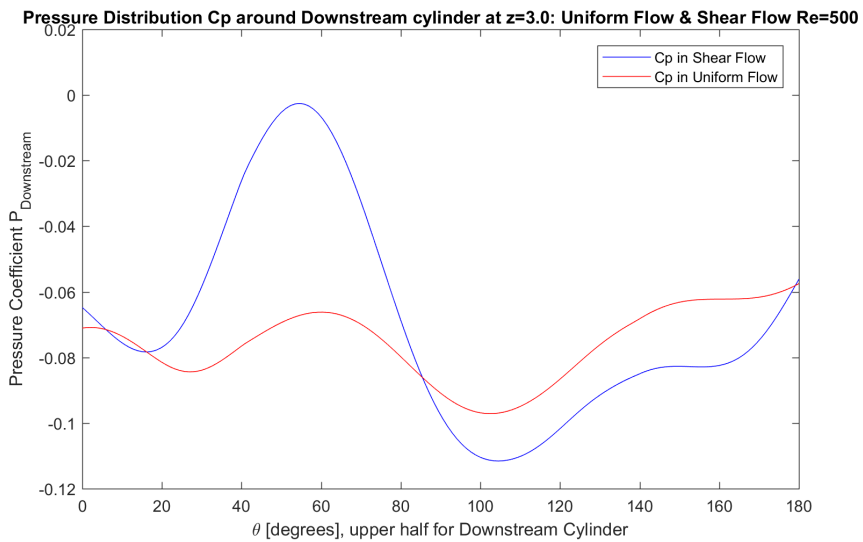


Figure 6.12: Pressure distribution around the upper half  $0 < \theta < 180$  degrees of the Downstream Cylinder for Shear Flow  $K = 0.2$  and Uniform Flow at Reynolds number 500 at  $t = 500s$ . The flow problem is presented in Appendices .5 and .11.

The shear flow problem around a single cylinder becomes unstable around time instant  $t = 142 - 143s$ . The pressure distribution at three different probes are presented in figure 6.13.

The simulation breaks due to large pressure jumps. At this time instant, the stability criterion of Courant-Friedrichs-Levy number exceeds it's limit. The Courant-Friedrichs-Levy number consists of the cell dimensions  $\Delta x$ ,  $\Delta y$  and  $\Delta z$  with velocities in x-, y- and z-direction. The PISO algorithm calculates the pressure with use of the velocity in a cell at each time instant.

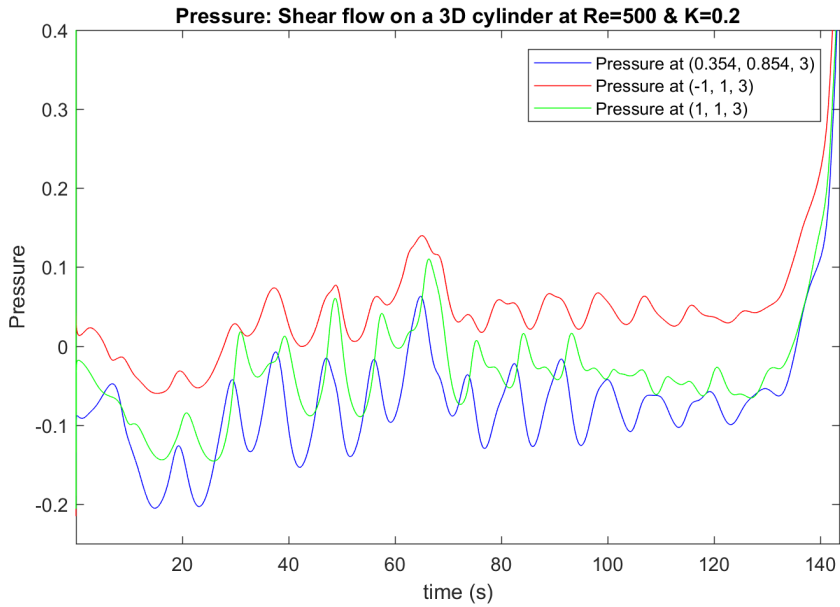


Figure 6.13: Pressure fluctuation with respect to time simulation for Probe1 (0.354, 0.854, 3), Probe 2 (-1.0, 1.0, 3.0) & Probe 3 (1.0, 1.0, 3.0).

The pressure distribution in figure 6.14 presents the pressure at time instant  $t = 100s$ . At this time instant, the pressure distribution is oscillating stable at the measured probe locations. Figure 6.15 presents the pressure distribution at time instant  $t = 140s$ , right before the numerical simulation breaks. At this time instant the pressure distribution around the whole domain increases, such that the results obtained are not corrects.

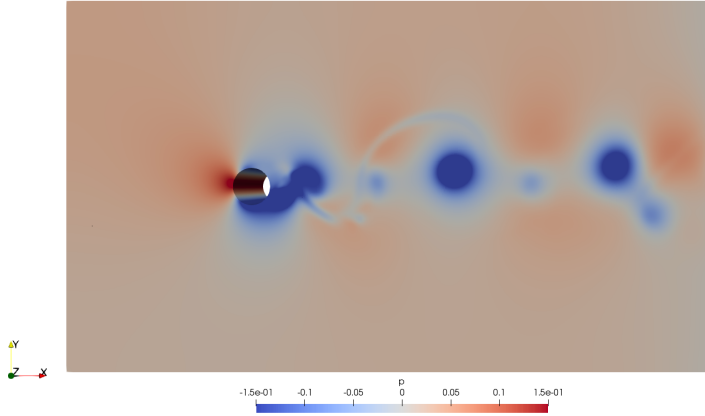


Figure 6.14: Pressure distribution for Shear flow at  $R_e = 500$  for  $K = 0.2$  at time instant  $t = 100s$ , when the pressure stable.

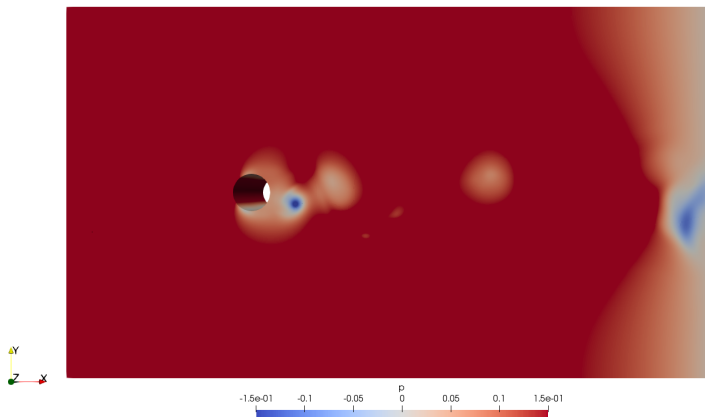


Figure 6.15: Pressure distribution for Shear flow at  $R_e = 500$  for  $K = 0.2$  at time instant  $t = 140s$  before breaking the simulation with  $\Delta t = 0.002$ .

### 6.2.3 Comparison of Vorticity in z-direction $\omega_z$

The vorticity distribution in z-direction  $\omega_z$  visualizes the level of vorticity in the computational domain. The vorticity describes how the flow behaves and reveals vortex sheddings, 3D effects span-wise and turbulent effects downstream. The magnitude of vorticity will reveal how vortices are behaving in-between the tandem cylinders and when travelling far downstream.

Figure 6.16 presents the vorticity in z-direction for the shear flow problem around tandem cylinders at time instant  $t = 500s$ . The flow moves smoothly around the tandem cylinders with 3D effects occurring in-between the tandem cylinders. The grid system in z-direction consists of 180 elements, such that an increase of elements could reveal more detailed 3D effects span-wise along the cylinder length.

Downstream in the wake region, vortices are shedded from the downstream cylinder, and 3D effects makes the flow turbulent as it begins to move in z-direction. The grid is coarser downstream, such that flow details may not be resolved as for the boundary layer. There are negative vorticities occurring on the high velocity side, while there are positive vorticities occurring on the low velocity side of the tandem cylinders.

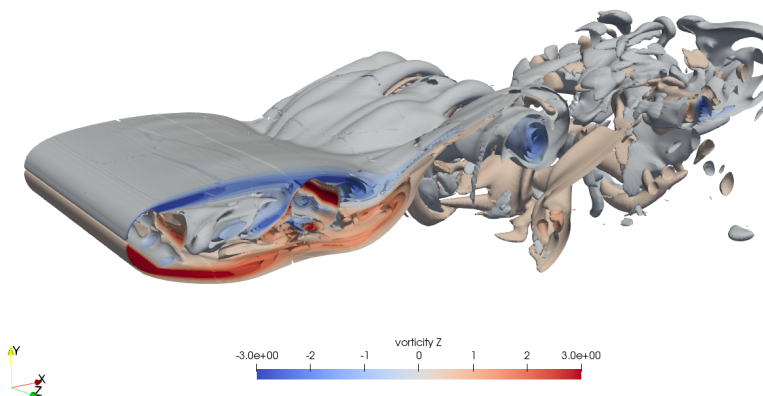


Figure 6.16: Vorticity in z-direction  $\omega_z$  for shear flow around tandem cylinder for  $R_e = 500$  &  $K = 0.2$  at time instant  $t = 500s$ .

Figure 6.17 presents the same vorticity distribution in z-direction as figure 6.16, where the figure presents the development of  $\omega_z$  in x-y-plane. The figure presents the alternating vortex shedding downstream, and how the vortices becomes irregular and turbulent. The flow moves smoothly around the tandem cylinders, with some vortices in-between the cylinders.

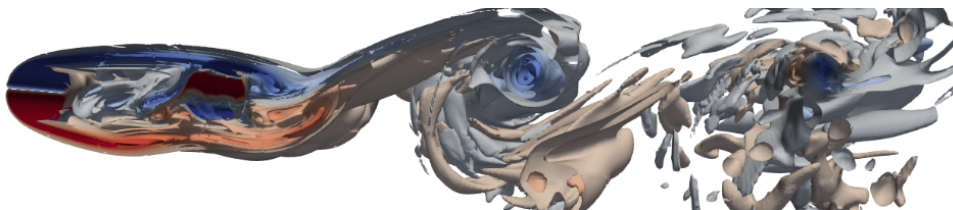


Figure 6.17: Vorticity in z-direction  $\omega_z$  for shear flow around tandem cylinder for  $R_e = 500$  &  $K = 0.2$  at time instant  $t = 500s$  in x-y-plane.

Figure 6.18 is a close-up view of figure 6.17 of the area in-between the cylinders. One can observe vortices in-between the cylinders, but no clear vortex shedding from the upstream cylinder towards the downstream cylinder.

The expectation of the Shear layer re-attachment behaviour or the re-attachment region for the tandem cylinders with a longitudinal length - diameter ratio  $L/D > 3.0$  did not occur for  $R_e = 500$ . Based on wake interference map in figure 3.23, the re-attachment will occur for the intermediate longitudinal length - diameter ratio ( $L/D$ ) and for Reynolds number around 10 000 in turbulence regime [Sumner, 2010], [Zdravkovich, 1987] & [Zhou and Yiu, 2006].

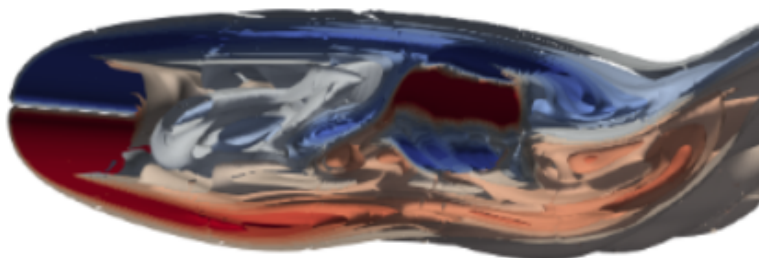


Figure 6.18: Vorticity in z-direction  $\omega_z$  for shear flow around tandem cylinder for  $R_e = 500$  &  $K = 0.2$  at time instant  $t = 500s$ . Close up of  $\omega_z$  in-between the tandem cylinders.

The vorticity distribution in z-direction is presented in figure 6.19 for the uniform flow problem around tandem cylinders at time instant  $t = 500s$ . The flow moves smoothly around the tandem cylinders, with vorticities in-between the tandem cylinders. At Reynolds number 500, it is expected 3D effects occurring for the vortices shed and travelling downstream.

Comparing the distribution of  $\omega_z$  in figure 6.19 with figure 6.16, one can observe more turbulent wake behaviour occurring downstream in figure 6.16.

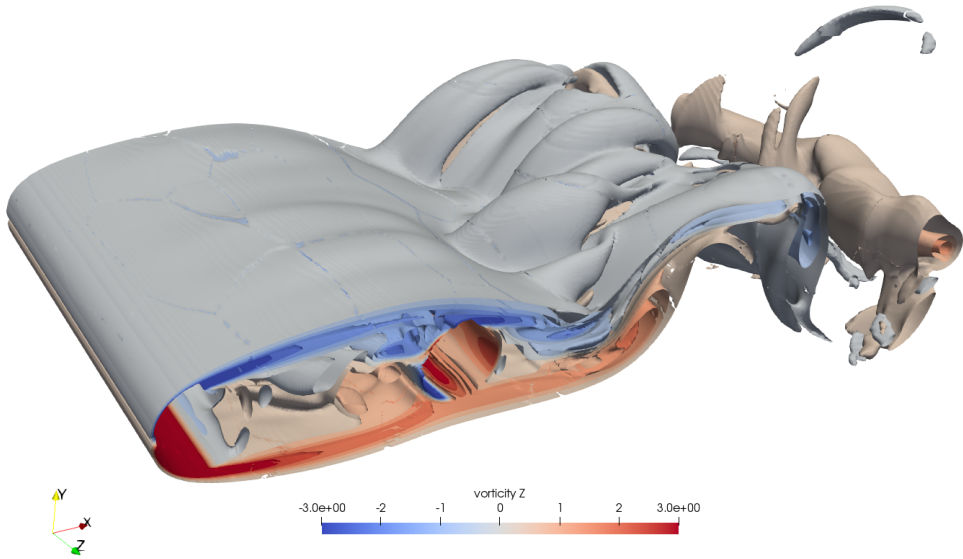


Figure 6.19: Vorticity in z-direction  $\omega_z$  for uniform flow around tandem cylinder for  $R_e = 500$  at time instant  $t = 500s$ .

Figure 6.20 presents vorticity distribution in z-direction, where alternating vortex sheddings are visualized in the x-and-y-plane.

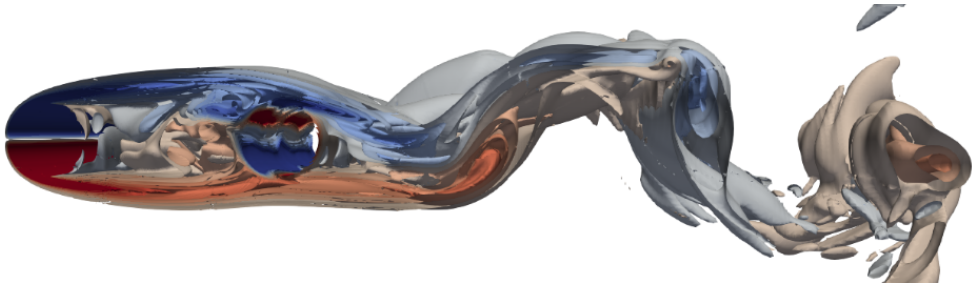


Figure 6.20: Vorticity in z-direction  $\omega_z$  for uniform flow around tandem cylinder for  $Re = 500$  at time instant  $t = 500s$  in x-y-plane.

Figure 6.21 presents a close up view of the vortices in-between the tandem cylinders in uniform flow. Observing the degree of vorticity in-between the tandem cylinders, one could assume that there are some vortices shedded from upstream cylinder. This corresponds with theory of Shear Layer Re-attachment for  $L/D > 3$  from figure 3.22 from section 3 for turbulent flow regime [Sumner, 2010], [Zdravkovich, 1987] & [Zhou and Yiu, 2006].

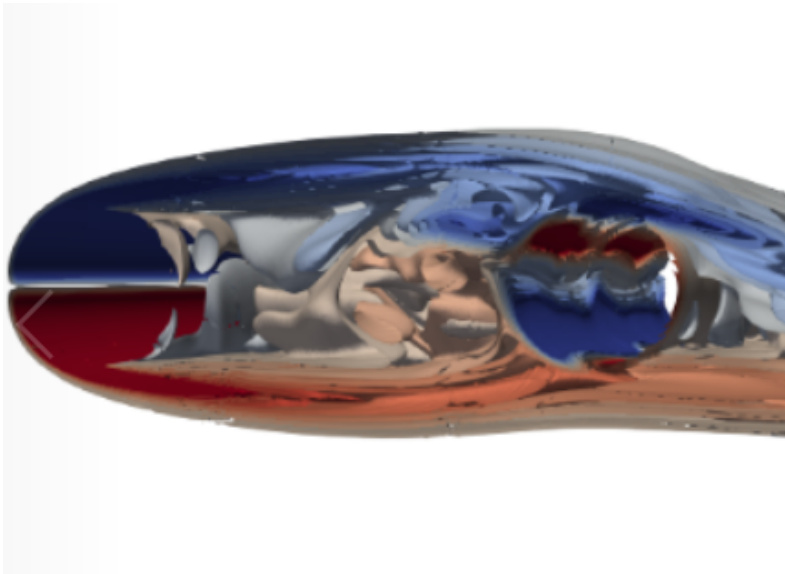


Figure 6.21: Vorticity in z-direction  $\omega_z$  for uniform flow around tandem cylinder for  $Re = 500$  at time instant  $t = 500s$ . Close up of  $\omega_z$  in-between the tandem cylinders.

Figure 6.22 presents the vorticity distribution in z-direction for a shear flow subjected on a single cylinder. The flow moves smoothly around the cylinder, and sheds alternating vortices with 3D effects. As the vortices travel downstream, the 3D effects will make the vortices behave with large irregularities and becomes turbulent.

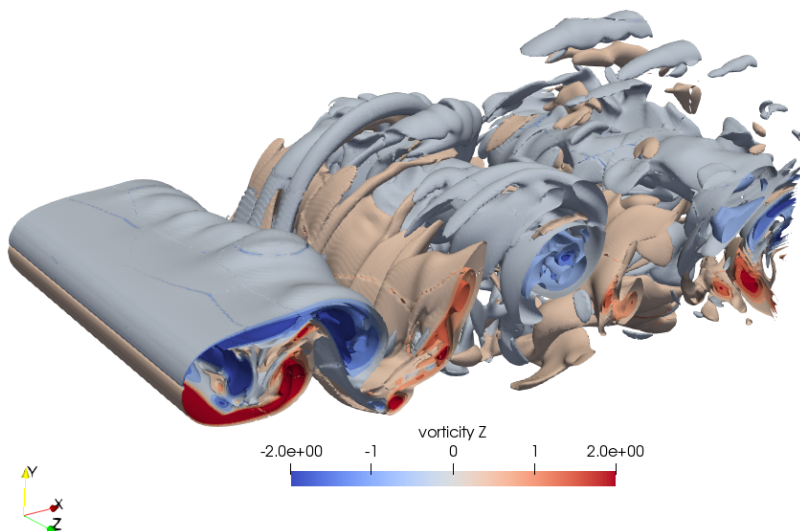


Figure 6.22: Vorticity in z-direction  $\omega_z$  for Shear flow at  $Re = 500$  for  $K = 0.2$  at time instant  $t = 140s$  right before simulation breaks.

The distribution of vorticity in z-direction  $\omega_z$  when a uniform flow is subjected on a single cylinder are presented in figure A.86 and A.87 for Reynolds number 300 in Appendix .6. The computational domain for the uniform flow around a single cylinder described in table A.1, where single cylinder has span-wise length of 4D, while the single cylinder subjected to a shear flow has 6D of span-wise length.

The numerical simulation is performed towards time instant  $t = 250s$ , where the simulation is stable at this point. The flow problem sheds alternating vortices downstream with 3D effects along the span-wise length. The wake behavior downstream is similar when a shear - or uniform flow is subjected on a single cylinder. For the shear flow problem, the domain along the y-axis ranges from  $-5.0 < y < 5.0$ , while the uniform flow problem has a domain range of  $-8.0 < y < 8.0$ . The top - and bottom boundary is closer to the single cylinder in the shear flow problem, and would have given large pressure distribution in the computational domain.



# Chapter 7

## Conclusion

Western Norway introduces the idea of removing all ferry connections with fixed links. This idea becomes a new infrastructural projects called Coastal Highway E39 or Ferry Free E39. The *Submerged Floating Tube Bridge (SFTB)* is a proposed concept, where two tunnels are submerged 30 m under the fjord surface. Combining technologies from offshore industry and civil engineering, the proposed concepts of a Submerged Floating Tube Bridge (SFTB) can be designed with respect to structural design and hydrodynamic loads.

Analyzing the SFTB, the proposed concept is simplified as tandem cylinders. The tandem configuration is subjected by a current velocity, with a linear varying profile called *shear flow*. The title of the Master Thesis is: *Numerical Simulation of a Viscous Shear Flow Around Tandem Cylinders*. Analysis' are performed by numerical simulation with use of the Computational Fluid Dynamic tool, OpenFOAM. The title explains that a *viscous shear flow* is subjected on *tandem cylinder* configuration. The cylinders are positioned with a longitudinal length - diameter ratio of  $L/D = 3.2$ , which is obtained from the actual ratio of the proposed SFTB. Numerical simulation gives observations of how the fluid flow will move around the tandem configuration, behave in-between the cylinders and occurrence of flow phenomena downstream in wake region.

The results obtained for the shear flow problem around tandem cylinders are discussed with respect to deviation of 2D and 3D simulations. When analyzing the problem of a shear flow subjected on tandem cylinders, one must evaluate the effects of shear flow compared to a uniform flow, and the effects of having tandem cylinders instead of a single cylinder.

Uniform current profiles do not exist in the experimental world. A linear approximation of the current velocity will be a new approach, which is based on measured current data at fjord surface and at 30 m depth. Using the current velocity at surface level and the velocity subjected normal to the SFTB,  $U_c = 0.32$  m/s, a linear gradient is found to be  $G = 0.0223$  and a shear rate of  $K = 0.07$ . Numerical analysis in OpenFOAM are performed with a velocity  $U_c = 0.5$  and a gradient  $G = 0.1$ .

Performing numerical simulations, boundary conditions are chosen to simulate the flow problem within the computational domain. Two-dimensional (2D) and three-dimensional (3D) analysis are performed with a shear flow described with shear rate  $K = 0.2$  around tandem cylinders. The results obtained for the 2D and 3D shear flow problems are presented in table 5.2 and 5.3 in section 5, while graphical visualization plots are presented in Appendix.

The 2D shear flow problems are performed with Reynolds 100, 300 and 500, while the 3D shear flow problems are performed with Reynolds number 100 and 500. Comparing the results from 2D and 3D flow problems with Reynolds number 100, the obtained results are identical, such that no 3D effects occur when simulating a flow with Reynolds number 100.

Results obtained for the 2D shear flow simulation at  $Re = 300$  and  $Re = 500$ , presents oscillations of velocity and force coefficients with two or more frequencies. When simulating the 3D shear flow at  $Re = 500$ , the vorticity distribution in z-direction  $\omega_z$  presents how the 3D effects occur along the span-wise length and how turbulent effects occur downstream. The 2D shear flow problems will restrict flow behaviour in span-wise direction, and the flow will oscillate with different frequencies and obtain incorrect values of forces, velocity - and pressure distribution.

The 3D shear flow problem simulated with  $Re = 500$  is compared to the flow problems of *a shear flow around a single cylinder* and *a uniform flow around tandem cylinders* at  $Re = 500$ . Comparing the effect of shear - and uniform flow around tandem cylinders, one will observe that shear flow will give high velocities at the upper half of the domain, and lower velocities at the lower half of the domain. The shear flow problem around a single cylinder presents the same tendency. Stagnation point is supposed to occur at the high velocity region on the first cylinder in a shear flow problem. For the simulated shear flow problems, the stagnation point occurred in-front of the upstream cylinder and for the single cylinder. Based on the pressure distributions, one can not conclude that the stagnation points occur at the high-velocity side.

The pressure distribution for the shear flow problem around a single cylinder becomes unstable, such that the simulation breaks at  $t = 140 - 143$ . The pressure distribution around the tandem cylinders with uniform and shear flow, follows the same pressure distribution curve with some deviations. The upstream cylinder experience larger pressure coefficient  $C_p$  around  $0 < \theta < 180$  degrees. The downstream cylinder experience larger pressure fluctuations, when subjected to a shear flow than a uniform flow. The downstream cylinder obtains negative pressure  $C_p$  when subjected by shear - and uniform flow.

The velocities behind the upstream cylinders in the tandem configuration are close to zero, when subjected by a uniform - or shear flow. The tandem cylinders subjected by uniform flow, will not obtain any oscillation periods or frequencies as velocity fluctuation is close to zero. For the shear flow problem around tandem cylinders, some period and frequencies are found, but the velocities are fluctuating so close to zero, that the results are incorrect.

The vorticity distribution in z-direction  $\omega_z$  reveals 3D effects and how the flow behaves downstream. The tandem configurations reveals that the flow moves smoothly over the cylinders, but will gain 3D effects as vortices travel downstream. In the wake region for the shear flow problem around tandem cylinder, the flow behaves more turbulent, compare the uniform flow problem. The shear flow problem around a single cylinder visualizes alternating vortex shedding with 3D effects occurring along the span-wise length of the vortices.

Tandem configurations with longitudinal length (L) ratio of  $L/D = 3.2$  in uniform flow assumes some Shear Layer Re-attachment to occur, as the upstream cylinder sheds vortices towards downstream cylinder. The distribution of vorticity in-between the tandem configuration presents some re-attachment phenomena in the uniform flow problem, shown in figure 6.21. In-between the tandem cylinders in the shear flow problem, vortex shedding from upstream cylinder are not clearly visualized.

Comparing the tandem configuration to a single cylinder, the inlet velocity flow has to move around the tandem configurations before shedding vortices downstream. The flow problem around a single cylinder will therefore obtain vortex shedding for an earlier time instant, than for tandem cylinder. The vortices downstream will obtain 3D effects when shedded from the single cylinder, while the tandem cylinders will experience turbulent effects downstream when subjected to a shear flow.

Constructing the Submerged Floating Tube Bridge (SFTB), the inlet shear flow will be the crucial factor as the pressure around the cylinder must be taken in account and the effects of turbulence downstream in a fjord. The longitudinal length ratio  $L/D$  is 3.2 is also of importance, as one could expect re-attachment layers for turbulent regimes and different oscillation period behind each cylinder. The analysis is performed with shear rate of  $K = 0.2$ , which is much larger than the actual shear rate of  $K = 0.07$  in the Bjørnafjord. One could assume that a uniform simulation is a good enough approximation, or either take use of a higher order inlet profile.

## 7.1 Future Work

The analysis performed, simplifies the SFTB as tandem cylinders with span-wise length of  $6D$  and diameter of  $D = 1$ . The numerical simulation is performed with a laminar solver at Reynolds number 500. Future work is to create a computational domain with finer grid. The elements could be more denser around the cylinders and in-between the cylinders. The computational domain can be increased with wider top and bottom boundary, and a longer wake region to visualize the flow phenomena occurring far downstream. The comparison between shear flow and uniform flow around single cylinder and tandem cylinders can be analyzed for higher Reynolds number and with a computational domain of the same dimensions in x, - y - and z-range.

The tandem cylinders can also be modelled with a larger span-wise length and with more elements along the span-wise length, to visualize the three-dimensional (3D) effects of vorticity distribution in z-direction. Changing the tandem configuration in terms of longitudinal length (L) and vertical length (T) to analyze the changes in velocity, pressure and vorticity for the tandem configuration, and understanding the importance of the distance between tandem cylinders.

The concept of SFTB are underwater tunnels, where the tunnel-ends will be connected to solid surfaces. Simulating tandem cylinders, where the ends are solid or fixed, will give understanding in the flow behaviour of the tunnels as they become integrated into the rock. Further, the analysis can be performed for turbulent inlet velocity with turbulence models. Current velocities as sea and fjords are turbulent, and therefore analyzing turbulent flows will give a better approximation of forces and flow behaviour for a shear flow problem around tandem cylinders.

The current load can be changed in terms of amplitude and profile. Uniform flow problems have been analyzed, and now linearly varying shear profiles are used. Further, the profile can be changed to higher order inlet profiles. The Submerged Floating Tube Bridge (SFTB) will have less effect of wind as it is submerged under water, but the effects of waves can also be added with the current velocity.

Marine technology and the knowledge obtained from the department can be used in several interdisciplinary project, as the Coastal Highway E39. The simulation and results obtained can further be studied with a structural approach, and understanding the forces subjected on tandem cylinders with respect to different materials, oscillation and fatigue of the bridge structure. At last, one must understand the costs that will involve creating a Submerged Floating Tube Bridge (SFTB) and the use of the bridge as a solution replacing an existing ferry route.

# Bibliography

- [Aarnes and Haugen, 2018] Aarnes, A. and Haugen (2018). Numerical investigation of free-stream turbulence effects on the transition-in-wake state of flow past a circular cylinder. Journal of Turbulence (2018). Taylor & Francis.
- [Akosile and Sumner, 2003] Akosile, O. and Sumner, D. (2003). On uniform planar shear flow around a circular cylinder at sub-critical Reynolds number. Journal of Fluid and Structures 18 (2003), 441-454.
- [Barkley and Henderson, 1996] Barkley and Henderson (1996). Three-dimensional Floquet stability analysis of the wake of a circular cylinder. Journal of Fluid Mechanics (1996), vol 322, pp. 215-241.
- [Behara and Mittal, 2010] Behara, S. and Mittal, S. (2010). Flow past a circular cylinder at low Reynolds number: Oblique vortex shedding. Physics of Fluids 22, 054102 (2010). American Institute of Physics.
- [Bejan and Kraus, 2003] Bejan and Kraus (2003). Heat transfer handbook volume 1.
- [Braza et al., 1986] Braza et al. (1986). Numerical study and physical analysis of the pressure and velocity fields in the near wake of a circular cylinder.
- [Cao and Wan, 2010] Cao, H. and Wan, D. (2010). Appliation of OpenFOAM to Simulate three-Dimensional Flows past a Single and Two Tandem Circular Cylinders. The International Society of Offshore and Polar Engineering (ISOPE).
- [Cao et al., 2010] Cao, S. et al. (2010). Numerical simulation of Reynolds number effects on velocity shear flow around a circular cylinder. Journals of Fluid and Structures 26 (2006) 685-702.
- [Cengel and Cimbala, 2014] Cengel and Cimbala (2014). Fluid Mechanics: Fundamentals and Applications. 3rd edition in SI units, McGraw-Hill Education.
- [Dimmen et al., 2016] Dimmen, A. et al. (2016). Utviklingsstrategi for ferjefri og utbetra E39. Nasjonal transportplan 2018-2019, Vedlegg 4, Statents Vegvesen.
- [Ding et al., 2007] Ding et al. (2007). Numerical simulation of flows around two circular cylinders by mesh-free square-based finite difference method. International Journal for Numerical Methods in Fluids 2007; 53:305-332.

- [Dunham, 2016] Dunham, K. K. (2016). Coastal Highway Route E30 - extreme crossings. *Transportation Research Procedia* 14 (2016) 494-498.
- [Faltinsen, 1990] Faltinsen, O. (1990). Sea Loads in Ships and offshore structures. Cambridge University Press.
- [Fey et al., 1998] Fey et al. (1998). A new strouhal-reynolds-number relationship for the circular cylinder in the range  $47 \leq Re \leq 2 \times 10^5$ .
- [Friehe, 1980] Friehe, C. A. (1980). Vortex shedding from cylinders at low reynolds numbers.
- [Greenshields, 2015] Greenshields, C. (2015). OpenFOAM. The Open Source CFD Toolbox. Programmer's Guide. OpenFOAM Foundation Ltd. & CFD Direct Ltd.
- [Hussain, 1995] Hussain, J. . (1995). On the identification of a vortex.
- [Igarashi, 1981] Igarashi, T. (1981). Characteristics of the Flow around Two Circular Cylinders Arranged in Tandem (1st Report). *Bulletin of the JSME*, Vol 24, No. 188, February 1981.
- [Johansen, 2016] Johansen, I. L. (2016). Technology Qualification of Extreme Fjord Crossings. *Proceeding of ASME 2016 35th International Conference on OMAE*, 2016-54419.
- [Kalvig et al., 2016] Kalvig, K. et al. (2016). Numerical Investigation of 3D flow around Two Tandem Cylinders. *The International Society of Offshore and Polar Engineering (ISOPE)*.
- [Kalvig, 2015] Kalvig, R. (2015). Numerical Investigation of 3D Flow Around Two Tandem Cylinders. Master thesis, Department of Marine Technology. Norwegian University of Science and Technology.
- [Kang, 2006] Kang, S. (2006). Uniform-shear flow over a circular cylinder at low Reynolds numbers. *Journals of Fluid and Structures* 22 (2006) 541-555.
- [Kiya et al., 1980] Kiya, M. et al. (1980). Vortex shedding from a circular cylinder in moderate-Reynolds-number shear flow. *J. Fluid Mech* (1980), col 141, part 4, pp721-735.
- [Kwon et al., 1992] Kwon, T. et al. (1992). Experiemental Investigation of Uniform-Shear Flow Past a Circular Cylinder. *Journal of Fluids Mechanics*, vol 114 (1992).
- [Larsen and Jakobsen, 2010] Larsen, R. and Jakobsen, S. (2010). Submerged floating tunnels for crossing of wide and deep fjords. *ISAB-2010. Procedia Engineering* 4 (2010) 135-143.
- [Lei et al., 2000] Lei, C. et al. (2000). A finite difference solution of the shear flow over a circular cylinder. *Ocean Engineering* 27 (2000) 271-290. Elsevier Science Ltd.

- [Meneghini et al., 2001] Meneghini et al. (2001). Numerical simulation of flow interference between two circular cylinders in tandem and side-by-side arrangements. *Journal of Fluids and Structures* (2001) 15, 327-350.
- [Minoretti et al., 2016] Minoretti, A. et al. (2016). The Submerged Floating Tube Bridge: The invisible bridge crossing the Bjørnafjord. IABSE Congress Stockholm 2016. Challenges in Design and Construction of an Innovative and Sustainable Built Environment.
- [Moukalled and Darwish, 2015] Moukalled, M. and Darwish (2015). The Finite Volume Method in Computational Fluid Dynamics: An Advanced Introduction with OpenFOam and Matlab. Springer.
- [Myhr et al., 2016] Myhr, A. et al. (2016). The Submerged Floating Tube Bridge: Design Philosophy and Concept Development. IABSE Congress Stockholm 2016 - Challenges in Design and Construction of an Innovative and Sustainable Built Environment.
- [Müller, 2017] Müller, B. (2017). Introduction to Computational Fluid Dynamics. Department of Energy and Process Engineering, Norwegian University of Science and Technology (NTNU).
- [NPRA and NVF, 2017] NPRA and NVF (2017). Coastal Highway Route E39. [vegvesen.no/teknologidagene](http://vegvesen.no/teknologidagene).
- [Pettersen, 2007] Pettersen, B. (2007). TMR4247 Marin Teknikk 3 Hydrodynamikk. Akademika Forlag.
- [Pletcher et al., 2013] Pletcher et al. (2013). Computational Fluid Mechanics and Heat Transfer. Third Edition, CRC Press. Taylor Francis Group, LLC.
- [Rajani et al., 2009] Rajani et al. (2009). Numerical simulation of laminar flow past a circular cylinder.
- [Reinertsen et al., 2016] Reinertsen et al. (2016). Bjørnafjord Submerged Floating Tube Bridge. K3/K4 Technical Report. Norwegian Public Road Administration (NPRA).
- [Reiso et al., 2015] Reiso, M. et al. (2015). Vertical stiffness for tube bridges: Comparing pontoons and tethers. IABSE Conference Geneva, Switzerland 2015 - Structural Engineering: Providing Solutions to Global Challenges
- [Sumer, 1997] Sumer, B. (1997). Hydrodynamics around cylindrical structures, volume vol. 12 of Advanced series on ocean engineering. World Scientific, Singapore.
- [Sumner, 2010] Sumner, D. (2010). Two circular cylinders in cross-flow: A review. *Journal of Fluid and Structures* 26 (2010), 849-899.
- [Tamura et al., 1980] Tamura, H. et al. (1980). Numerical Study on Viscous Shear Flow Past a Circular Cylinder. *Bulletin of the JSME*, Vol. 23, No. 186, Decembre 1980. Paper no. 186-2.
- [Tennekes and Lumley, 1972] Tennekes and Lumley (1972). A first course in turbulence.

- [Tveit, 2010] Tveit, P. (2010). Submerged floating tunnels (SFTs) for Norwegian fjords. ISAB-2010. *Procedia Engineering* 4 (2010) 135-143.
- [White, 2006] White, M. (2006). Chapter 4: Laminar Boundary Layers, VISCOUS FLUID FLOWS. McGraw-Hill Education.
- [Williamson, 1996] Williamson, C. (1996). Vortex Dynamics in the Cylinder Wake. *Annual Review of Fluid Mechanics* 1996. 28:477-539.
- [Wu and Chen, 1999] Wu and Chen (1999). Laminar boundary-layer separation over a circular cylinder in uniform shear flow. *Acta Mechanica* 144, 71-82.
- [Wu et al., 2004] Wu et al. (2004). Experimental and numerical study of the separation angle for flow around a circular cylinder at low reynolds number.
- [Xu and Zhou, 2004] Xu, G. and Zhou, Y. (2004). Strouhal numbers in the wake of two inline cylinders. *Experiments in Fluids* 37 248-256.
- [Zdravkovich, 1987] Zdravkovich, M. M. (1987). The effects of interference between circular cylinders in cross flow. *Journal of Fluid and Structures* (1987) 1, 239-261.
- [Zhou and Yiu, 2006] Zhou, Y. and Yiu, M. (2006). Flow structure, momentum and heat transport in a two-tandem-cylinder wake. *Journal of Fluid Mechanics* 548, 17-48.





# APPENDIX

## .1 2D Shear Flow Around Tandem Cylinders at $R_e = 100$ and $K = 0.2$

The results obtained for the 2D shear flow around tandem cylinders, gives a lift coefficients oscillating around zero. The downstream cylinders obtains larger oscillation amplitudes or root mean square value for lift. The mean force coefficients are found for the last 65 % of the results. The upstream cylinder will have a drag which oscillate around  $\bar{C}_D = 1.236$ , while the downstream cylinder obtains  $\bar{C}_D = -0.0197$ .

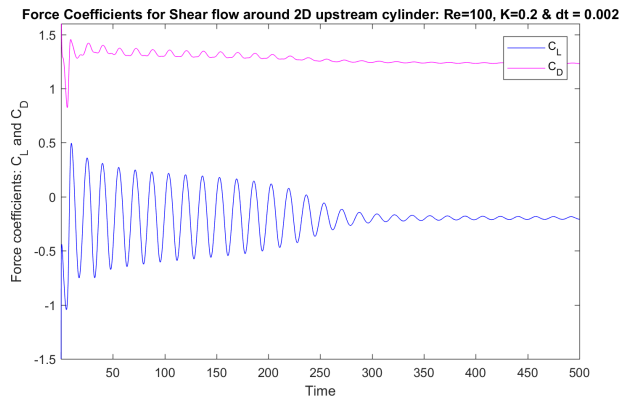


Figure A.1: Drag - and Lift Coefficients for Upstream Cylinder in Shear Flow at  $R_e = 100$ ,  $K = 0.2$  and  $\Delta t = 0.002$ .

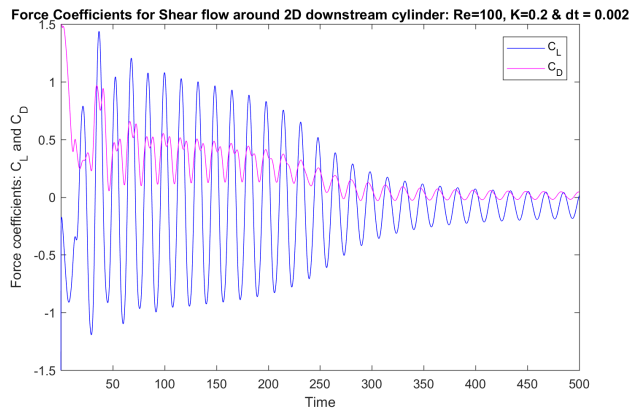


Figure A.2: Drag - and Lift Coefficients for Downstream Cylinder in Shear Flow at  $R_e = 100$ ,  $K = 0.2$  and  $\Delta t = 0.002$ .

The velocity in x-direction is found for a probe behind upstream cylinder at  $(x, y, z) = (-1.0, 0.354, 0.0)$  and behind downstream cylinder at  $(x, y, z) = (2.2, 0.354, 0.0)$ . The origin is placed in-between the tandem cylinders. The velocity behind the both cylinders oscillates stable, but changes root mean square around  $t = 300s$ . The velocities behind the upstream and downstream cylinders are used to compute the Power Spectral Density curves.

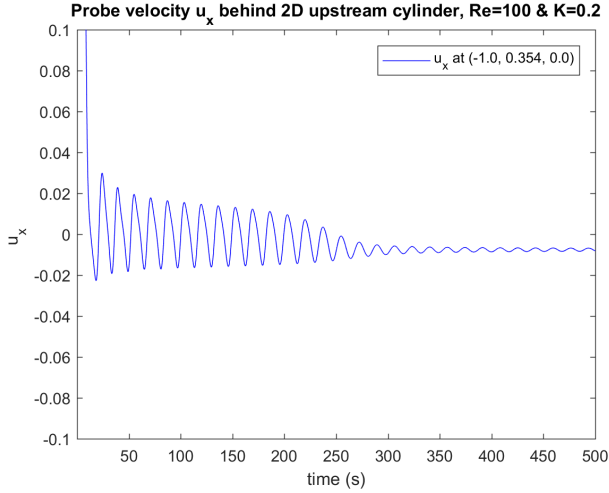


Figure A.3:  $U_x$  velocity probe behind Upstream Cylinder  $(x, y, z) = (-1.0, 0.354, 0.0)$  at  $R_e = 100$ ,  $K = 0.2$  at  $\Delta t = 0.002$ .

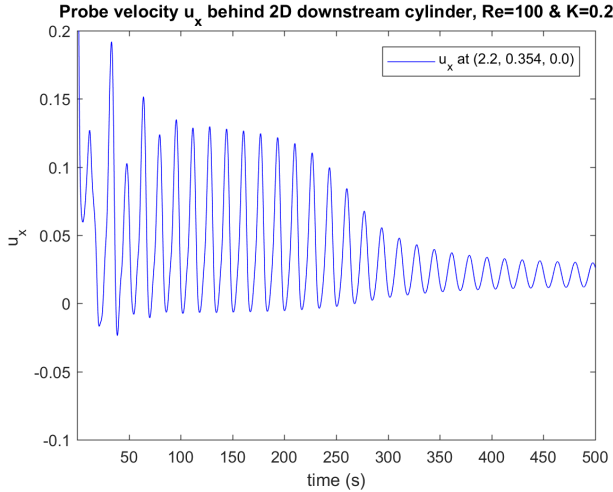


Figure A.4:  $U_x$  velocity probe behind Downstream Cylinder  $(x, y, z) = (2.2, 0.354, 0.0)$  at  $R_e = 100$  at  $\Delta t = 0.002$ .

The Power Spectral Density curves for the upstream cylinder represents what period the fluid is oscillation towards. The oscillation period is obtained from the figure, and it  $T_v = 16.67$ . The frequency can be found by the relation:  $f_v = 1/T_v [Hz]$ . The frequency is  $f_v = 0.06$ , with Strouhals number equals to  $S_t = 0.12$ . These values are also obtained for the downstream cylinder.

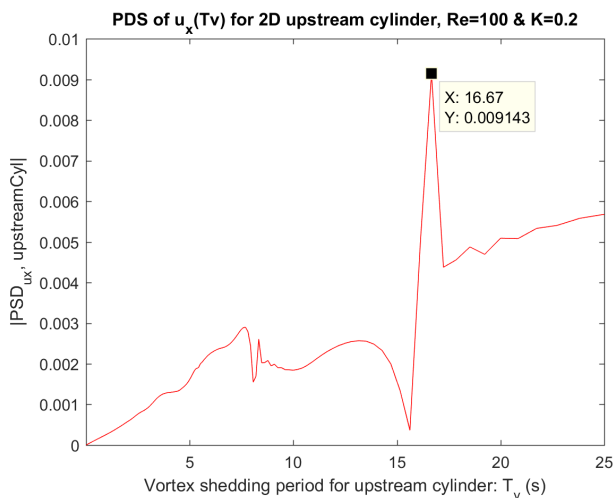


Figure A.5: The power spectral density of probe velocity  $U_x$  with respect to vortex shedding period  $T_v$  for: Upstream Cylinder at  $R_e = 100$ ,  $K = 0.2$  and  $\Delta t = 0.002$ .

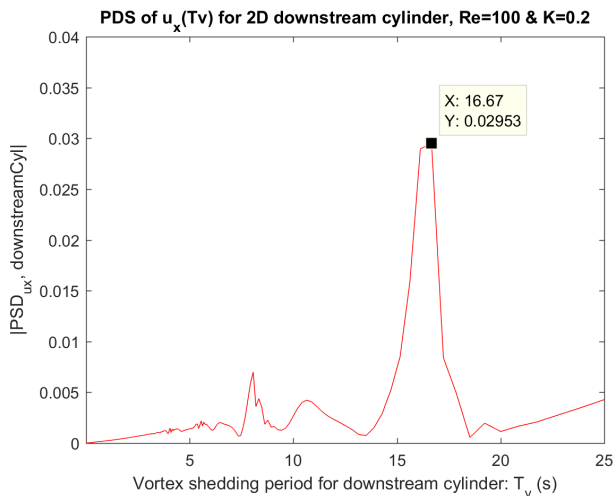


Figure A.6: The power spectral density of probe velocity  $U_x$  with respect to vortex shedding period  $T_v$  for: Downstream Cylinder at  $R_e = 100$ ,  $K = 0.2$  and  $\Delta t = 0.002$ .

The velocity magnitude at time instant  $t = 250s$  presents the how the absolute value for the velocities are within the domain. At this time instant the the force coefficients are still oscillating with large root mean squares for both upstream and downstream cylinder. At time instant  $t = 500s$ , the flow problem is stable and one can observe a low velocities as a ribbon behind the tandem cylinders.

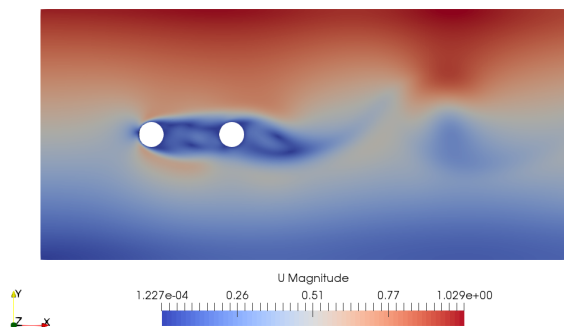


Figure A.7: Velocity magnitude for shear flow around tandem cylinders for  $R_e = 100$  &  $K = 0.2$  at time instant  $t = 250s$ .

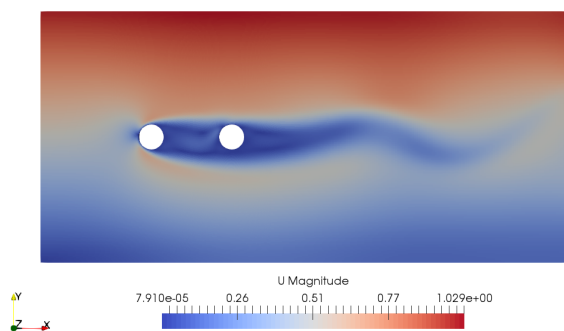


Figure A.8: Velocity magnitude for shear flow around tandem cylinders for  $R_e = 100$  &  $K = 0.2$  at time instant  $t = 500s$ .

The pressure distribution presents the stagnation point in front of the upstream cylinder with a high pressure zone, while there are pressure drops behind upstream cylinder, downstream cylinder and in the wake region. The low pressure zones on the upstream cylinder could be due to the flow moving along the cylinder surface.

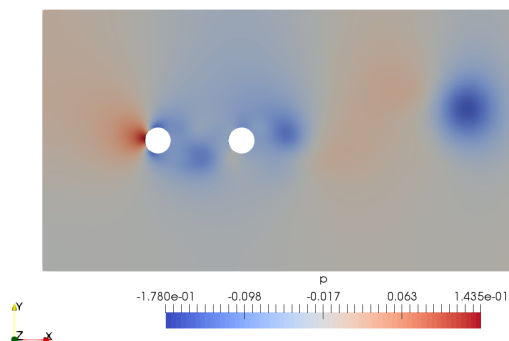


Figure A.9: Pressure distribution for shear flow around tandem cylinders for  $R_e = 100$  &  $K = 0.2$  at time instant  $t = 250s$ .

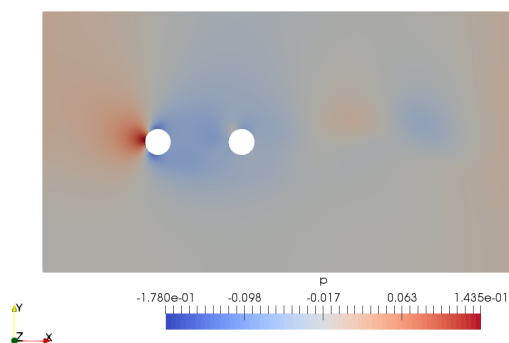


Figure A.10: Pressure distribution for shear flow around tandem cylinders for  $R_e = 100$  &  $K = 0.2$  at time instant  $t = 500s$ .

## .2 2D Shear Flow Around Tandem Cylinders at $R_e = 300$ and $K = 0.2$

Flow problems at Reynolds number 300 has oscillating drag - and lift coefficients. The lift coefficient is oscillating around zero, with root mean square of  $C_{L,RMS} = 0.86768$  for the upstream cylinder and  $C_{L,RMS} = 1.49092$  for the downstream cylinder. These values are larger than the results obtained for 2D shear flow with  $R_{100}$ .

The upstream cylinder experience a mean drag force  $\bar{C}_D = 1.44934$ , while the downstream cylinder will experience a much smaller drag force of  $\bar{C}_D = 0.40348$ . The upstream cylinder will experience a larger drag force.

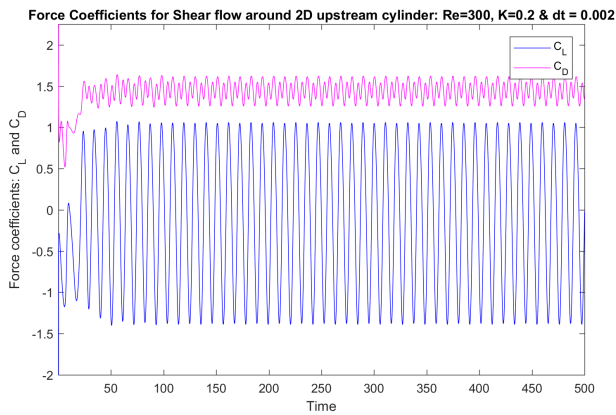


Figure A.11: Drag - and Lift Coefficients for Upstream Cylinder in Shear Flow at  $R_e = 300$ ,  $K = 0.2$  and  $\Delta t = 0.002$ .

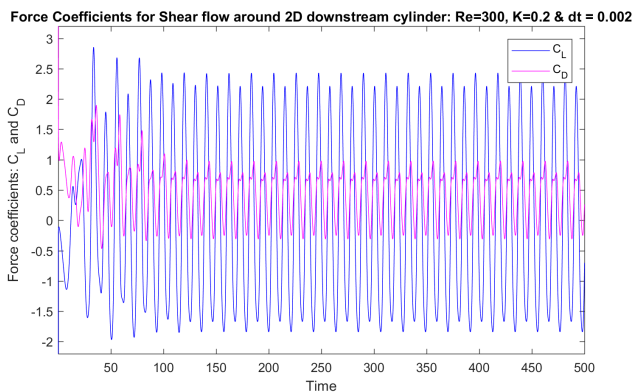


Figure A.12: Drag - and Lift Coefficients for Downstream Cylinder in Shear Flow at  $R_e = 300$ ,  $K = 0.2$  and  $\Delta t = 0.002$ .

The velocities behind upstream and downstream cylinder will both oscillate with two frequencies. This could be due the restrictions in the domain in z-direction, such that 3D effects are restricted to occur.

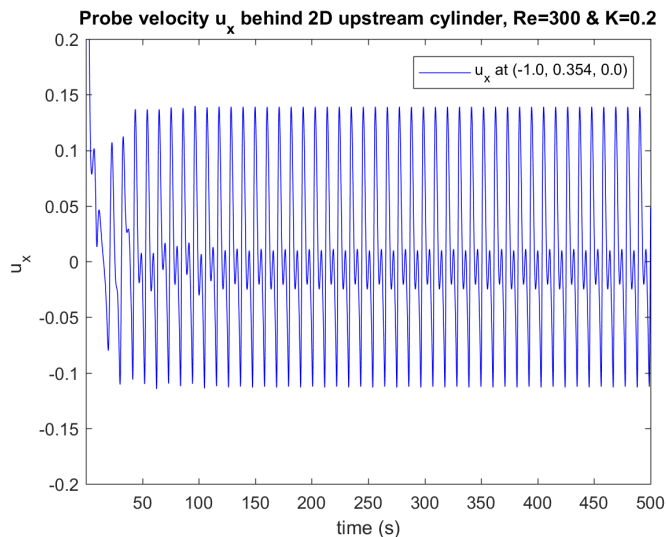


Figure A.13:  $U_x$  velocity probe behind Upstream Cylinder  $(x, y, z) = (-1.0, 0.354, 0)$  at  $Re = 300$ ,  $K = 0.2$  at  $\Delta t = 0.002$ .

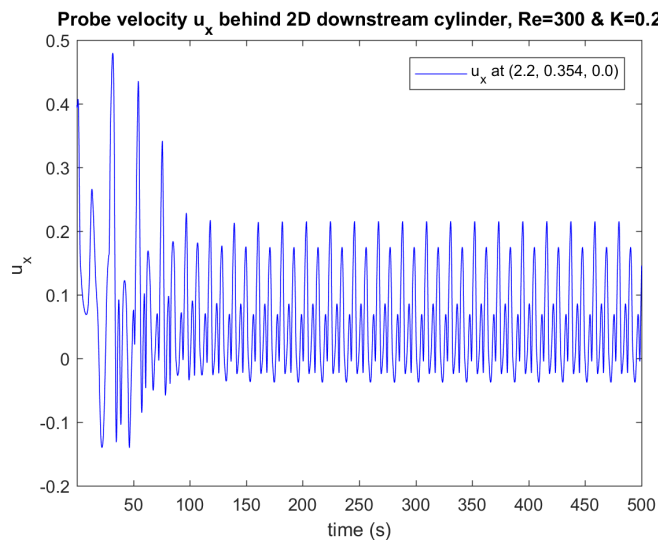


Figure A.14:  $U_x$  velocity probe behind Downstream Cylinder  $(x, y, z) = (2.2, 0.354, 0)$  at  $Re = 300$  at  $\Delta t = 0.002$ .



The Power Spectral Density curves presents the main oscillation period and frequency occurring right behind the upstream and downstream cylinder. Both cylinders are experiencing a oscillation periods of  $T_v = 5.319$  and  $T_v = 10.64$  and frequencies of  $f_v = 0.188$  and  $f_v = 0.094$ . The Strouhals number are  $S_t = 0.376$  and  $S_t = 0.188$ .

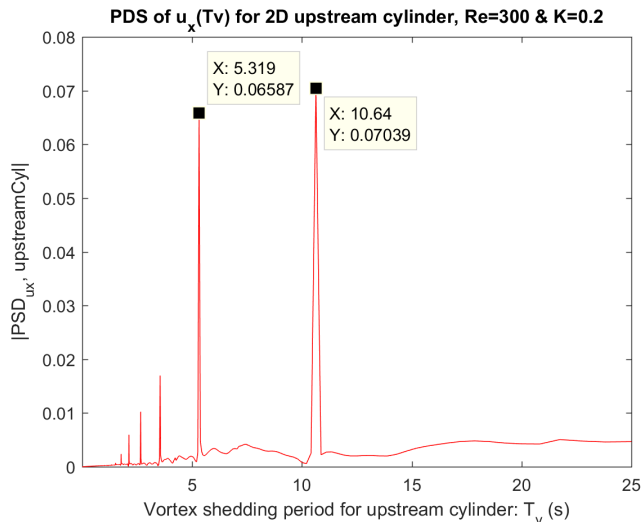


Figure A.15: The power spectral density of probe velocity  $U_x$  with respect to vortex shedding period  $T_v$  for: 2D Upstream Cylinder at  $R_e = 300$ ,  $K = 0.2$  and  $\Delta t = 0.002$ .

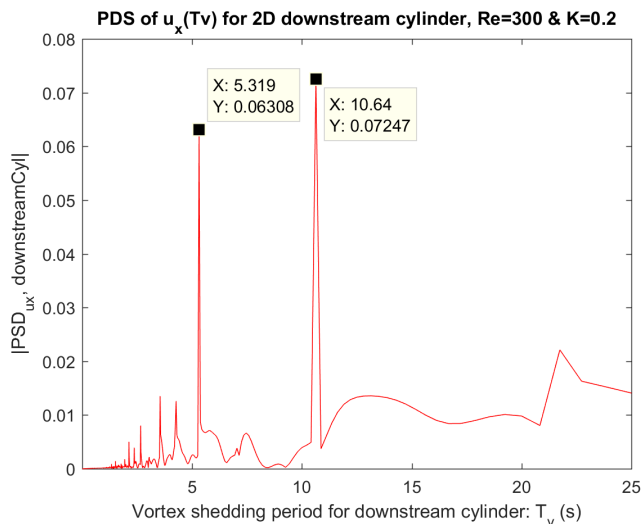


Figure A.16: The power spectral density of probe velocity  $U_x$  with respect to vortex shedding period  $T_v$  for: Downstream Cylinder at  $R_e = 300$ ,  $K = 0.2$  and  $\Delta t = 0.002$ .

The velocity magnitude is presented at time instant  $t = 500s$ , where there are velocities moving in-between the tandem cylinders. The downstream cylinder will therefore be affected by the wake from the upstream cylinder.

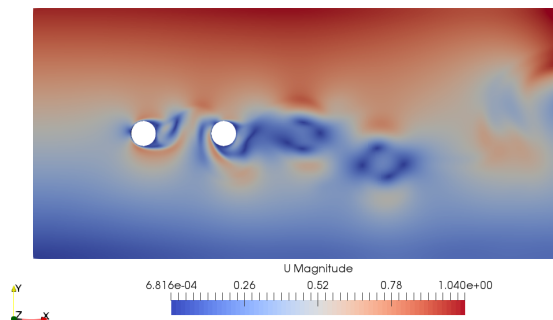


Figure A.17: Velocity magnitude for shear flow around tandem cylinders for  $R_e = 300$  &  $K = 0.2$  at time instant  $t = 500s$ .

The pressure distribution illustrated low pressure zones around the upstream cylinder, which represent the high velocities around the upstream cylinder. In the wake there are several low pressure zones, which represents vortex sheddings.

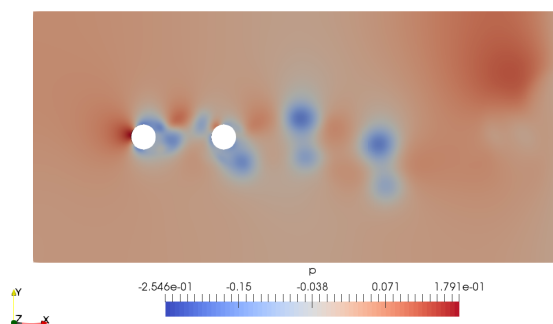


Figure A.18: Pressure distribution for shear flow around tandem cylinders for  $R_e = 300$  &  $K = 0.2$  at time instant  $t = 500s$ .

### .3 2D Shear Flow Around Tandem Cylinders at $Re = 500$ and $K = 0.2$

Flow problems at Reynolds number 500 has oscillating drag - and lift coefficients. The lift coefficient is still oscillating close to zero, with larger root mean square values compared to the flow problems with Reynolds number 100 and 300. The root mean square for the lift coefficients are  $C_{L,RMS} = 1.04621$  for the upstream cylinder and  $C_{L,RMS} = 1.60544$  for the downstream cylinder.

The upstream cylinder experience a mean drag force  $\bar{C}_D = 1.54587$ , while the drag around the downstream cylinder is close to zero at  $\bar{C}_D = 0.60668$ . Comparing the drag around upstream and downstream cylinder, the drag around the downstream cylinder is close to zero, but is increasing with the Reynolds number. The drag around the upstream cylinder is also increasing with Reynolds number for the flow problem with a 2D domain. At Reynolds number 500, the flow wants to act in 3D, such that a 2D domain will restrict the flow behaviour.

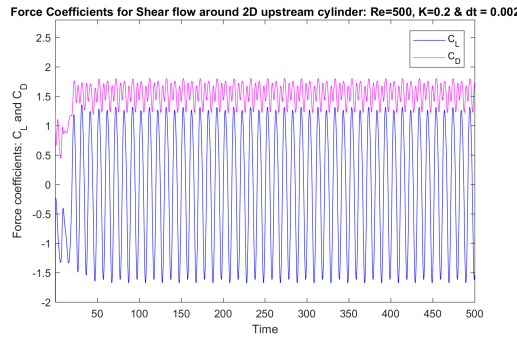


Figure A.19: Drag - and Lift Coefficients for Upstream Cylinder in Shear Flow at  $Re = 500$ ,  $K = 0.2$  and  $\Delta t = 0.002$ .

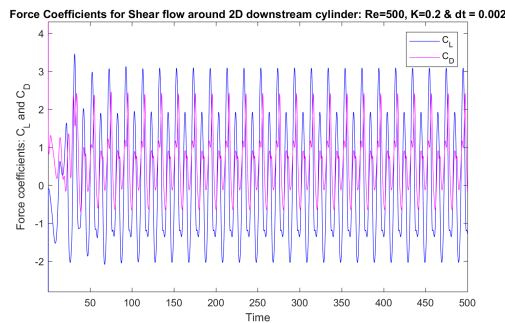


Figure A.20: Drag - and Lift Coefficients for Downstream Cylinder in Shear Flow at  $Re = 500$ ,  $K = 0.2$  and  $\Delta t = 0.002$ .

The velocity in x-direction behind upstream and downstream cylinder is oscillating periodically for the time simulation, but are oscillating with several periods and frequencies.

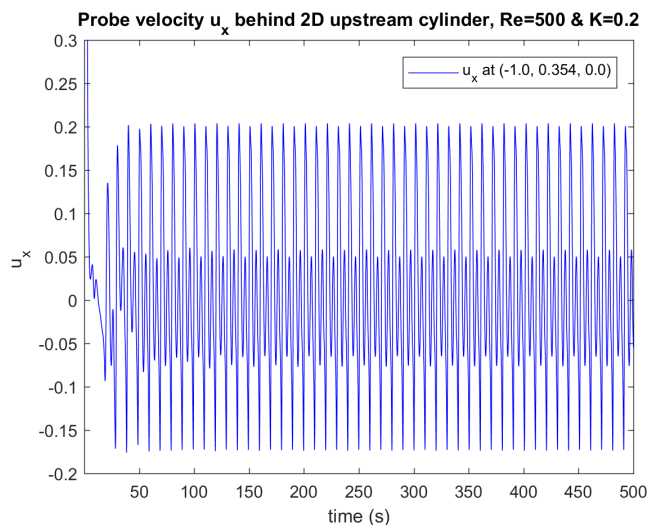


Figure A.21:  $U_x$  velocity probe behind Upstream Cylinder  $(x, y, z) = (-1.0, 0.354, 0)$  at  $R_e = 500$ ,  $K = 0.2$  at  $\Delta t = 0.002$ .

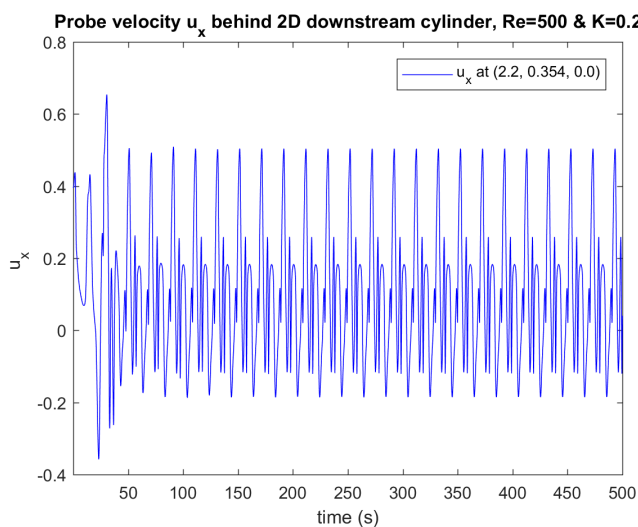


Figure A.22:  $U_x$  velocity probe behind Downstream Cylinder  $(x, y, z) = (2.2, 0.354, 0)$  at  $R_e = 500$  at  $\Delta t = 0.002$ .

The upstream cylinder is oscillating with the periods  $T_v = 5.05$  and  $T_v = 10$ , and frequencies  $f_v = 0.2$  and  $f_v = 0.1$ . The Strouhals numbers for the upstream cylinder are  $S_t = 0.4$  and  $S_t = 0.2$ .

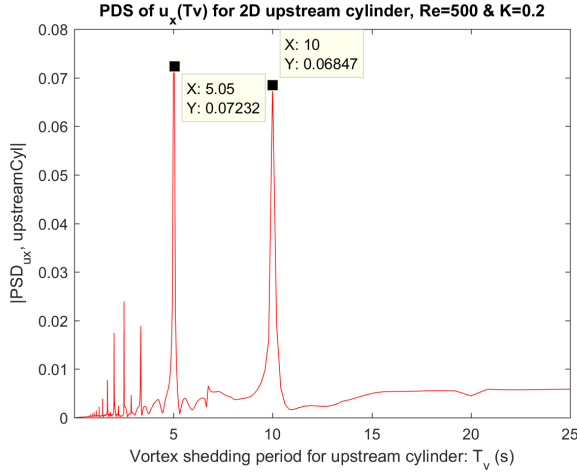


Figure A.23: The power spectral density of probe velocity  $U_x$  with respect to vortex shedding period  $T_v$  for: 2D Upstream Cylinder at  $R_e = 500$ ,  $K = 0.2$  and  $\Delta t = 0.002$ .

The downstream cylinder have to main peaks which gives oscillation periods  $T_v = 10$  and  $T_v = 20$ , and frequencies  $f_v = 0.1$  and  $f_v = 0.05$ . The Strouhals numbers for the upstream cylinder are  $S_t = 0.2$  and  $S_t = 0.1$ .

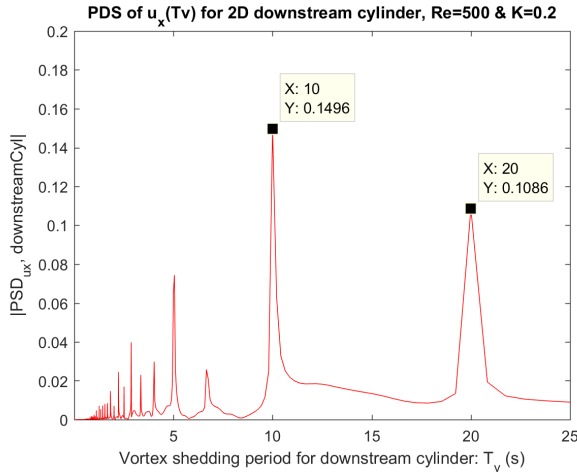


Figure A.24: The power spectral density of probe velocity  $U_x$  with respect to vortex shedding period  $T_v$  for: Downstream Cylinder at  $R_e = 500$ ,  $K = 0.2$  and  $\Delta t = 0.002$ .

Velocity magnitude illustrated the absolute velocities at time instant  $t = 500s$  for a flow problem with Reynolds number  $R_e = 500$ . There are velocities moving in-between the tandem cylinder, such that the downstream cylinder will be effected by the wake from the upstream cylinder. Downstream behind the downstream cylinder there are vortex sheddings occurring as there are alternating vortices shedding from each side of the downstream cylinder. This is also visualized in the pressure distribution as low pressure zones.

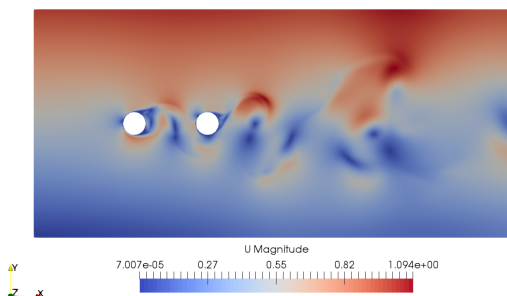


Figure A.25: Velocity magnitude for shear flow around tandem cylinders for  $R_e = 500$  &  $K = 0.2$  at time instant  $t = 500s$ .

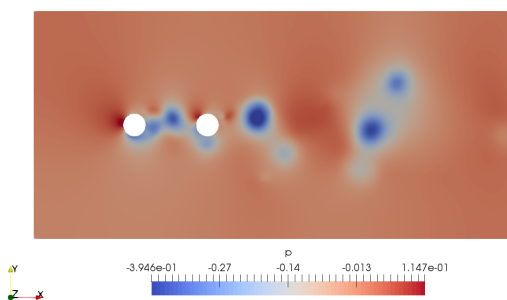


Figure A.26: Pressure distribution for shear flow around tandem cylinders for  $R_e = 500$  &  $K = 0.2$  at time instant  $t = 500s$ .

## .4 3D Shear Flow Around Tandem Cylinders at $R_e = 100$ and $K = 0.2$

The Shear flow problem with a shear rate  $K = 0.2$  and Reynolds number  $R_e = 100$  around Tandem cylinder gives psccillating force dowfficients for the upstream and downstream cylinder. The upstream cylinder experience an oscillation around the mean value of  $\bar{C}_D = 1.236$  and  $\bar{C}_L = -0.0197$ , while the downstream cylinder experience oscillation around the  $\bar{C}_D = 0.0196$  and  $\bar{C}_L = -0.074$ . These mean force coefficients with the root mean square values are identical to the 2D Shear flow problem at Reynolds number 100.

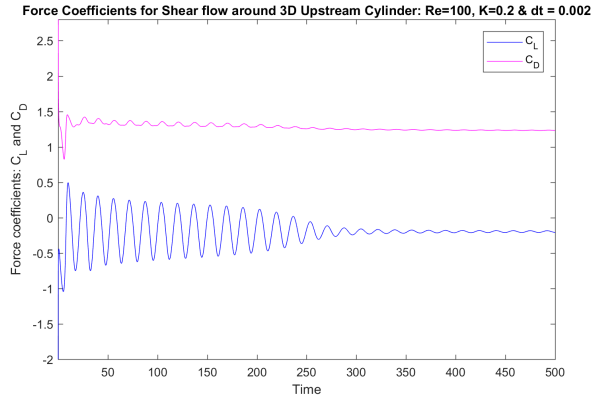


Figure A.27: Drag - and Lift Coefficients for 3D Upstream Cylinder in Shear Flow at  $R_e = 100$ ,  $K = 0.2$  and  $\Delta t = 0.002$ .

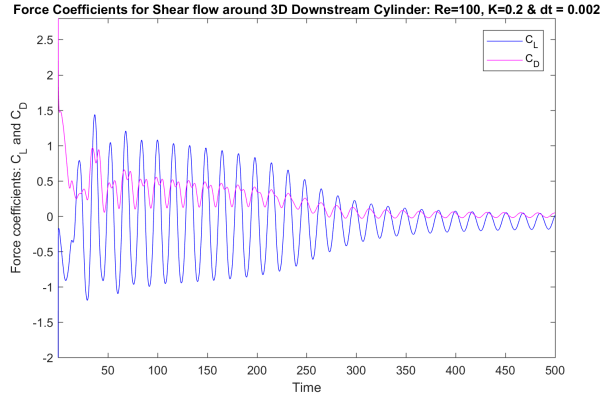


Figure A.28: Drag - and Lift Coefficients for 3D Downstream Cylinder in Shear Flow at  $R_e = 100$ ,  $K = 0.2$  and  $\Delta t = 0.002$ .

Velocity fluctuation behind upstream and downstream cylinder is also oscillating with the same period and frequency as for the 2D shear flow problem described in section .1. The first values obtained for the time simulation are unstable, and could have been removed for the graphical plot.

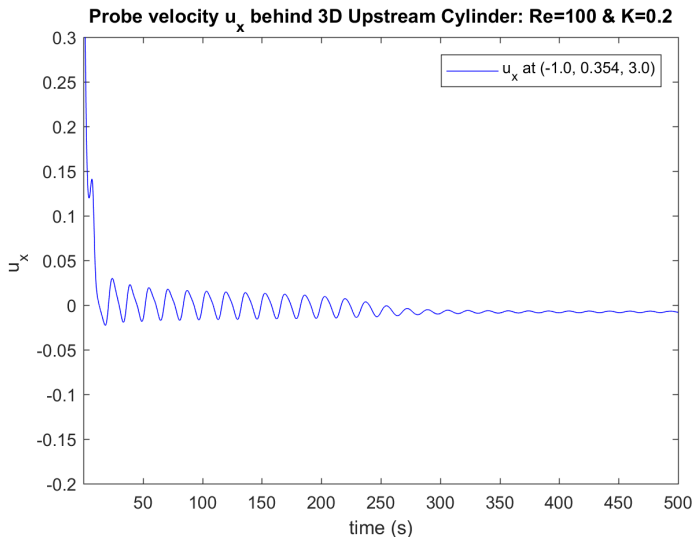


Figure A.29:  $U_x$  velocity probe behind 3D Upstream Cylinder  $(x, y, z) = (-1.0, 0.354, 3.0)$  at  $Re = 100$ ,  $K = 0.2$  at  $\Delta t = 0.002$ .

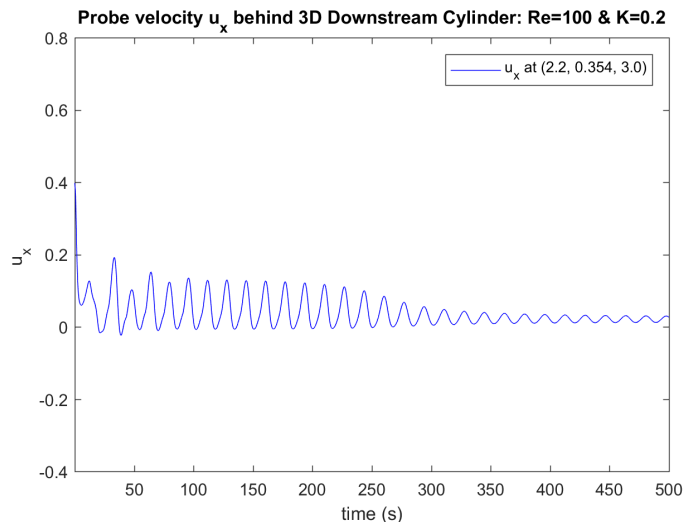


Figure A.30:  $U_x$  velocity probe behind 3D Downstream Cylinder  $(x, y, z) = (2.2, 0.354, 3.0)$  at  $Re = 100$  at  $\Delta t = 0.002$ .



The Spectral Density curves are found by Fourier Transform of the velocity fluctuations, and will reveal the main oscillation periods and peaks behind upstream and downstream cylinder. The periods and frequencies for the 3D shear flow problem are the same for the 2D problem, where the values are  $T_V = 16.67$ ,  $f_v = 0.06$  and Strouhals number  $S_t = 0.12$  for both upstream and downstream cylinder.

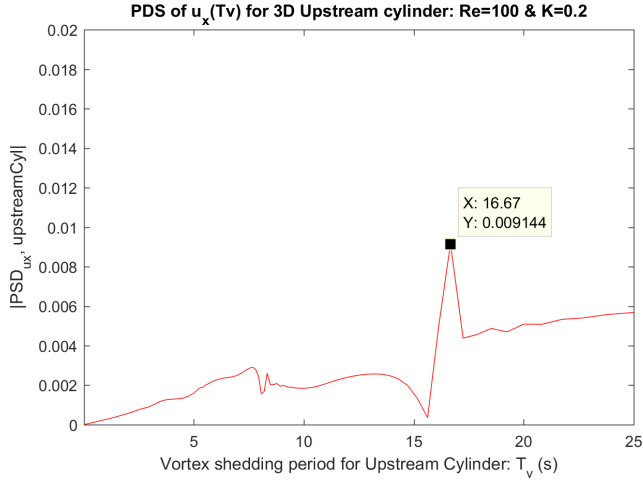


Figure A.31: The power spectral density of probe velocity  $U_x$  with respect to vortex shedding period  $T_v$  for: 3D Upstream Cylinder at  $R_e = 100$ ,  $K = 0.2$  and  $\Delta t = 0.002$ .

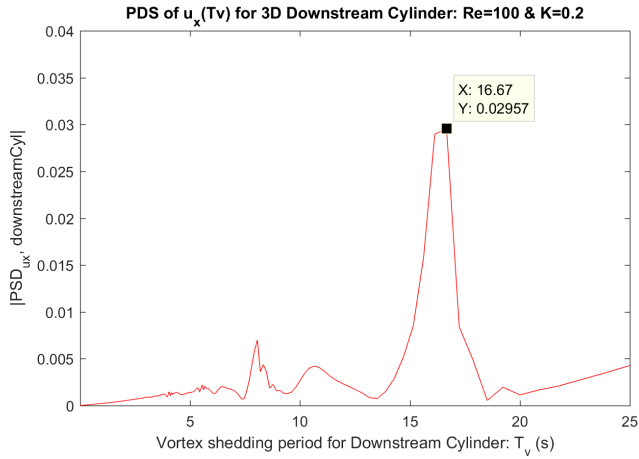


Figure A.32: The power spectral density of probe velocity  $U_x$  with respect to vortex shedding period  $T_v$  for: 3D Downstream Cylinder at  $R_e = 100$ ,  $K = 0.2$  and  $\Delta t = 0.002$ .

Figure A.33 and A.34 presents the velocity magnitude and pressure distribution for the 3D Shear for problem at time instant  $t = 150s$ . At this time instant the velocity behind the cylinders and the force coefficients are oscillating stable.

There are velocities in-between the tandem cylinder, and downstream there are vortices shedded. This is also visualized in the pressure distribution.

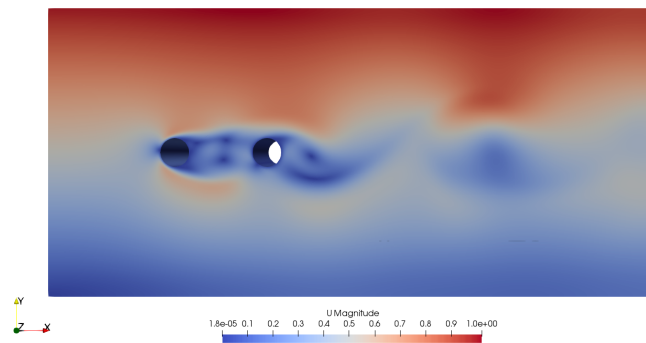


Figure A.33: Velocity magnitude for shear flow around tandem cylinders for  $R_e = 100$  &  $K = 0.2$  at time instant  $t = 150s$ .

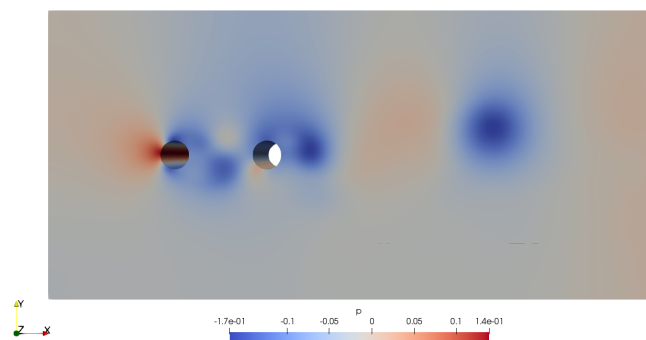


Figure A.34: Pressure distribution for shear flow around tandem cylinders for  $R_e = 100$  &  $K = 0.2$  at time instant  $t = 150s$ .

Velocity magnitude is presented in figure A.35 and the pressure distribution is presented in figure A.36 at time instant  $t = 250s$ . At this time instant the velocity behind the cylinders and the force coefficients decreases its root mean square while oscillating stable. This means that the velocities behind the cylinders decreases.

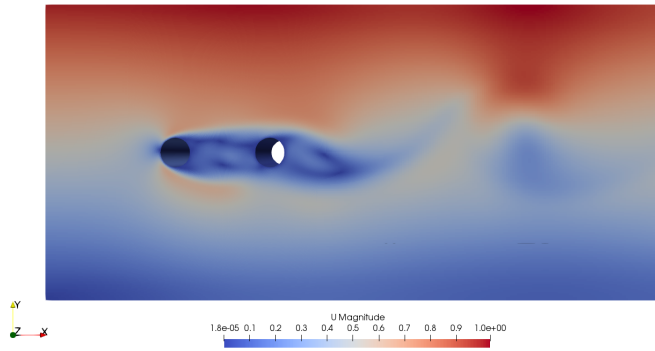


Figure A.35: Velocity magnitude for shear flow around tandem cylinders for  $R_e = 100$  &  $K = 0.2$  at time instant  $t = 250s$ .

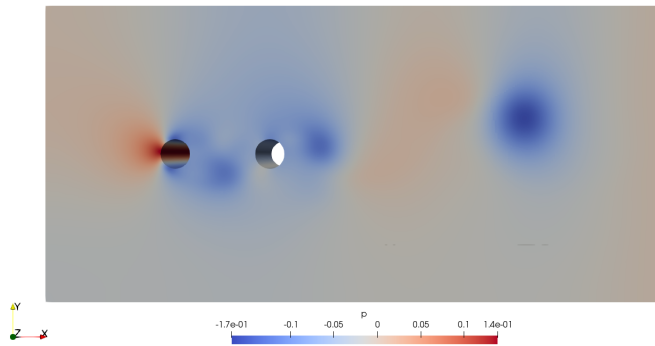


Figure A.36: Pressure distribution for shear flow around tandem cylinders for  $R_e = 100$  &  $K = 0.2$  at time instant  $t = 250s$ .

The velocity magnitude and pressure distribution is presented at time instant  $t = 500s$  in figure A.37 and A.38. The inlet current will flow around the tandem cylinders, and there will occur a ribbon in the wake region with low velocities which is oscillating. There are no vortex shedding occurring at this time instant in our domain. One could increase the wake region to observe how the flow is evolving far downstream.

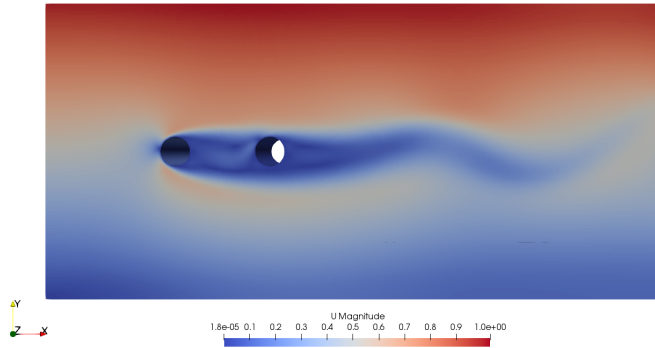


Figure A.37: Velocity magnitude for shear flow around tandem cylinders for  $R_e = 100$  &  $K = 0.2$  at time instant  $t = 500s$ .

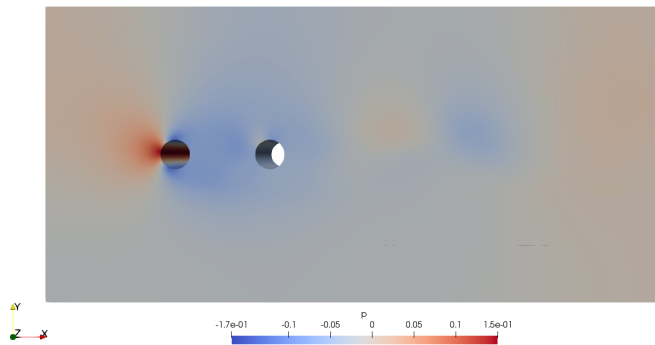


Figure A.38: Pressure distribution for shear flow around tandem cylinders for  $R_e = 100$  &  $K = 0.2$  at time instant  $t = 500s$ .

At time instant  $t = 150s$  the is observed vortices shedded in figure A.33 and A.34 for velocity magnitude and pressure distribution. The Vorticity in z-direction presents how the fluid behaves span-wise along the cylinder in terms of the degree of vorticity.

Figure A.39 presents the vorticity in z-direction  $\omega_z$  at time instant  $t = 150s$  where there are vorticity occurring in-between the cylinders. The downstream cylinder will experience the effect of vorticity from the upstream cylinder. Far downstream there are vortex sheddings occurring. Figure A.40 presents  $\omega_z$  in a different angle for the same time instant. Span-wise along the cylinder the flow moves smoothly around the cylinder. There are no three-dimensional effects occurring, due to the low Reynolds number 100.

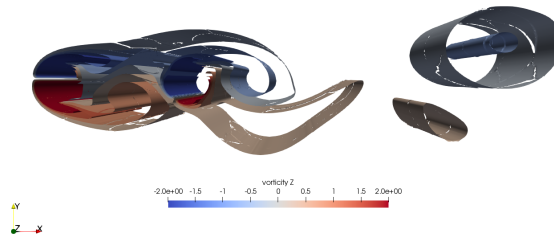


Figure A.39: Vorticity in z-direction  $\omega_z$  for shear flow around tandem cylinder for  $R_e = 100$  &  $K = 0.2$  at time instant  $t = 150s$ .

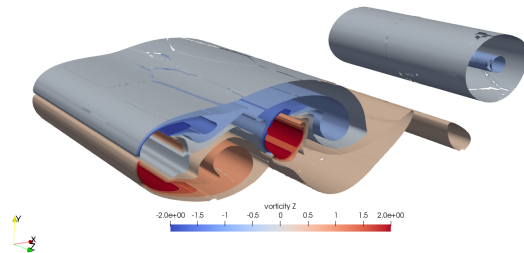


Figure A.40: Vorticity in z-direction  $\omega_z$  for shear flow around tandem cylinder for  $R_e = 100$  &  $K = 0.2$  at time instant  $t = 150s$ . Different angle.

Figure A.41 presents the distribution of vorticity in z-direction  $\omega_z$  at time instant  $t = 250s$ . At this time instant the oscillation decreases the root mean square value. There are less vortices in-between the cylinders, compared to the time instant  $t = 150s$ . The flow must also flow more downstream before shedding vortices, and the flow begins to act like more like ribbons downstream than shedded vortices.

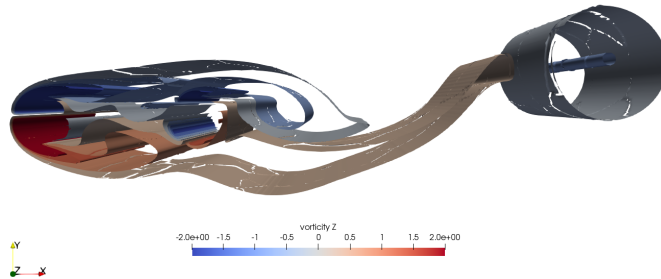


Figure A.41: Vorticity in z-direction  $\omega_z$  for shear flow around tandem cylinder for  $Re = 100$  &  $K = 0.2$  at time instant  $t = 250s$ .

Figure A.42 presents the vorticity distribution in z-direction  $\omega_z$  at time instant  $t = 250s$  in a different angle. There are no three-dimensional effects span-wise along the cylinder.

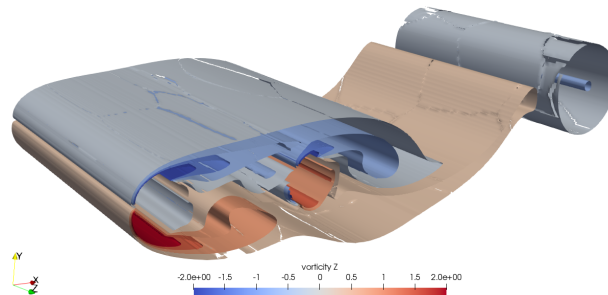


Figure A.42: Vorticity in z-direction  $\omega_z$  for shear flow around tandem cylinder for  $Re = 100$  &  $K = 0.2$  at time instant  $t = 250s$ . Different angle.

At time instant  $t = 500s$  the flow downstream in the wake region begins to behave like a ribbon. The vorticity distribution in z-direction  $\omega_z$  in figure A.43 presents how the vorticity in the flow and how the flow behaves downstream. There are no vortex shedding occurring in the domain, but if the domain far downstream is increased, there would be possible vortex shedding occurring. Figure A.44 presents the vorticity distribution for a different angle, where there are no three-dimensional effects along the span-wise cylinders or the flow downstream.

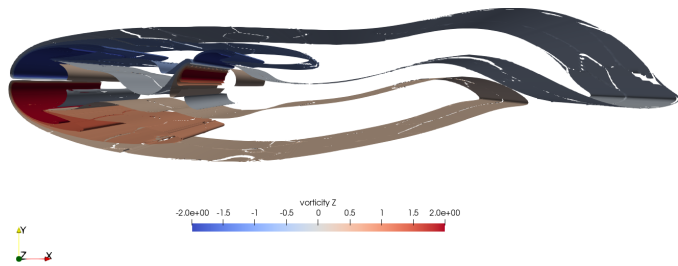


Figure A.43: Vorticity in z-direction  $\omega_z$  for shear flow around tandem cylinder for  $R_e = 100$  &  $K = 0.2$  at time instant  $t = 500s$ .

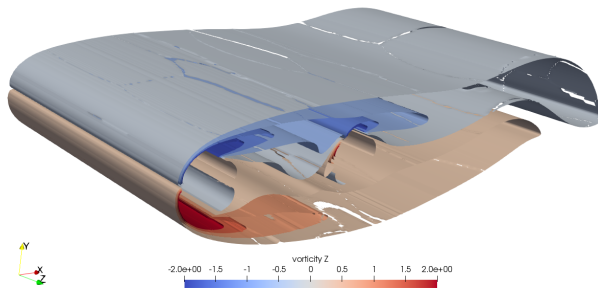


Figure A.44: Vorticity in z-direction  $\omega_z$  for shear flow around tandem cylinder for  $R_e = 100$  &  $K = 0.2$  at time instant  $t = 500s$ . Different angle.

## .5 3D Shear Flow Around Tandem Cylinders at $R_e = 500$ and $K = 0.2$

For time first 100 s of the time simulation, the force coefficients will oscillate with a certain root mean square value. Time simulation from  $t = 100 - 500$ s, the forces will oscillate with a different frequency and smaller root mean square as the 3D effects occur. The mean values are obtained for the last 65 % of the time simulation.

The mean force coefficients are  $\bar{C}_D = 1.027$  and  $\bar{C}_L = -0.123$  for the upstream cylinder. The downstream cylinder obtains mean values at  $\bar{C}_D = -0.158$  and  $\bar{C}_L = -0.078$ . The mean drag force for the 2D upstream cylinder from section .3 is  $\bar{C}_D = 1.545$ , where the flow problem is restricted for 3D effects.

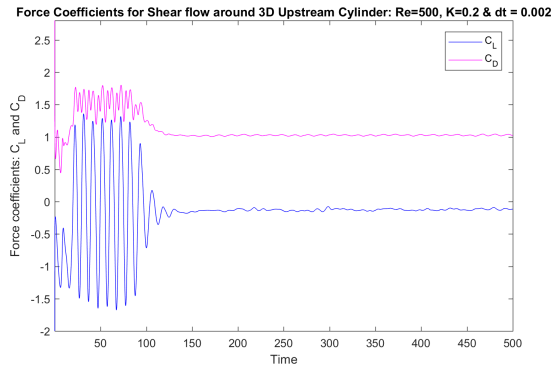


Figure A.45: Drag - and Lift Coefficients for 3D Upstream Cylinder in Shear Flow at  $R_e = 500$ ,  $K = 0.2$  and  $\Delta t = 0.002$ .

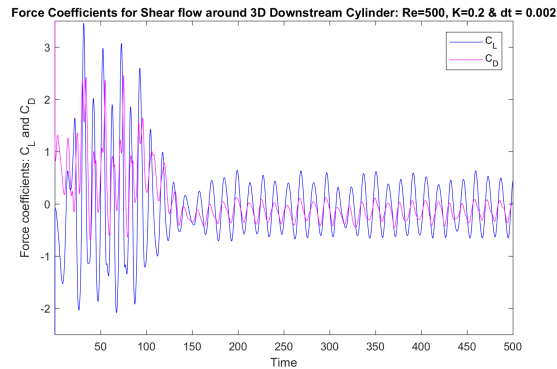


Figure A.46: Drag - and Lift Coefficients for 3D Downstream Cylinder in Shear Flow at  $R_e = 500$ ,  $K = 0.2$  and  $\Delta t = 0.002$ .



The velocity fluctuation behind the upstream cylinder is presented in figure A.47. The velocity fluctuation has a stable oscillation towards  $t = 100s$ , before oscillating unstable towards  $t = 500s$  and is oscillating close to zero with several local peaks. The fluctuation seems unstable as the local peaks occur.

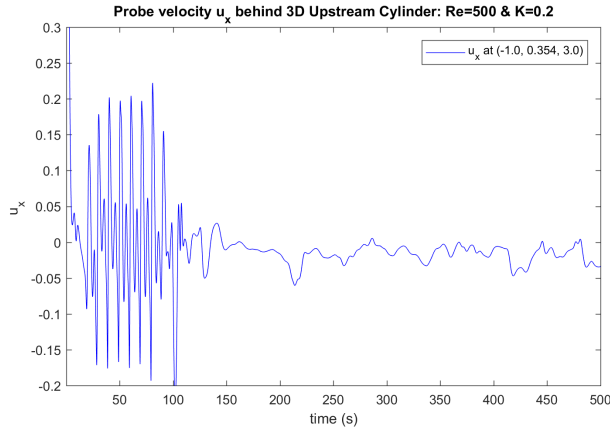


Figure A.47:  $U_x$  velocity probe behind 3D Upstream Cylinder  $(x, y, z) = (-1.0, 0.354, 3.0)$  at  $Re = 500$ ,  $K = 0.2$  at  $\Delta t = 0.002$

The velocity fluctuation behind the downstream cylinder is presented in figure A.48, where the velocity oscillated stable towards  $t = 500s$ , but changes its oscillation amplitude (root mean square) and frequency around time instant  $t = 100s$ . The downstream cylinder obtains a periodically fluctuating, but the velocity is close to zero right behind the upstream cylinder.

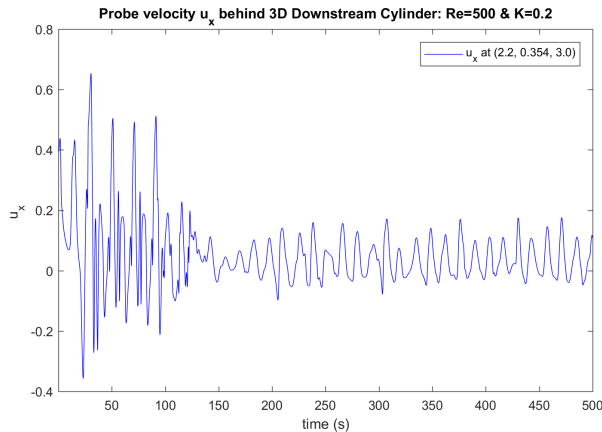


Figure A.48:  $U_x$  velocity probe behind 3D Downstream Cylinder  $(x, y, z) = (2.2, 0.354, 3.0)$  at  $Re = 500$ ,  $K = 0.2$  at  $\Delta t = 0.002$

Far downstream the velocity fluctuation is measured at point  $(x, y, z) = (3.5, 0.354, 3.0)$  and presented in figure A.49. The velocity at this point oscillated with the same period and frequency as for the velocity right behind the downstream cylinder.

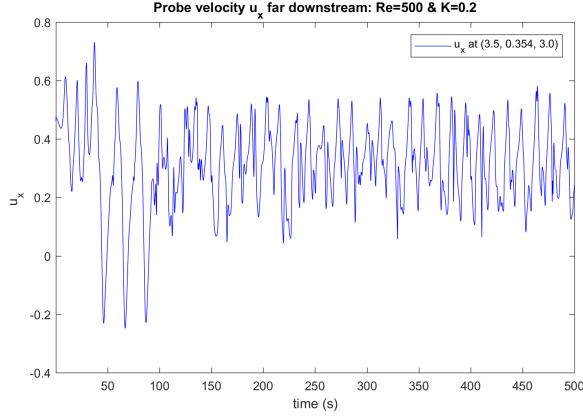


Figure A.49:  $U_x$  velocity probe far downstream  $(x, y, z) = (3.5, 0.354, 3.0)$  at  $R_e = 500$ ,  $K = 0.2$  at  $\Delta t = 0.002$ .

Pressure distribution at four different probes presents the fluctuation at the given points, behind upstream cylinder  $(x, y, z) = (-1.0, 0.354, 3.0)$ , in-between tandem cylinders  $(z, y, z) = (0, 0.354, 3.0)$ , behind downstream cylinder  $(x, y, z) = (2.2, 0.354, 3.0)$  and far downstream  $(x, y, z) = (3.5, 0.354, 3.0)$ . The pressure is highly unstable for the first 100 s of the time simulation, but is stable towards  $t = 500$ s.

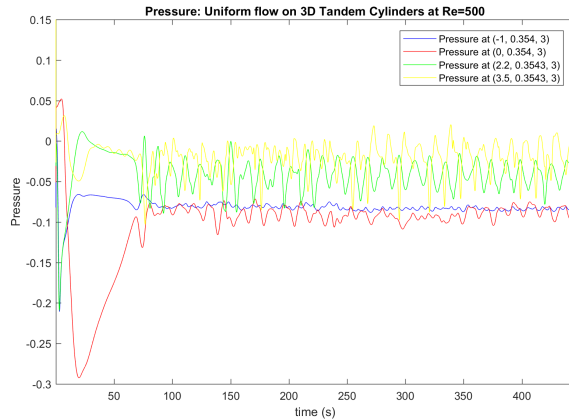


Figure A.50: Pressure fluctuation with respect to time simulation for Probe1  $(-1, 0.354, 3)$ , Probe 2  $(0, 0.354, 3)$ , Probe 3  $(2.2, 0.354, 3)$  and probe 4  $(3.5, 0.354, 3)$  for a Shear Flow around 3D Tandem Cylinders with  $R_e = 500$ ,  $K = 0.2$   $\Delta t = 0.002$ .

The velocity fluctuation behind the upstream cylinder is unstable, but the Power Spectral Density gives out two peak value for oscillation periods and frequencies. Due to the unstable velocity fluctuation presented in figure A.49, the periods and frequencies obtained for the upstream cylinder is not ideal results.

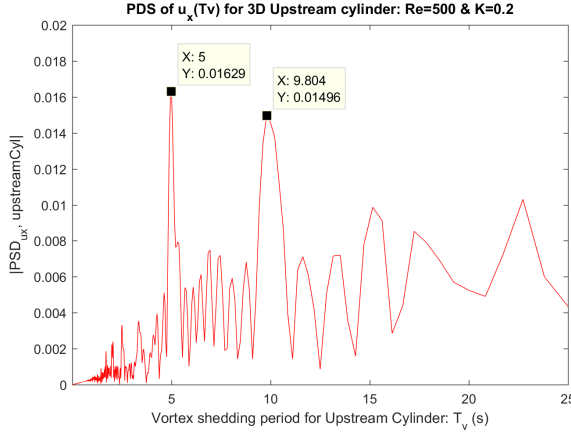


Figure A.51: The power spectral density of probe velocity  $U_x$  with respect to vortex shedding period  $T_v$  for: 3D Upstream Cylinder at  $R_e = 500$ ,  $K = 0.2$  and  $\Delta t = 0.002$ .

The downstream cylinder experience oscillation period of  $T_v = 13.89$  and a frequency of  $f_v = 0.072$ . The Strouhals number for the downstream cylinder is  $S_t = 0.144$ . Comparing these results with the results obtained for the uniform flow problem around tandem cylinders with  $R_e = 500$  in section .11, the oscillation period, frequency and Strouhals number are approximately the same.

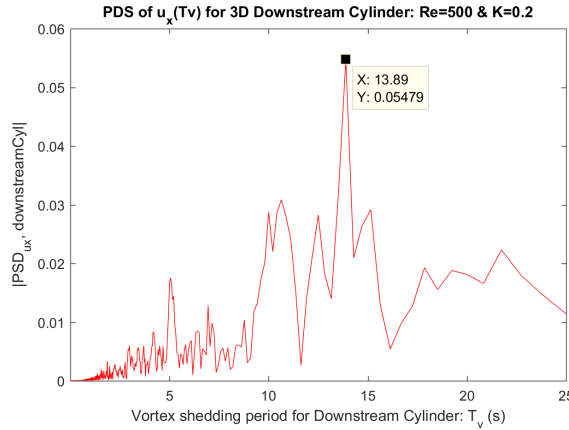


Figure A.52: The power spectral density of probe velocity  $U_x$  with respect to vortex shedding period  $T_v$  for: 3D Downstream Cylinder at  $R_e = 500$ ,  $K = 0.2$  and  $\Delta t = 0.002$ .

Velocity magnitude in figure A.53 and pressure distribution in figure A.54 is at time instant  $t = 50s$ , where the flow is oscillating with amplitude and frequency for the 2D shear flow problem with no 3D effects, while the pressure is unstable. There are velocity fluctuation in-between the tandem cylinders, such that the downstream cylinder will be effected by the wake of the upstream cylinders. There are alternating vortex shedding occurring downstream.

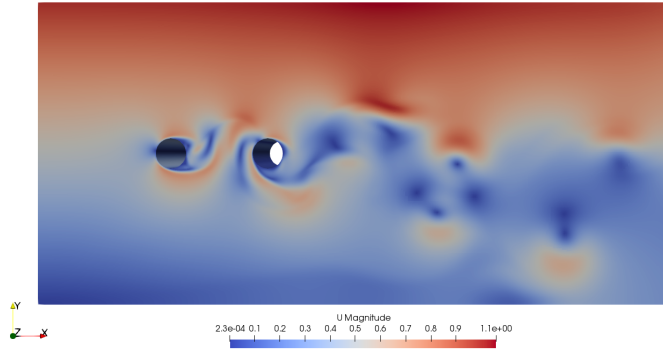


Figure A.53: Velocity magnitude for shear flow around tandem cylinders for  $R_e = 500$  &  $K = 0.2$  at time instant  $t = 50s$ .

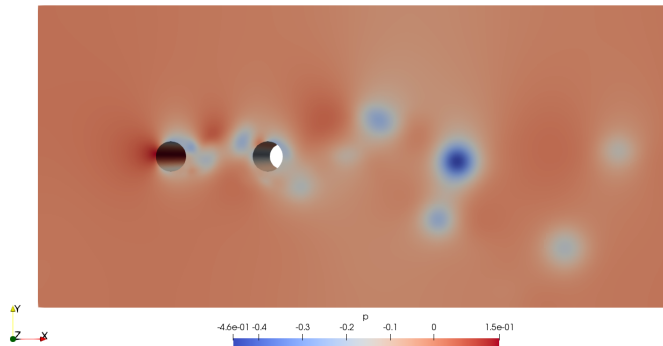


Figure A.54: Pressure distribution for shear flow around tandem cylinders for  $R_e = 500$  &  $K = 0.2$  at time instant  $t = 50s$ .

At time instant  $t = 100s$ , the velocity fluctuations behind upstream and downstream cylinder begins to oscillate with a different amplitude (root mean square). The pressure begins to stabilize and oscillate periodically.

Figure A.55 presents the velocity magnitude, where there are velocity fluctuations in-between the tandem cylinders. The upstream cylinder is shedding vortices towards the downstream cylinder. Far downstream there will be vortex shedding, but now 3D effects will effects the flow span-wise along the cylinder. The pressure distribution in figure A.56 presents low pressure zones for the areas of alternating vortex shedding in the downstream region.

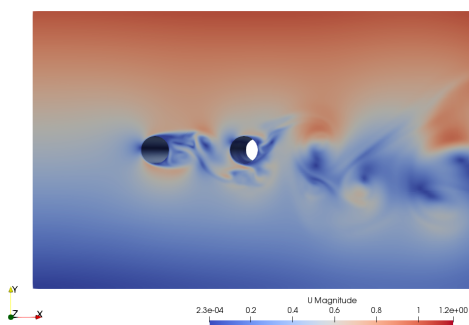


Figure A.55: Velocity magnitude for shear flow around tandem cylinders for  $R_e = 500$  &  $K = 0.2$  at time instant  $t = 100s$ .

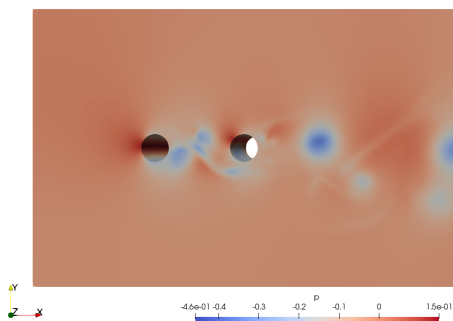


Figure A.56: Pressure distribution for shear flow around tandem cylinders for  $R_e = 500$  &  $K = 0.2$  at time instant  $t = 100s$ .

At time instant  $t = 150s$  the flow problem has stabilized with a new oscillation period, frequency and amplitude (root mean square).

Figure A.57 presents the velocity magnitude. At this time instant the velocity in-between the cylinder is approximately zero, with small and irregular velocity fluctuations. In the downstream wake region, there are vortex shedding occurring.

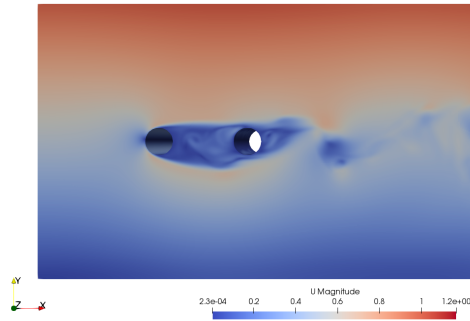


Figure A.57: Velocity magnitude for shear flow around tandem cylinders for  $R_e = 500$  &  $K = 0.2$  at time instant  $t = 150s$ .

The pressure distribution in figure A.38 presents the stagnation point in-front of the upstream cylinder with a high pressure zone, and lower pressure areas in-between the tandem cylinders.

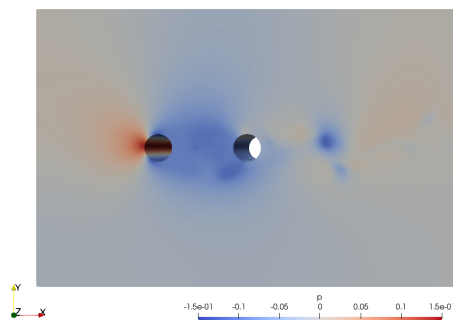


Figure A.58: Pressure distribution for shear flow around tandem cylinders for  $R_e = 500$  &  $K = 0.2$  at time instant  $t = 150s$ .

The velocity magnitude at time instant  $t = 500s$  is presented in figure A.59 visualize the low velocities in-between the cylinders. Downstream wake area consist of alternating vortices. The pressure distribution is presented in A.60 presents the stagnation point, and the low pressure areas around the tandem cylinders. The low pressure zones in the wake region are due to high velocities due vortex shedding.

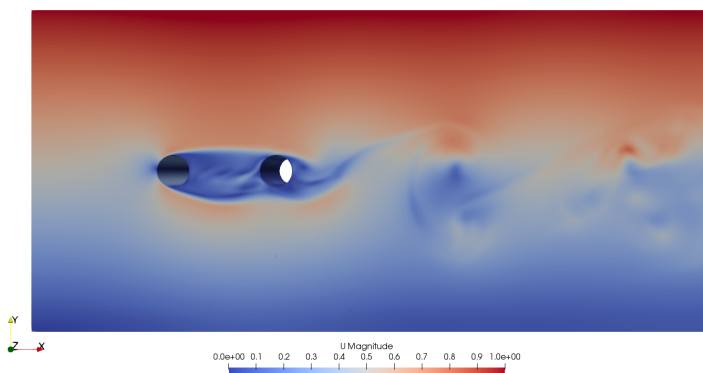


Figure A.59: Velocity magnitude for shear flow around tandem cylinders for  $R_e = 500$  &  $K = 0.2$  at time instant  $t = 500s$ .

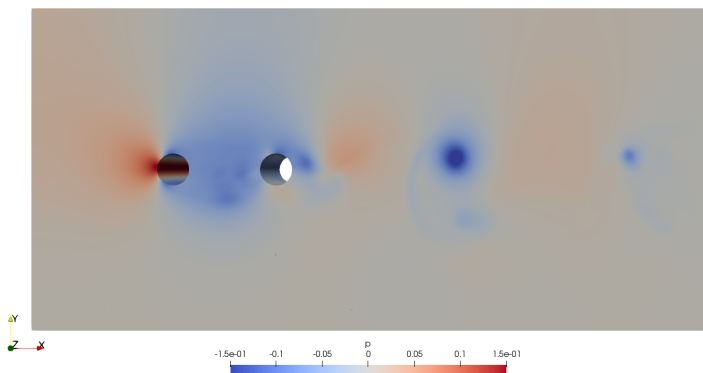


Figure A.60: Pressure distribution for shear flow around tandem cylinders for  $R_e = 500$  &  $K = 0.2$  at time instant  $t = 500s$ .

Figure A.61 and A.62 presents the velocities in  $y$  - direction and  $z$ -direction. The figures presents approximately no velocities for  $U_y$  and  $U_z$ . The velocity magnitude presented in figure A.59 consist of contribution from velocity in  $x$ -direction  $U_x$ .

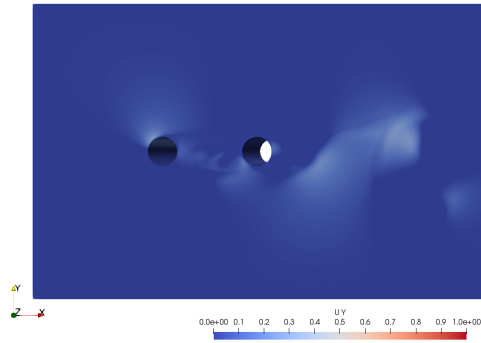


Figure A.61: Velocity in  $y$  - direction  $U_y$  for Uniform Flow around tandem cylinders with  $Re = 500$  at time instant  $t = 500s$ .

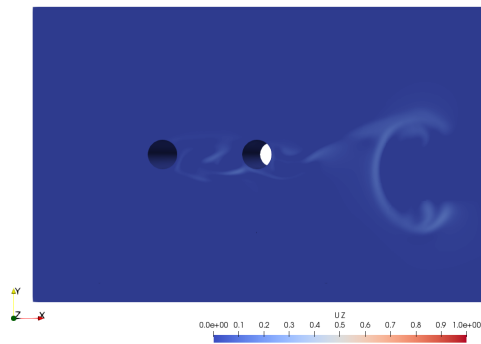


Figure A.62: Velocity in  $z$  - direction  $U_z$  for Uniform Flow around tandem cylinders with  $Re = 500$  at time instant  $t = 500s$ .



Figure A.63 presents  $\omega_z$ , where there are vorticities in-between the cylinder which are shedded from the upstream cylinder towards the downstream cylinder. In figure A.64 the vorticity in z-direction is visualized for a different angle at time instant  $t = 50s$ . The figure visualize no 3D effects along the cylinder or the alternating vortex shedding.

At time instant  $t = 50s$  the flow oscillates as in the 2D shear flow problem with  $Re = 500$ , where there are no 3D effects occurring along the span-wise length. There are several alternating vortex shedding occurring at this time step, which is visualized downstream.

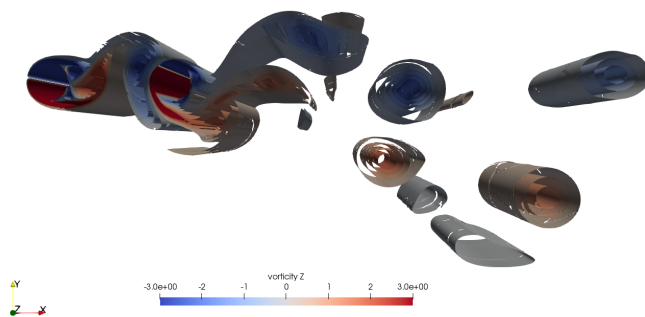


Figure A.63: Vorticity in z-direction  $\omega_z$  for shear flow around tandem cylinder for  $Re = 500$  &  $K = 0.2$  at time instant  $t = 50s$ .

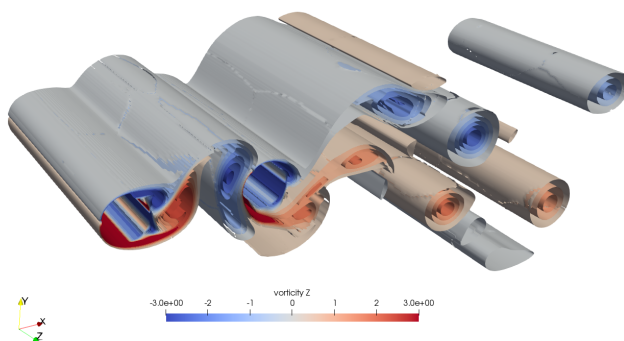


Figure A.64: Vorticity in z-direction  $\omega_z$  for shear flow around tandem cylinder for  $Re = 500$  &  $K = 0.2$  at time instant  $t = 50s$ . Different angle.

Figure A.65 presents the vorticity in z-direction  $\omega_z$ , where the vortex sheddings downstream are effected by the 3D effects. The vortices downstream begin to obtain irregularities which is turbulence along the span-wise length presented in figure A.66.

In-between the tandem cylinders, there are vortices shedded from the upstream cylinder towards the downstream cylinder. The flow around the upstream cylinders seems smooth over the span-wise length, while the turbulent behaviour occur as the flow moves around the downstream cylinder and sheds vortices far downstream.

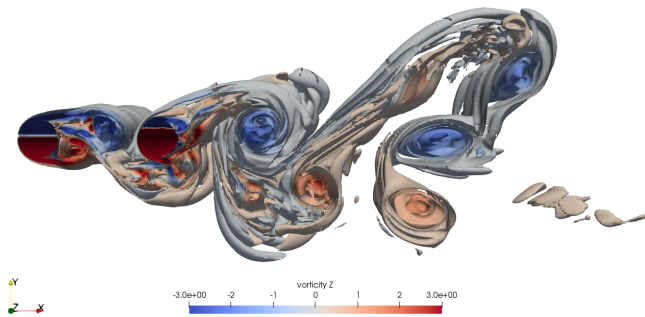


Figure A.65: Vorticity in z-direction  $\omega_z$  for shear flow around tandem cylinder for  $R_e = 500$  &  $K = 0.2$  at time instant  $t = 100s$ .

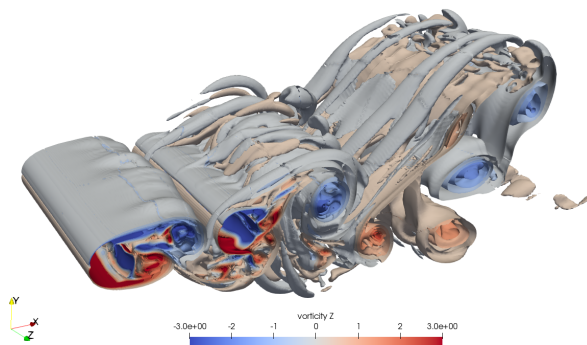


Figure A.66: Vorticity in z-direction  $\omega_z$  for shear flow around tandem cylinder for  $R_e = 500$  &  $K = 0.2$  at time instant  $t = 100s$ . Different angle.

At time instant  $t = 150s$  the flow begins to move around both tandem cylinders, but there are still small vortices in-between the cylinders which are shedded from the upstream cylinder. Far downstream the downstream cylinder will shed vortices, which experience 3D effects, as the fluid starts to move in  $z$ -direction. The vortices no longer look like vortices as the flow contains turbulence behaviour downstream.

Figure A.67 presents the vorticity distribution, where one can observe hoe the flow behaves downstream. Figure A.68 presents the vorticity distribution in a different angle, where the flow around the tandem cylinders are smooth with almost no 3D effects, until the fluid flow is shedded from the downstream cylinder far downstream.

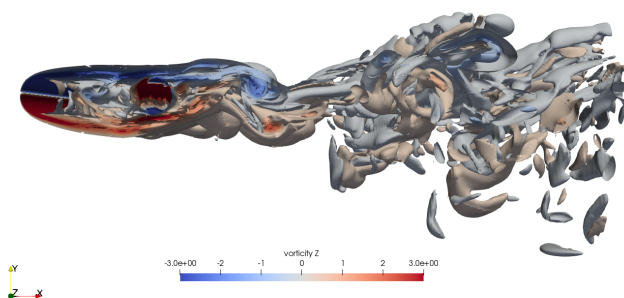


Figure A.67: Vorticity in  $z$ -direction  $\omega_z$  for shear flow around tandem cylinder for  $R_e = 500$  &  $K = 0.2$  at time instant  $t = 150s$ .

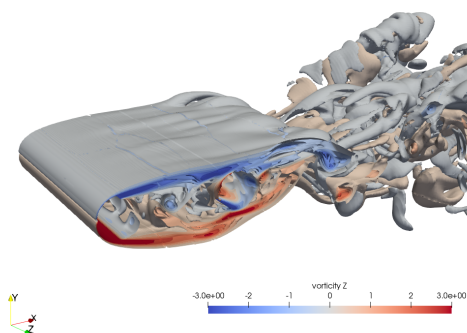


Figure A.68: Vorticity in  $z$ -direction  $\omega_z$  for shear flow around tandem cylinder for  $R_e = 500$  &  $K = 0.2$  at time instant  $t = 150s$ . Different angle.

The shear flow problem around 3D tandem cylinder with shear rate  $K = 0.2$  and  $Re = 500$  is simulated towards  $t = 500s$ . The figure A.69 presents the vorticity in z-direction  $\omega_z$  where vortex shedding occurs behind the downstream cylinder. Figure A.70 presents  $\omega_z$  in a different angle, where one can observe no 3D effects of the flow around the tandem cylinder.

The 3D effects will affect the vortex shedding downstream. The wake region consist of shedded vortices with turbulent behaviour, such that the vortex shedding becomes more unclear.

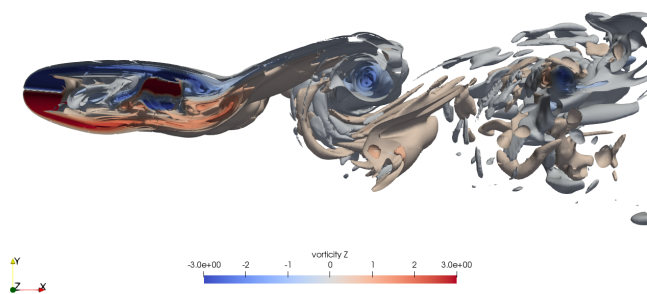


Figure A.69: Vorticity in z-direction  $\omega_z$  for shear flow around tandem cylinder for  $Re = 500$  &  $K = 0.2$  at time instant  $t = 500s$ .

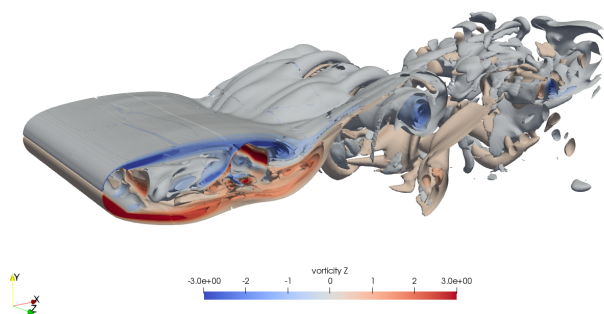


Figure A.70: Vorticity in z-direction  $\omega_z$  for shear flow around tandem cylinder for  $Re = 500$  &  $K = 0.2$  at time instant  $t = 500s$ . Different angle.

## .6 Uniform Flow around a 3D Circular Cylinder

This section presents the uniform flow problem with Reynolds number 100, 200 and 300, analyzed around a single circular cylinder with time step  $\Delta t = 0.005$ . The domain size and cylinder dimensions are given in table A.1.

Table A.1: Domain size and Cylinder dimensions.

Domain Range and Dimensions:	
$X_{range}$ :	$-3 < x < 12.5$
$Y_{range}$ :	$-8 < y < 8$
$Z_{range}$ , 3D:	$0 < z < 4$
Diameter D	1
Cylinder origo:	$(x,y,z) = (0, 0, 0)$

Figure A.71 presents the mesh generated around a circular cylinder for the domain presented in table A.1.

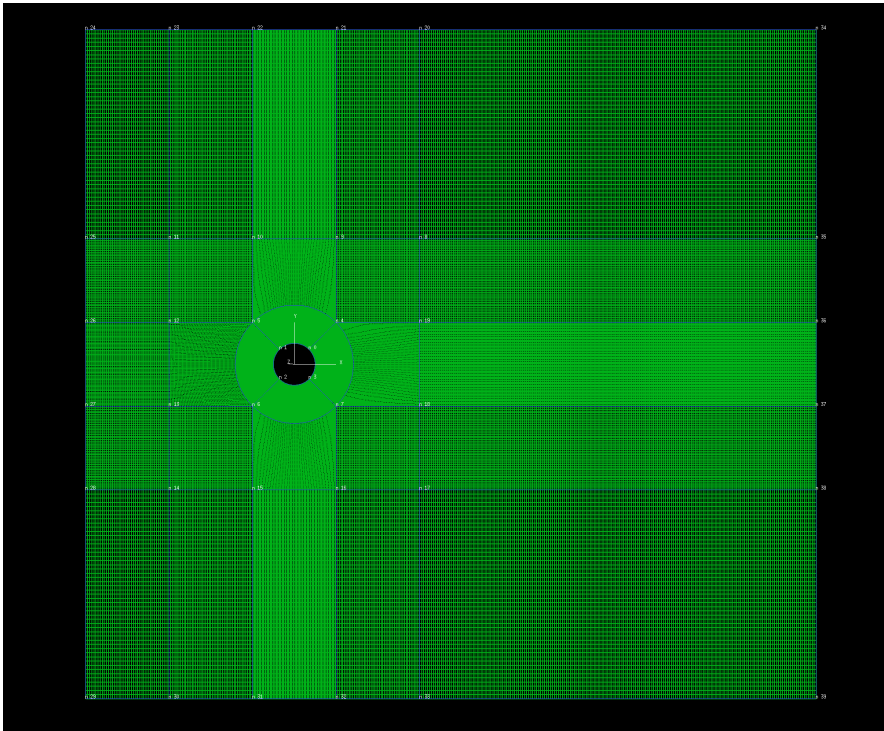


Figure A.71: Mesh generated in MEGA: 2D Single Cylinder with  $D = 1$ .

Table A.2 presents the boundary constraint which are used to analyze a uniform flow around a single circular cylinder for various Reynolds numbers.

Table A.2: Defining boundary conditions in OpenFOAM [Greenshields, 2015].

Defined boundaries:	Geometric constraint:	Velocity U:	Pressure P:
front	empty (2D)	empty (2D)	empty (2D)
	cyclic (3D)	cyclic (3D)	cyclic (3D)
back	empty (2D)	empty (2D)	empty (2D)
	cyclic (3D)	cyclic (3D)	cyclic (3D)
cylinder	wall	fixedValue	zeroGradient
inlet	patch	fixedValue	zeroGradient
outlet	patch	zeroGradient	fixedValue
topAndBottom	slip	slip	slip

Table A.3 presents the mean values and the root mean square values of drag - and lift coefficient. The values are found for the last 80 % results for the time simulation towards  $t = 180s$  with time step  $\Delta t = 0.005$ .

Oscillation period  $T_v$ , frequency  $f_v$  and Strouhal number  $S_t$  are found for the flow problem with Reynolds number 100, while for Reynolds number  $Re = 200$  and  $Re = 300$  the values are obtained for time simulation towards  $t = 250s$  with time step  $\Delta t = 0.005$ .

To increase the Reynolds number for each flow case, the inlet velocity is changed, while the kinematic viscosity  $\nu$  is set to 0.01. In further simulations the viscosity will be changes to obtain the desired Reynolds number, while the inlet velocity is unchanged for the various flow problems.

Table A.3: Values for test case: Uniform flow around a circular cylinder for  $t = 180s$ .

$Re$	<b>100</b>	<b>200</b>	<b>300</b>
U	1	2	3
magUInf	1	2	3
viscosity $\nu$	0.01	0.01	0.01
$\Delta t$	0.005	0.005	0.005
mean $C_L$	-0.01231	0.00027	0.00323
mean $C_D$	1.46210	1.37041	1.36400
RMS $C_L$	0.25080	0.41337	0.47233
RMS $C_D$	0.00737	0.04764	0.04694
$T_v[s]$	5.80	-	-
$f_v[Hz]$	0.1722	-	-
$S_t[-]$	0.1722	-	-

The mean vales and root mean square values for drag - and lift coefficient for Reynolds number 200 and 300 are presented in table A.4, for time simulation towards  $t = 250s$  with time step  $\Delta t = 0.005$ .

Table A.4: Values for test case: Uniform flow around a circular cylinder for  $t = 250s$ .

$R_e$	<b>200</b>	<b>300</b>
mean $C_L$	0.00030	0.00314
mean $C_D$	1.36486	1.39338
RMS $C_L$	0.40231	0.53586
RMS $C_D$	0.05103	0.04704
$T_v[s]$	2.5 & 2.632	1.623
$f_v[Hz]$	0.38 & 0.4	0.616
$S_t[-]$	0.19 & 0.2	0.20533

## PLOTS: Single Cylinder in Uniform Flow at $Re = 100$

The figure A.72 presents how the drag - and lift coefficient oscillates. The flow stabilize around  $t = 20 - 30s$ , where the oscillation is stable towards  $t = 180s$ .

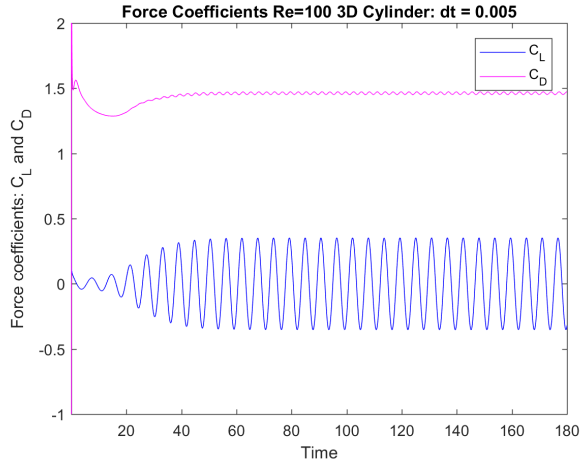


Figure A.72: Drag - and Lift Coefficients at  $\Delta t = 0.005$  for  $Re = 100$ .

The Power Spectral Density (PDS) curves are found by Fourier Transform of the lift coefficient  $C_L$ . The PDS's curve presented the period  $T_v = 5.806s$  for the 65 % last values for the time simulation, where the frequency  $f_v = 1/T_v = 0.1722Hz$ . The Strouhals number for this flow problem is  $S_t = 0.1722$ .

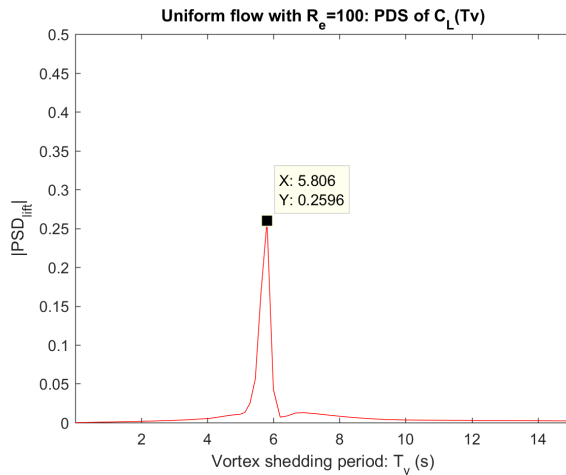


Figure A.73: The power spectral density of lift coefficients  $C_L$  with respect to vortex shedding period  $T_v$  at  $Re = 100$ .



Figure A.74 presents the velocity magnitude at the stable time instant  $t = 180s$ . The plot presents vortex shedding in the wake region, and low velocity regions behind the wake.

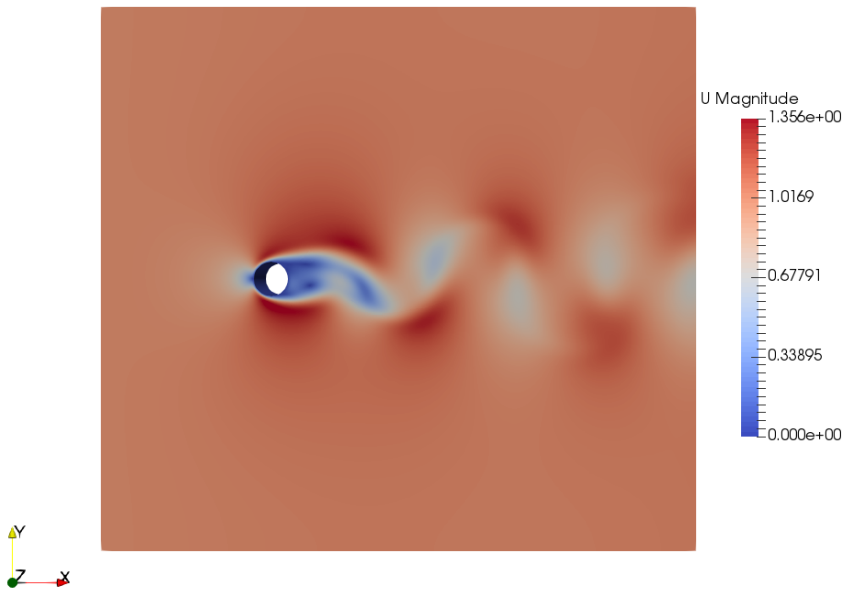


Figure A.74: Velocity magnitude for uniform flow at  $R_e = 100$  at time instant  $t = 180s$ .

Figure A.75 presents the pressure distribution at the stable time instant  $t = 180s$  as vortex shedding occurs. There is a high pressure zone located in-front of the cylinder due to stagnation point.

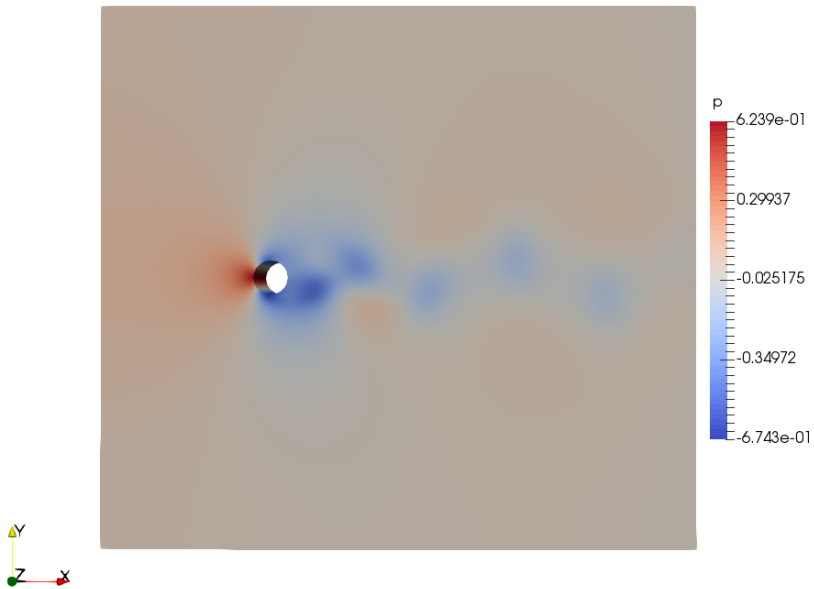


Figure A.75: Pressure distribution for uniform flow at  $R_e = 100$  at time instant  $t = 180s$ .

Figure A.76 presents the vorticity distribution in z-direction  $\omega_z$ . The figure presents how the vortex shedding occurs for each side of the cylinder. For the flow problem at Reynolds number 100, the flow is two-dimensional, such that there are no three-dimensional effects along the span-wise length of the cylinder.

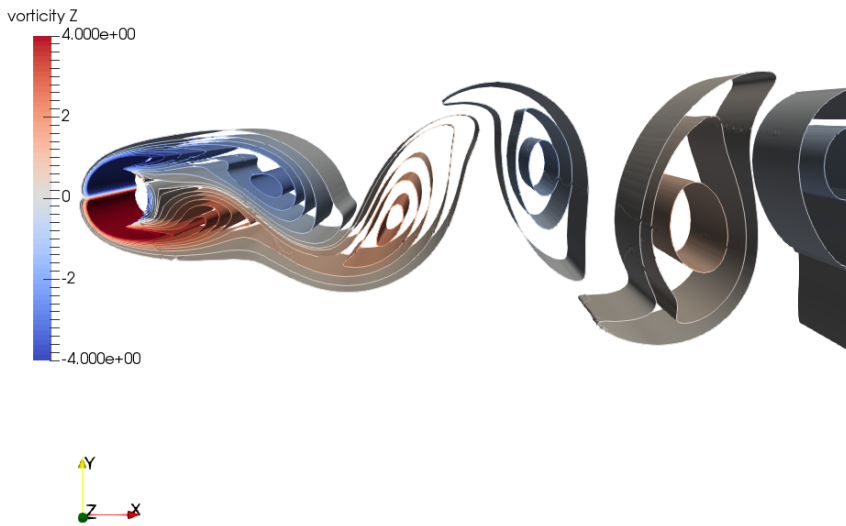


Figure A.76: Vorticity in z-direction  $\omega_z$  for uniform flow at  $R_e = 100$  at time instant  $t = 180s$ .

## PLOTS: Single Cylinder in Uniform Flow at $Re = 200$

The figure A.77 presents how the drag - and lift coefficient oscillates. The flow seems stable towards  $t = 130s$ , where the flow begins to oscillate with various root mean square values. The simulation is run to time instant  $t = 250s$ .

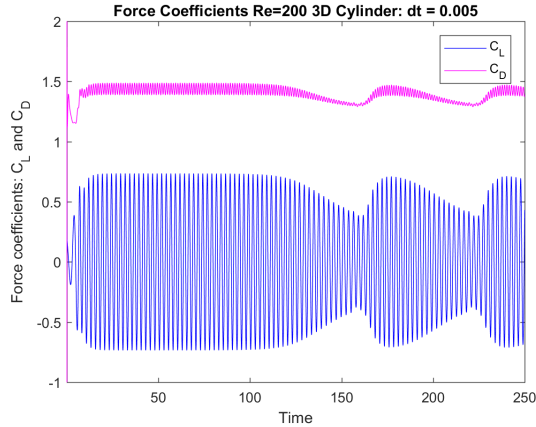


Figure A.77: Drag - and Lift Coefficients at  $\Delta t = 0.005$  for  $Re = 200$ .

The Power Spectral Density curves presents two peaks for oscillation period and frequency found by Fourier Transform of the lift coefficient  $C_L$ . The two peaks occur due to the flow will have one oscillation frequency towards  $t = 130s$ , but also an alternating oscillation frequency with different root mean square values between  $t = 130s$  and  $t = 250s$ .

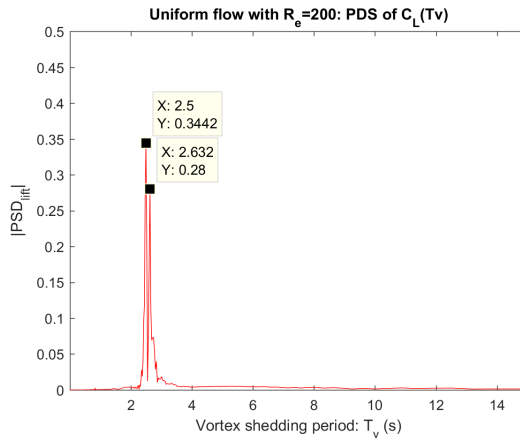


Figure A.78: The power spectral density of lift coefficients  $C_L$  with respect to vortex shedding period  $T_v$  at  $Re = 200$ .

The figures A.79 and A.80 present the velocity magnitude and pressure distribution at time instant  $t = 250s$ . Vortex shedding is presented clearly for the velocity magnitude plot and in with low pressure zones in the wake region.

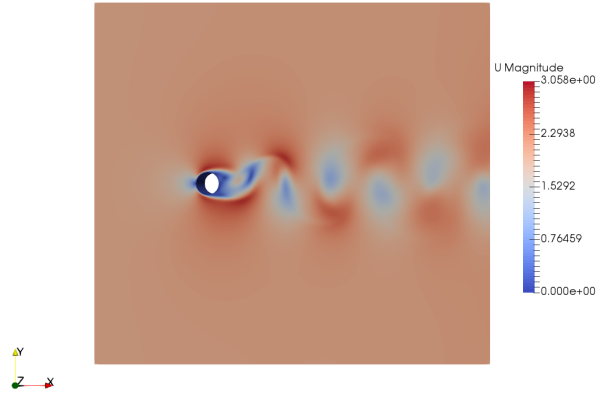


Figure A.79: Velocity magnitude for uniform flow at  $R_e = 200$  at time instant  $t = 250s$ .

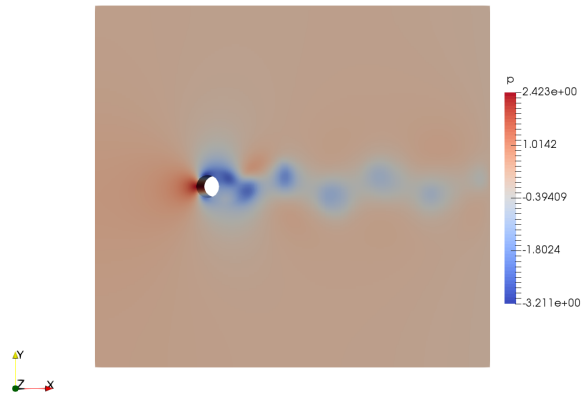


Figure A.80: Pressure distribution for uniform flow at  $R_e = 200$  at time instant  $t = 250s$ .

The vorticity distribution in  $z$ -direction  $\omega_z$  in figure A.76 presents the vorticity distribution from  $-5.0 < \omega_z < 5.0$ , where the vortex sheddings have alternating vorticity value. For Reynolds number 200 there are some 3D effects occurring along the span-wise length.

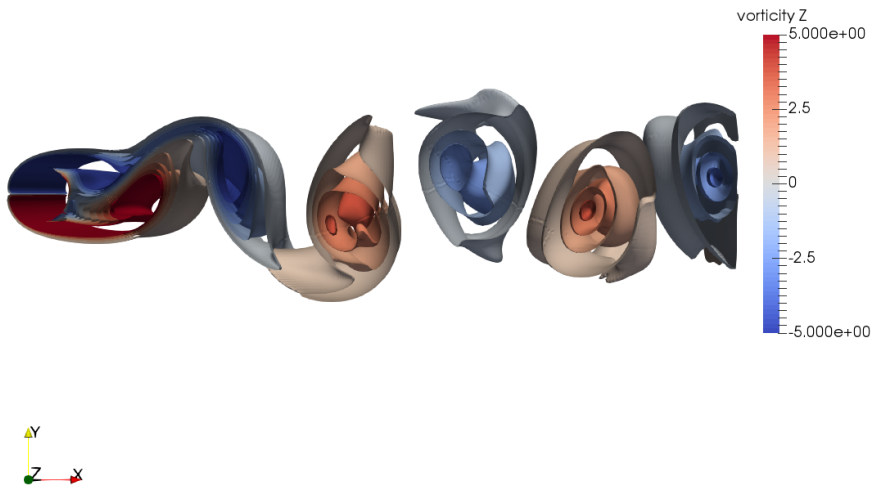


Figure A.81: Vorticity in  $z$ -direction  $\omega_z$  for uniform flow at  $Re = 200$  at time instant  $t = 250s$ .

## PLOTS: Single Cylinder in Uniform Flow at $Re = 300$

Figure A.82 presents the drag - and lift oscillation for the flow problem. The Oscillation has varying root mean square value, but it stable for the time simulation towards  $t = 250s$ .

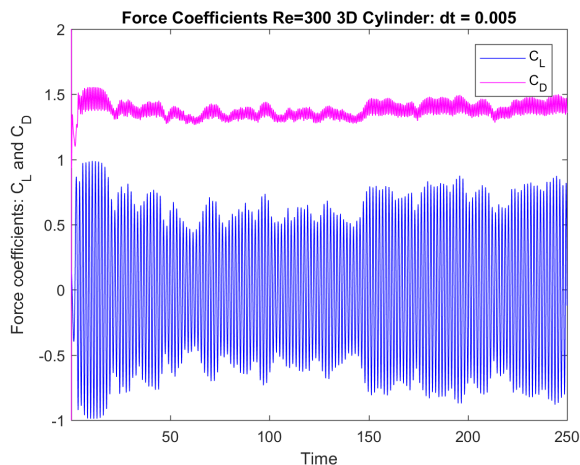


Figure A.82: Drag - and Lift Coefficients at  $\Delta t = 0.005$  for  $Re = 300$ .

The Power Spectral Density presents the Fourier transformation of the lift coefficient  $C_L$ , where the Strouhals number is  $S_t = 0.205$ .

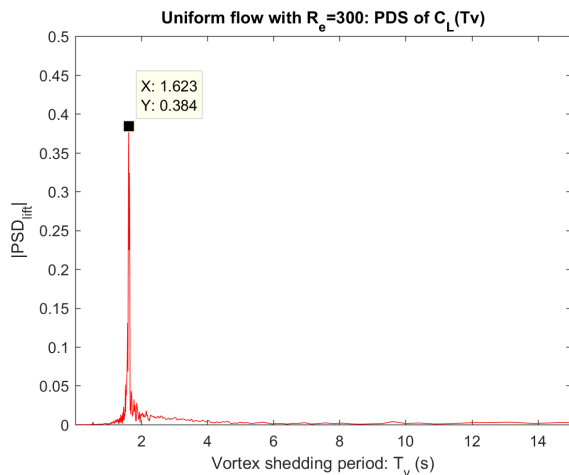


Figure A.83: The power spectral density of lift coefficients  $C_L$  with respect to vortex shedding period  $T_v$  at  $Re = 300$ .

The figures A.84 and A.85 present the velocity magnitude and pressure distribution at time instant  $t = 250s$  for the uniform flow problem with Reynolds number 300. As for the uniform flow problem with Reynolds number 200, one can observe vortex shedding for both velocity magnitude plot and pressure distribution plot.

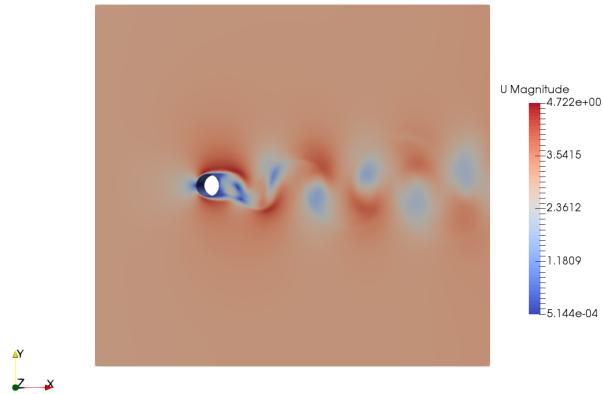


Figure A.84: Velocity magnitude for uniform flow at  $R_e = 300$  at time instant  $t = 250s$ .

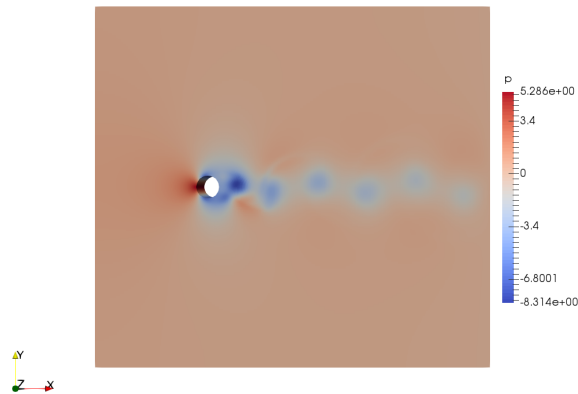


Figure A.85: Pressure distribution for uniform flow at  $R_e = 300$  at time instant  $t = 250s$ .



The vorticity distribution of  $\omega_z$  at time instant  $t = 250s$  are presented in figure A.86 and in a different angle for figure A.87. One can observe the 3D effects occurring span-wise along the cylinder for each vortex shedding.

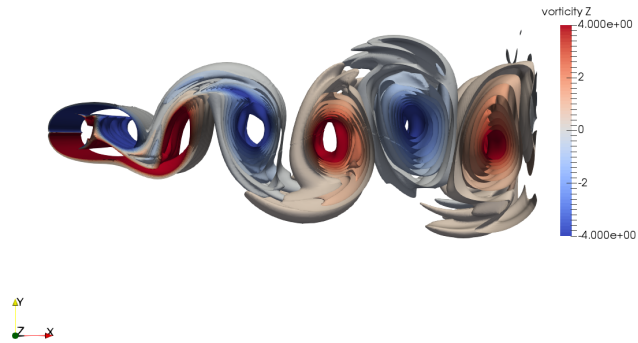


Figure A.86: Vorticity in z-direction  $\omega_z$  for uniform flow at  $Re = 300$  at time instant  $t = 250s$ .

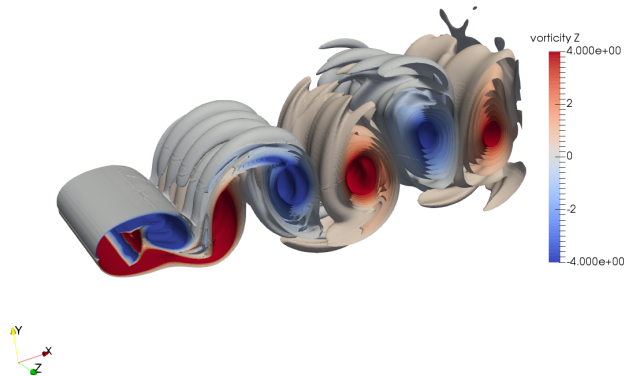


Figure A.87: Vorticity in z-direction  $\omega_z$  for uniform flow at  $Re = 300$  at time instant  $t = 250s$ . Different angle.

## .7 Uniform Flow around a 3D Circular cylinder with Boundary conditions for Slip and Symmetry

An analysis is performed with uniform flow and Reynolds number 300 around a three-dimensional cylinder, where the boundary conditions for front and back patches are changed to slip and symmetric. The boundary conditions are presented in table A.5 for slip-condition, and in table A.6 for symmetry-condition.

Table A.5: Boundary conditions: Slip

Defined boundaries	Geometric constraint	Velocity U	Pressure P
front	slip	slip	slip
back	slip	slip	slip
cylinder	wall	fixedValue	zeroGradient
inlet	patch	fixedValue	zeroGradient
outlet	patch	zeroGradient	fixedValue
topAndBottom	slip	slip	slip

Table A.6: Boundary conditions: Symmetric

Defined boundaries	Geometric constraint	Velocity U	Pressure P
front	symmetric	symmetric	symmetric
back	symmetric	symmetric	symmetric
cylinder	wall	fixedValue	zeroGradient
inlet	patch	fixedValue	zeroGradient
outlet	patch	zeroGradient	fixedValue
topAndBottom	slip	slip	slip

The flow properties are presented in table A.7, where the three-dimensional domain is presented in table A.1 in section .6.

Table A.7: Flow properties at  $R_e = 300$

Properties of Uniform Flow:	
inlet velocity $U$	1
viscosity $\nu$	0.003333
Cylinder diameter	1
Span-wise length	4D
$\Delta t$	0.005

The results obtained for the slip-condition and symmetry-condition are almost equivalent to the results in the values for drag - and lift compared to the results obtained for the three-dimensional flow problem for Reynolds number 300 in section .6.

The mean values for drag and lift coefficients as well as the root mean square for the last 80 % for the analysis are presented in table A.8.

The differences is the value for the mean drag coefficient, where the slip - and - symmetric condition gave a value  $C_D = 1.37$ , while from table A.4 in section .6 with cyclic-condition gave  $C_D = 1.39$ . The Strouahls number roughly the same.

Table A.8: Values for test case: Uniform flow around a circular cylinder with different boundary conditions  $R_e = 300$

Boundary condition	<b>slip</b>	<b>symmetric</b>
mean $C_L$	-0.00806	0.01082
mean $C_D$	1.37633	1.37791
RMS $C_L$	0.47349	0.47124
RMS $C_D$	0.04088	0.03807
$T_v[s]$	4.717	4.762
$f_v[Hz]$	0.212	0.21
$S_t[-]$	0.212	0.21

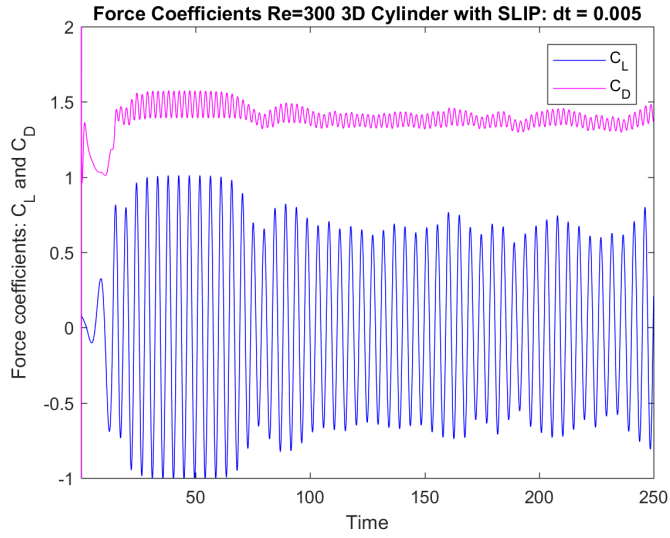


Figure A.88: Drag - and Lift Coefficients for slip condition at boundaries topAndBottom, front and back at  $\Delta t = 0.005$  for  $Re = 300$ .

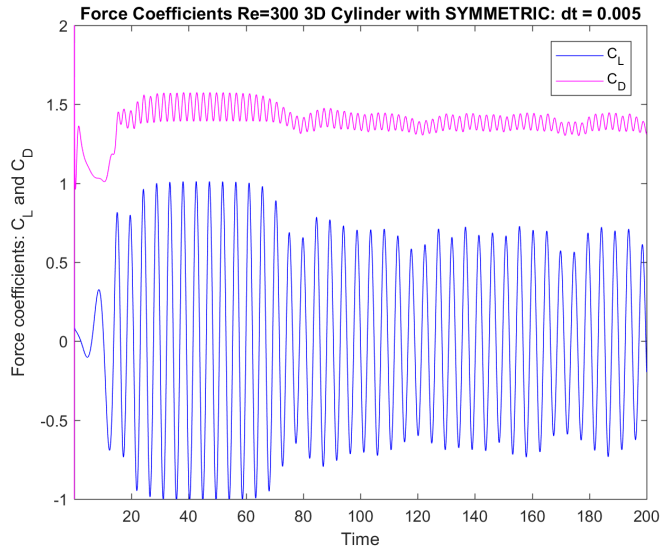


Figure A.89: Drag - and Lift Coefficients for symmetry condition at front and back boundaries at  $\Delta t = 0.005$  for  $Re = 300$ .

The figures below presents the Power Spectral Density curves for the Slip-condition with respect to oscillation period and frequency, by taking the Fourier Transform of the lift coefficient.

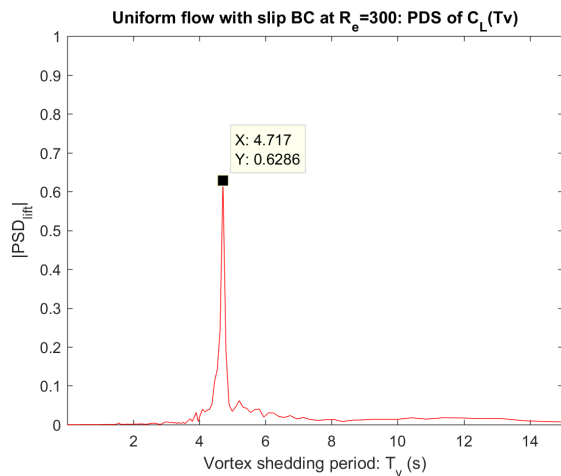


Figure A.90: The power spectral density of lift coefficients  $C_L$  with respect to vortex shedding period  $T_v$  with slip BC at  $Re = 300$ .

The figures below presents the Power Spectral Density curves for the Symmetry-condition with respect to oscillation period and frequency, by taking the Fourier Transform of the lift coefficient.

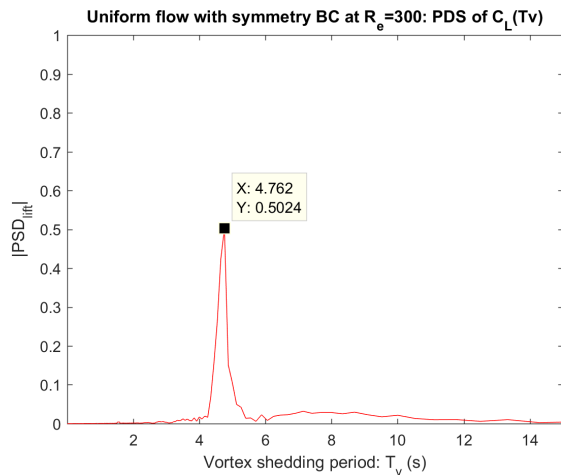


Figure A.91: The power spectral density of lift coefficients  $C_L$  with respect to vortex shedding period  $T_v$  with symmetry BC at  $Re = 300$ .

## .8 Shear Flow around a 2D Circular Cylinder

Flow problems with Shear Flow is performed for different shear rate  $K$ . The Shear Flow is subjected on a single circular cylinder with dimensions and domain size presented in table A.1 in section .6. The analysis is performed with Reynolds number 100 and time step  $\Delta t = 0.002$ , with boundary constraint given in table A.2 in section .6.

The domain size spans for  $y = -8.0$  to  $y = 8.0$ , such that some shear cases will have their shear flow inlet at different origins.

Table A.9: Properties of Shear Flow.

2D Shear Flow $Re = 100$	$Uc$	$G$	origin
$K = 0.125$	0.25	$\frac{1}{32}$	$y = -8.0$
$K = 0.2$	1.0	$\frac{1}{5}$	$y = -5.0$
$K = 0.5$	0.25	$\frac{1}{8}$	$y = -2.0$
$K = 1.0$	0.125	$\frac{1}{8}$	$y = -1.0$
$K = 2.0$	0.125	$\frac{1}{4}$	$y = -0.5$

The table A.10 presents the mean force coefficients, root mean square and the oscillation period, frequency and Strouhals number for flow problem with different Shear rate  $K$ . The values are found for the last 65 % results for the time simulation. The flow problems with shear rate  $K = 0.5$ ,  $K = 1.0$  and  $K = 2.0$  do not show any results as the flow problem becomes unstable during the simulation.

Table A.10: Shear flow around a 2D cylinder at  $Re = 100$  for various Shear Rates  $K$ .

	$K = 0.125$	$K = 0.2$	$K = 0.5$	$K = 1.0$	$K = 2.0$
mean $C_L$	-0.14555	-0.22123	-	-	-
mean $C_D$	1.43570	1.28658	-	-	-
RMS $C_L$	0.26600	0.39034	-	-	-
RMS $C_D$	0.01708	0.05908	-	-	-
$T_v [s]$	23.08	7.317	-	-	-
$f_v [Hz]$	0.04333	0.1367	-	-	-
$S_t [-]$	0.17332	0.1367	-	-	-

### PLOTS: Shear Flow around a Cylinder: $Re = 100$ & $K = 0.125$

This shear flow problem has origin at  $y = -8.0$ , which is at the bottom boundary. This flow problem is stable during the simulation time towards time instant  $t = 300s$ . The presented plots for velocity magnitude and pressure are presented for this time instant.

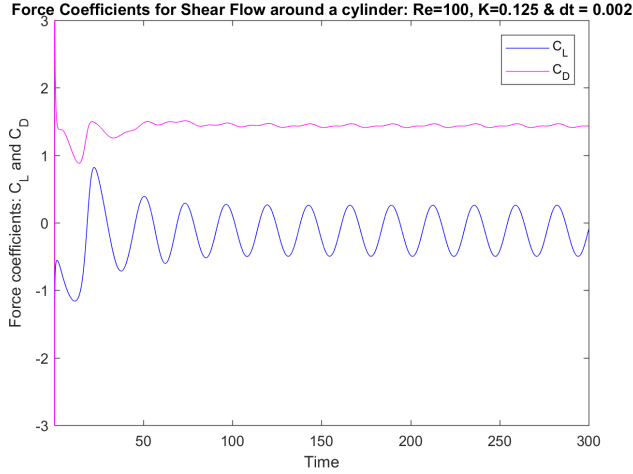


Figure A.92: Drag - and Lift Coefficients for: 2D Shear flow with  $Re = 100$ ,  $K = 0.125$  and  $\Delta t = 0.002$

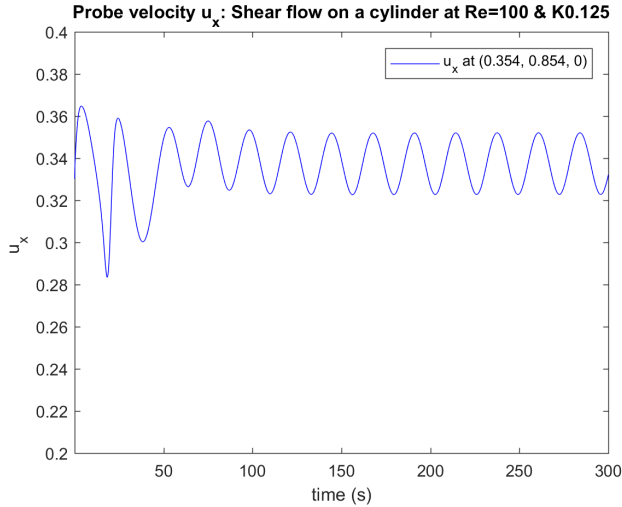


Figure A.93:  $U_x$  velocity probe at  $(x, y, z) = (0.354, 0.854, 0)$  with respect to time for: 2D Shear flow with  $Re = 100$ ,  $K = 0.125$  and  $\Delta t = 0.002$

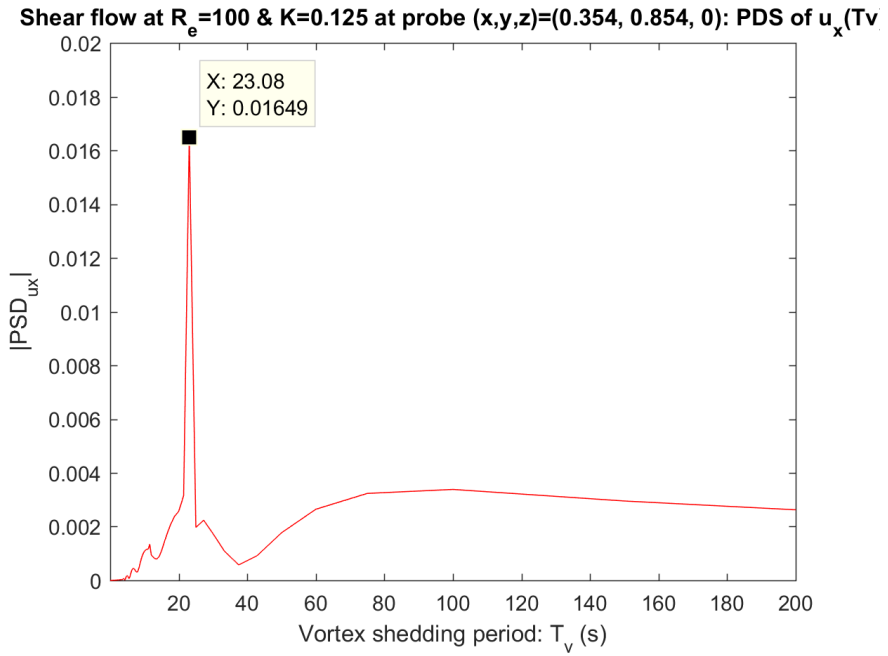


Figure A.94: The power spectral density of probe velocity  $U_x$  with respect to vortex shedding period  $T_v$  for: 2D Shear flow with  $R_e = 100$ ,  $K = 0.125$  and  $\Delta t = 0.002$ .



The figures below present the velocity magnitude at time instant  $t = 5s$  and  $t = 250s$ . At time instant  $t = 5s$  the flow will be unstable, before becoming stable as alternating vortices occur.

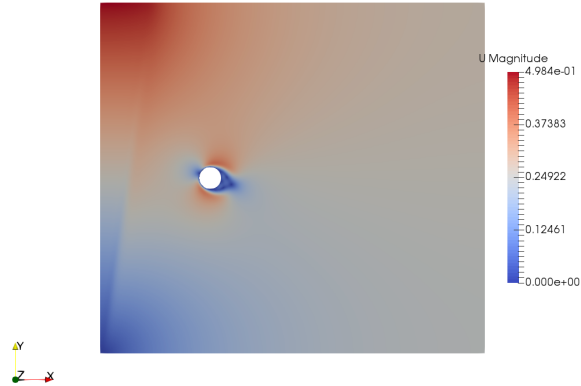


Figure A.95: Velocity magnitude at time instant  $t = 5s$  for shear current on a 2D cylinder at  $Re = 100$ ,  $K = 0.125$  and  $\Delta t = 0.002$ .

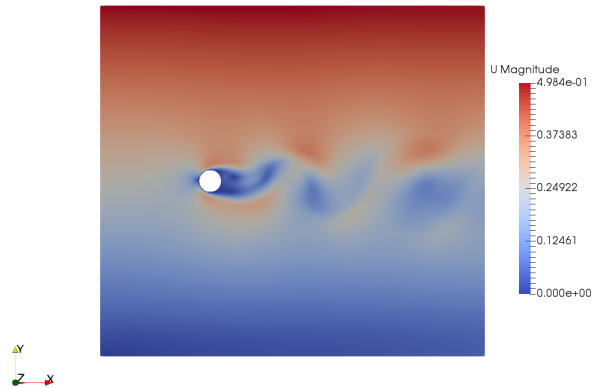


Figure A.96: Velocity magnitude at time instant  $t = 250s$  for shear current on a 2D cylinder at  $Re = 100$ ,  $K = 0.125$  and  $\Delta t = 0.002$ .

The pressure distribution is also presented for time instant  $t = 5s$  and  $t = 250s$ .

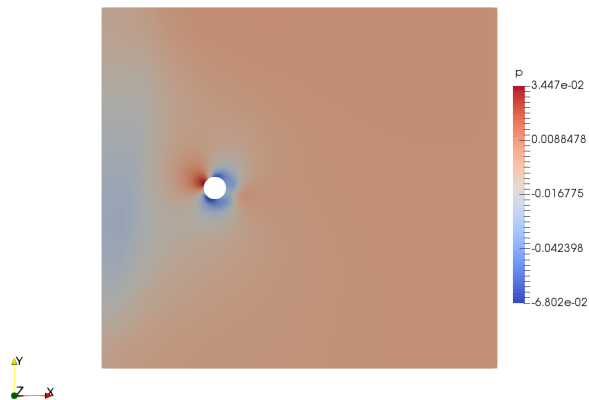


Figure A.97: Pressure distribution at time instant  $t = 5s$  for shear current on a 2D cylinder at  $Re = 100$ ,  $K = 0.125$  and  $\Delta t = 0.002$ .

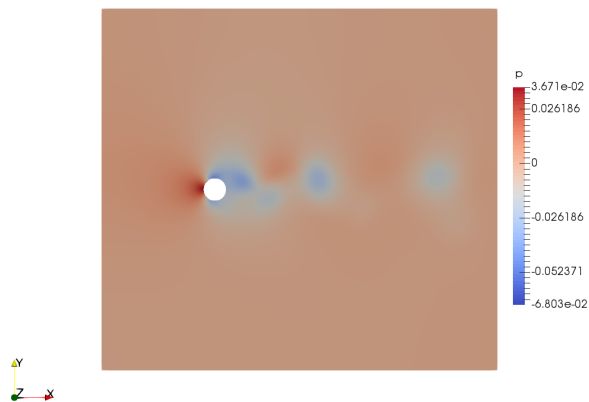


Figure A.98: Pressure distribution at time instant  $t = 260s$  for shear current on a 2D cylinder at  $Re = 100$ ,  $K = 0.125$  and  $\Delta t = 0.002$ .

### PLOTS: Shear Flow around a Cylinder: $R_e = 100$ & $K = 0.2$

This shear flow problem with shear rate  $K = 0.2$  has origin at  $y = -5.0$  while the domain span begins at  $y = -8.0$ , which can give incorrect values. Therefore a new domain is created to analyze flow problems with shear rate  $K = 0.2$ . The domain will have a span of  $y = -5.0$  to  $y = 5.0$ .

The force coefficients and the velocity in x-direction behind the cylinder are both stable, and oscillates with a constant period and frequency. This can indicate that the results are fairly correct, but not ideal due to shear flow inlet origin.

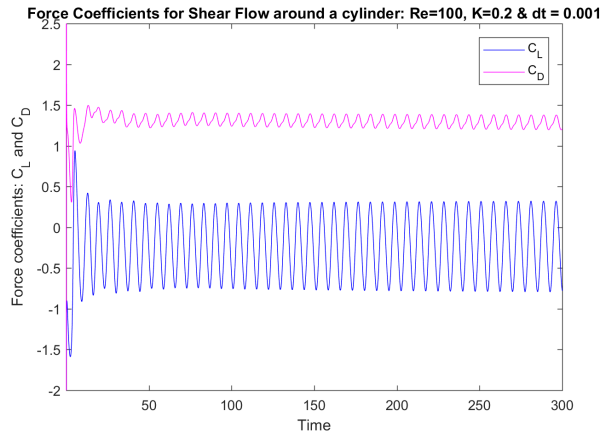


Figure A.99: Drag - and Lift Coefficients for: 2D Shear flow with  $R_e = 100$ ,  $K = 0.2$  and  $\Delta t = 0.001$

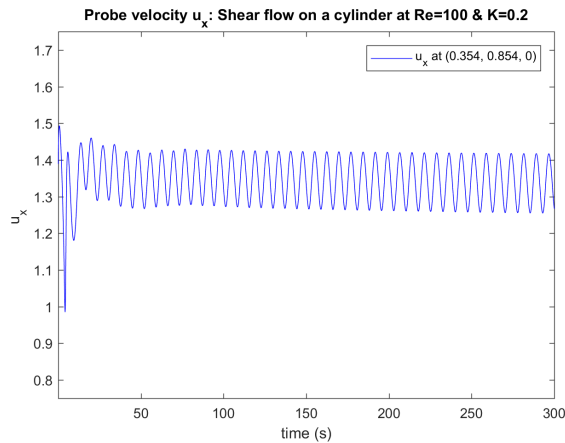


Figure A.100:  $U_x$  velocity probe at  $(x, y, z) = (0.354, 0.854, 0)$  with respect to time for: 2D Shear flow with  $R_e = 100$ ,  $K = 0.2$  and  $\Delta t = 0.001$

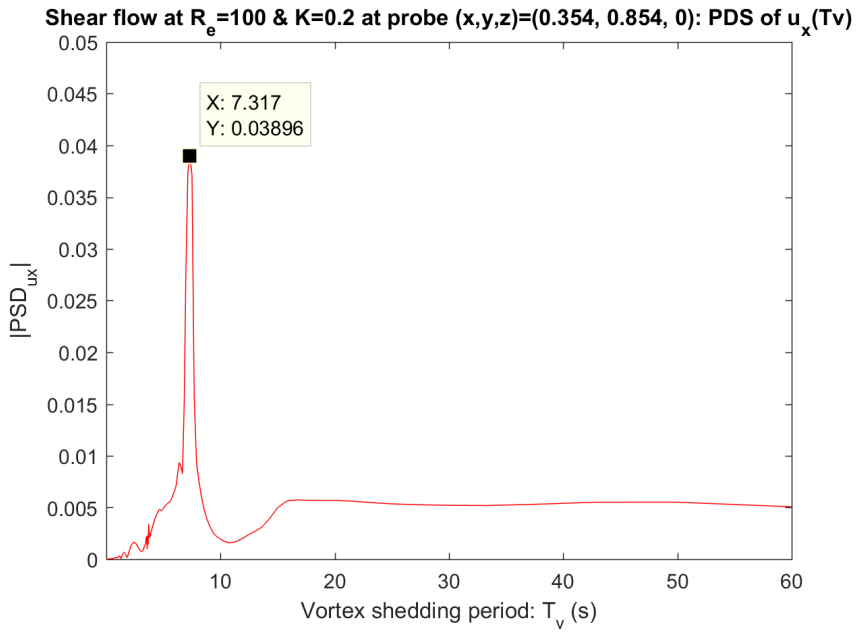


Figure A.101: The power spectral density of probe velocity  $U_x$  with respect to vortex shedding period  $T_v$  for: 2D Shear flow with  $R_e = 100$ ,  $K = 0.2$  and  $\Delta t = 0.001$ .

Since the inlet velocity begins at  $y = -5.0$ , there will be large jumps velocity in the domain, as as the lower boundary will not have any inlet velocity.

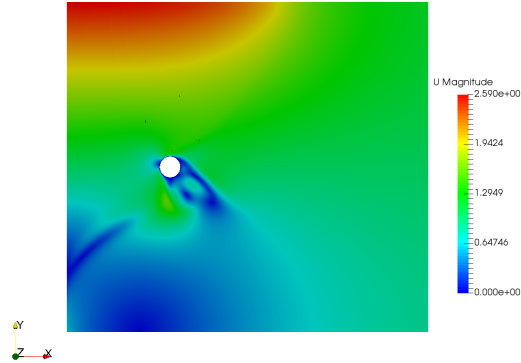


Figure A.102: Velocity magnitude at time instant  $t = 5s$  for shear current on a 2D cylinder at  $Re = 100$ ,  $K = 0.2$  and  $\Delta t = 0.001$ .

At time instant  $t = 300s$  the velocity magnitude presents no velocity behind the cylinder in the wake region and along the bottom boundary.

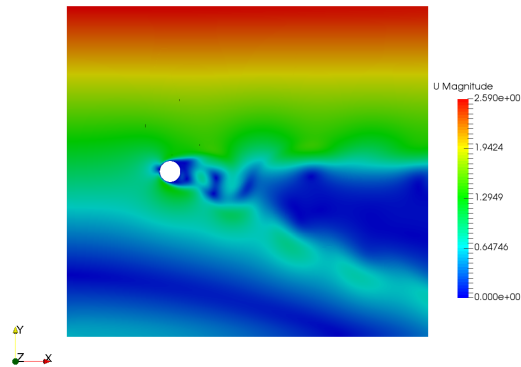


Figure A.103: Velocity magnitude at time instant  $t = 300s$  for shear current on a 2D cylinder at  $Re = 100$ ,  $K = 0.2$  and  $\Delta t = 0.001$ .

### PLOTS: Shear Flow around a Cylinder: $Re = 100$ & $K = 0.5$

This shear flow problem with  $K = 0.5$  has origin at  $t = -2.0$  while the domain span begins at  $y = -8.0$ . This gives incorrect values, as the values of force coefficients are highly unstable (even though it simulated the shear flow problem towards  $t = 300$ ).

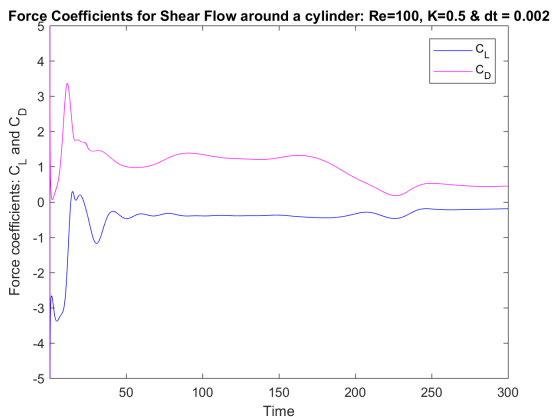


Figure A.104: Drag - and Lift Coefficients for: 2D Shear flow with  $Re = 100$  &  $K = 0.5$

The velocity magnitude at time instant  $t = 300s$  is varying around the domain, as there are approximately no velocity in- front and behind the cylinder.

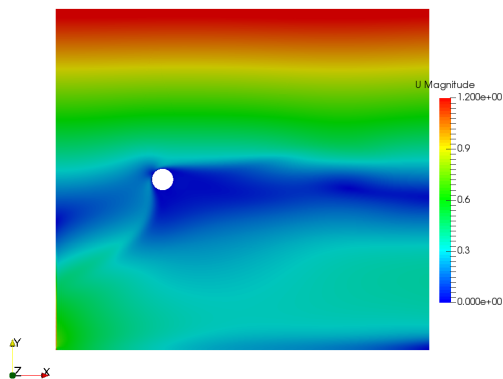


Figure A.105: Velocity magnitude at time instant  $t = 300s$  for shear current on a 2D cylinder at  $Re = 100$ ,  $K = 0.5$  and  $\Delta t = 0.002$ .

### PLOTS: Shear Flow around a Cylinder: $Re = 100$ & $K = 1.0$

This shear flow problem with  $K = 1.0$  has origin at  $t = -1.0$  while the domain span begins at  $y = -8.0$ . The results are unstable and the simulation breaks at time instant  $t = 66.5$ , where the time step  $\Delta t$  is reduced from 0.001 to 0.0001.

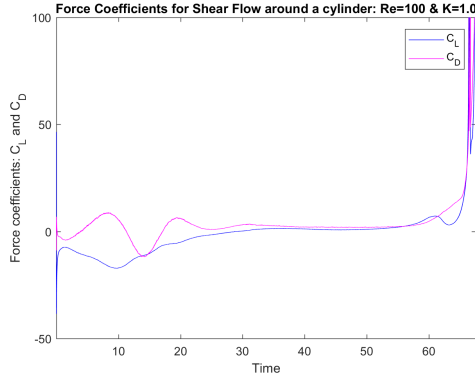


Figure A.106: Drag - and Lift Coefficients for: 2D Shear flow with  $Re = 100$  &  $K = 1.0$

The velocity distribution is highly unstable and the whole domain consist of almost no velocity, while there are high velocity zones at the bottom boundary. It is not sure why and how this occurs, but the inlet flow seems to be the factor in obtaining an unstable flow as it breaks at  $t = 66.5s$ .

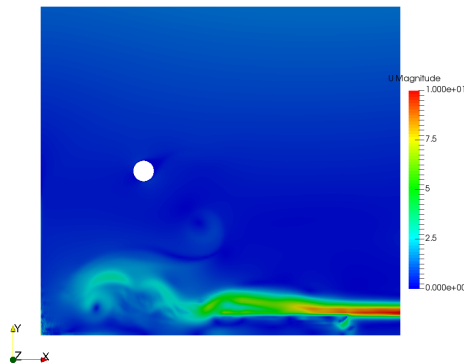


Figure A.107: Velocity magnitude at time instant  $t = 66.5s$  for shear current on a 2D cylinder at  $Re = 100$  &  $K = 1.0$ .

### PLOTS: Shear Flow around a Cylinder: $Re = 100$ & $K = 2.0$

This shear flow problem with  $K = 2.0$  has origin at  $t = -0.5$  while the domain span begins at  $y = -8.0$ . The results are unstable and the simulation breaks at time instant  $t = 66.5$ , where the time step  $\Delta t$  is reduced from 0.001 to 0.0001.

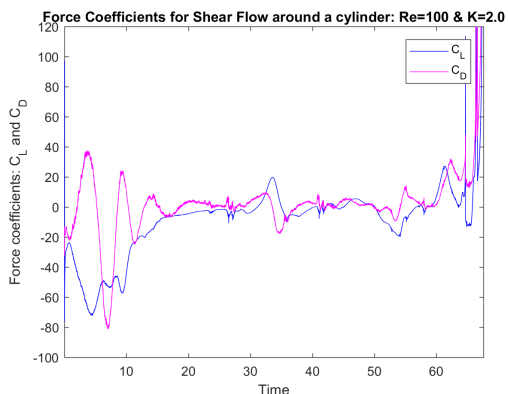


Figure A.108: Drag - and Lift Coefficients for: 2D Shear flow with  $Re = 100$  &  $K = 2.0$

The velocity distribution for this shear flow problem visualizes approximately no velocity in the domain at time instant  $t = 66.5s$  as the flow breaks. There are high velocity zone close to the bottom boundary. It is not sure why this occurs, but mainly due to inlet velocity.

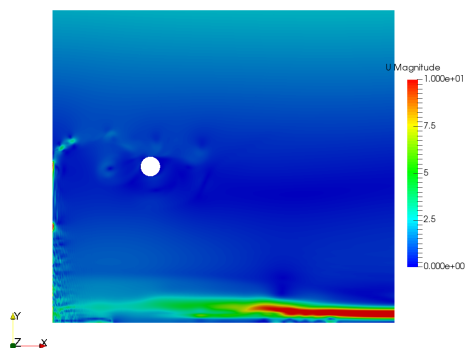


Figure A.109: Velocity magnitude at time instant  $t = 66.5s$  for shear current on a 2D cylinder at  $Re = 100$  &  $K = 2.0$ .



## .9 Shear Flow with Shear Rate $K = 0.2$ around a 2D & 3D Circular Cylinders

Shear flow problems are analyzed for shear rate  $K = 0.2$  with Reynolds number 100, 200 and 300. The domain size is changed, such that the inlet shear flow will have origin at bottom boundary  $y = -5.0$ .

The domain size and cylinder dimensions are presented in table A.11 and boundary constraints are presented in table A.2. The flow problems are analyzed for both two-dimensions (2D) and three-dimensions (3D), where the span-wise length  $Z_{range}$  the cylinder is 6 times the diameter length.

Table A.11: Domain size and Cylinder dimensions.

Domain Range and Dimensions	
$X_{range}$ :	$-5 < x < 12.5$
$Y_{range}$ :	$-5 < y < 5$
$Z_{range}$ , 3D:	$0 < z < 6$
Diameter D	1
Cylinder origo:	$(x,y,z) = (0, 0, 0)$

Figure A.110 presents the mesh used to analyze the shear flow problem with shear rate  $K = 0.2$  for various Reynolds numbers.

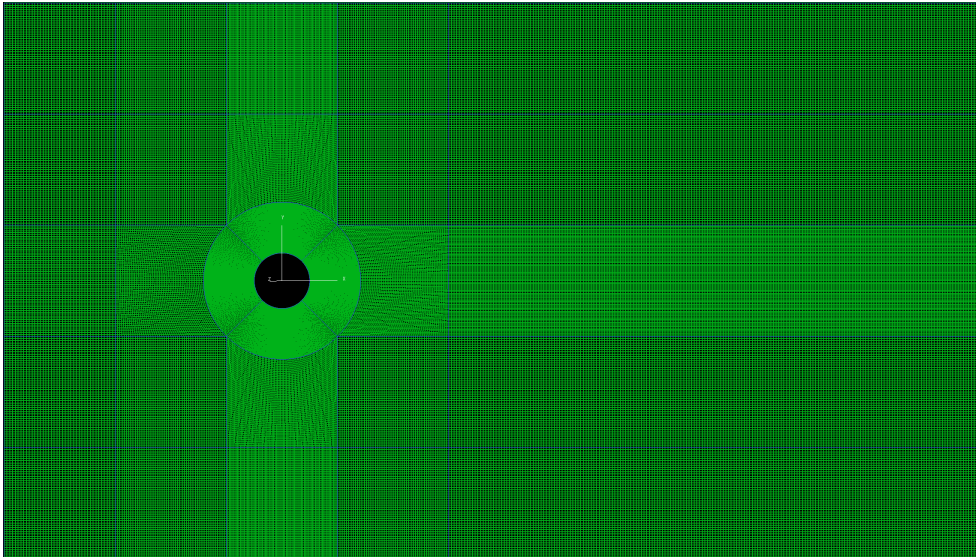


Figure A.110: Mesh generated in MEGA: 2D Single Cylinder with domain and cylinder dimensions given in table A.11.

Table A.12 presents the shear flow properties for a shear flow problem with shear rate  $K = 0.2$ .

Table A.12: Shear Flow properties: Shear Rate  $K$  & Reynolds numbers

Shear Flow $K = 0.2$	
$G$	1/10
$U_c$	0.5
inlet origin	$y = -5.0$
$R_e = 100$	$\nu = 0.005$
$R_e = 300$	$\nu = 1/600$
$R_e = 500$	$\nu = 1/1000$

Table A.13 below presents the properties and resulting values for uniform flow problem at  $R_e = 100$  for both domain sizes:  $-8.0 < y < 8.0$  and  $-5.0 < y < 5.0$ .

The comparison is performed to clarify that the new domain with y-axis span of  $-5.0 < y < 5.0$  is large enough to obtain correct results. As we reduce the y-axis span, the cylinder will take 10 % domain span in y-axis with a diameter of 1 while the total span is 10. The mean drag coefficient increases to  $\bar{C}_D = 1.491$  with a domain of  $-5.0 < y < 5.0$ , compared to  $\bar{C}_D = 1.462$  with a domain  $-8.0 < y < 8.0$ .

Table A.13: Uniform flow around a Cylinder  $K = 0.0$ : Comparing domain sizes.

$R_e = 100$	domain: $-8.0 < 8.0$ 3D & $t = 180s$	domain: $-5.0 < 5.0$ 2D & $t = 300$
U	1	1
magUInf	1	1
viscosity $\nu$	0.01	0.01
mean $C_L$	-0.01231	0.00468
mean $C_D$	<b>1.46210</b>	<b>1.49089</b>
RMS $C_L$	0.25080	0.25250
RMS $C_D$	0.00737	0.00763
$T_v[s]$	5.80	5.66
$f_v[Hz]$	0.1721	0.1767
$S_t[-]$	0.1721	0.1767

Table A.14 presents the mean values for drag - and lift coefficients, with the root mean square. Oscillation periods and frequencies are found from Power Spectral Density curves of x-direction velocity  $U_x$  behind the cylinder. Strouhals number is also presented. The values are found for the last 65 % results for the time simulation.

Table A.14: Shear flow  $K = 0.2$  a around a 2D and 3D Cylinder.

-	2D			3D		
Reynolds Number	$Re_e = 100$	$Re_e = 300$	$Re_e = 500$	$Re_e = 100$	$Re_e = 300$	$Re_e = 500$
mean $C_L$	-0.18199	-0.13409	-0.15547	-0.18198	-0.16091	-0.10392
mean $C_D$	1.42987	1.44789	1.50445	1.42981	1.33070	1.29849
RMS $C_L$	0.28235	0.73430	0.92095	0.28227	0.45317	0.43352
RMS $C_D$	0.02563	0.07812	0.12751	0.02561	0.06140	0.08907
$T_v[s]$	11.54	9.375	8.823	11.54	9.516	8.936
$f_v[Hz]$	0.08667	0.1067	0.1133	0.08667	0.1051	0.1119
$S_t[-]$	0.17334	0.2134	0.2266	0.17334	0.2102	0.2238

**PLOTS: Uniform Flow around a 2D Cylinder:  $Re_e = 100$  &  $K = 0.0$**

Analysis is performed for  $K = 0.0$ , which is equivalent to uniform flow with domain size  $-5.0 < y < 5.0$ .

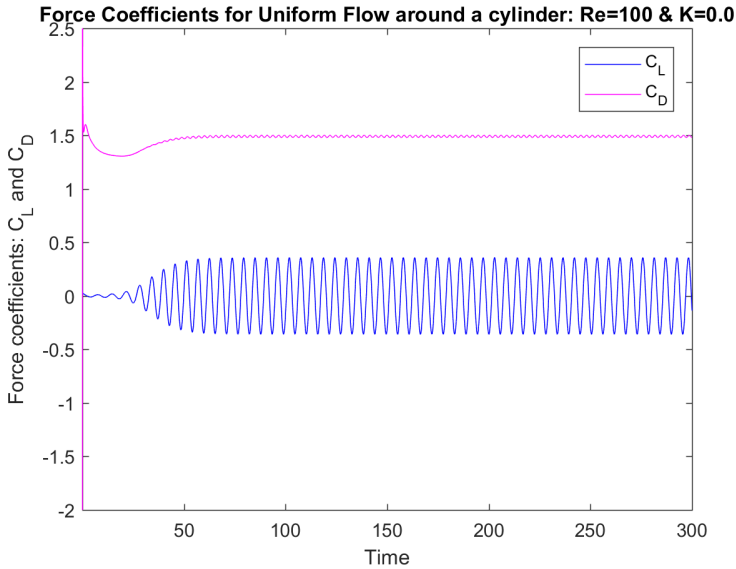


Figure A.111: Drag - and Lift Coefficients for: 2D Uniform flow with  $Re_e = 100$  and  $K = 0.0$ .

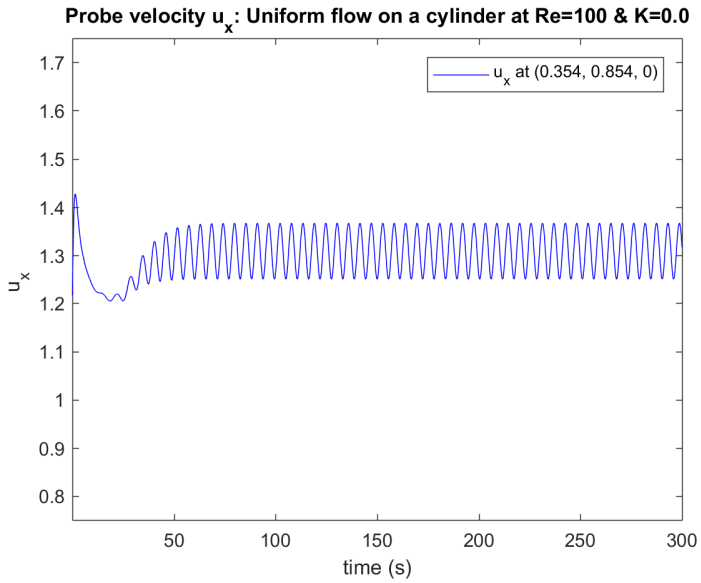


Figure A.112:  $U_x$  velocity probe at  $(x, y, z) = (0.354, 0.854, 0)$  with respect to time for: Uniform flow with  $Re = 100$  and  $K = 0.0$ .

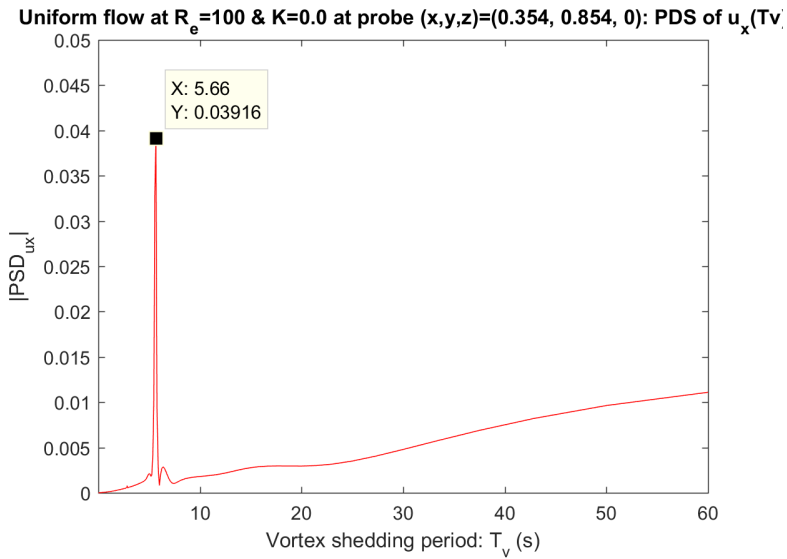


Figure A.113: The power spectral density of probe velocity  $U_x$  with respect to vortex shedding period  $T_v$  for: Uniform flow with  $Re = 100$  and  $K = 0.0$ .

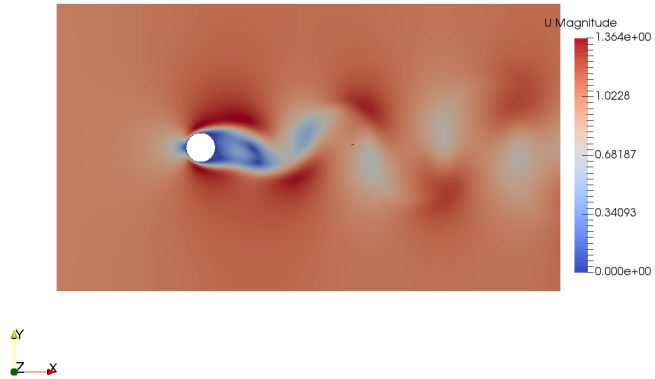


Figure A.114: Velocity magnitude for uniform flow at  $R_e = 100$  for  $K = 0.0$  at time instant  $t = 300s$ .

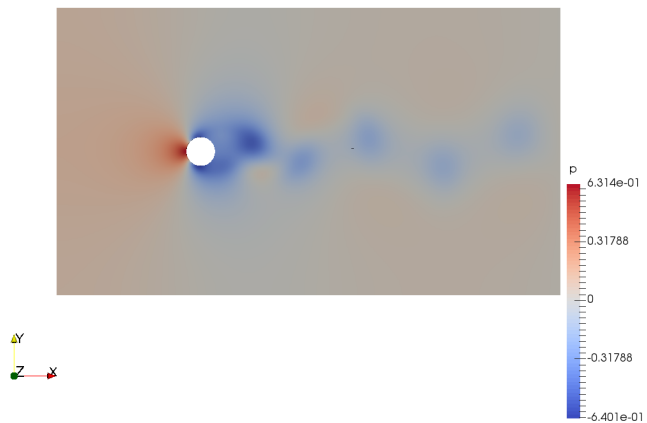


Figure A.115: Pressure distribution for uniform flow at  $R_e = 100$  for  $K = 0.0$  at time instant  $t = 300s$ .

**PLOTS: Shear Flow around a 2D Cylinder:  $R_e = 100$  &  $K = 0.2$**

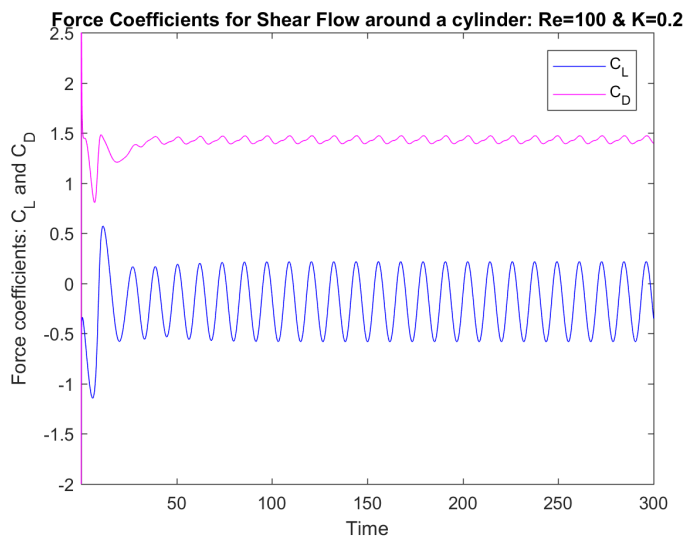


Figure A.116: Drag - and Lift Coefficients for: 2D Shear flow with  $R_e = 100$  and  $K = 0.2$ .

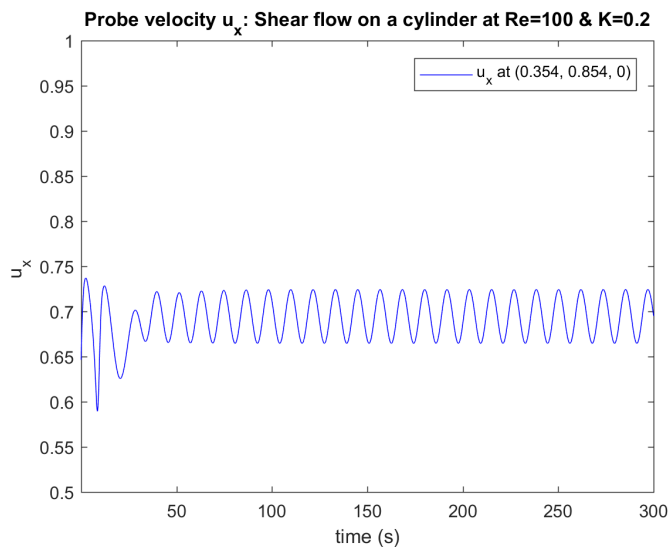


Figure A.117:  $U_x$  velocity probe at  $(x, y, z) = (0.354, 0.854, 0)$  with respect to time for: Shear flow with  $R_e = 100$  and  $K = 0.2$ .

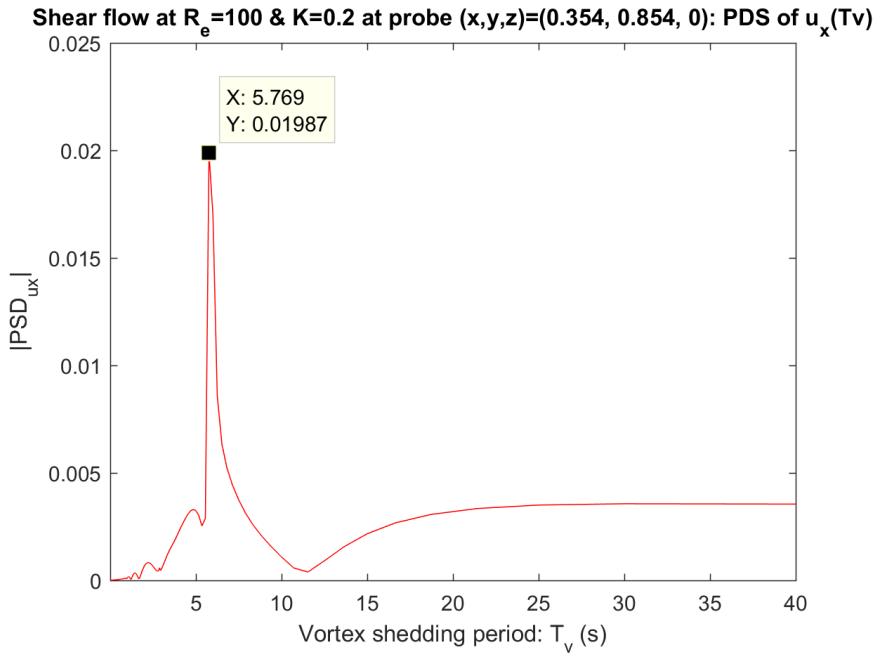


Figure A.118: The power spectral density of probe velocity  $U_x$  with respect to vortex shedding period  $T_v$  for: Shear flow with  $Re = 100$  and  $K = 0.2$ .

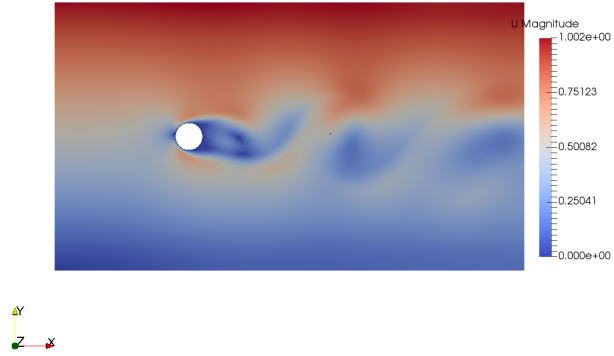


Figure A.119: Velocity magnitude for Shear flow at  $R_e = 100$  for  $K = 0.2$  at time instant  $t = 300s$ .

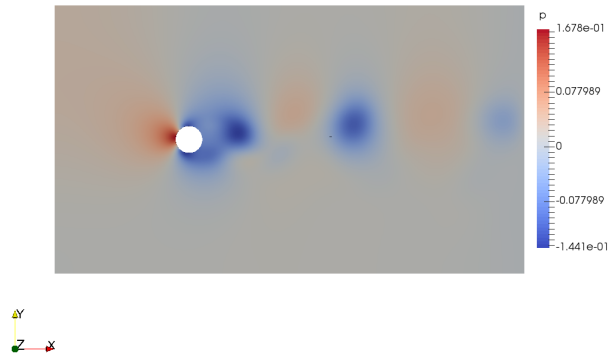


Figure A.120: Pressure distribution for Shear flow at  $R_e = 100$  for  $K = 0.2$  at time instant  $t = 300s$ .



**PLOTS: Shear Flow around a 2D Cylinder:  $R_e = 300$  &  $K = 0.2$**

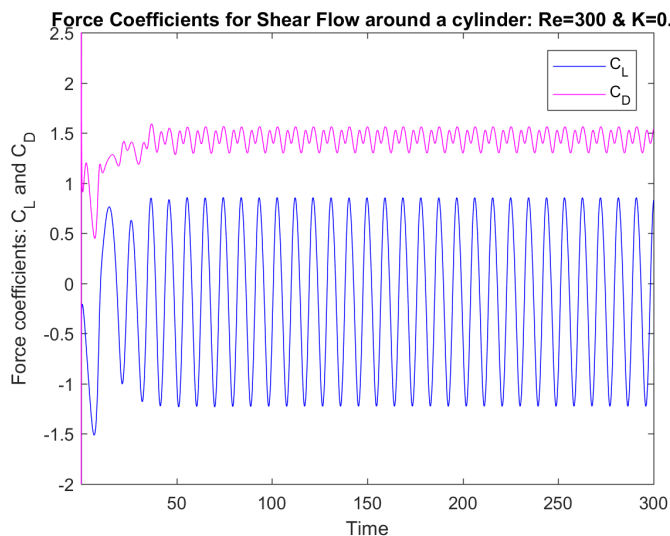


Figure A.121: Drag - and Lift Coefficients for: 2D Shear flow with  $R_e = 300$  and  $K = 0.2$ .

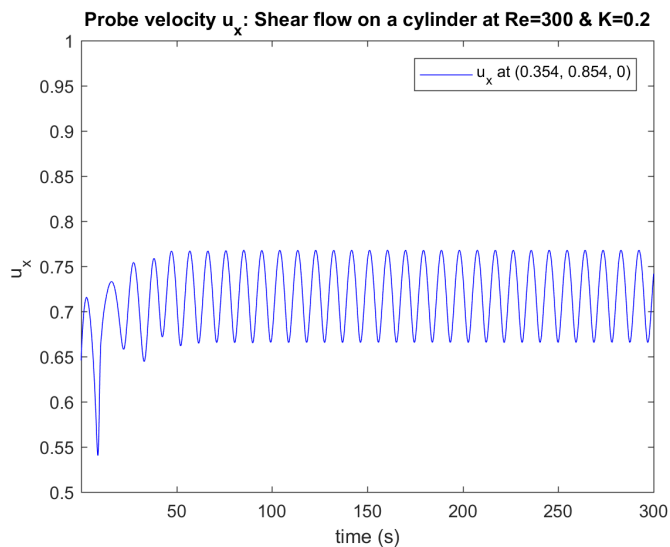


Figure A.122:  $U_x$  velocity probe at  $(x, y, z) = (0.354, 0.854, 0)$  with respect to time for: Shear flow with  $R_e = 300$  and  $K = 0.2$ .

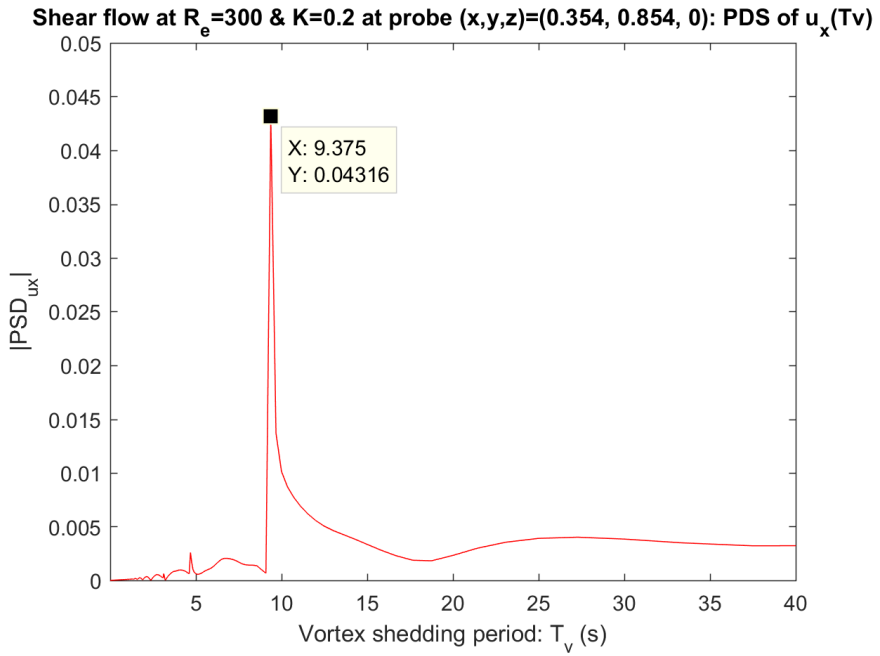


Figure A.123: The power spectral density of probe velocity  $U_x$  with respect to vortex shedding period  $T_v$  for: Shear flow with  $R_e = 300$  and  $K = 0.2$ .

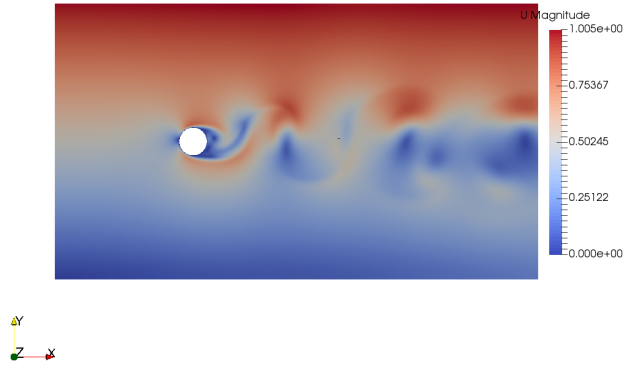


Figure A.124: Velocity magnitude for Shear flow at  $R_e = 300$  for  $K = 0.2$  at time instant  $t = 300s$ .

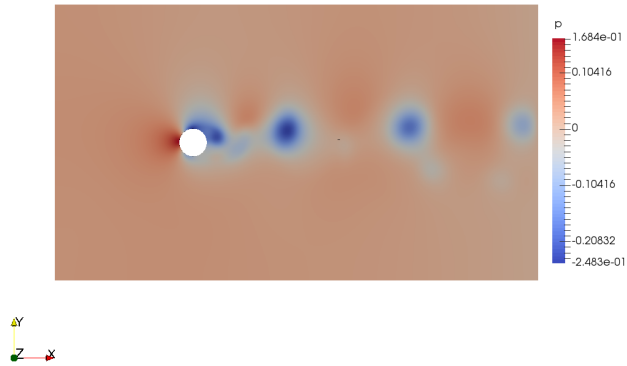


Figure A.125: Pressure distribution for Shear flow at  $R_e = 300$  for  $K = 0.2$  at time instant  $t = 300s$ .

**PLOTS: Shear Flow around a 2D Cylinder:  $R_e = 500$  &  $K = 0.2$**

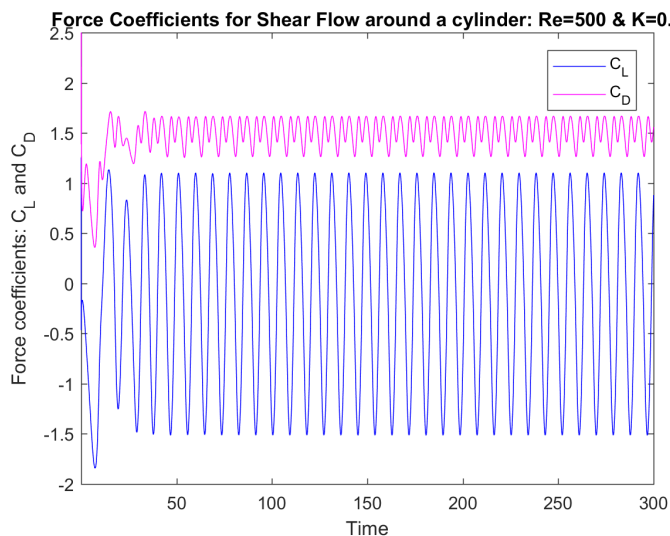


Figure A.126: Drag - and Lift Coefficients for: 2D Shear flow with  $R_e = 500$  and  $K = 0.2$ .

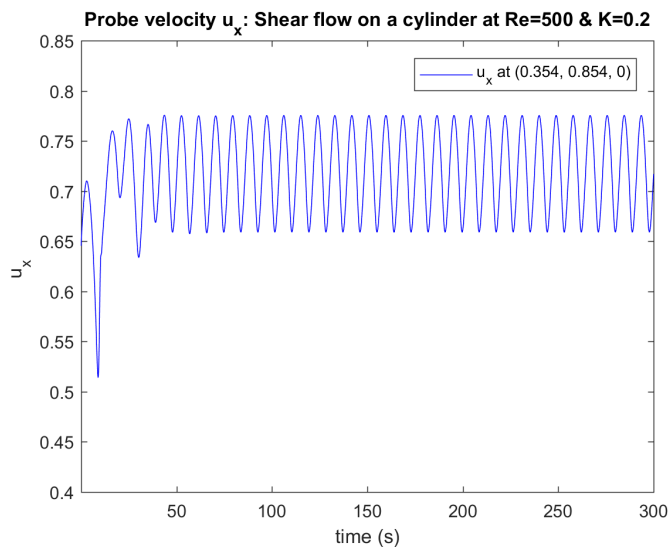


Figure A.127:  $U_x$  velocity probe at  $(x, y, z) = (0.354, 0.854, 0)$  with respect to time for: Shear flow with  $R_e = 500$  and  $K = 0.2$ .

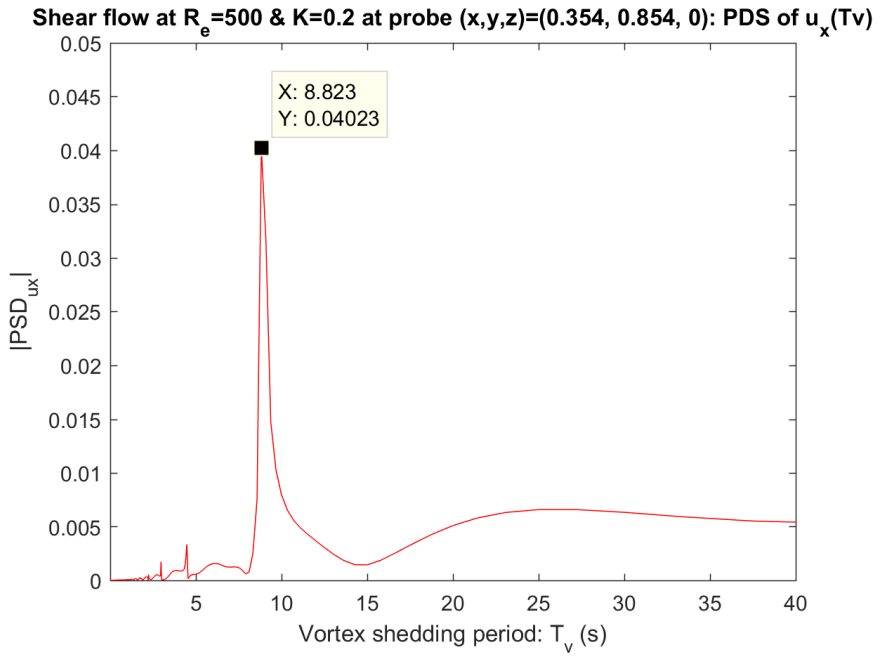


Figure A.128: The power spectral density of probe velocity  $U_x$  with respect to vortex shedding period  $T_v$  for: Shear flow with  $R_e = 500$  and  $K = 0.2$ .

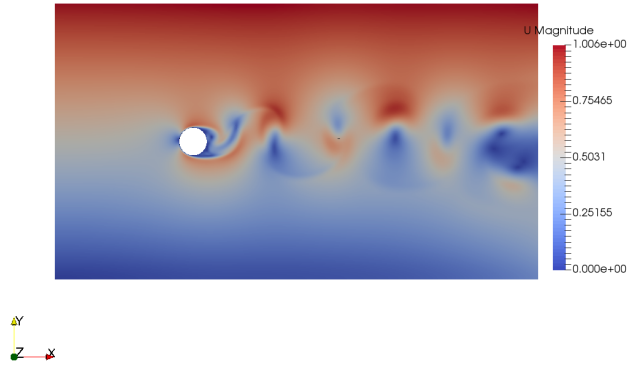


Figure A.129: Velocity magnitude for Shear flow at  $R_e = 500$  for  $K = 0.2$  at time instant  $t = 300s$ .

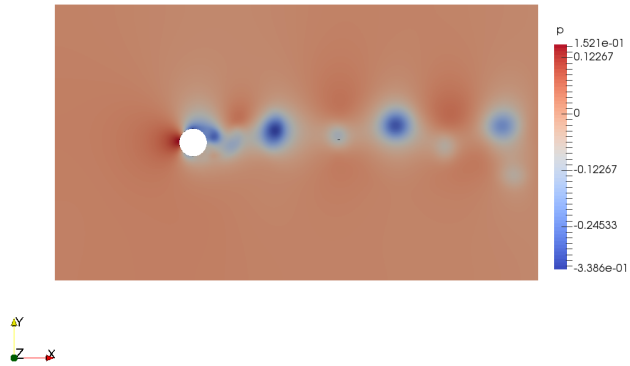


Figure A.130: Pressure distribution for Shear flow at  $R_e = 500$  for  $K = 0.2$  at time instant  $t = 300s$ .

**PLOTS: Shear Flow around a 3D Cylinder:  $R_e = 100$  &  $K = 0.2$**

Values for mean drag, lift and Strouhals number for this 3D flow problem are equivalent to the 2D flow problem with Reynolds number 100 and shear rate  $K=0.2$ . The velocity magnitude plot and pressure distribution will be identical for the 2D flow problem for the same time instant.

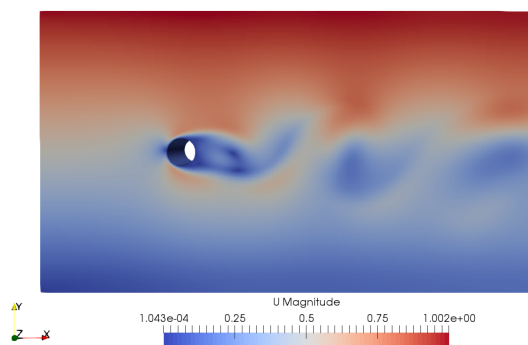


Figure A.131: Velocity magnitude for Shear flow at  $R_e = 100$  for  $K = 0.2$  at time instant  $t = 300s$ .

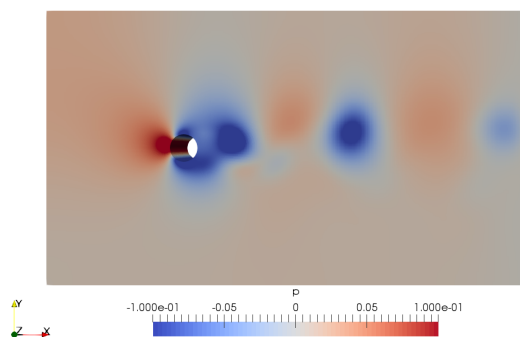


Figure A.132: Pressure distribution for Shear flow at  $R_e = 100$  for  $K = 0.2$  at time instant  $t = 300s$ .

The vorticity in z-direction  $\omega_z$  presents the vortex shedding with respect to vorticity  $-1.0 < \omega_z < 1.0$ . A shear problem at Reynolds number 100 will not have 3D effects along the span-wise cylinder, such that the flow will move smoothly around the span-wise cylinder.

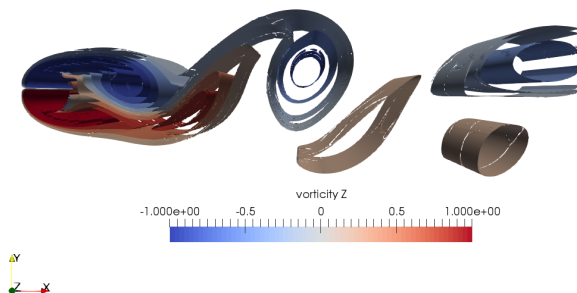


Figure A.133: Vorticity in z-direction  $\omega_z$  for Shear flow at  $Re = 100$  for  $K = 0.2$  at time instant  $t = 300s$ .

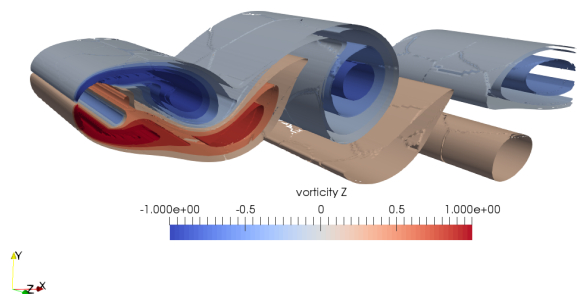


Figure A.134: Vorticity in z-direction  $\omega_z$  for Shear flow at  $Re = 100$  for  $K = 0.2$  at time instant  $t = 300s$ . Different angle.



**PLOTS: Shear Flow around a 3D Cylinder:  $Re = 300$  &  $K = 0.2$**

The drag force for the first 150s is similar to the results obtained for the 2D shear flow case  $K = 0.2$  with Reynolds number 300. After  $t = 150s$  the 3D effects will effect the drag of the cylinder. One can observe changes in velocity of  $U_x$  at the same time instant, and change in oscillation frequency.

The mean drag coefficient  $\bar{C}_D$  for the equivalent flow problem is  $\bar{C}_D = 1.44789$ , but is decreased to  $\bar{C}_D = 1.33070$  for the 3D flow problem . This change in mean root square of the drag coefficient is fairly similar.

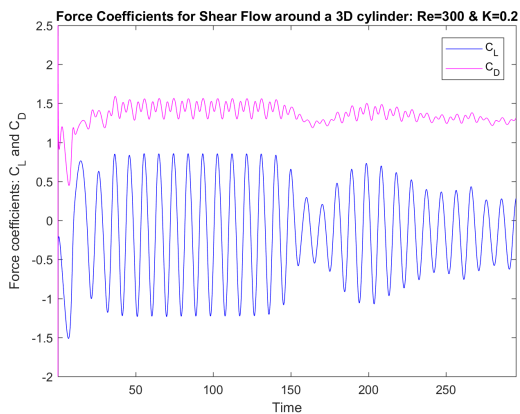


Figure A.135: Drag - and Lift Coefficients for: 3D Shear flow with  $Re = 300$  and  $K = 0.2$ .

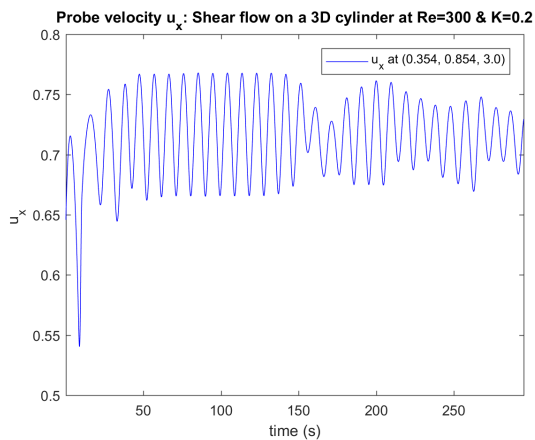


Figure A.136:  $U_x$  velocity probe at  $(x, y, z) = (0.354, 0.854, 3.0)$  with respect to time for: Shear flow with  $Re = 300$  and  $K = 0.2$ .

The Strouhals number  $S_t$  is found from the oscillation period and frequency. The oscillation periods and frequency are approximately similar for the 2D and 3D flow problem with Reynolds number 300 with shear rate  $K = 0.2$ .

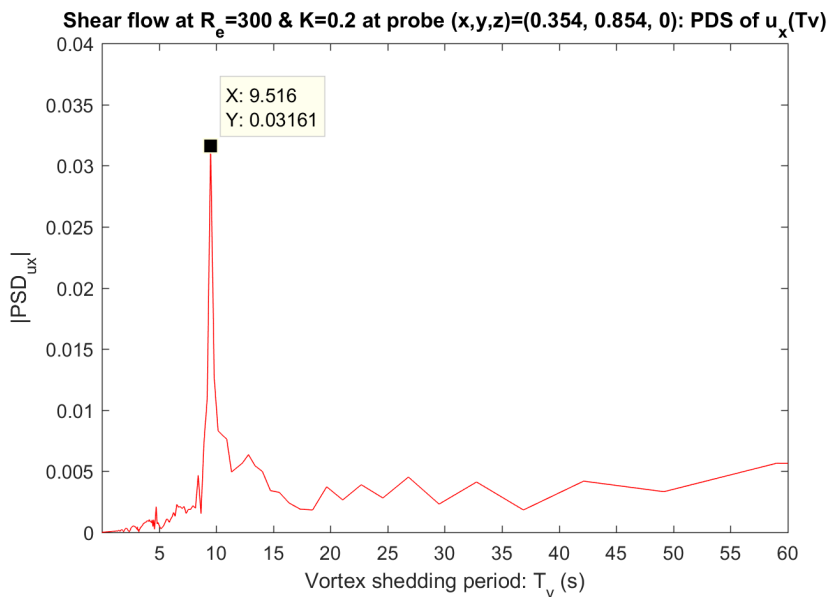


Figure A.137: The power spectral density of probe velocity  $U_x$  with respect to vortex shedding period  $T_v$  for: Shear flow with  $R_e = 300$  and  $K = 0.2$ .

The plots below presents the velocity magnitude at time instant  $t = 160s$  and  $t = 300s$ . At time instant  $t = 160s$  the drag - and lift coefficient will oscillate with a different frequency and with smaller amplitude before stabilizing before time instant  $t = 300$ .

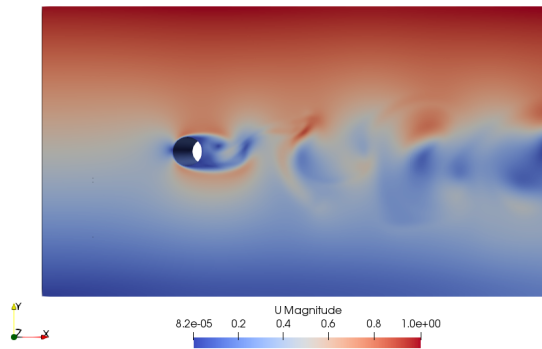


Figure A.138: Velocity magnitude for Shear flow at  $R_e = 300$  for  $K = 0.2$  at time instant  $t = 160s$ .

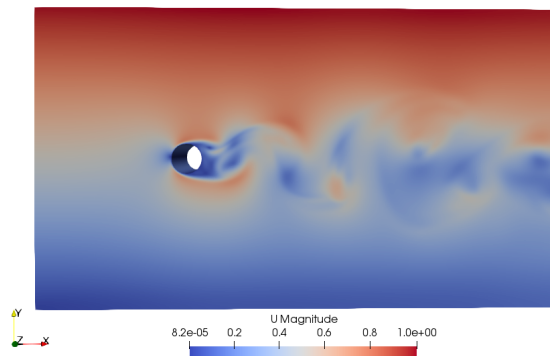


Figure A.139: Velocity magnitude for Shear flow at  $R_e = 300$  for  $K = 0.2$  at time instant  $t = 300s$ .

The pressure distributions below are presented at time instant  $t = 160s$  and  $t = 300s$ .

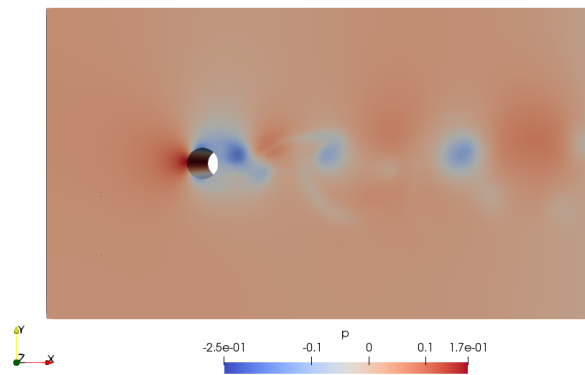


Figure A.140: Pressure distribution for Shear flow at  $R_e = 300$  for  $K = 0.2$  at time instant  $t = 160s$ .

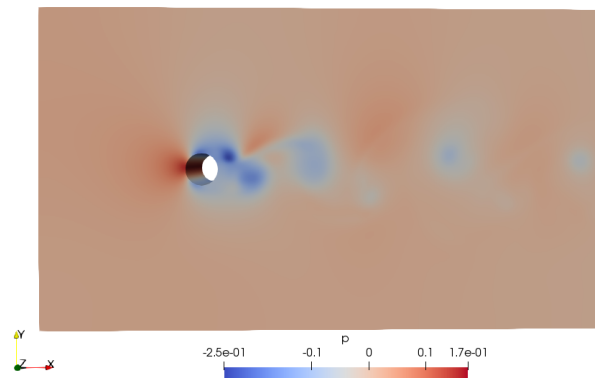


Figure A.141: Pressure distribution for Shear flow at  $R_e = 300$  for  $K = 0.2$  at time instant  $t = 300s$ .

The plots below presents vorticity in z-direction  $\omega_z$  for time instant  $t = 160s$ , where there observed a sudden change in oscillation frequency. The Vortex sheddings are shown, with the corresponding 3D effects along the span-wise length.

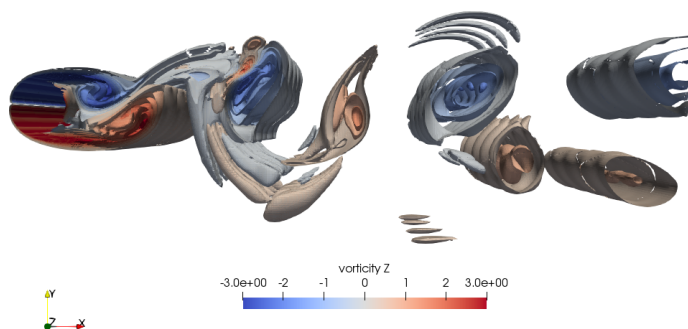


Figure A.142: Vorticity in z-direction  $\omega_z$  for Shear flow at  $Re = 300$  for  $K = 0.2$  at time instant  $t = 160s$ .

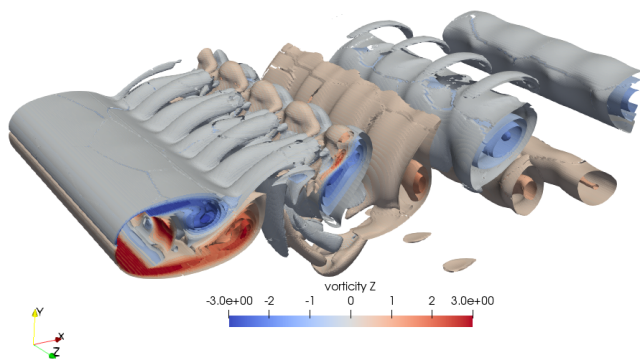


Figure A.143: Vorticity in z-direction  $\omega_z$  for Shear flow at  $Re = 300$  for  $K = 0.2$  at time instant  $t = 160s$ . Different angle.

The plots below presents vorticity in z-direction  $\omega_z$  for time instant  $t = 300s$ . The flow problem at this point is stable, and one can observe the vortex shedding with disturbances. The 3D effects along the span-wise length and the vortex shedding downstream have clearly changed since time instant  $t = 160s$ .

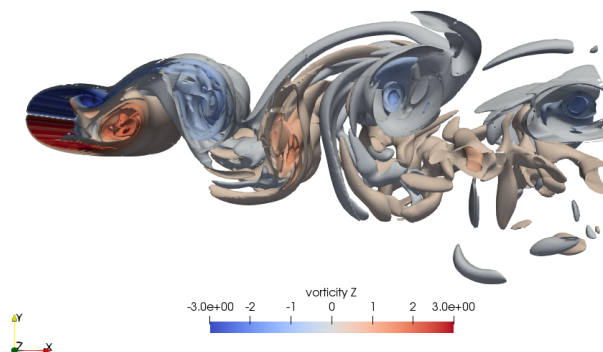


Figure A.144: Vorticity in z-direction  $\omega_z$  for Shear flow at  $R_e = 300$  for  $K = 0.2$  at time instant  $t = 300s$ .

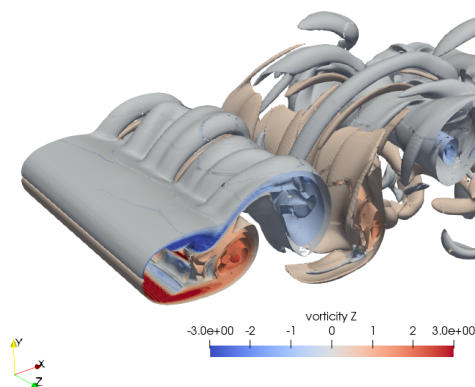


Figure A.145: Vorticity in z-direction  $\omega_z$  for Shear flow at  $R_e = 300$  for  $K = 0.2$  at time instant  $t = 300s$ . Different angle.

**PLOTS: Shear Flow around a 3D Cylinder:  $Re = 500$  &  $K = 0.2$**

The 3D flow problem with Reynolds number 500 and shear rate  $K = 0.2$  simulated until  $t = 145s$  before breaking du large pressure fluctuations. This is due to large jumps in pressure in the flow domain. The 3D flow problem becomes unstable, while the equivalent 2D flow problem was stable for the whole time simulation towards  $t = 300s$ .

The mean drag coefficient  $\bar{C}_D$  for the flow problem is  $\bar{C}_D = 1.29849$  for the last 65 % of the time simulation towards breaking point  $t = 145s$ . The stable 2D flow problem has a mead drag coefficient of  $\bar{C}_D = 1.50445$ .

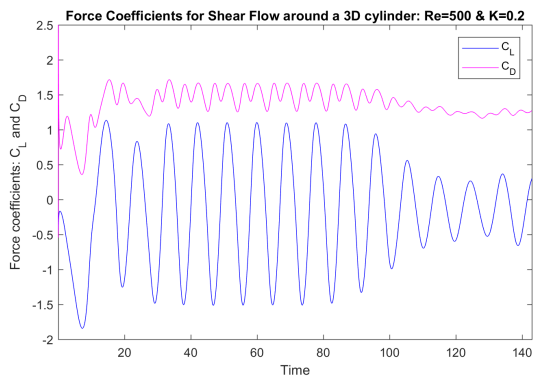


Figure A.146: Drag - and Lift Coefficients for: 3D Shear flow with  $Re = 500$  and  $K = 0.2$ .

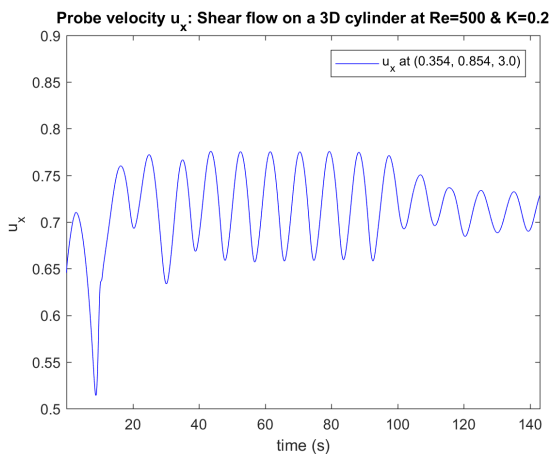


Figure A.147:  $U_x$  velocity probe at  $(x, y, z) = (0.354, 0.854, 3.0)$  with respect to time for: Shear flow with  $Re = 500$  and  $K = 0.2$ .

The oscillation periods, frequency and Strouhals number are remaining the same for both 2D and 3D flow problem at Reynolds number 500 and shear rate  $K = 0.2$ .

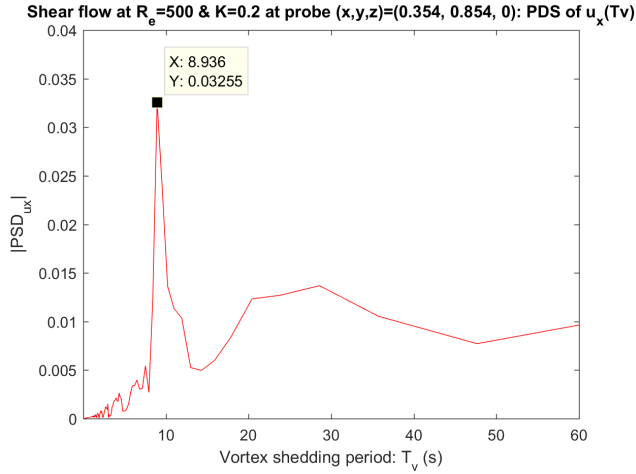


Figure A.148: The power spectral density of probe velocity  $U_x$  with respect to vortex shedding period  $T_v$  for: Shear flow with  $Re = 500$  and  $K = 0.2$ .

The graph below presents the pressure fluctuation for three different probes around the cylinder. The pressure is fluctuating with an irregular frequency, and at time instant  $t = 140 - 143$  the pressure rapidly increases and the flow becomes unstable and breaks simulation.

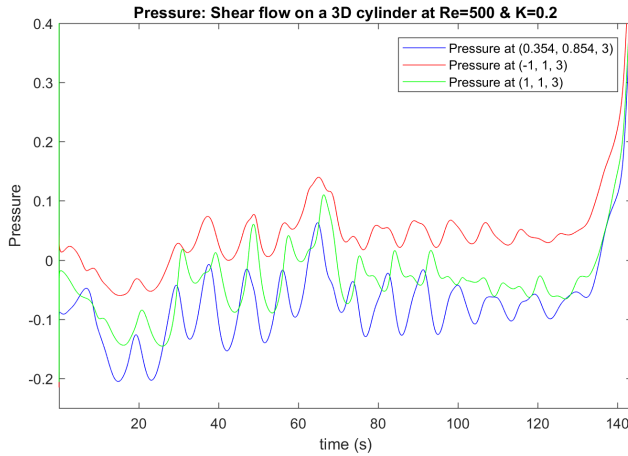


Figure A.149: Pressure fluctuation with respect to time simulation for Probe1 (0.354, 0.854, 3), Probe 2 (-1, 1, 3) & Probe 3 (1, 1, 3).



The plots below presents the velocity magnitude at time instant  $t = 70s$  and  $t = 140s$ . At time instant  $t = 70s$  the drag - and lift coefficient will oscillate with a stable frequency before changing amplitude around  $t = 100$ . At time instant  $t = 140$  the simulation for this flow problem will crash/break due to large pressure jumps.

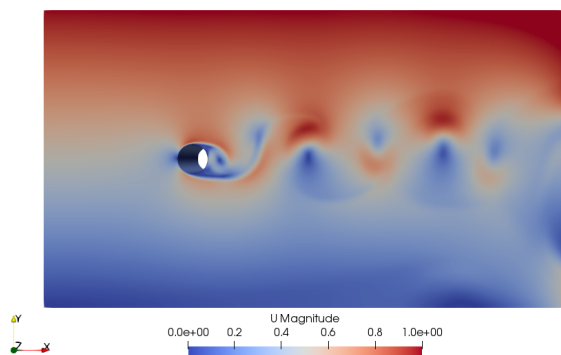


Figure A.150: Velocity magnitude for Shear flow at  $R_e = 500$  for  $K = 0.2$  at time instant  $t = 70s$ .

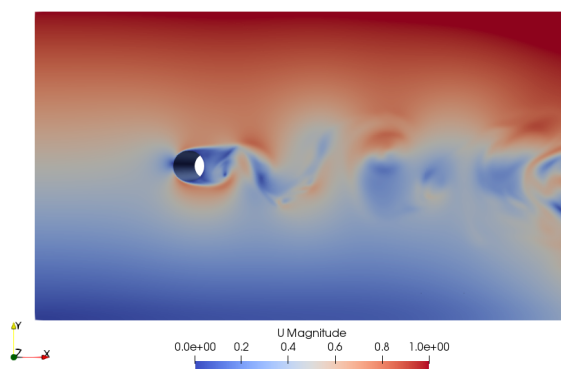


Figure A.151: Velocity magnitude for Shear flow at  $R_e = 500$  for  $K = 0.2$  at time instant  $t = 140s$  before breaking the simulation with  $\Delta t = 0.002$ .

Figure A.152 and A.153 presents the velocity distribution in y-and-z-direction  $U_y$  and  $U_z$ . The velocities are approximately zero, such that the absolute velocity magnitude consist for the distribution from the velocity in x-direction  $U_x$ .

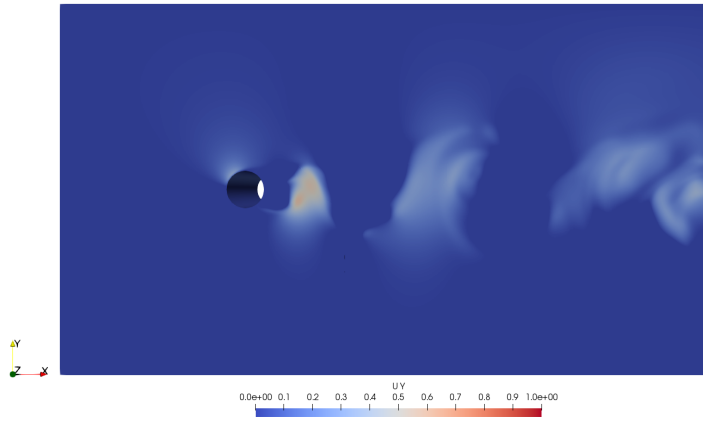


Figure A.152: Velocity in y - direction  $U_y$  for Shear Flow at  $Re = 500$  for  $K = 0.2$  at time instant  $t = 140s$ .

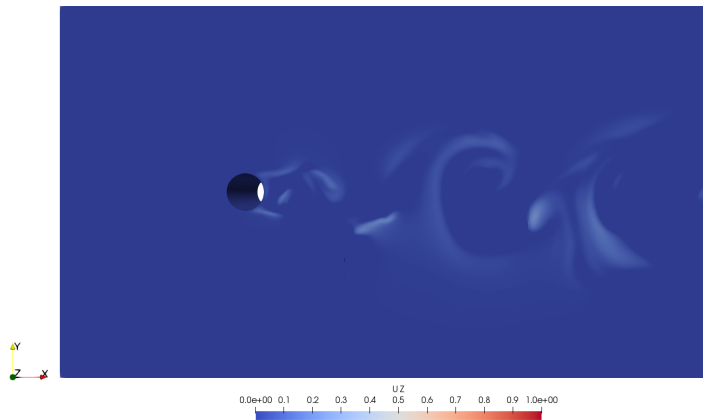


Figure A.153: Velocity in z - direction  $U_z$  for Shear Flow at  $Re = 500$  for  $K = 0.2$  at time instant  $t = 140s$ .

The pressure distributions below are presented at time instant  $t = 70s$  and  $t = 140s$ . At time instant  $t = 70s$ , one can observe pressure drops for areas with vortex shedding, but for time instant  $t = 140s$  the domain has an absolute value of larger pressure distribution.

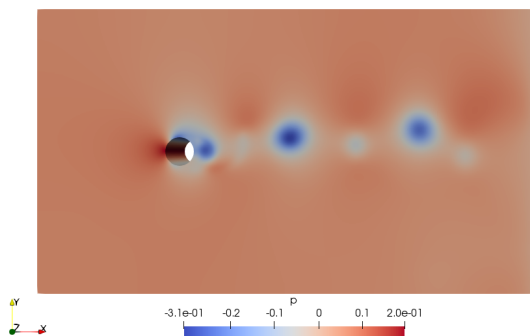


Figure A.154: Pressure distribution for Shear flow at  $R_e = 500$  for  $K = 0.2$  at time instant  $t = 70s$ .

The plot below presents absolute values for pressure distribution around the domain for time instant  $t = 140s$ , which is right before the simulation breaks.

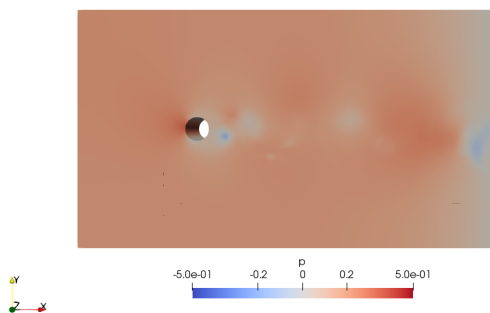


Figure A.155: Pressure distribution for Shear flow at  $R_e = 500$  for  $K = 0.2$  at time instant  $t = 140s$  before breaking the simulation with  $\Delta t = 0.002$ .

The plots below presents vorticity in z-direction  $\omega_z$  for time instant  $t = 70s$  where the flow problem is shedding vortices with a stable frequency. The vortex shedding are clearly visualized with smooth surfaces with little disturbances.

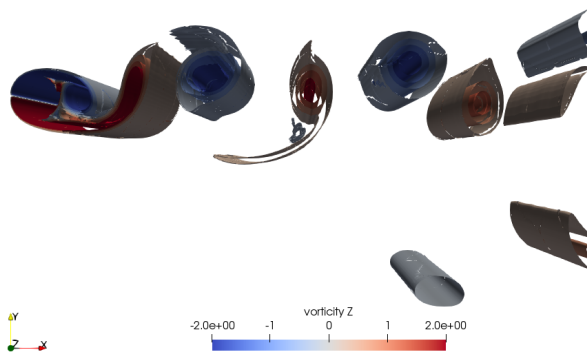


Figure A.156: Vorticity in z-direction  $\omega_z$  for Shear flow at  $Re = 500$  for  $K = 0.2$  at time instant  $t = 70s$ .

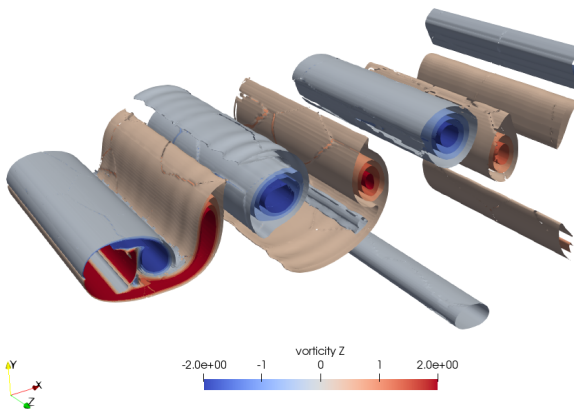


Figure A.157: Vorticity in z-direction  $\omega_z$  for Shear flow at  $Re = 500$  for  $K = 0.2$  at time instant  $t = 70s$ . Different angle.

The plots below presents vorticity in z-direction  $\omega_z$  for time instant  $t = 140s$ . The flow problem at this time instant will break due to large pressure jumps, and the vortices downstream are effected by large 3D effects in span-wise direction.

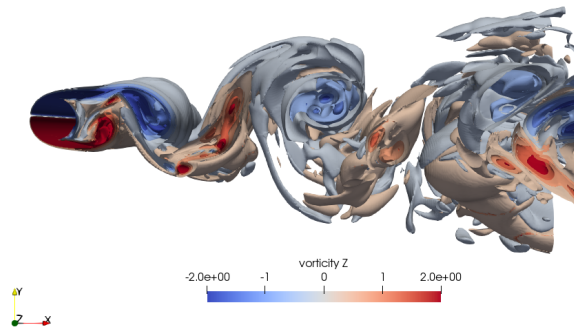


Figure A.158: Vorticity in z-direction  $\omega_z$  for Shear flow at  $R_e = 500$  for  $K = 0.2$  at time instant  $t = 140s$  right before simulation breaks.

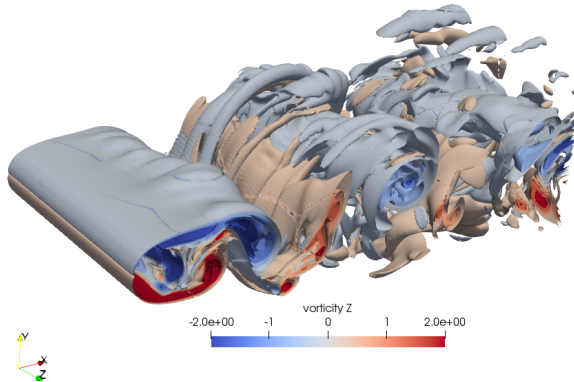


Figure A.159: Vorticity in z-direction  $\omega_z$  for Shear flow at  $R_e = 500$  for  $K = 0.2$  at time instant  $t = 140s$  right before simulation breaks. Different angle.

## .10 Uniform Flow around 2D Tandem Cylinder

When analyzing tandem cylinders, a new domain and mesh is generated with tandem cylinders presented in figure A.160. The analysis is performed with uniform flow with Reynolds number 100, 200 and 300 presented in table A.15.

Table A.15: Properties for Uniform flow for different Reynolds numbers.

Properties of Uniform Flow:			
$Re$	100	200	300
U	1	1	1
magUInf	1	1	1
viscosity $\nu$	0.01	0.005	0.003333
$\Delta t$	0.002	0.002	0.002

Table A.16 presents the domain size and cylinder dimensions for the tandem flow problem. The flow problems are analyzed for both two-dimension and three-dimensions, there the span-wise length of the cylinder is 6 times the diameter length.

Table A.16: Domain size and Cylinder dimensions.

Domain Range and Dimensions:	
$X_{range}$ :	$-6 < x < 12$
$Y_{range}$ :	$-6 < y < 6$
$Z_{range}$ , 3D:	$0 < z < 6$
Diameter D	1
Upstream cylinder origo:	(x,y,z)= (-1.6, 0, 0)
Downstream cylinder origo:	(x,y,z)= (1.6, 0, 0)
Longitudinal gap	3.2xD

Table A.17 presents the boundary constraint which are used to analyze a uniform flow around a single circular cylinder for various Reynolds numbers.

Table A.17: Defining boundary conditions in OpenFOAM [Greenshields, 2015].

Defined boundaries:	Geometric constraint:	Velocity U:	Pressure P:
front	empty (2D)	empty (2D)	empty (2D)
	cyclic (3D)	cyclic (3D)	cyclic (3D)
back	empty (2D)	empty (2D)	empty (2D)
	cyclic (3D)	cyclic (3D)	cyclic (3D)
upstreamCyl	wall	fixedValue	zeroGradient
downstreamCyl	wall	fixedValue	zeroGradient
inlet	patch	fixedValue	zeroGradient
outlet	patch	zeroGradient	fixedValue
topAndBottom	slip	slip	slip

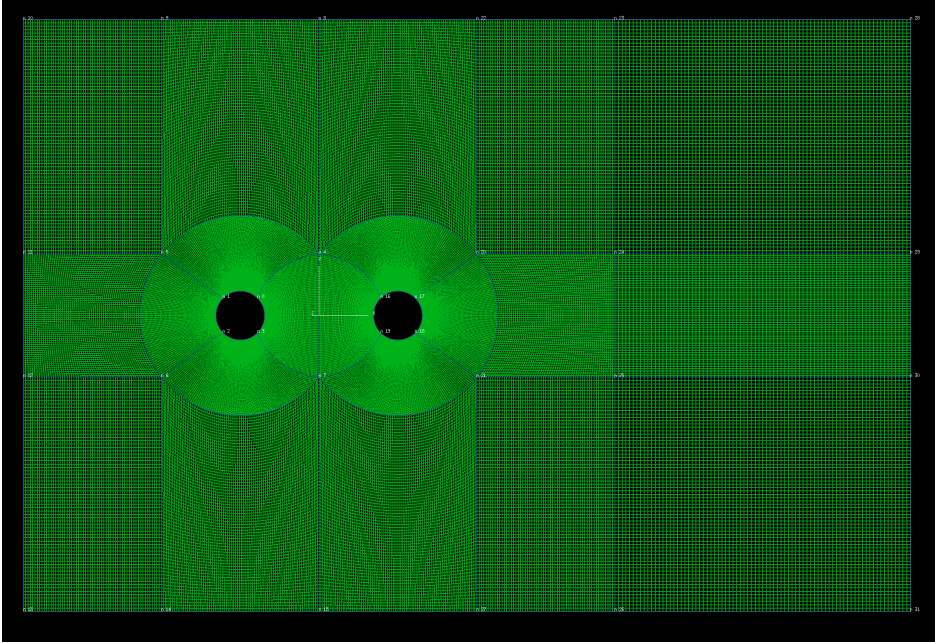


Figure A.160: Mesh generated in MEGA: 2D Tandem Cylinders with  $D = 1$ .

Table A.18 presents mean force coefficients, root mean square values, oscillation period, frequency and Strouhals number behind both upstream and downstream cylinder. The values are found for the last 65 % results for the time simulation. It is performed analysis for Reynolds number 100, 200 and 300.

Table A.18: Values for test case: Uniform flow around 2D tandem cylinders for  $t = 500s$ .

<b>Properties of Uniform Flow:</b>						
-	$Re = 100$		$Re = 200$		$Re = 300$	
Values	Upstream	Downstream	Upstream	Downstream	Upstream	Downstream
mean $C_L$	0.00006	0.00202	0.00046	-0.00701	.005080	0.08367
mean $C_D$	1.30039	-0.0042	1.13620	-0.13492	1.50550	0.94505
RMS $C_L$	0.00965	0.09697	0.01770	0.23108	0.86000	1.73471
RMS $C_D$	0.00008	0.00160	0.00039	0.00931	0.10338	0.46961
$T_v[s]$	7.936	8.064	7.353	7.353	5 & 2.488	-
$f_v[Hz]$	0.126	0.124	0.136	0.136	0.2 & 0.402	-
$S_t$	0.126	0.124	0.136	0.136	0.2 & 0.402	-

## PLOTS: Tandem Cylinders in Uniform Flow at $Re = 100$

The figures below presents the oscillation of the force coefficient for upstream and downstream cylinder. The upstream cylinder is oscillating with small root mean square, such that the axis could have been scaled to visualized the oscillation.

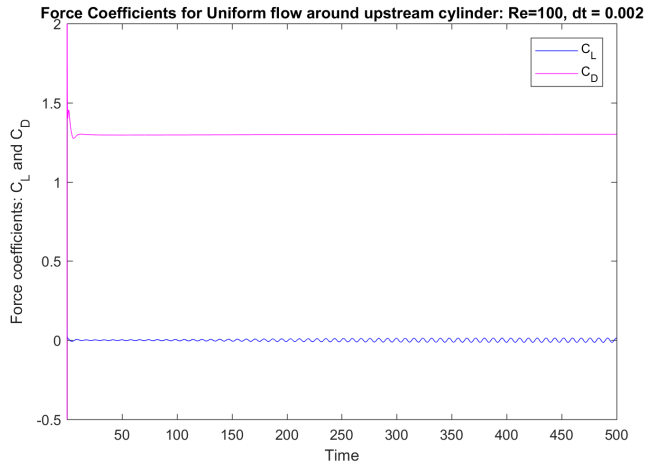


Figure A.161: Drag - and Lift Coefficients for Upstream Cylinder in uniform flow at  $Re = 100$  and  $\Delta t = 0.002$ .

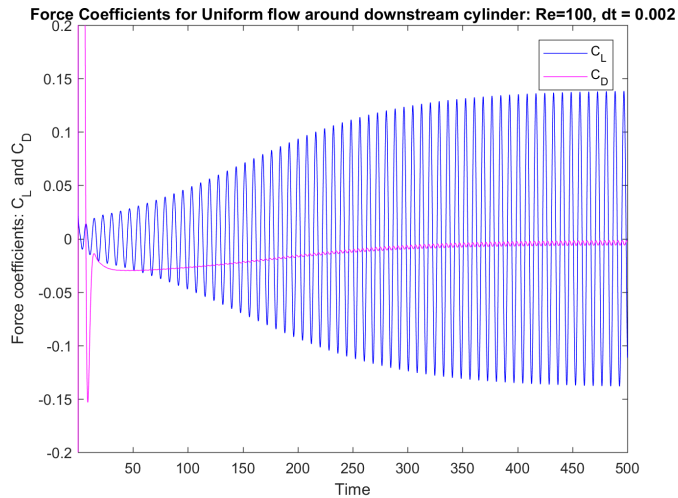


Figure A.162: Drag - and Lift Coefficients for Downstream Cylinder in uniform flow at  $Re = 100$  and  $\Delta t = 0.002$ .



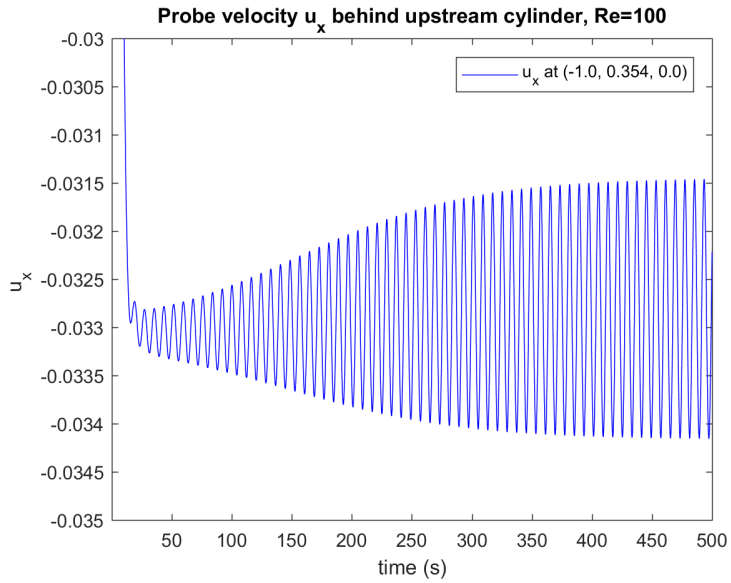


Figure A.163:  $U_x$  velocity probe behind Upstream Cylinder  $(x, y, z) = (-1.0, 0.354, 0)$  at  $Re = 100$  at  $\Delta t = 0.002$ .

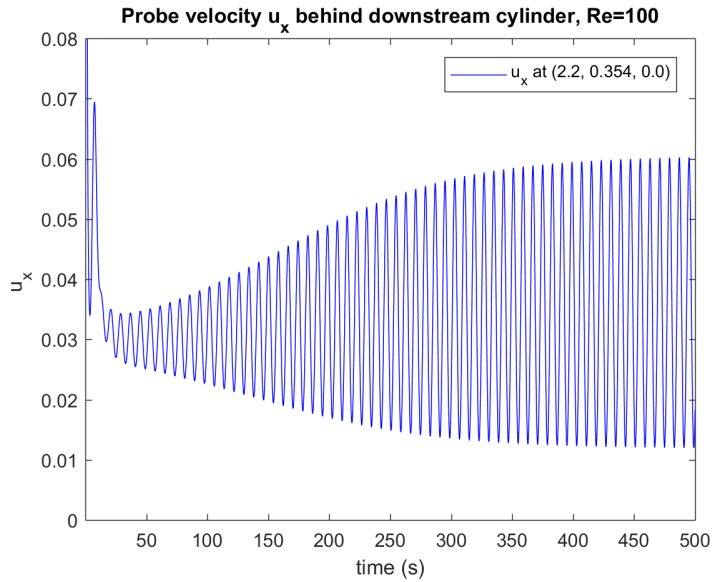


Figure A.164:  $U_x$  velocity probe behind Downstream Cylinder  $(x, y, z) = (2.2, 0.354, 0)$  at  $Re = 100$  at  $\Delta t = 0.002$ .

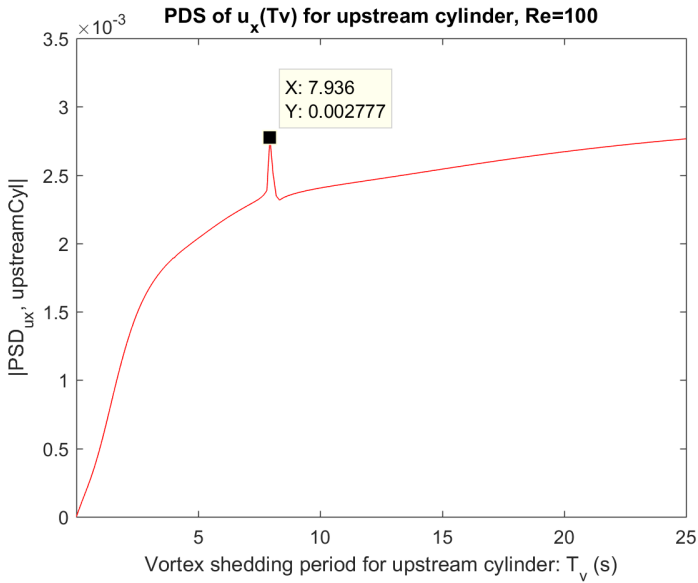


Figure A.165: The power spectral density of probe velocity  $U_x$  with respect to vortex shedding period  $T_v$  for: Upstream Cylinder at  $Re = 100$  and  $\Delta t = 0.002$ .

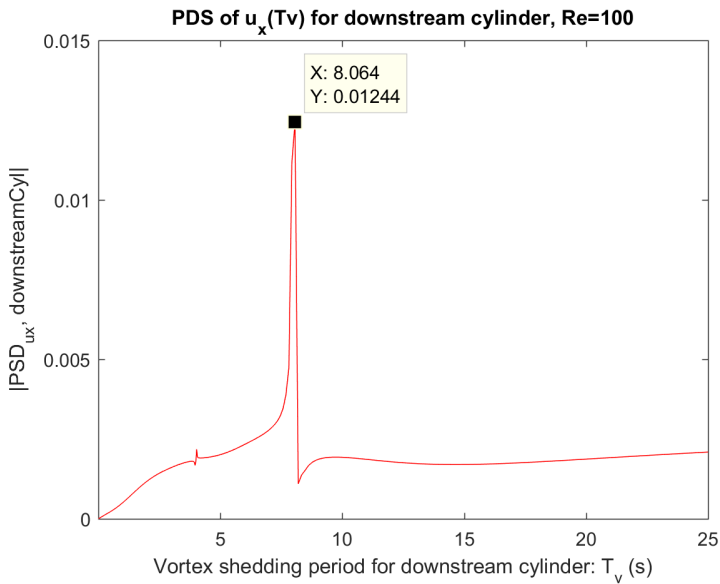


Figure A.166: The power spectral density of probe velocity  $U_x$  with respect to vortex shedding period  $T_v$  for: Downstream Cylinder at  $Re = 100$  and  $\Delta t = 0.002$ .

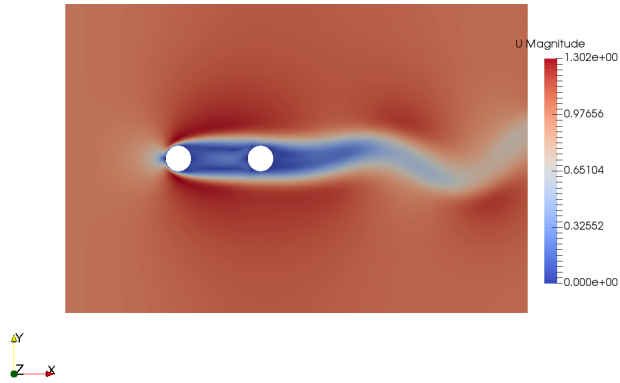


Figure A.167: Velocity magnitude for uniform flow at  $R_e = 100$  at time instant  $t = 1000s$ .

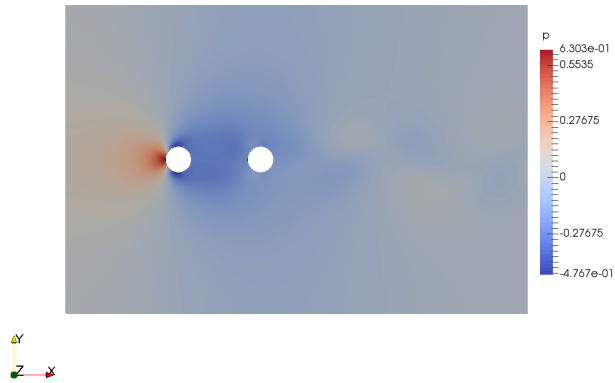


Figure A.168: Pressure distribution for uniform flow at  $R_e = 100$  at time instant  $t = 1000s$ .

## PLOTS: Tandem Cylinders in Uniform Flow at $Re = 200$

The figures below present the oscillation of force coefficients. The oscillations have small root mean square, such that the axisis could have been scales to visualize the oscillation, especially for the drag force oscillation.

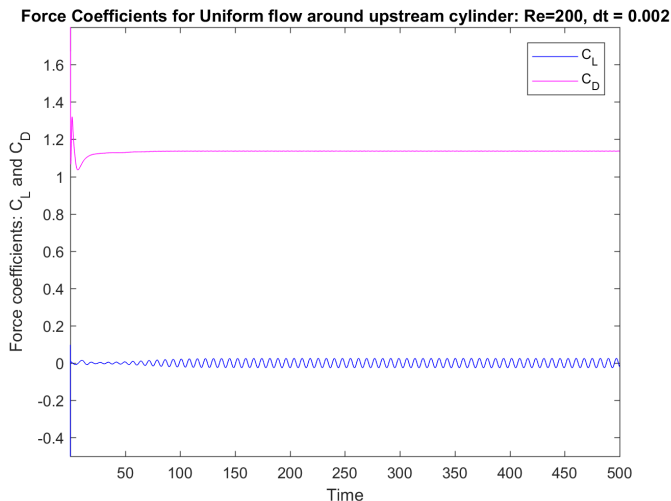


Figure A.169: Drag - and Lift Coefficients for Upstream Cylinder in uniform flow at  $Re = 200$  and  $\Delta t = 0.002$ .

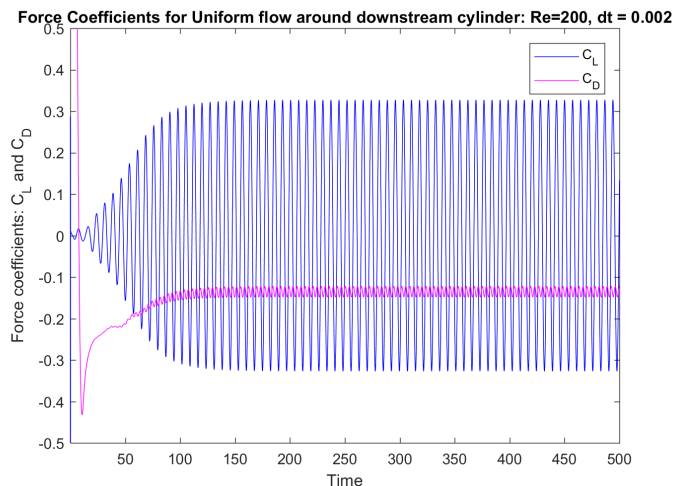


Figure A.170: Drag - and Lift Coefficients for Downstream Cylinder in uniform flow at  $Re = 200$  and  $\Delta t = 0.002$ .

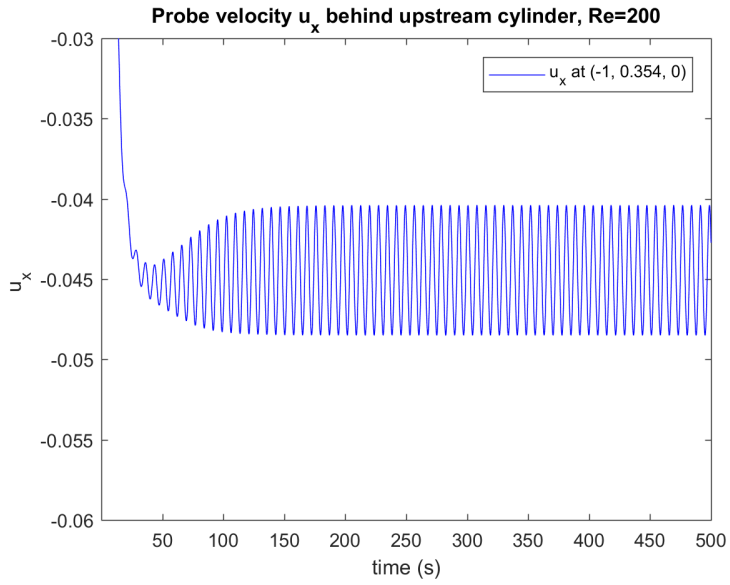


Figure A.171:  $U_x$  velocity probe behind Upstream Cylinder  $(x, y, z) = (-1.0, 0.354, 0)$  at  $Re = 200$  at  $\Delta t = 0.002$ .

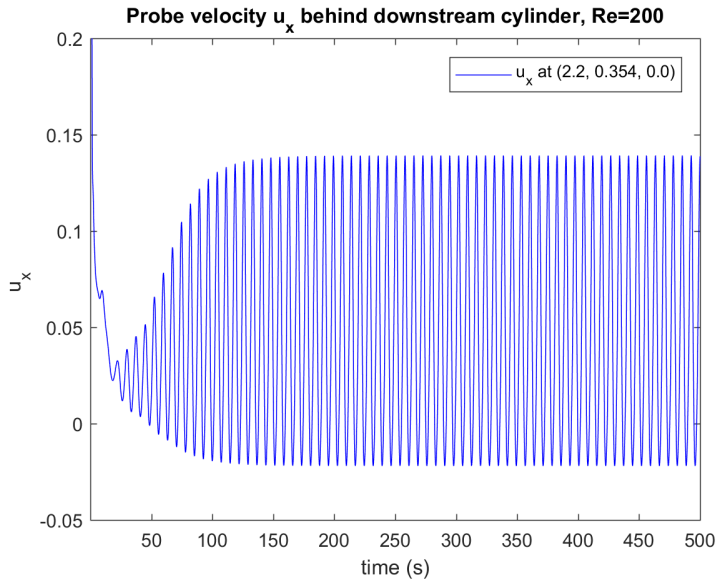


Figure A.172:  $U_x$  velocity probe behind Downstream Cylinder  $(x, y, z) = (2.2, 0.354, 0)$  at  $Re = 200$  at  $\Delta t = 0.002$ .

The oscillation period for the upstream and downstream cylinder is both at  $T_v = 7.353$ , with frequency  $f_v = 0.136$  Hz.

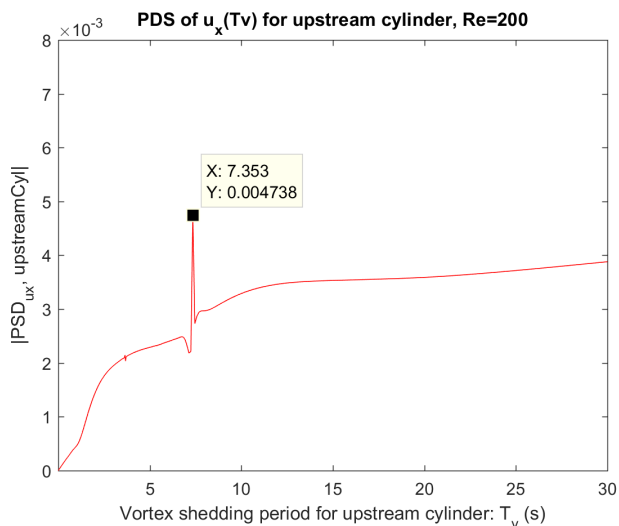


Figure A.173: The power spectral density of probe velocity  $U_x$  with respect to vortex shedding period  $T_v$  for: Upstream Cylinder at  $Re = 200$  and  $\Delta t = 0.002$ .

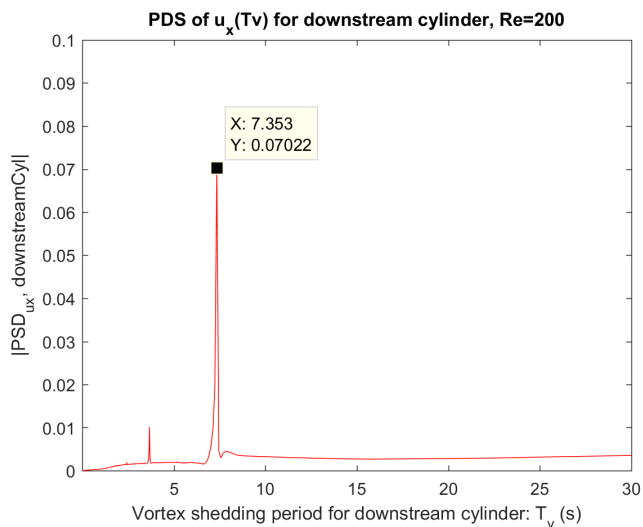


Figure A.174: The power spectral density of probe velocity  $U_x$  with respect to vortex shedding period  $T_v$  for: Downstream Cylinder at  $Re = 200$  and  $\Delta t = 0.002$ .

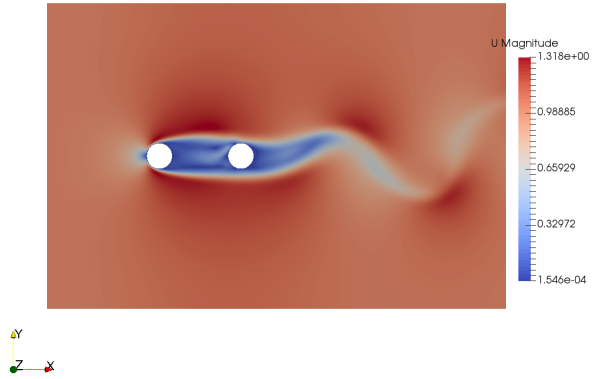


Figure A.175: Velocity magnitude for uniform flow at  $R_e = 200$  at time instant  $t = 500s$ .

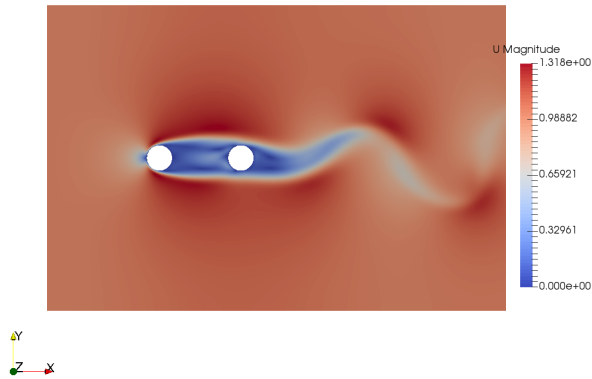


Figure A.176: Velocity magnitude for uniform flow at  $R_e = 200$  at time instant  $t = 1000s$ .

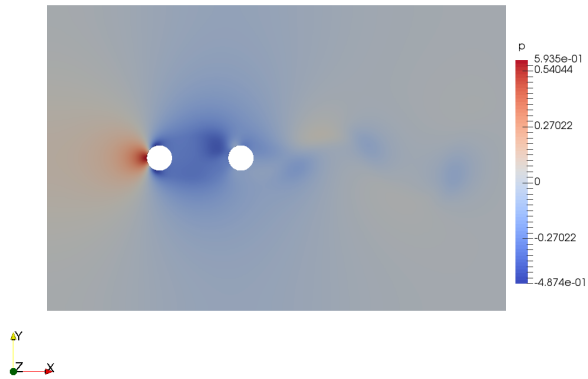


Figure A.177: Pressure distribution for uniform flow at  $R_e = 200$  at time instant  $t = 500s$ .

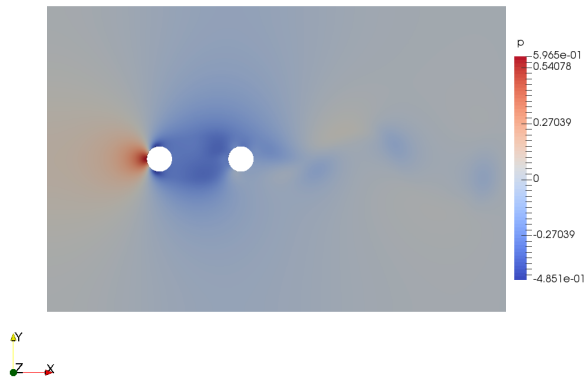


Figure A.178: Pressure distribution for uniform flow at  $R_e = 200$  at time instant  $t = 1000s$ .



## PLOTS: Tandem Cylinders in Uniform Flow at $Re = 300$

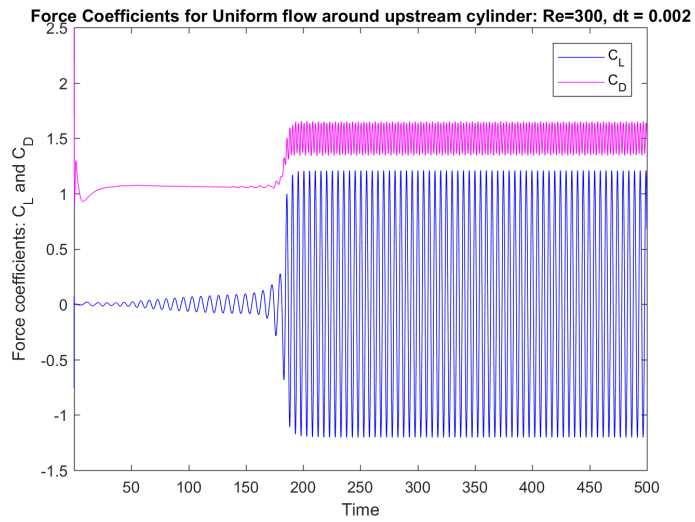


Figure A.179: Drag - and Lift Coefficients for Upstream Cylinder in uniform flow at  $Re = 300$  and  $\Delta t = 0.002$ .

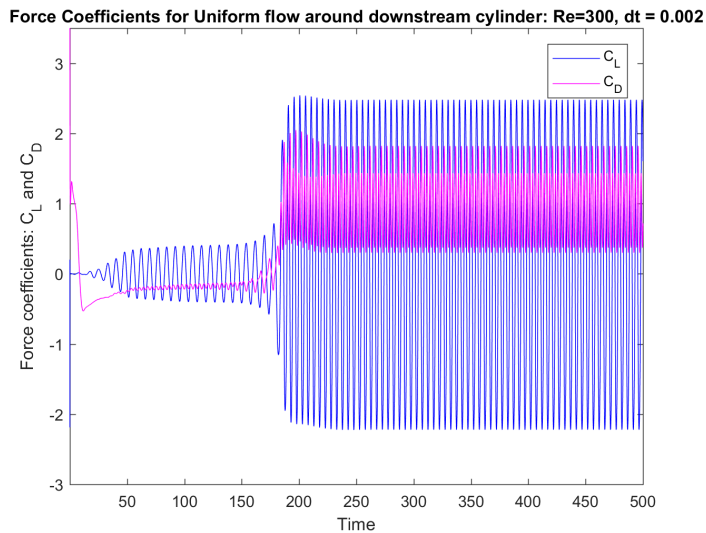


Figure A.180: Drag - and Lift Coefficients for Downstream Cylinder in uniform flow at  $Re = 300$  and  $\Delta t = 0.002$ .

The 2D flow problem gives stable probe velocity behind the upstream cylinder around time instant 180, but is oscillating with two frequencies. The velocity in x-direction behind the downstream cylinder is close to zero ( $1 \times 10^{-300}$ ), such that there is hardly any velocity or oscillation frequency to find. To obtain the oscillation frequency a probe must be places further downstream behind the downstream cylinder wake.

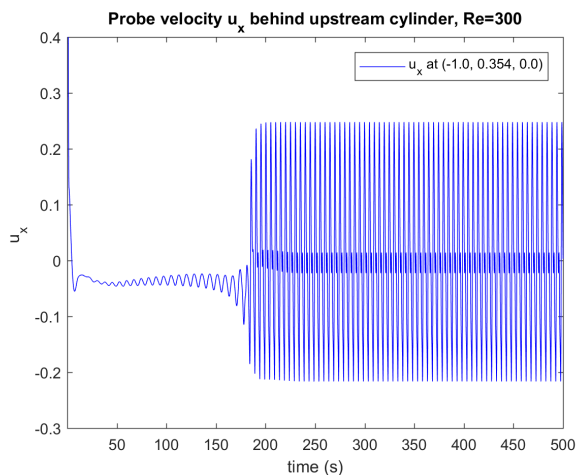


Figure A.181:  $U_x$  velocity probe behind Upstream Cylinder  $(x, y, z) = (-1.0, 0.354, 0)$  at  $Re = 200$  at  $\Delta t = 0.002$ .

The velocity fluctuation behind the upstream cylinder is oscillating with a period of  $T_v = 2.488s$  and  $T_v = 5s$ . The frequencies obtained are  $f_v = 0.402$  and  $f_v = 0.2$ .

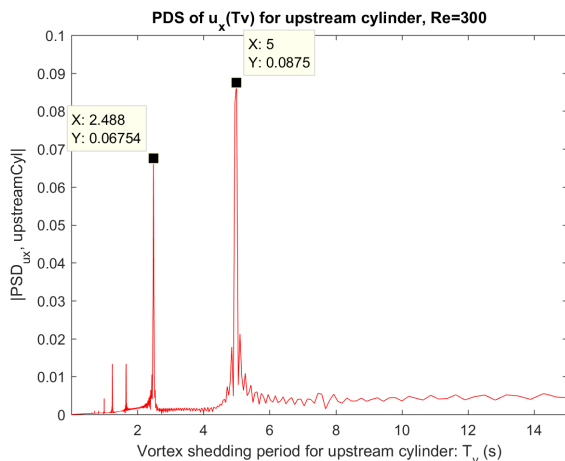


Figure A.182: The power spectral density of probe velocity  $U_x$  with respect to vortex shedding period  $T_v$  for: Upstream Cylinder at  $Re = 300$  and  $\Delta t = 0.002$ .

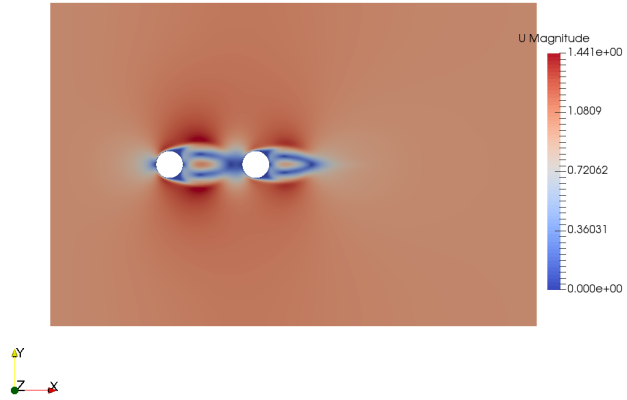


Figure A.183: Velocity magnitude for uniform flow at  $Re = 300$  at time instant  $t = 5s$ .

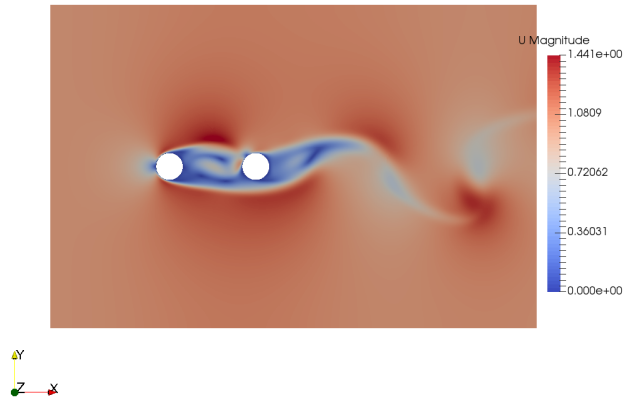


Figure A.184: Velocity magnitude for uniform flow at  $Re = 200$  at time instant  $t = 175s$ .

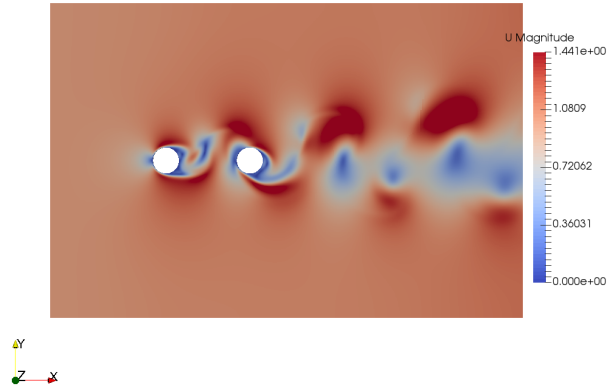


Figure A.185: Velocity magnitude for uniform flow at  $R_e = 300$  at time instant  $t = 200s$ .

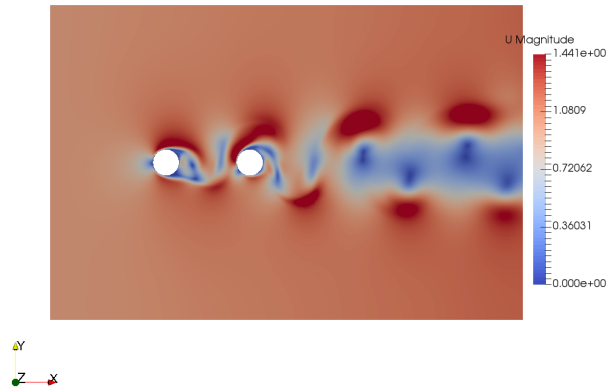


Figure A.186: Velocity magnitude for uniform flow at  $R_e = 300$  at time instant  $t = 500s$ .

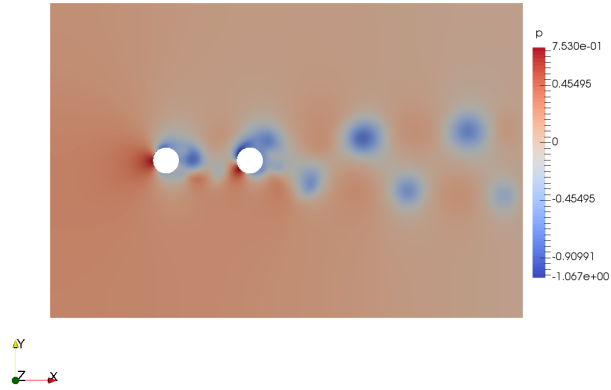


Figure A.187: Pressure distribution for uniform flow at  $R_e = 300$  at time instant  $t = 500s$ .

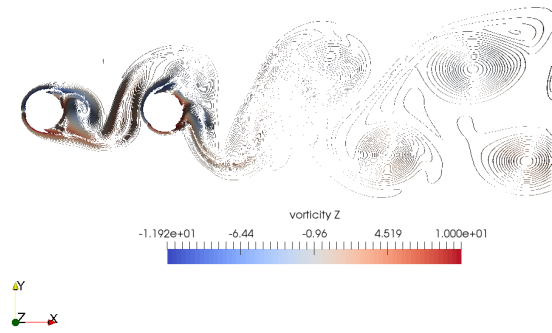


Figure A.188: Vorticity in z-direction  $\omega_z$  for uniform flow at  $R_e = 300$  at time instant  $t = 500s$ .

## .11 Uniform Flow around a 3D Tandem Cylinder

An analysis of how tandem cylinders will behave in uniform flow is performed for three-dimensional flow problems with a span-wise cylinder length of 6 times the diameter length, where the domain size and cylinder properties are presented in table A.16. The analysis is performed for Reynolds number 100, 300 and 500 with  $\Delta t = 0.002$ , where the flow properties are presented in table A.19.

Table A.19: Properties for Uniform flow for different Reynolds numbers.

Properties of Uniform Flow:			
$R_e$	100	300	500
U	1	1	0.5
magUInf	1	1	0.5
viscosity $\nu$	0.01	0.003333	0.001

The results obtained are given in table A.20 for uniform flow around 3D tandem cylinders. The values presented are found for the last 65 % of time simulation up to  $t = 500s$ .

Table A.20: Uniform flow around tandem cylinders towards  $t = 500s$ .

Properties of Uniform Flow:						
	$R_e = 100$		$R_e = 300$		$R_e = 500$	
Values	Upstream	Downstream	Upstream	Downstream	Upstream	Downstream
mean $C_L$	0.00009	-0.00166	0.00033	-0.00137	0.00312	0.00505
mean $C_D$	1.30024	-0.00503	1.07441	-0.11942	1.05257	-0.17424
RMS $C_L$	0.00946	0.09483	0.03816	0.33021	0.01562	0.35311
RMS $C_D$	0.00012	0.00162	0.00495	0.05064	0.00241	0.04071
$T_v[s]$	8.133	8.002	-	7.143	-	13.16
$f_v[Hz]$	0.123	0.125	-	0.14	-	0.076
$S_t$	0.123	0.125	-	0.14	-	0.152

## PLOTS: Uniform Flow around 3D Tandem Cylinders at $Re = 100$

The 3D uniform flow problem at  $Re = 100$  around tandem cylinders presents stable oscillation for both upstream and downstream cylinders (the results from the 2D and 3D cases for  $Re = 100$  are accurate, check appendix .10).

The upstream cylinder has a mean drag coefficient at 1.3, while the 3D uniform flow problem around a Single cylinder (presented in appendix .6) has a drag coefficient at 1.46. The downstream cylinder has a lift coefficient oscillating around 0 (zero), while the drag coefficient is close to zero too. The upstream cylinder will therefore obtain a larger drag force than the downstream cylinder.

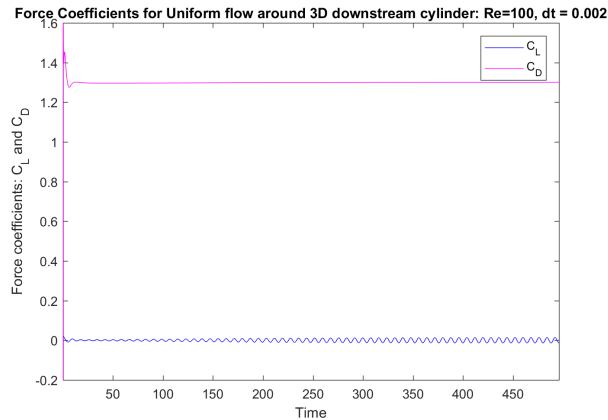


Figure A.189: Drag - and Lift Coefficients for 3D Upstream Cylinder in uniform flow at  $Re = 100$  and  $\Delta t = 0.002$ .

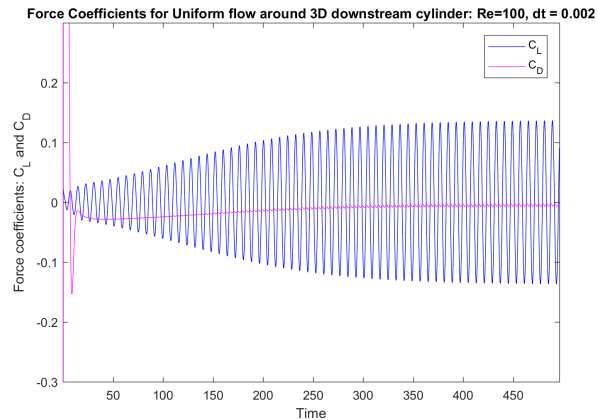


Figure A.190: Drag - and Lift Coefficients for 3D Downstream Cylinder in uniform flow at  $Re = 100$  and  $\Delta t = 0.002$ .

The Strouhals number for a 3D single cylinder in uniform flow at  $Re = 100$  will be at 0.172, while both upstream and downstream cylinder will have Strouhals number close to 0.12. Such that both upstream and downstream will shed for equal period and frequencies.

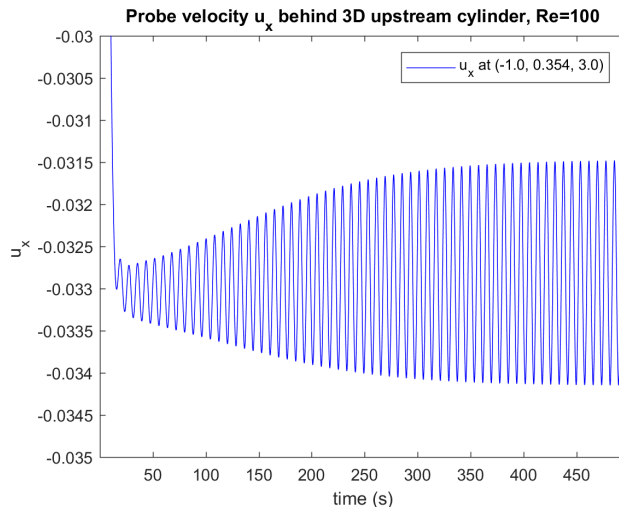


Figure A.191:  $U_x$  velocity probe behind 3D Upstream Cylinder  $(x, y, z) = (-1.0, 0.354, 3.0)$  at  $Re = 100$  at  $\Delta t = 0.002$ .

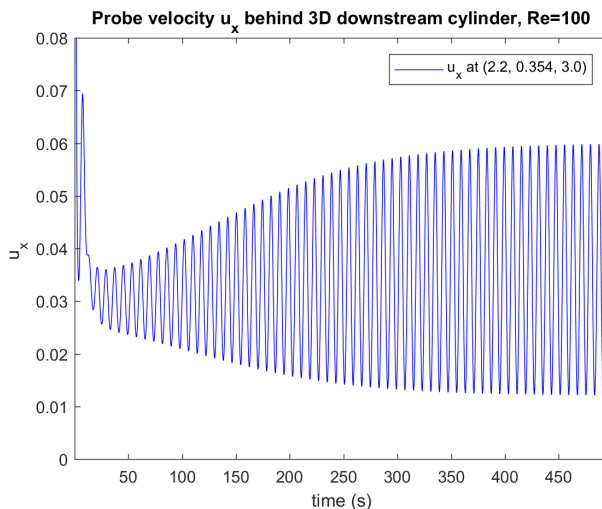


Figure A.192:  $U_x$  velocity probe behind 3D Downstream Cylinder  $(x, y, z) = (2.2, 0.354, 3.0)$  at  $Re = 100$  at  $\Delta t = 0.002$ .



The oscillation period behind upstream cylinder is  $T_v = 8.113s$ , which is close to the oscillation period behind the downstream cylinder at  $T_v = 8.002s$ ,

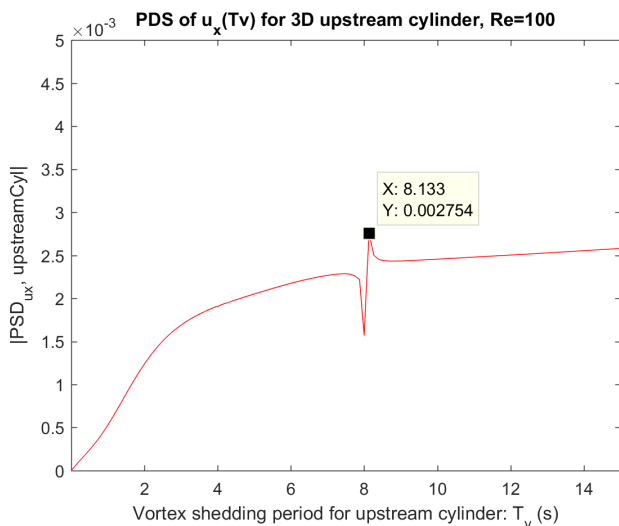


Figure A.193: The power spectral density of probe velocity  $U_x$  with respect to vortex shedding period  $T_v$  for: 3D Upstream Cylinder at  $Re = 100$  and  $\Delta t = 0.002$ .

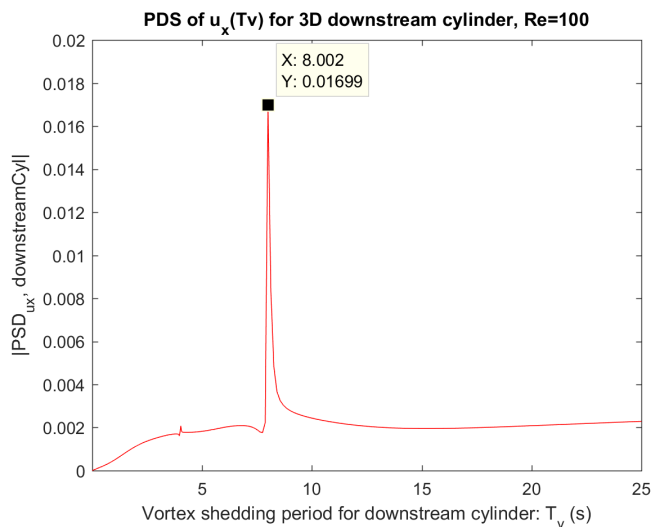


Figure A.194: The power spectral density of probe velocity  $U_x$  with respect to vortex shedding period  $T_v$  for: 3D Downstream Cylinder at  $Re = 100$  and  $\Delta t = 0.002$ .

The plots for velocity magnitude and pressure distribution are at time instant  $t = 500s$ , where the flow problem is stable. These plots are similar for the 2D flow problem with Reynolds number 100.

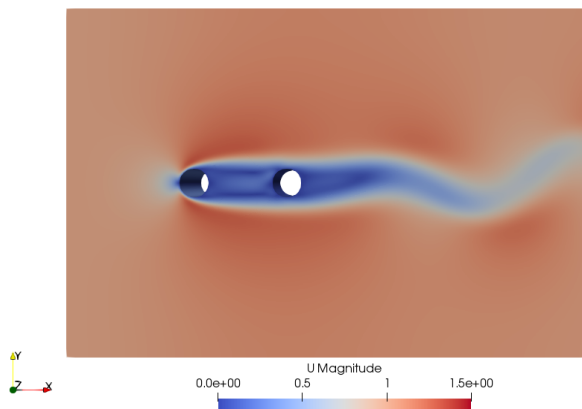


Figure A.195: Velocity magnitude for uniform flow around tandem cylinders for  $R_e = 100$  at time instant  $t = 500s$ .

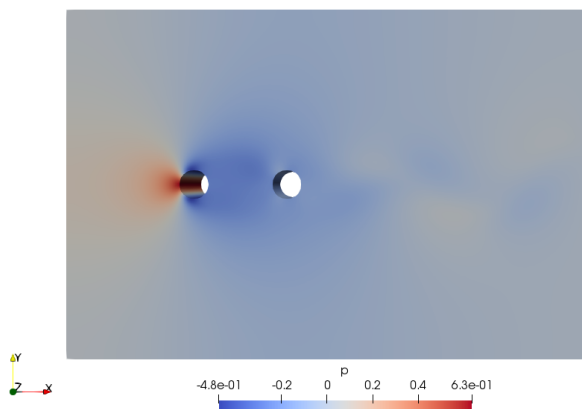


Figure A.196: Pressure distribution for uniform flow around tandem cylinders for  $R_e = 100$  at time instant  $t = 500s$ .

OmegaZ gives a view of how the fluid is behaving and the degree of vorticity. One can observe how a fluid flow acts around solid objects to vortex shedding phenomena in the wake area. The 3D uniform problem around a single cylinder (appendix .6) presents vortex shedding and layered vortices at time instant 180s, where the flow is stable.

For the 3D uniform problem around tandem cylinders, one must simulate for almost 400-500 second for the wake behind the downstream cylinder to become stable. For low Reynolds number as 100, there will not be observed any vortex shedding phenomena, such that OmegaZ around tandem cylinders will only show how the uniform flow is behaving behind the upstream and downstream cylinder.

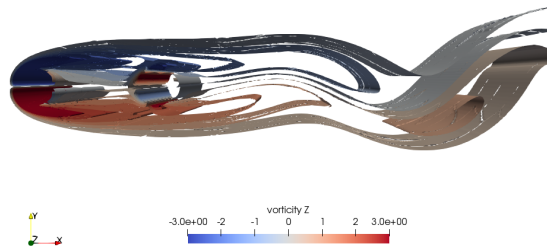


Figure A.197: Vorticity in z-direction  $\omega_z$  for uniform flow around tandem cylinder for  $R_e = 100$  at time instant  $t = 500s$ .

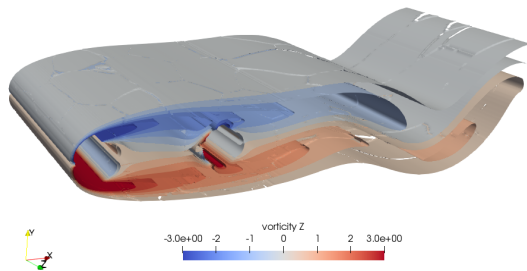


Figure A.198: Vorticity in z-direction  $\omega_z$  for uniform flow around tandem cylinder for  $R_e = 100$  at time instant  $t = 500s$ .

## PLOTS: Uniform Flow around 3D Tandem Cylinders at $Re = 300$

The 3D uniform flow problem around tandem cylinders at  $Re = 300$  presents oscillating force coefficients around upstream and downstream cylinder. The results obtained for the 3D flow problem with  $Re = 300$  differs from the results obtained for the equivalent 2D flow problem. The mean lift coefficient is oscillating around zero for upstream and downstream cylinder for both 2D and 3D flow problem. The root mean square or the oscillation amplitude is larger for the 2D flow problem, as it is restricted for three-dimensional effects.

The drag coefficients for the 2D flow problem is  $\bar{C}_D = 1.50550$  for the upstream cylinder and  $\bar{C}_D = 0.94505$  for the downstream cylinder. For the 3D flow problem the mean drag coefficients are reduced to  $\bar{C}_D = 1.07441$  for the upstream cylinder, while the downstream cylinder obtains a negative value at  $\bar{C}_D = -0.11942$ .

Comparing the upstream cylinder with the flow problem for a single cylinder subjected to a uniform with Reynolds number 300, one can observe that the upstream cylinder for the tandem for problem will have smaller oscillation amplitudes (root mean square values) than for the flow problem with a single cylinder in section .6.

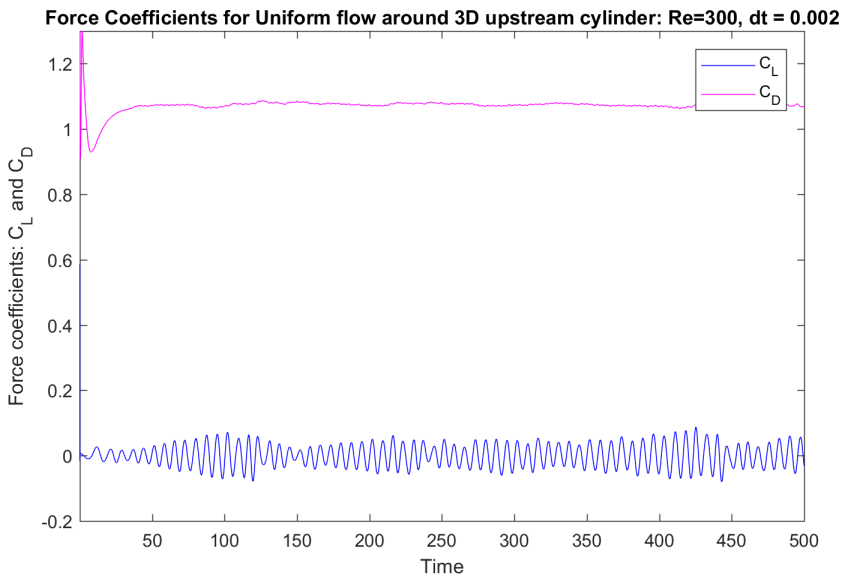


Figure A.199: Drag - and Lift Coefficients for 3D Upstream Cylinder in uniform flow at  $Re = 300$  and  $\Delta t = 0.002$ .

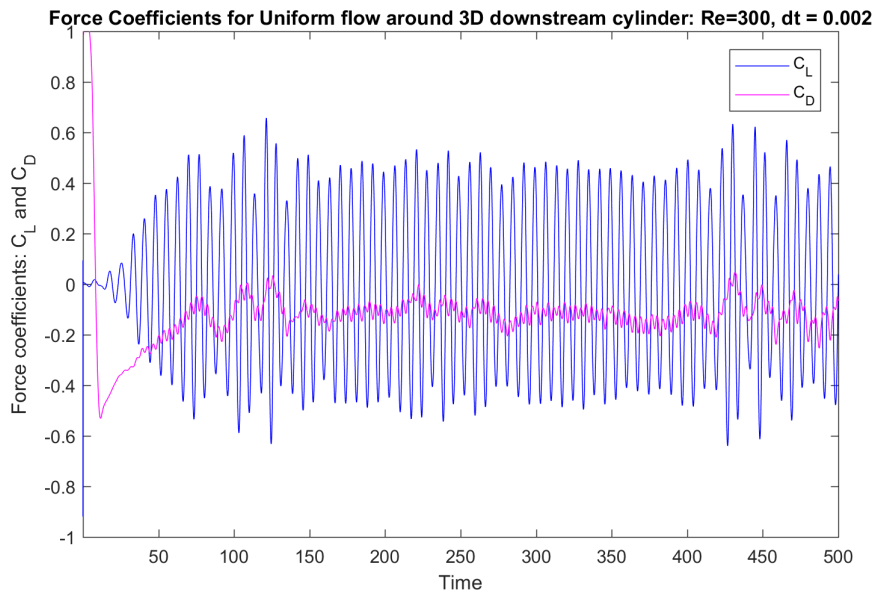


Figure A.200: Drag - and Lift Coefficients for 3D Downstream Cylinder in uniform flow at  $Re = 300$  and  $\Delta t = 0.002$ .

The probe velocity for the upstream cylinders is unstable with varying local tops. These probe data cannot be used to find the value for oscillation period and frequency. There will be velocities fluctuating around zero right behind the upstream cylinder, as the inlet velocity flows around the tandem cylinders as one whole solid object.

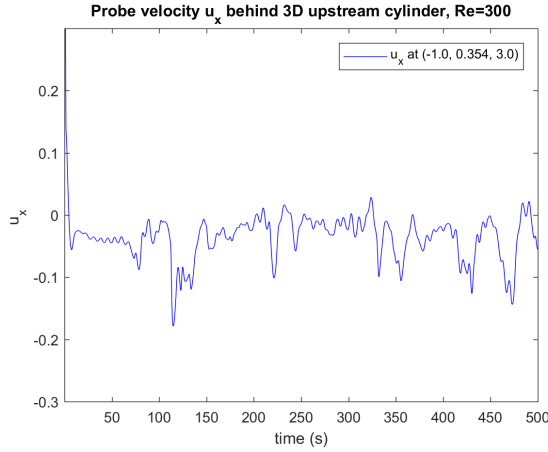


Figure A.201:  $U_x$  velocity probe behind 3D Upstream Cylinder  $(x, y, z) = (-1.0, 0.354, 3.0)$  at  $Re = 300$  at  $\Delta t = 0.002$ .

The probe velocity behind the downstream cylinder is oscillating with one top and bottom within a period, such that the oscillation period and frequencies are found. Comparing to the equivalent 2D fluid problem, the oscillation period and frequency are not found for the downstream cylinder (appendix .10).

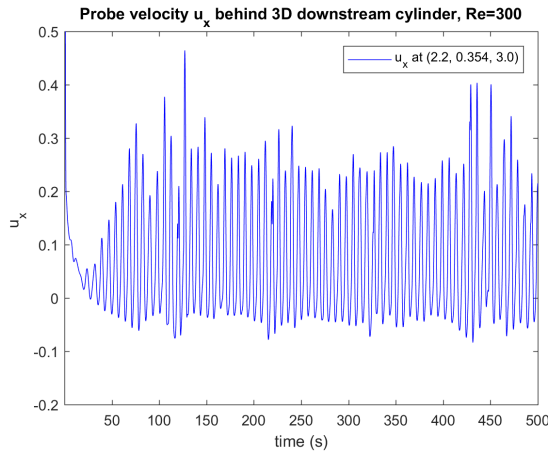


Figure A.202:  $U_x$  velocity probe behind 3D Downstream Cylinder  $(x, y, z) = (2.2, 0.354, 3.0)$  at  $Re = 300$  at  $\Delta t = 0.002$ .

The vortex shedding period is not easy to find with the given figures.

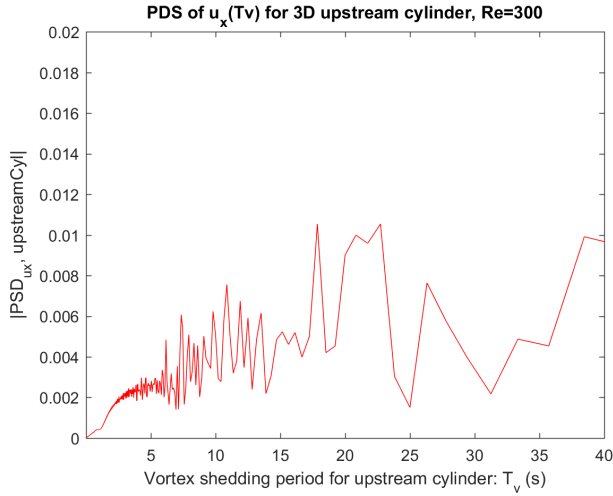


Figure A.203: The power spectral density of probe velocity  $U_x$  with respect to vortex shedding period  $T_v$  for: 3D Upstream Cylinder at  $Re = 300$  and  $\Delta t = 0.002$ .

The vortex shedding period is found for the downstream cylinder for the 3D tandem flow case, with a oscillation period of  $T_v = 7.143$ , frequency and Strouhals number of 0.14.

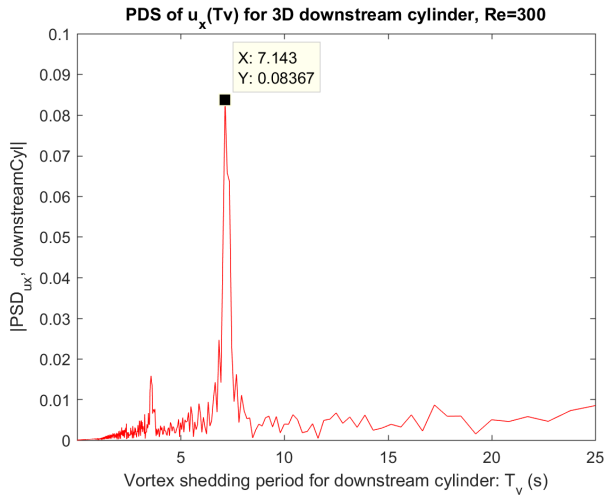


Figure A.204: The power spectral density of probe velocity  $U_x$  with respect to vortex shedding period  $T_v$  for: 3D Downstream Cylinder at  $Re = 300$  and  $\Delta t = 0.002$ .

The plots for velocity magnitude and pressure distribution at time instant 500s. During the simulation the Force coefficients are oscillating with irregular amplitudes with a frequency for both upstream and downstream cylinder for all time instants.

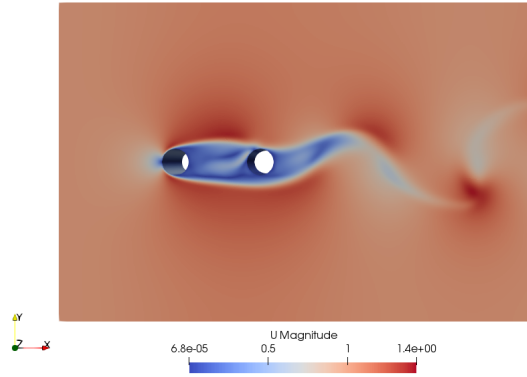


Figure A.205: Velocity magnitude for uniform flow around tandem cylinders for  $R_e = 300$  at time instant  $t = 500s$ .

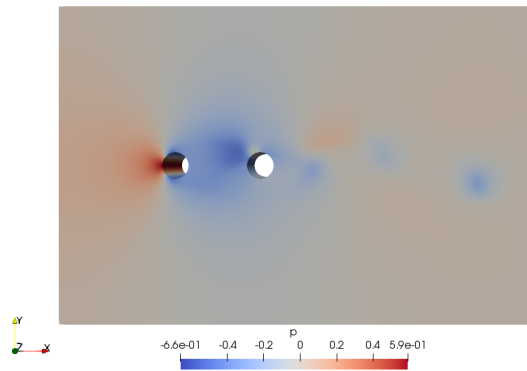


Figure A.206: Pressure distribution for uniform flow around tandem cylinders for  $R_e = 300$  at time instant  $t = 500s$ .



The omegaZ  $\omega_z$  visualizes how the uniform flow at Reynolds number 300 behaves around tandem cylinders. The plots are given for time instant  $t = 500s$ . The fluid acts all smooth around both cylinders, where the two solid surfaces acts as one large body.

There are vortices acting behind the upstream cylinder (in-between the tandem cylinders), which could be why it was unable to find the oscillation periods and frequencies for the upstream cylinder. There are no clear vortex sheddings, and the wake region becomes unclear. In the wake region the shedding occurs with 3D effects along the cylinder.

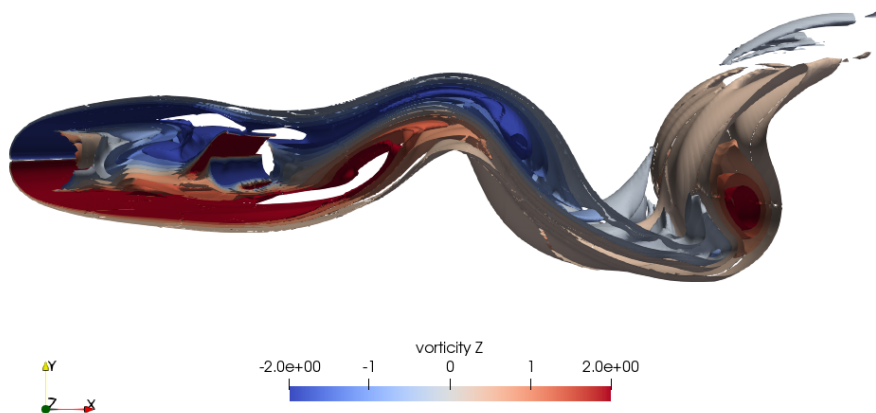


Figure A.207: Vorticity in z-direction  $\omega_z$  for uniform flow around tandem cylinder for  $R_e = 300$  at time instant  $t = 150s$ .

The plots below presents the flow problem of a uniform flow at  $R_e = 300$  around a single cylinder with span-wise length of 4 diameters (appendix .6), while the tandem cylinders have a span-wise length of 6 diameters. For the flow problem around a single cylinder, there are several vortex shedding presented in the plot, with 3D effects along the span-wise length. The flow problem with tandem cylinders shows the two cylinders acting almost as a single object, where the fluid moves around the tandem cylinders. There will be vortices and velocities between the upstream and downstream cylinder, but no clear 3D effects along the span-wise length.

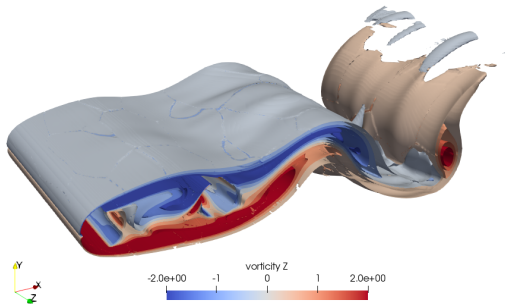


Figure A.208: Vorticity in z-direction  $\omega_z$  for uniform flow around tandem cylinder for  $R_e = 300$  at time instant  $t = 500s$ .

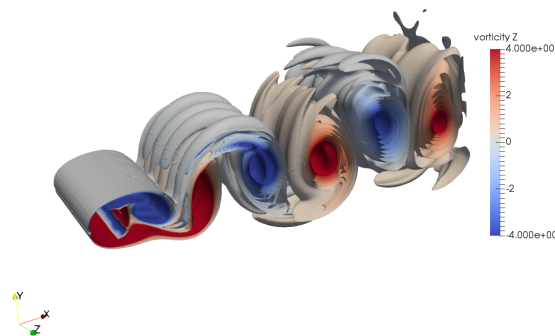


Figure A.209: Vorticity in z-direction  $\omega_z$  for uniform flow at  $R_e = 300$  at time instant  $t = 250s$ . Different angle.

## PLOTS: Uniform Flow around 3D Tandem Cylinders at $Re = 500$

The 3D uniform flow problem around tandem cylinders at  $Re = 500$  gives oscillating drag - and lift coefficients around upstream and downstream cylinder. The mean value of drag around upstream cylinder is  $\bar{C}_D = 1.05257$ . while the lift coefficient oscillated around zero.

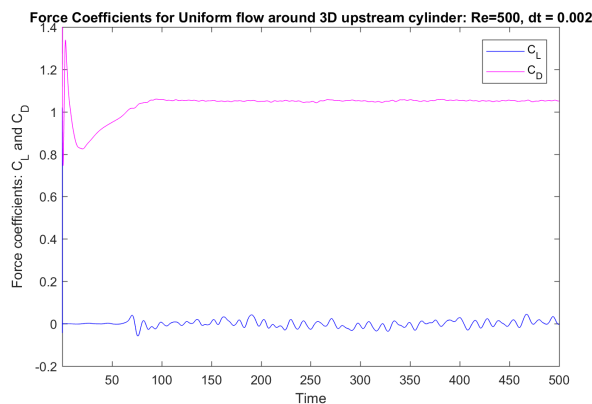


Figure A.210: Drag - and Lift Coefficients for 3D Upstream Cylinder in uniform flow at  $Re = 500$  and  $\Delta t = 0.002$ .

The downstream cylinder will experience a negative drag coefficient of  $\bar{C}_D = -0.17424$ . The lift coefficient will still oscillate around mean value of zero, but the root mean square (oscillation amplitude) is larger than for the upstream cylinder. One can observe that the flow is stable around  $t = 100s$ .

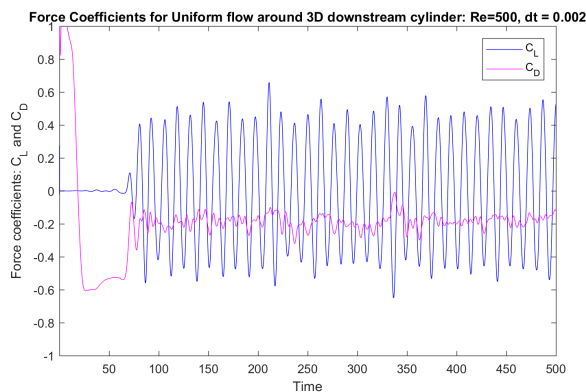


Figure A.211: Drag - and Lift Coefficients for 3D Downstream Cylinder in uniform flow at  $Re = 500$  and  $\Delta t = 0.002$ .

The velocity behind the upstream cylinder is unstable, as the figure below presents the velocity with varying local tops. The probe velocity is also varying around the mean value of zero, which means that there are small velocities behind the upstream cylinder. One can therefore not obtain the oscillation period, frequency or the Strouhals number for the upstream cylinder. The 3D uniform flow problem with  $Re = 300$  also experiences small fluctuating velocities behind the upstream cylinder.

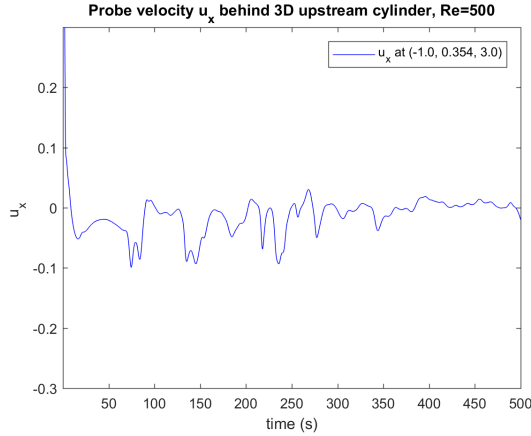


Figure A.212:  $U_x$  velocity probe behind 3D Upstream Cylinder  $(x, y, z) = (-1.0, 0.354, 3.0)$  at  $Re = 500$  at  $\Delta t = 0.002$ .

The probe velocity behind the downstream cylinder oscillates with one top and bottom within a period, such that the oscillation period, frequency and Strouhals number is found.

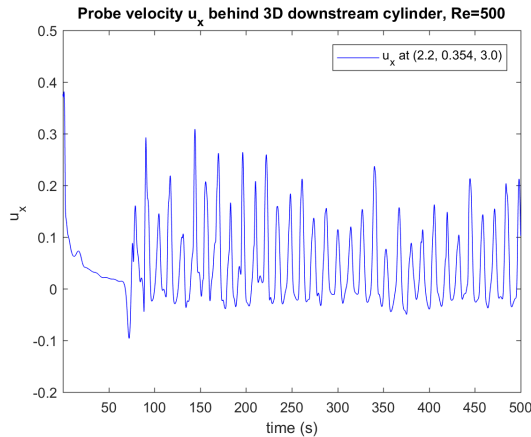


Figure A.213:  $U_x$  velocity probe behind 3D Downstream Cylinder  $(x, y, z) = (2.2, 0.354, 3.0)$  at  $Re = 500$  at  $\Delta t = 0.002$ .

The velocity fluctuation far downstream at probe  $(3.5, 0.354, 3.0)$  is presented in the figure below. The oscillation of the velocity in x-direction  $U_x$  is similar to the oscillation right behind the downstream cylinder.

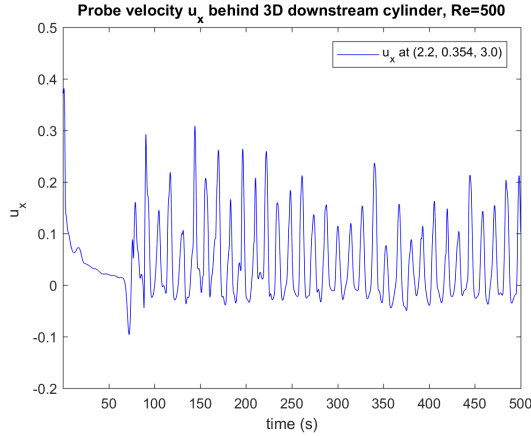


Figure A.214:  $U_x$  velocity probe far downstream  $(x, y, z) = (3.5, 0.354, 3.0)$  at  $R_e = 500$  at  $\Delta t = 0.002$ .

The figure below presents the pressure fluctuation for four different probes around the cylinder. Time simulations before  $t = 100s$  is unstable as the pressure is varying. The flow problems stabilizes and the pressure fluctuates periodically.

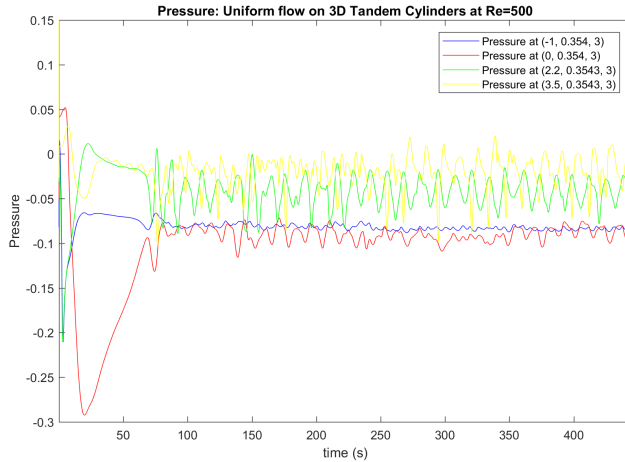


Figure A.215: Pressure fluctuation with respect to time simulation for Probe1  $(-1, 0.354, 3)$ , Probe 2  $(0, 0.354, 3)$ , Probe 3  $(2.2, 0.354, 3)$  and probe 4  $(3.5, 0.354, 3)$  for Uniform Flow around 3D Tandem Cylinders with  $R_e = 500$  &  $\Delta t = 0.002$ .

The Power Spectral Density curves are presented for the upstream cylinder. There are no obvious periods or frequencies which are dominated the flow behind the upstream cylinder. This is due to the velocity behind the upstream cylinder is fluctuating irregular around zero.

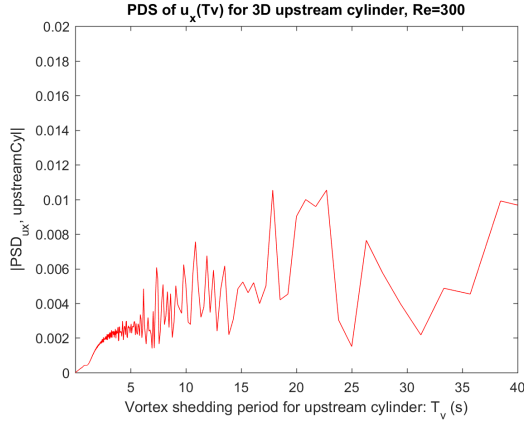


Figure A.216: The power spectral density of probe velocity  $U_x$  with respect to vortex shedding period  $T_v$  for: 3D Upstream Cylinder at  $Re = 300$  and  $\Delta t = 0.002$ .

The downstream cylinder experiences fluctuating velocities with a period  $T_v = 13.61$  and a frequency of  $f_v = 0.076$ . The Strouhals number is  $St = 0.152$ , which is close to the the value obtained for flow problem with Reynolds number 300. The periods and frequency are deviating from the 3D flow problem with  $Re = 300$  due to different inlet velocity. All results for 3D uniform flow are presented in table A.20.

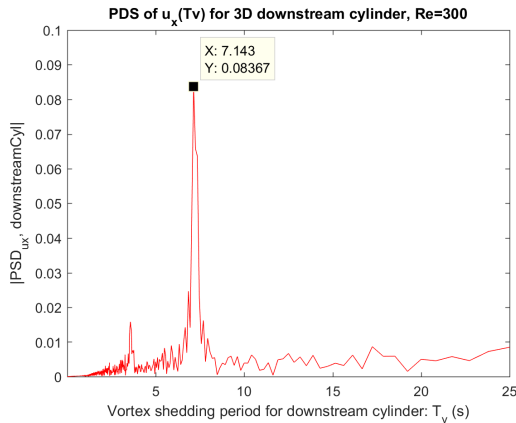


Figure A.217: The power spectral density of probe velocity  $U_x$  with respect to vortex shedding period  $T_v$  for: 3D Downstream Cylinder at  $Re = 300$  and  $\Delta t = 0.002$ .

Velocity magnitude is presented in the plots below at time instant  $t = 100s$  and  $t = 500s$ . At time instant  $t = 100s$  the flow problem has stabilized and continue to stay stable towards time instant  $t = 500s$ .

The velocities behind the upstream cylinders as close to zero, such that the inlet current velocity is moving around the tandem cylinders as a single solid body. Velocities behind the downstream cylinder and far downstream oscillated periodically due to the vortex shedding phenomena in the wake region.

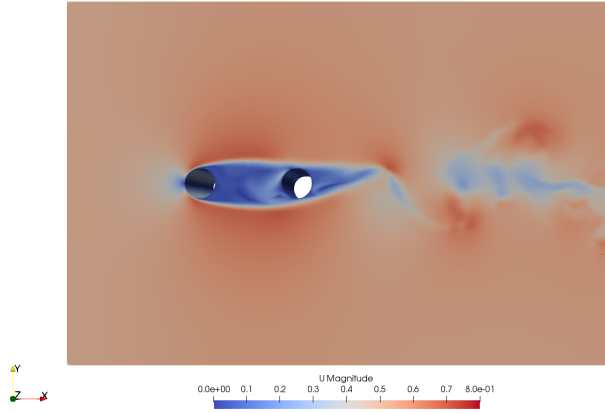


Figure A.218: Velocity magnitude for uniform flow around tandem cylinders for  $R_e = 500$  at time instant  $t = 100s$ .

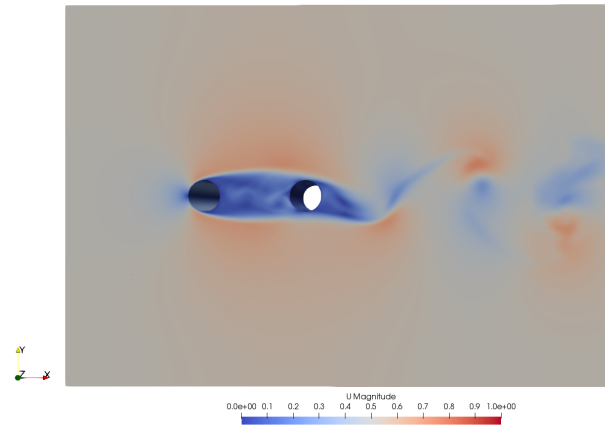


Figure A.219: Velocity magnitude for uniform flow around tandem cylinders for  $R_e = 500$  at time instant  $t = 500s$ .

Figure A.220 and A.221 presents the velocity distribution in y - and z - direction  $U_y$  and  $U_z$ , which is approximately zero. The velocity in x-direction will dominate the absolute velocity magnitude in the domain.

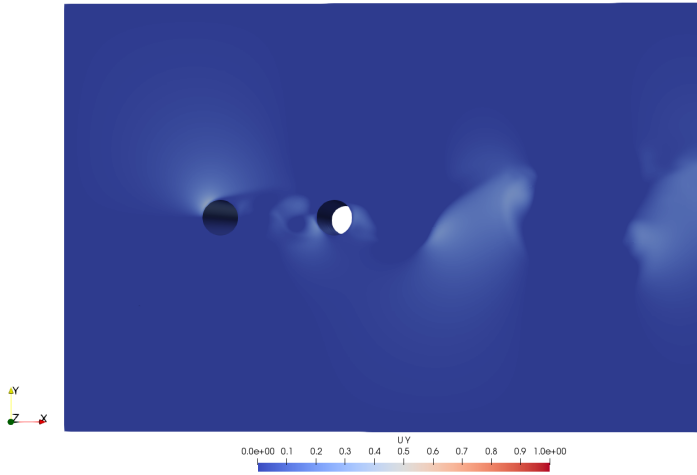


Figure A.220: Velocity in y - direction  $U_y$  for Uniform Flow around tandem cylinders with  $Re = 500$  at time instant  $t = 500s$ .

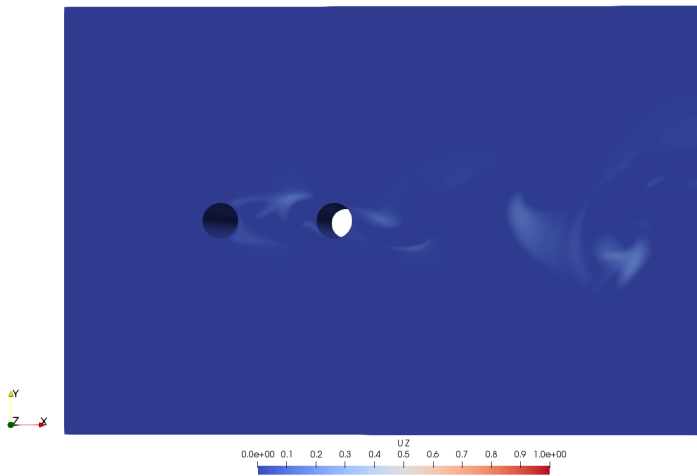


Figure A.221: Velocity in z - direction  $U_z$  for Uniform Flow around tandem cylinders with  $Re = 500$  at time instant  $t = 500s$ .



Pressure distribution at time instant  $t = 100s$  and  $t = 500s$  looks similar as the flow is stable at both time instants. One can observe a stagnation point in the area in-front of the upstream cylinder with a high pressure zone. There is low pressure zones in-between the tandem cylinders, and far downstream in the wake region due to vortex shedding phenomena.

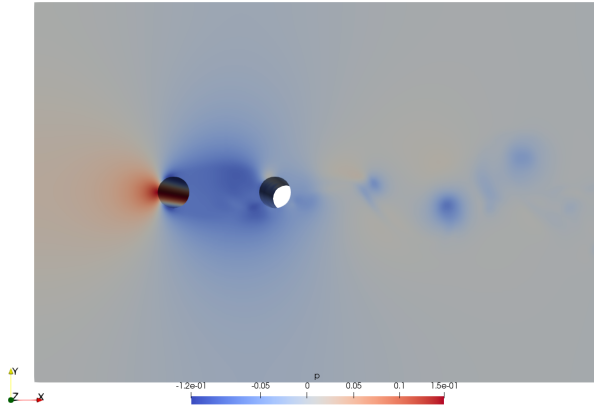


Figure A.222: Pressure distribution for uniform flow around tandem cylinders for  $R_e = 500$  at time instant  $t = 100s$ .

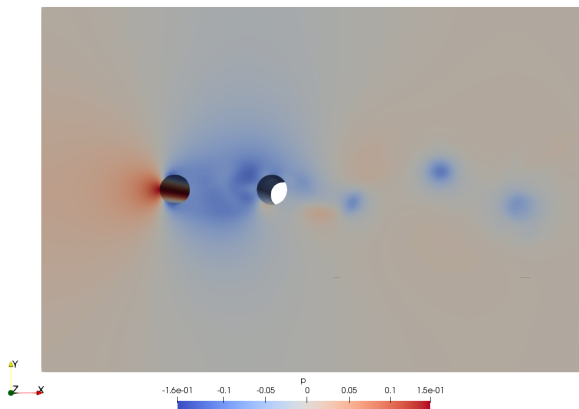


Figure A.223: Pressure distribution for uniform flow around tandem cylinders for  $R_e = 500$  at time instant  $t = 500s$ .

Vorticity distribution in z-direction  $\omega_z$  is presented at time instant  $t = 100s$ . The fluid motion is moving around the tandem cylinders, with vorticities close to zero in-between the tandem cylinders. The fluid around the tandem cylinders have little 3D effects as the flow moves smoothly over the tandem cylinders a single solid surface. Downstream in the the wake area consist of vortex shedding with 3D effects along the vortex downstream.

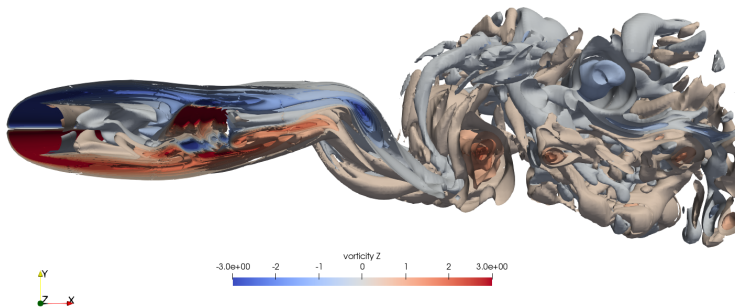


Figure A.224: Vorticity in z-direction  $\omega_z$  for uniform flow around tandem cylinder for  $R_e = 500$  at time instant  $t = 100s$ .

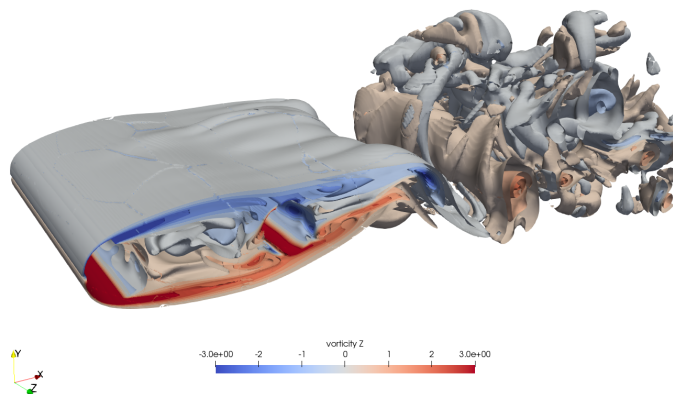


Figure A.225: Vorticity in z-direction  $\omega_z$  for uniform flow around tandem cylinder for  $R_e = 500$  at time instant  $t = 100s$ . Different angle.

Vorticity in z-direction  $\omega_z$  is presented at time instant  $t = 500s$ . The vorticity will describe the fluid motion around the tandem cylinder, in-between the cylinders and behaviour far downstream. Fluid moves smoothly around the tandem cylinders, will fluid motions in-between the tandem cylinders. Downstream the flow will gain vortex sheddings and 3D effects occur. At time instant  $t = 500s$  the 3D effects downstream follow the vortex shedding. The vortex shedding seems more periodically for this time instant, compares to time instant  $t = 100s$  where the downstream flow is chaotic and irregular.

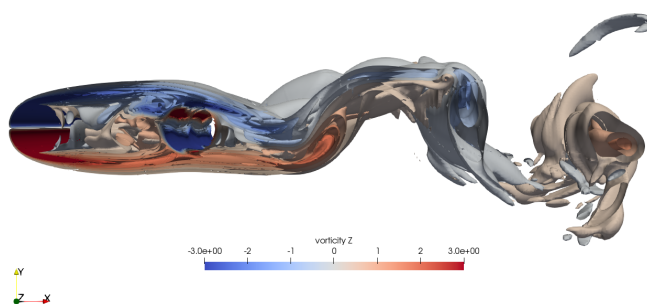


Figure A.226: Vorticity in z-direction  $\omega_z$  for uniform flow around tandem cylinder for  $Re = 500$  at time instant  $t = 500s$ .

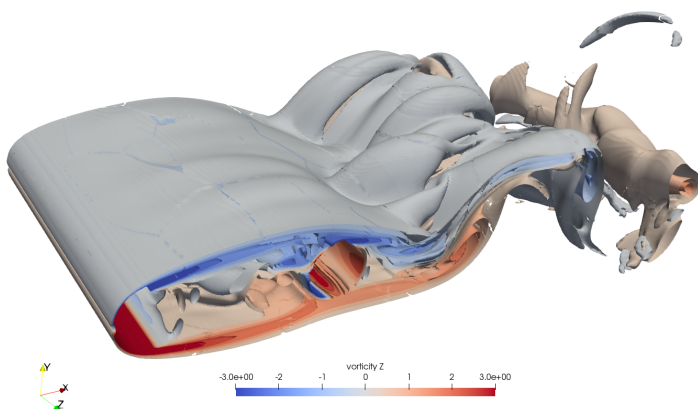


Figure A.227: Vorticity in z-direction  $\omega_z$  for uniform flow around tandem cylinder for  $Re = 500$  at time instant  $t = 500s$ . Different angle.

## .12 MATLAB SCRIPTS:

```
%CALCULATING MEAN VALUES OF DRAG AND LIFT
%Plotting force coefficients with respect to time simulation
clear all;
clc;

% Reading dat.-file , & converting into matrix
fid=fopen('forceCoeffs_downstream3D_uniRe500.dat','r');
datacell=textscan(fid, '%f%f%f%f%f', 'Headerlines', 10, 'collect', 1);
fclose(fid);
datamat = cell2mat(datacell);

% collecting data from matrix
Cl = datamat(:, 4);
Cd = datamat(:, 3);
time = datamat(:, 1);

figure(1)
plot(time, Cl, 'b', time, Cd, 'm')
axis([min(time) max(time) -1.0 1.0])
title('Force Coefficients for Uniform flow around '
'3D downstream cylinder:Re=500, dt = 0.002');
xlabel('Time');
ylabel('Force coefficients: C_{L} and C_{D}');
legend('C_L', 'C_D');

%Finding mean and max/min values of coefficients
%Taking the mean of 80 % last values

meanCl = mean(Cl(end*0.65:end));
meanCd = mean(Cd(end*0.65:end));

%RMS – root mean square
RMS_Cd = rms(Cd(end*0.65 : end)-meanCd);
RMS_Cl = rms(Cl(end*0.65 : end)-meanCl);

fprintf('The mean Cl is %4.5f \n', meanCl)
fprintf('The mean Cd is %4.5f \n', meanCd)
fprintf('The RMS of Cl is %4.5f \n', RMS_Cl)
fprintf('The RMS of Cd is %4.5f \n', RMS_Cd)
```

```
%FINDING VORTEX FREQUENCY AND STROUHALS NUMBER
```

```
clear all; clc;
```

```
% Reading dat.-file , & converting into matrix
```

```
fid = fopen('Utot_3Dtandem_uniRe500.dat','r');
datacell = textscan(fid, '%f (%f %f %f) (%f %f %f) (%f %f %f)'
''(%f %f %f)', 'Headerlines', 6);
fclose(fid);
datamat = cell2mat(datacell);
```

```
time = datamat(:, 1);
ux_p1 = datamat(:, 2);      %Ux at probe1: (-1.0, 0.354, 0)
ux_p2 = datamat(:, 8);      %Ux at probe2: (2.2, 0.354, 0)
ux_p3 = datamat(:, 11);     %Ux at probe3: (3.5, 0.354, 3)
dt = 0.002 ;                %Sampling period, time step
Fs = 1/dt;                   %Sampling frequency
L = length(time);           %Length of signal, simulation
```

```
%Plot of lift coefficient with respect to time simulation:
```

```
figure(1)
plot(time, ux_p1, 'b')
axis([min(time) max(time) -0.3 0.3])
title('Probe velocity u- $\{x\}$  behind 3D upstream cylinder, Re=500')
xlabel('time (s)')
ylabel('u- $\{x\}$  ')
legend('u- $\{x\}$  at (-1.0, 0.354, 3.0)')
```

```
figure(2)
plot(time, ux_p2, 'b')
axis([min(time) max(time) -0.2 0.5])
title('Probe velocity u- $\{x\}$  behind 3D downstream cylinder, Re=500')
xlabel('time (s)')
ylabel('u- $\{x\}$  ')
legend('u- $\{x\}$  at (2.2, 0.354, 3.0)')
```

```
figure(3)
plot(time, ux_p3, 'b')
axis([min(time) max(time) -0.4 0.8])
title('Probe velocity u- $\{x\}$  far downstream: Re=500')
xlabel('time (s)')
ylabel('u- $\{x\}$  ')
legend('u- $\{x\}$  at (3.5, 0.354, 3.0)')
```

```
%Power Spectral Density with respect to vortex shedding period
```

```
Y_p1 = fft(ux_p1);
prob1_P2 = abs(Y_p1/L);
```

```

prob1_P1 = prob1_P2(1:L/2+1);
prob1_P1(2:end-1) = 2*prob1_P1(2:end-1);

Y_p2 = fft(ux_p2);
prob2_P2 = abs(Y_p2/L);
prob2_P1 = prob2_P2(1:L/2+1);
prob2_P1(2:end-1) = 2*prob2_P1(2:end-1);

fv = Fs*(0:(L/2))/L;
Tv=1./fv;

%Power Spectral Density with respect to vortex shedding period
figure(4)
plot(Tv, prob1_P1, 'r')
axis([min(time) 40 0 0.02])
title('PDS of u_{x}(Tv) for 3D upstream cylinder, Re=500')
xlabel('Vortex shedding period for upstream cylinder: T_{v} (s)')
ylabel('|PSD_{ux}, upstreamCyl|')

%Power Spectral Density with respect to vortex shedding frequency
figure(5)
plot(fv, prob1_P1, 'r')
axis([0 0.2 0 0.02])
title('PDS of u_{x}(fv) for 3D upstream cylinder, Re=500')
xlabel('Vortex shedding frequency for upstream cylinder: f_{v} (Hz)')
ylabel('|PSD_{ux}, upstreamCyl|')

%Power Spectral Density with respect to vortex shedding period
figure(6)
plot(Tv, prob2_P1, 'r')
axis([min(time) 25 0 0.1])
title('PDS of u_{x}(Tv) for 3D downstream cylinder, Re=500')
xlabel('Vortex shedding period for downstream cylinder: T_{v} (s)')
ylabel('|PSD_{ux}, downstreamCyl|')

%Power Spectral Density with respect to vortex shedding frequency
figure(7)
plot(fv, prob2_P1, 'r')
axis([0 0.2 0 0.1])
title('PDS of u_{x}(fv) for 3D downstream cylinder, Re=500')
xlabel('Vortex shedding frequency for downstream cylinder: f_{v} (Hz)')
ylabel('|PSD_{ux}, downstreamCyl|')

```

```
%PLOT OF PRESSURE MEASURES AT PROBES
```

```
clear all;  
clc;
```

```
% Reading dat.-file , & converting into matrix  
fid = fopen('Ptot_3Dtandem_uniRe500.dat','r');  
datacell = textscan(fid, '%f%f%f%f%f%f', 'Headerlines', 6);  
fclose(fid);  
datamat = cell2mat(datacell);
```

```
%extracting desired data for time and ux for all three probes:  
time = datamat(:, 1);           %timestep  
p1 = datamat(:, 2);           %Probe 1: (-1, 0.354, 3)  
p2 = datamat(:, 3);           %Probe 2: (0, 0.354, 3)  
p3 = datamat(:, 4);           %Probe 3: (2.2, 0.3543, 3)  
p4 = datamat(:, 5);           %Probe 4: (3.5, 0.3543, 3)
```

```
%Plot of lift coefficient with respect to time simulation:  
figure(1)  
plot(time, p1, 'b', time, p2, 'r', time, p3, 'g', time, p4, 'y' )  
axis([min(time) max(time) -0.3 0.15])  
title('Pressure: Uniform flow on 3D Tandem Cylinders at Re=500')  
xlabel('time (s)')  
ylabel('Pressure')  
legend('Pressure at (-1, 0.354, 3)', 'Pressure at (0, 0.354, 3)',  
'Pressure at (2.2, 0.3543, 3)', 'Pressure at (3.5, 0.3543, 3)');
```

```

%PRESSURE DISTRIBUTION AROUND CYLINDERS
clear all; clc;

%Upstream Cylinder in Shear Flow: Reading csv.-file
data_up_shear=csvread('upstream_slice_shearRe500_t500.csv',1,0);

%Downstream Cylinder in Shear flow: Reading dat.-file
data_down_shear=csvread('downstream_slice_shearRe500_t500.csv',1,0);

%Upstream Cylinder in Uniform Flow: Reading csv.-file
data_up_uni=csvread('upstream_slice_uniRe500_t500.csv',1,0);

%Downstream Cylinder in Uniform Flow: Reading dat.-file
data_down_uni=csvread('downstream_slice_uniRe500_t500.csv',1,0);

%Extracting value of pressure for Upstream Cylinder Shear Flow Problem
p1_up_shear = data_up_shear(117:146, 5);
p2_up_shear = data_up_shear(1:86, 5);
p3_up_shear = data_up_shear(232:266, 5);
p-up-shear= [p1_up_shear; p2_up_shear; p3_up_shear];

%Extracting value of pressure for Downstream Cylinder Shear Flow Problem
p1_down_shear = data_down_shear(276:310, 5);
p2_down_shear = data_down_shear(1:121, 5);
p-down-shear = [p1_down_shear; p2_down_shear];

%Extracting value of pressure for Upstream Cylinder Uniform Flow Problem
p1_up_uni = data_up_uni(117:146, 5);
p2_up_uni = data_up_uni(1:86, 5);
p3_up_uni = data_up_uni(232:266, 5);
p-up-uni= [p1_up_uni; p2_up_uni; p3_up_uni];

%Extracting value of pressure for Downstream Cylinder Uniform Flow Problem
p1_down_uni = data_down_uni(276:310, 5);
p2_down_uni = data_down_uni(1:121, 5);
p-down-uni = [p1_down_uni; p2_down_uni];

%p_tot_up consist of 151 elements
theta_up = (180/pi)*transpose(linspace(0, pi, 151));
theta_down = (180/pi)*transpose(linspace(0, pi, 156));

%Plot of Pressure coefficient around upper half of cylinders
figure(1)
plot(theta_up, p-up-shear, 'b', theta_up, p-up-uni, 'r')
axis([0 180 -0.15 0.2])

```



```
title('Pressure Distribution Cp around Upstream cylinder at z=3.0: Uniform Flow')
xlabel('\theta [degrees], upper half for Upstream Cylinder')
ylabel('Pressure Coefficient Cp_{Upstream}')
legend('Cp in Shear Flow', 'Cp in Uniform Flow');
```

```
figure(2)
plot(theta_down, p_down_shear, 'b', theta_down, p_down_uni, 'r')
axis([0 180 -0.12 0.02])
title('Pressure Distribution Cp around Downstream cylinder at z=3.0: Uniform Flow')
xlabel('\theta [degrees], upper half for Downstream Cylinder')
ylabel('Pressure Coefficient P_{Downstream}')
legend('Cp in Shear Flow', 'Cp in Uniform Flow');
```

```
%VALIDATION OF TOP AND BOTTOM BOUNDARY CONDITION
```

```
clear all; clc;
```

```
%Upstream Cylinder: Reading dat.-file , & converting into matrix  
data_bottom = csvread('bottomBC_ShearRe100_t500.csv', 1, 0);
```

```
%Downstream Cylinder: Reading dat.-file , & converting into matrix  
data_top = csvread('topBC_ShearRe100_t500.csv', 1, 0);
```

```
%Extracting values for bottom boundary
```

```
P_bottom = data_bottom(:, 1);  
Ux_bottom = data_bottom(:, 2);  
Uy_bottom = data_bottom(:, 3);  
Uz_bottom = data_bottom(:, 4);  
arc_bottom = data_bottom(:, 10);  
x_bottom = data_bottom(:, 11);
```

```
%Extracting values for top boundary
```

```
P_top = data_top(:, 1);  
Ux_top = data_top(:, 2);  
Uy_top = data_top(:, 3);  
Uz_top = data_top(:, 4);  
arc_top = data_top(:, 10);  
x_top = data_top(:, 11);
```

```
%Values for bottom boundary
```

```
figure(1)  
plot(x_bottom, Ux_bottom, 'b', x_bottom, Uy_bottom, 'r',  
x_bottom, P_bottom, 'm')  
axis([min(x_bottom) max(x_bottom) -0.05 0.23])  
title('Ux and P at Bottom Boundary for  $-6.0 < x < 15$ ')  
xlabel('X_{range}')  
%ylabel('')  
legend('Ux at Bottom Boundary', 'Uy at Bottom Boundary',  
'P at Bottom Boundary');
```

```
%Values for top boundary
```

```
figure(2)  
plot(x_top, Ux_top, 'b', x_top, Uy_top, 'r', x_top, P_top, 'm')  
axis([min(x_top) max(x_top) -0.1 1.3])  
title('Ux and P at Top Boundary for  $-6.0 < x < 15$ ')  
xlabel('X_{range}')  
%ylabel('')  
legend('Ux at Top Boundary', 'Uy at Top Boundary', 'P at Top Boundary');
```

```

%VALIDATION OF BOUNDARY LAYER RESOLUTION
clear all; clc;

%Upstream Cylinder: Reading dat.-file , & converting into matrix
data_up = csvread('upstream_ShearRe100_t500.csv', 1, 0);

%Downstream Cylinder: Reading dat.-file , & converting into matrix
data_down = csvread('downstream_ShearRe100_t500.csv', 1, 0);

%Extracting values for upstream cylinder
Ux_up = data_up(:, 2);
Uy_up = data_up(:, 3);
Uz_up = data_up(:, 4);
y_up = data_up(:, 12);

%Extracting values for downstream cylinder
Ux_down = data_down(:, 2);
Uy_down = data_down(:, 3);
Uz_down = data_down(:, 4);
y_down = data_down(:, 12);

%Values for upstream cylinder
figure(1)
plot(y_up, Ux_up, 'b', y_up, Uy_up, 'g', y_down, Ux_down, 'r',
y_down, Uy_down, 'm')
axis([min(y_up) max(y_up) -0.2 1.4])
title('Ux and Uy above Upstream and Downstream Cylinder for  $0.5 < y < 5.0$ ')
xlabel('Y_{arch}, ranging  $0.5 < y < 5.0$ ')
%ylabel('')
legend('Ux above Upstream Cylinder', 'Uy above Upstream Cylinder',
'Ux above Downstream Cylinder', 'Uy above Downstream Cylinder');

```

## .13 BASH SCRIPTS:

*Bash scripts performs gmshToFoam on Vilje:*

```
#!/bin/bash
#PBS -N mesh
#PBS -l walltime=01:00:00
#PBS -l select=4:ncpus=32:mpiprocs=16
#PBS -A nn9191k
cd $PBS_O_WORKDIR
module load gcc/6.2.0
module load mpt/2.14
module load openfoam/5.0
gmshToFoam 4_tandem3D_6dia.msh
```

*Bash scripts performs decomposePar, checkMesh and pisoFoam on Vilje:*

```
#!/bin/bash
#PBS -N name
#PBS -l walltime=68:00:00
#PBS -l select=4:ncpus=32:mpiprocs=16
#PBS -A nn9191k
cd $PBS_O_WORKDIR
module load gcc/6.2.0
module load mpt/2.14
module load openfoam/5.0
decomposePar
mpiexec_mpt checkMesh -parallel
mpiexec_mpt pisoFoam -parallel
```

*Bash scripts deletes undesired time steps for the performed analysis in each processor folder from 0 to 63:*

```
#!/bin/bash
#PBS -N deleting
#PBS -l walltime=01:00:00
#PBS -l select=1:ncpus=32:mpiprocs=16
#PBS -A nn9191k
cd $PBS_O_WORKDIR

for i in {0..63}
do
cd processor\${i}
rm -rf 5 10 15 20 25 30 35 40 45 55 60 65 70 75 80
cd ..
done
```

## .14 OpenFOAM SCRIPTS

### .14.1 OpenFOAM: boundary

```
/*-----*- C++ -*-----*\
| ===== |
| \\ / F i e l d | OpenFOAM: The Open Source CFD Toolbox |
| \\ / O p e r a t i o n | Version: 5.0 |
| \\ / A n d | Web: www.OpenFOAM.org |
| \\ / M a n i p u l a t i o n |
\*-----*/
FoamFile
{
    version      2.0;
    format       binary;
    class        polyBoundaryMesh;
    location     "constant/polyMesh";
    object       boundary;
}
// ***** //
7
(
    upstreamCyl
    {
        type            wall;
        physicalType    wall;
        nFaces          36000;
        startFace       39451400;
    }
    back
    {
        type            cyclic;
        physicalType    cyclic;
        nFaces          110200;
        startFace       39487400;
    }
    neighbourPatch front;
}
    front
    {
        type            cyclic;
        physicalType    cyclic;
        nFaces          110200;
        startFace       39597600;
    }
    neighbourPatch back;
}
```

```

topAndBottom
{
    type            slip;
    physicalType    slip;
    nFaces          98400;
    startFace       39707800;
}
inlet
{
    type            patch;
    physicalType    patch;
    nFaces          24000;
    startFace       39806200;
}
downstreamCyl
{
    type            wall;
    physicalType    wall;
    nFaces          37200;
    startFace       39830200;
}
outlet
{
    type            patch;
    physicalType    patch;
    nFaces          25200;
    startFace       39867400;
}
)
// ***** //

```

## .14.2 OpenFOAM: velocity U

```
/*-----* C++ *-----*\
| ===== |
| \\ / F i e l d | OpenFOAM: The Open Source CFD Toolbox |
| \\ / O p e r a t i o n | Version: 4.1 |
| \\ / A n d | Web: www.OpenFOAM.org |
| \\ / M a n i p u l a t i o n |
\*-----*/
FoamFile
{
    version      2.0;
    format       ascii;
    class        volVectorField;
    object       U;
}
// *****
dimensions      [0 1 -1 0 0 0 0];
internalField   uniform (0 0 0);
boundaryField
{
    front
    {
        type      cyclic;
    }
    back
    {
        type      cyclic;
    }
    topAndBottom
    {
        type      slip;
    }
    upstreamCyl
    {
        type      fixedValue;
        value     uniform (0 0 0);
    }
    downstreamCyl
    {
        type      fixedValue;
        value     uniform (0 0 0);
    }
    inlet
    {
        type      fixedProfile;
    }
}
```

```
        profile      polynomial
        (
          ( (0.1 0 0)      (1 0 0) )
        );

direction      (0 1 0);
      origin      -5.0;
    }
  outlet
  {
    type      zeroGradient;
  }

}
// ***** //
```



### .14.3 OpenFOAM: pressure P

```
/*-----* C++ *-----*\
| ===== |
| \\      / F i e l d      | OpenFOAM: The Open Source CFD Toolbox |
| \\      / O p e r a t i o n | Version: 4.1 |
| \\      / A n d | Web: www.OpenFOAM.org |
|  \\    / M a n i p u l a t i o n |
\*-----*/
FoamFile
{
    version      2.0;
    format       ascii;
    class        volScalarField;
    object       p;
}
// ***** //

dimensions      [0 2 -2 0 0 0 0];

internalField   uniform 0;

boundaryField
{
    front
    {
        type      cyclic;
    }

    back
    {
        type      cyclic;
    }

    upstreamCyl
    {
        type      zeroGradient;
    }

    downstreamCyl
    {
        type      zeroGradient;
    }

    topAndBottom
    {

```

```
    type      slip;
}

inlet
{
    type      zeroGradient;
}

outlet
{
    type      fixedValue;
    value     uniform 0;
}
}
// ***** //
```

## .14.4 OpenFOAM: vorticity

```
/*-----*- C++ -*-----*\
=====
\\      /   F ield      |
 \\    /    O peration  |   OpenFOAM: The Open Source CFD Toolbox
  \\  /     A nd        |   Web:      www.OpenFOAM.org
   \\ /      M anipulation |
-----*-----*/

Description
    Calculates the vorticity field, i.e. the curl of the velocity field.

/*-----*- C++ -*-----*/

type          vorticity;
libs          ("libfieldFunctionObjects.so");

field         U;

executeControl writeTime;
writeControl   writeTime;

// ***** //
```

## .14.5 OpenFOAM: controlDict

```
/*-----*- C++ -*-----*\
| ===== |
| \\ / F i e l d | OpenFOAM: The Open Source CFD Toolbox |
| \\ / O p e r a t i o n | Version: 4.1 |
| \\ / A n d | Web: www.OpenFOAM.org |
| \\ / M a n i p u l a t i o n |
\*-----*/
FoamFile
{
    version      2.0;
    format       ascii;
    class        dictionary;
    location     "system";
    object       controlDict;
}
// ***** //

application     pisoFoam;

startFrom       latestTime;

startTime       0;

stopAt          endTime;

endTime         500;

deltaT          0.002;

writeControl    timeStep;

writeInterval   2500;

purgeWrite      100;

writeFormat     binary;

writePrecision  6;

writeCompression off;

timeFormat      general;

timePrecision   6;
```

```

runTimeModifiable no;
\newpage

functions
{
    Probes
    {
        type                probes;
        functionObjectLibs  ("libsampling.so");
        enabled              true;
        writeControl         timeStep;
        writeInterval        1;
        probeLocations
        (
            ( -1.0 0.354 3)
            (  0  0.354 3)
(  2.2 0.354 3)
(  3.5 0.354 3)

        );
        fields
        (
            p U
        );
    }

    forceCoeffs_upstreamCyl
    {
        type                forceCoeffs;
        functionObjectLibs  ( "libforces.so" );
        writeControl         timeStep;
        writeInterval        1;
        patches              ( upstreamCyl );
        pName                p;
        UName                U;
        rho                  rhoInf;
        rhoInf               1000;
        magUInf              0.5;
        log                  true;
        liftDir              (0 1 0);
        dragDir              (1 0 0);
        CofR                 (0 0 0);
        pitchAxis            (0 0 1);
        lRef                 1;
        Aref                 6;
    }
}

```

```

}

forceCoeffs_downstreamCyl
{
    type                forceCoeffs;
    functionObjectLibs ( "libforces.so" );
    writeControl        timeStep;
    writeInterval       1;
    patches              ( downstreamCyl );
    pName               p;
    UName               U;
    rho                 rhoInf;
    rhoInf              1000;
    magUInf             0.5;
    log                 true;
    liftDir              (0 1 0);
    dragDir              (1 0 0);
    CofR                (0 0 0);
    pitchAxis           (0 0 1);
    lRef                1;
    Aref                6;
}

#includeFunc singleGraph
#includeFunc Q
#includeFunc vorticity
}
// ***** //

```

## .14.6 OpenFOAM: decomposeParDict

```
/*-----*- C++ -*-----*\
| ===== |
| \\ / F i e l d | OpenFOAM: The Open Source CFD Toolbox |
| \\ / O p e r a t i o n | Version: 4.1 |
| \\ / A n d | Web: www.OpenFOAM.org |
| \\ / M a n i p u l a t i o n |
\*-----*/
FoamFile
{
    version      2.0;
    format       ascii;
    class        dictionary;
    location     "system";
    object       decomposeParDict;
}
// ***** //

numberOfSubdomains 64;

method            scotch;

simpleCoeffs
{
    n              (8 8 1);
    delta          0.001;
}

hierarchicalCoeffs
{
    n              (8 8 1);
    delta          0.001;
    order          xyz;
}

manualCoeffs
{
    dataFile       "";
}

distributed       no;

roots             ( );
// ***** //
```